12-2019

Dynamics and viscoelastic properties of Hydrogen-bonding telechelic associating polymers

Kunyue Xing
University of Tennessee, kxing@vols.utk.edu

To the Graduate Council:

I am submitting herewith a dissertation written by Kunyue Xing entitled "Dynamics and viscoelastic properties of Hydrogen-bonding telechelic associating polymers." I have examined the final electronic copy of this dissertation for form and content and recommend that it be accepted in partial fulfillment of the requirements for the degree of Doctor of Philosophy, with a major in Chemistry.

Alexei Sokolov, Major Professor

We have read this dissertation and recommend its acceptance:

Sheng Dai, Brian Long, Joshua Sangoro

Accepted for the Council:

Dixie L. Thompson

Vice Provost and Dean of the Graduate School

(Original signatures are on file with official student records.)

Dynamics and Viscoelastic Properties of Hydrogen-bonding Telechelic Associating Polymers

A Dissertation Presented for the

Doctor of Philosophy

Degree

The University of Tennessee, Knoxville

Kunyue Xing

May 2020

Acknowledgements

First of all, I would like to express my heartfelt gratitude to my advisor, Professor Alexei P. Sokolov for his guidance, patience, encouragement and support throughout my doctoral study. I feel extremely lucky to be able to work closely with him and learn about various aspects of polymer physics and many professional skills. He is my life mentor not only in the field of scientific research, but also in how to become a kind, considerate, decent and wise person with critical thinking and professional spirit. Besides the Ph.D. research, he cares deeply for students' future development and is super supportive for us to explore various opportunities. His kindness to students, diligent and professional working spirit, aspiration to knowledge and passion for science have influenced me profoundly in the past six years and will keep inspiring me in my future life.

I want to thank my doctoral committee members: Professor Brian Long, Professor Joshua Sangoro, Professor Sheng Dai and Professor Jimmy Mays for serving on my doctoral committee and for their valuable suggestions and efforts to help me with my graduation.

I feel greatly blessed to work in our group with so many talented and kind colleagues. Thanks to Dr. Yangyang Wang, without whose help, I wouldn't have been able to transfer into this group and begin a wonderful journey in the next few years. Dr. Catalin Gainaru worked closely with me on my very first project and opened the door to scientific research for me by teaching me various experimental techniques and the underlying physical theory patiently. Dr. Pengfei Cao offered me great help on the material design and synthesis, assisted me to overcome the obstacles. I've learned a lot about rheology from Dr. Shiwang Cheng. Despite his many ongoing projects, he provided fruitful discussion and offered insight into my research. I'm especially grateful to work closely with Dr. Martin Tress, who was always willing to take time to help me by going through every detail when I was blocked on the project and uncertain about my next steps. When I was down and very upset about my Ph.D. career, he was there to encourage me and watch my back.

I would like to thank Dr. Fei Fan who taught me dielectric experiments and data analysis, Dr. Tao Hong who helped me with proposal writing, Bingrui Li who greatly helped me in the

synthesis lab. I want to thank Dr. Anne-Caroline Genix for helping us with SAXS experiments in France, Dr. Halie Martin and Dr. Mark Dadmun for SAXS experiments at University of Tennessee, Knoxville and University of South Carolina.

I would also like to acknowledge the collaborative efforts and many valuable discussions with members in the group: Dr. Tomonori Saito, Dr. Vladimir Novikov, Dr. Vera Bocharova, Dr. Dmitry N. Voylov, Dr. Zaneta Wojnarowska, Dr. Bobby Carroll, Dr. Adam Holt, Sirui Ge, Sheng Zhao and all former group members.

I want to thank my best friends, Xinyang He, Ziwei He, Xiaoyi Huang for the enduring encouragement and heart-warming comfort whenever I went down and got self-suspicious. I would also like to thank all my friends, especially Dr. Xinyi Lu, Jiali Li, Luna Liang, Kaizhong Guan. Last but not least, special thanks to my boyfriend Jiadi Hou. I won't achieve what I have today without his love and support.

I dedicate this dissertation to my beloved parents, Yunxia Jia and Keli Xing, for their unconditional love, support and encouragement.

Abstract

Supramolecular polymers (also termed as associating polymers), which are connected by non-covalent interactions between polymer chains, have become an increasingly important class of polymers and gained tremendous interest in the last few decades. The co-existence of reversible secondary interactions and covalent bonding makes supramolecular polymers promising candidates for functional materials with unique properties. Immense effort has been put on the development of chemical structure design, while the understanding of their physical properties is rather limited, especially in the melt state.

In this dissertation, we studied the dynamics and viscoelastic properties of H-bonded telechelic associating polymers by tuning the association strength, main chain length, flexibility and polarity. The supramolecular association of hydroxyl-terminated PDMS chains leads to the emergence in dielectric and mechanical relaxation spectra of the so-called Debye process traditionally observed in monohydroxy alcohols. Then we investigated telechelic associating PMDS with different hydrogen bonding end groups, *e.g.* NH_2, NHCO-COOH (amide-acid groups). Remarkably, a single species of end group forms two qualitatively different types of associates in PDMS-NHCO-COOH. In the following work, we studied telechelic PDMS and PPG with three types of H-bonding end-groups possessing different interaction strengths and a non-H-bonding end-group as reference were compared. In the end, we studied the role of the linker groups (-NHCO- vs. -S-) and the influence of phase separation. A systematical analysis was conducted by employing a combination of experimental techniques: dielectric spectroscopy, differential scanning calorimetry, rheology and small angle X-ray spectroscopy to get a deeper understanding of the dynamics of supramolecular polymers. Our results provide another experimental support to lifetime renormalization model and we found that the phase separation plays more important role than increase in strength of secondary interactions.

Unraveling the mechanisms of many molecular processes and structure-dynamics-property relationship in supramolecular polymers is of great importance for both fundamental studies and industrial applications. Findings in this work suggested that the backbone length, flexibility and polarity, the strength and lifetime of the associating groups, the ratio of

characteristic time scales between backbone and chain ends and the phase separation behavior should be considered in the design of associating polymers to achieve the desired properties.

Table of Contents

List of Tables

List of Figures

Introduction

Supramolecular polymers are applied in various field such as rheological modifiers, adhesives, superabsorbers, biomedical, self-healing and photovoltaic materials. Their reversible non-covalent bonding contributes to the good performance in processing and recycling. Considering that each polymer gets its properties from the unique chemical structure, its molecular weight and architecture, etc., it is of utmost significance to understand the relation between the chemical structure, the architecture, molecular weight and the macroscopic physical properties of supramolecular polymers.

The research on polymer dynamics focuses on seeking a quantitative microscopic description for observed macroscopic properties, and furthermore, tuning dynamics on various length and time scales may directly control materials' properties and industrial application. Although there's intensive work and effort in the past, the understanding of many processes and phenomena in supramolecular polymers, especially in the melt state, remains far from complete.

In this work, we expect to bridge the fields of H-bonded small molecules and supramolecular polymers, and reveal how the strength of secondary interactions, polymer backbone flexibility and molecular weight (MW) determine the dynamics and viscoelastic properties of supramolecular polymers on different time and length scales. Hydroxyl terminated Polydimethylsiloxane (PDMS-OH) with different MW were first studied with expectation that even single H-bonding at the chain ends can affect dynamics significantly at low temperatures. With a careful design of end-functionalization, we further introduced amine (NH_2), amide-acid (NHCO-COOH) groups based on PDMS to study how different H-bonding chain ends can affect the molecular dynamics on segmental and chain scales, and macroscopic viscoelastic properties. In PDMS-NHCO-COOH, a second glass transition temperature (the glass transition temperature, T_g is the temperature at which the material transits from glassy state to rubbery state) T_g is detected, indicating clearly that there's phase segregation in the system. We found that due to the reversibility of the cluster association, the PDMS-NHCO-COOH systems combine viscoelastic properties of short chains at high T, and those of crosslinked rubber below

the second T_g. This suggests a promising route to combine easy processability of low MW liquids with the desired mechanical performance of high MW polymers and even crosslinked networks.

Later, we compare the dielectric and rheological performance of associated PDMS with that of poly(propylene glycol) (PPG) with similar end groups (OH, NH_2, NHCO-COOH). The difference in glass transition temperature and viscosity as a function of MW can be explained by the lifetime ratio of the end-group associations to segmental and chain relaxation times of backbones. We demonstrated that the ratio of characteristic time scales should be considered in the design of associating polymers to achieve the desired properties. In the end, in order to dig deeper into the mechanisms and dynamics of PDMS-NHCO-COOH systems, we synthesized sulfur-acid terminated PDMS-S-COOH and employed Small-angle X-ray Scattering. It turns out that not just the end-group (-COOH in both case) but also the linker group (-NHCO- vs. -S-) plays an important role. Our analysis clearly demonstrate that phase separation affects viscoelastic properties stronger than the strength of the chain ends interactions. This dissertation has the following organization.

Introduction gives the organization of this dissertation.

Chapter 1 gives a concise overview of the historical background of supramolecular polymers and classic theories of supramolecular polymer dynamics.

Chapter 2 describes experimental techniques and procedures employed in this work. An introduction to the fundamental mechanisms and instrumentation of Broadband Dielectric Spectroscopy (BDS), Differential Scanning Calorimetry (DSC), rheology and Small-angle X-ray Scattering (SAXS) is included.

Chapter 3 shows materials, synthesis and characterization in this work. A detailed description of synthesis method, structure confirmation, molecular weight (MW) and degree of polymerization (*DP*) characterization is presented.

Chapter 4 presents a detailed investigation of the effect of chain-end hydrogen bonding on the dynamics of hydroxyl-terminated PDMS (PDMS-OH). Our analysis suggests that the

PDMS-OH oligomers may associate in brush-like or chain-like structures, depending on the size of their covalent chains. The effective length of the linear-associated chains was estimated from the rheological measurements.

Chapter 5 extends the work of Chapter 4 by introducing more H-bonding chain end groups (NH_2, NHCO-COOH) to PDMS. Observations provides insight into the underlying molecular mechanisms, and especially reveals that many end groups of the NHCO-COOH terminated chains phase segregate, while a certain fraction forms binary associates and remains non-segregated. In contrast, the NH_2-terminated systems form only binary associates increasing the effective chain length, whereas the NHCO-COOH-terminated system consist of two types of associates forming a crosslinked network.

Chapter 6 presents a systematic study on the impact of H-bonding end-groups on segmental and chain dynamics of telechelic poly(propylene glycol) (PPG) and PDMS with similar associating end groups (OH, NH_2, NHCO-COOH). The molecular weight dependence of glass transition temperature and viscosity are explained qualitatively by the ratio of lifetime of the end-group associations to segmental and chain relaxation times of polymer chains.

Chapter 7 further explores how phase separation affect the dynamics and viscoelastic properties of PDMS based associating polymers. A slight adjustment of the linker group (-NHCO- vs. -S-) could result in significant difference of the phase separation behavior. With additional lateral packing (-NHCO-), the amide-acid groups (-NHCO-COOH) aggregate prominently even at room temperature, leading to a pronounced phase separation as evident from the SAXS measurements; the absence of higher order peaks suggests that the spatial arrangement of the aggregates is not highly ordered.

At the end, conclusions are summarized and presented.

Chapter I

Historical Background and Classical Theories

1.1 Supramolecular polymers

Associating polymers form a relatively new class of materials generically defined as "arrays of monomeric units that are held together by highly directional and reversible noncovalent interactions. These interactions result in properties that are characteristic for high molecular weight polymers or cross-linked networks in solution and bulk".[1-5] The noncovalent (also termed as "secondary") interactions which can promote the formation of such supramolecular networks include hydrogen bonding,[6-9] metal-ligand bonding,[10-12] π-π interactions,[13, 14] ionic bonding,[15, 16] and host-guest interactions.[17, 18] Besides the utilization of a single secondary interaction, the combination of two or more different forces is also employed to explore the link of diverse strengths and dynamics.[17, 19, 20]

Among the interactions mentioned above, hydrogen (H-) bonding is the most common interaction involved in the formation of supramolecular polymers due to its intrinsic directionality, cooperative nature,[21] and variability of cohesive strength.[22-24] The latter can be tuned, for example, by increasing the number of H-bonding centers attached to the molecular constituents, from a single to several (e.g., triple,[25-29] quadruple,[6-8, 30] even sextuple[31, 32]) units. Classical examples of molecules designed for sustaining multiple H-bonds include thymine-2, 6-diaminotriazine (THY-DAT),[29] 2-ureido-4-pyrimidinone (UPy),[6, 7] 2, 7-diamido-1, 8-naphthyridine/urea of guanosine (DAN/UG),[30] and diaminopyridine-substituted isophthalamide and barbiturates motifs as shown in Fig. 1.1.[31] Because of the reversibility of hydrogen-bonding and tunable association strength, the topologies and dynamics of the transient supramolecular system can be tuned by specific design of H-bonding motifs as well as external stimuli such as temperature and applied mechanical force.

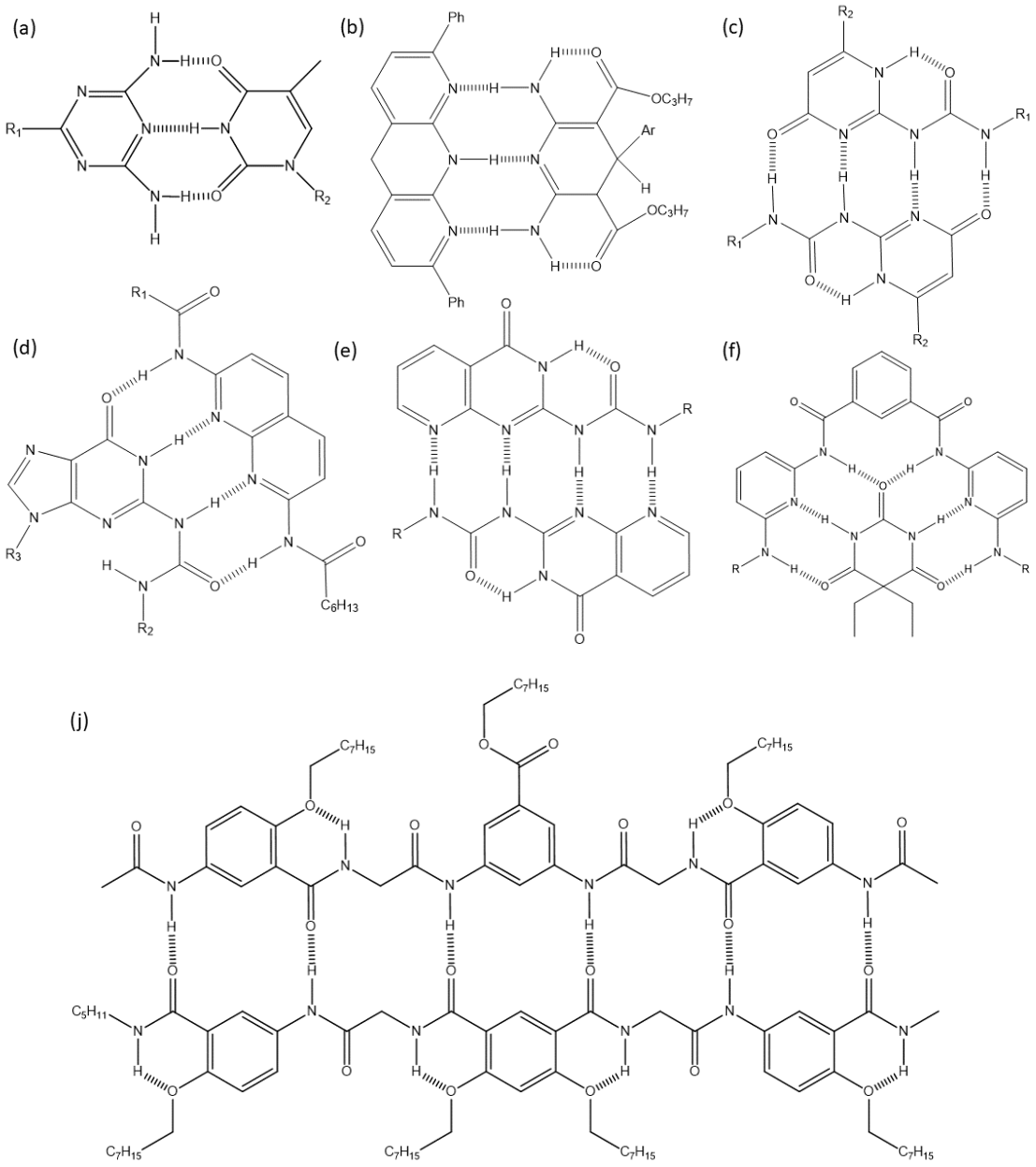

Figure 1. 1. Triple hydrogen-bonding motifs: a) thymine-2, 6-diaminotriazine (THY-DAT);[29] b) a triple motif according to Zimmerman and coworkers.[25] Quadrable hydrogen-bonding motifs: c) 2-ureido-4-pyrimidinone (UPy)[6]; d) 2, 7-diamido-1, 8-naphthyridine/urea of guanosine (DAN/UG); e) a quadrable motif by Zimmerman and coworkers.[8] Sextuple hydrogen-bonding arrays: f) diaminopyridine-substituted isophthalamide and barbiturates;[31] j) a sextuple motif reported by Gong *et al*.[32]

Besides the nature of the association strength, supramolecular polymers can also be classified by the number and the position of the associating moieties. Generally, they can be distributed at either the center or the chain ends to form main-chain supramolecular polymers,[33-36] or as pendant groups spread along the chain backbones to form side-chain systems (Fig. 1.2).[37-41] In main-chain supramolecular systems, when associative motifs are on both ends of chain building blocks, extended chains can be formed (Fig. 1.2 a) and the degree of supramolecular polymerization is correlated to the concentration and equilibrium number of active secondary forces. Utilization of non-linear chain building blocks[42, 43] or multi-functionality associative motifs[44, 45] can form transient networks (Fig. 1.2 a), thereby leading to more complicated rheological and mechanical behaviors. In side-chain supramolecular polymers, multiple stickers along the backbones can lead to cross-linked and grafted structures (Fig. 1.2 b).[41, 46-50]

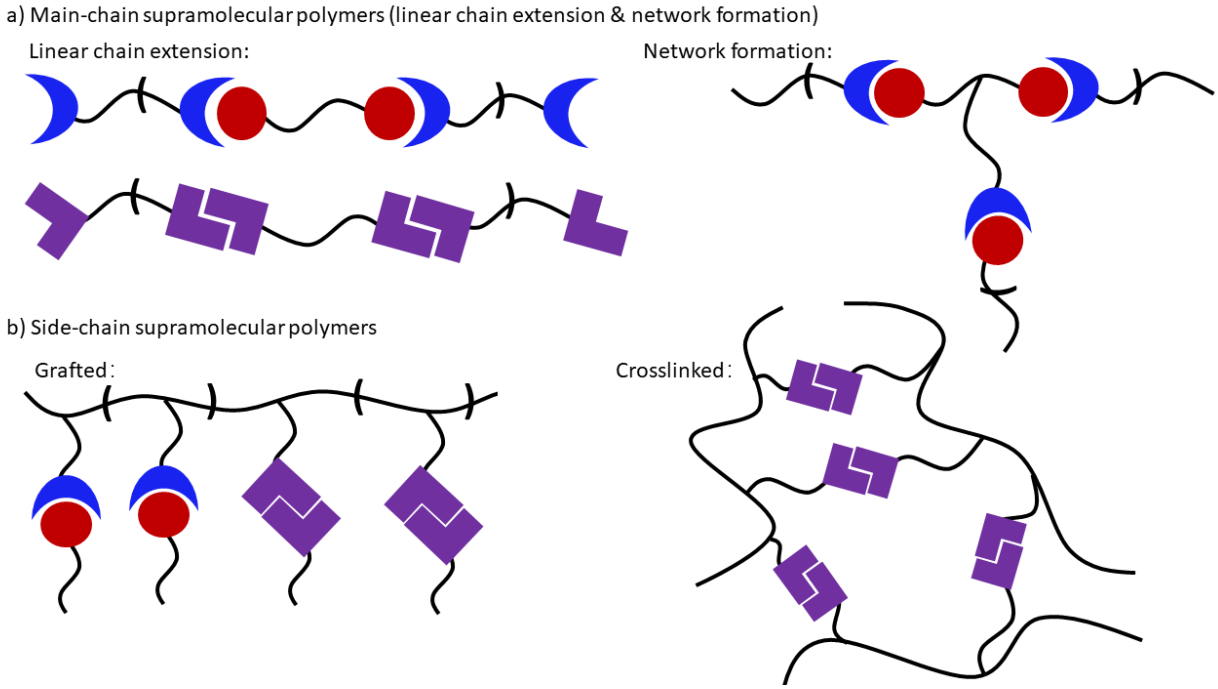

Figure 1. 2. a) Main-chain supramolecular polymers; b) side-chain supramolecular polymers. Purple puzzles represent same associating groups and blue-red puzzles represent complementary association from different groups.

The structural reversibility caused by the transient nature of secondary interactions renders supramolecular polymers as promising materials with unique properties, such as recyclable, degradable, stimuli-responsive, self-healing, and shape-memory behavior with great capacity for processability (Table 1.1).[3, 24, 37, 51-56] Conventional polymers have excellent properties as materials, but due to entanglement of their macromolecules, they usually exhibit high viscosity after melting. To solve this problem, high temperatures and pressures are typically applied to reduce viscosity for processing, which limit their applications. On the contrary, slight temperature increase can produce large reduction in viscosity above the melting point or glass transition temperature of supramolecular polymers according to the intrinsic characteristics of secondary interactions. This makes the materials ideal for easy processing and handling. To be specific, the primary pathway for stress relaxation in conventional polymers is reptation, which is the thermal motion of long, entangled macromolecules analogous to snakes slithering through one another.[57, 58] For supramolecular polymers, besides reptation, strain/stress can be released by non-covalent bonding groups dissociating and re-associating with other strain-free ones. This process even speeds up at higher temperatures, leading to liquid-like behavior when these polymers are rapidly reduced to shorter chains. Therefore, supramolecular polymer is a promising candidate that can combine the easy processing similar to low viscous melts (at slightly elevated temperatures) with good functional performance of high molecular weight materials at ambient temperatures.

1.2 Glass transition and structural dynamics

1.2.1 Glass transition and temperature dependence of segmental relaxation

The transition of a glassy material from a soft, rubber-like state to a glass-like non-crystalline solid is called the glass transition and is one of the most widely studied, yet incompletely understood phenomena. Upon cooling, the molecular motion will become so slow that an equilibrium of packing the molecules cannot be attained during the process. When this happens, we say that the polymer has undergone the glass transition. At the meantime, the materials' shear viscosity can change by 10-15 orders of magnitude over a temperature range

Table 1. 1. Summary of representative applications of supramolecular polymers.

Application	Literature
Self-healing	59-67
Functional behavior	3, 20, 24, 51, 53, 68-70
Functionalization of surfaces	69, 71-73
Stimuli responsive materials	63, 74-82
Controlled self-assembly	17, 83-87
Shape memory	88-90
Sensors	91
Controlled release drug delivery Biomedical applications	54, 55, 92
Biomimetic	55, 93-95

within a few hundred Kelvins. The temperature dependence of segmental relaxation is understood to be sensitive to the molecular structure and thermodynamic conditions.

The glass transition temperature, T_g is a thermodynamic property of the polymer, it is defined as a temperature at which a transition from liquid to solid state occurs without crystallization. In polymers, the glass transition is a result of slowing down of segmental motion. The segmental relaxation time is a characteristic of the polymer segment motion. In terms of relaxation time, T_g is conventionally defined as the temperature at which the segmental relaxation time (τ_α) of a polymeric material equals to 100 seconds. Generally, segmental relaxation is a local intermolecular motion that can be viewed as a rearrangement of segments through conformational changes. In order to perform conformation changes and have segmental rearrangements, the energy barrier between two conformations should be overcome and this barrier is often connected to the apparent activation energy for the segmental relaxation. Thus, segmental rearrangements could be regarded as a process of jumping over a potential energy barrier.

The systems often follow a simple Arrhenius dependence at high temperatures above T_A (T_A is called Arrhenius Temperature, often exceeds $2T_g$):[96]

$$\tau(T) = \tau_0 \exp(\frac{E_a}{RT}) \quad (1.1)$$

in which τ is the structural relaxation time, τ_0 is the attempt time (also termed as infinite temperature relaxation time) describing a unit oscillating in the potential well, E_a is the activation energy. In the temperature range from T_A to T_g, dynamics can be described by the Vogel-Fulcher-Tammann (VFT) equation:

$$\tau(T) = \tau_0 \exp(\frac{B}{T-T_0}) \quad (1.2)$$

T_0 is the so-called thermodynamic T_g, and B is a material specific parameter. The materials that follow VFT behavior show an increasing apparent activation energy upon cooling to T_g. The glass transition temperature T_g observed by techniques such as Differential Scanning Calorimetry (DSC) varies with the heating or cooling rate. Usually the higher the cooling rate, the higher glass transition temperature T_g obtained.[58]

As discussed above, it is the permanent connectivity between repeating units that determines many particular features of the segmental dynamics in conventional covalently-bonded polymers.[58] As it's been observed in all polymers without functional end groups, the segmental mobility would be restricted by increasing MW, thus resulting in higher T_g with elevated MW (Fig. 1.3).[97] In this field, the critical parameters that affect the glass transition temperature are chain and side groups' rigidity and bulkiness. As shown in Fig. 1.3, the increase in T_g with MW for flexible chains (*e.g.* polydimethylsiloxane, PDMS) appears relatively weaker, while a stronger dependence of T_g on MW is observed for rigid polymers (*e.g.* polystyrene, PS) due to more prominent restriction imposed on segmental relaxation.[97] Meanwhile, the local packing efficiency strongly relies on the intramolecular energy barriers. For supramolecular polymers with transient connections between molecular building blocks, the inner structure and architecture such as the strength of the non-covalent interactions, the molecular weight and flexibility of segmental blocks, and the number of functional groups can influence the segmental dynamics and lifetime of the supramolecular polymer. However, the study of the structural dynamics of associating supramolecular polymers in melt are quite incomplete. Therefore, it is important to explore the impact of transient secondary association on the segmental dynamics of supramolecular polymers, especially the influence on glass transition temperature and temperature dependence of segmental relaxation.

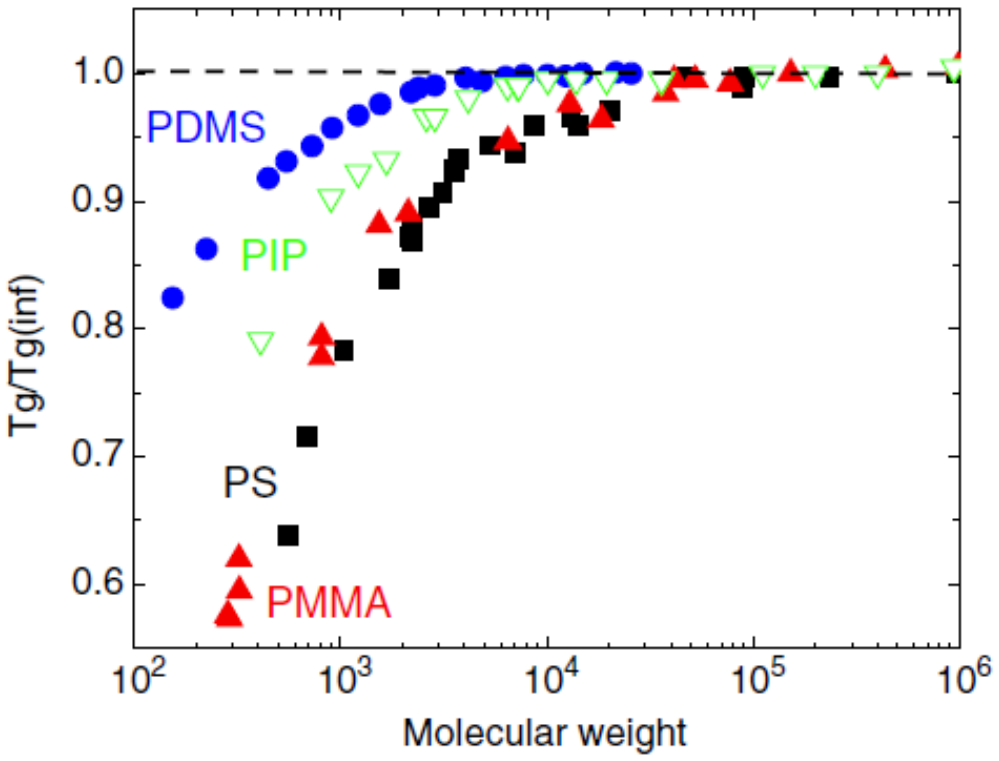

Figure 1. 3. The molecular weight dependence of glass transition temperature T_g scaled by $T_{g,inf}$ (T_g at high MW) for polystyrene (PS), Poly(methyl methacrylate) (PMMA), polyisoprene (PIP), poly(dimethyl siloxane) PDMS. The $T_{g,inf}$ is 373 K, 385 K, 206 K and 146 K, respectively.[97]

1.2.2 Fragility

Another important parameter is fragility index, *m*, which characterizes the steepness of the temperature-dependence of segmental relaxation time (τ_α) close to the glass transition temperature:

$$m = \left.\frac{\partial \log \tau_\alpha}{\partial (T_g/T)}\right|_{T=T_g} \quad (1.3)$$

The systems that exhibit a strongly non-Arrhenius temperature dependence of segmental dynamics with steep variations approaching to T_g (that is to say, with high fragility value) are called 'fragile', and the systems that show Arrhenius-like dependence of τ_α (with low fragility value) are called 'strong' as shown in Fig. 1.4.

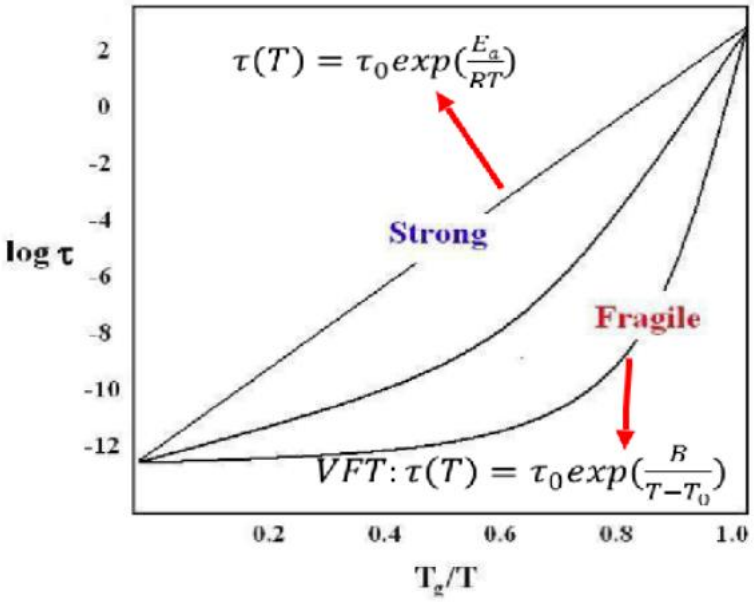

Figure 1. 4. A schematic representation of strong and fragile behaviors.

Fragility is commonly used to characterize glass-forming liquids based on the idea that strong materials perform higher resistance to properties variation with temperature, namely exhibit a relatively smooth transition from the rubbery state to the glassy state. In this view, systems with a higher fragility are supposed to have a relatively narrow glass transition temperature range. The earlier research revealed that the relative rigidity of the backbone and side group is a decisive factor in the fragility of regular covalent bonded polymers.[98] Rigid polymers usually show high values of *m* according to the packing frustration.[99, 100] On the contrary, weakly hydrogen-bonded liquids typically possess low fragilities. Comparing with conventional polymers with rigid chains or with pronounced difference in the stiffness of the backbone and side groups, weakly bonded associating liquids are expected to have better packing efficiency due to the transient nature of its secondary intermolecular interactions.

Several methods have been presented to calculate the fragility index *m*. One of the most commonly used ways is using VFT parameters. Combine equation 1.2 and 1.3 yields:

$$m = \frac{B/T_g}{ln10\left(1-T_0/T_g\right)^2} \quad (1.4)$$

1.2.3 Adam-Gibbs theory

Although the intrinsic physical picture underlying the glass transition behavior is still far from complete, there're several important theories developed as good references. For example, Adam-Gibbs theory proposed more than half a century ago describes the dynamics of supercooled liquids using thermodynamic arguments.[101] This molecular kinetic theory predicts the relaxation time based on the size of Cooperatively Rearranging Regions (CRRs) which increases with cooling. CRRs are referred to the smallest volumes of a liquid that can relax freely with the neglected environmental influence. These regions can overcome the individual temperature-independent potential energy barriers that hindering their cooperative rearrangement. It demonstrates that the size of the region is directly related to the macroscopic configuration entropy. The relaxation time of the supercooled liquid is expressed as:[101]

$$\tau(T) = \tau_\infty \exp\left(\frac{Z^* \Delta\mu}{k_B T}\right) \quad (1.5)$$

where $\Delta\mu$ is the individual potential energy barriers, τ_∞ is the relaxation time at infinite temperature, k_B is the Boltzmann constant, Z^* is the critical size of the cooperating region:

$$Z^* = \frac{N_A S_c^*}{S_c} \quad (1.6)$$

Where S_C is the macroscopic configuration entropy of the system, and S_C^* is the critical molar configuration entropy of a region with Z^* structural units. Combining Eq. 1.5 and 1.6, we have:

$$\tau(T) = \tau_\infty \exp\left(\frac{C}{S_c T}\right) \quad (1.7)$$

in which C is a temperature-independent constant. As temperature decreases, the size of CRR increases (~Z^*), thus reducing S_C. The system should become more densely packed and have a higher activation energy. On the other hand, at higher temperatures, the segmental motion is not collective, and the systems should have a temperature-independent barrier height, leading to Arrhenius behavior.[96]

1.2.4 Free volume models

The free volume models are used to describe the dynamics in viscous liquids and the glass transition. These models rely on the assumption that the local motion of a small molecule or a segment of polymers is determined by the free space available to it.[102] Normally when the melt is cooled down, the fraction of free volume decreases, which result in structural freezing. In polymeric systems, the free volume is usually ascribed to the chain ends according to their higher mobility. So shorter polymer chains are supposed to exhibit higher fraction of free volume compared to longer chains. This decrease in fractional free volume as chain length increases is generally accepted to be the reason behind the molecular weight dependence of T_g for conventional covalently bonded polymers (as shown in Fig. 1.3).[58]

1.3 Debye-like relaxation in hydrogen-bonded liquids and associating polymers

There's much research on the dynamics of weakly associating liquids, such as water,[103-105] secondary amides,[106] mono- and poly-alcohols.[107, 108] It's well known that hydrogen-bonded small molecule glass-forming liquids exhibit many peculiar characteristics that are not observed in regular van der Waals liquids, which is mainly related to the nature of their intermolecular interactions. For example, besides structural relaxation, a pronounced Debye-like (single-exponential) dielectric relaxation at low frequency is commonly observed in monohydroxy alcohols and it's regarded as a distinct signature of hydrogen-bonded simple liquids (as shown in Fig. 1.5 b). It's been proposed by Dr. Gainaru *et al.*[108, 109] that the Debye-like relaxation is a reflection of the fluctuation of the cumulative dipole moment along the chain-like supramolecular structure (Fig. 1.5 a), thus making it similar to the dielectric normal mode in type-A polymers.[110, 111]

The study of Debye-like relaxation has long been limited to hydrogen-bonded simple liquids, such as mono-alcohols and secondary amides. While a recent study of a self-complementary supramolecular polymer T-DAP9 based on thymine (T) and diamidopyridine (DAP) triple hydrogen-bonding motifs in melts demonstrated that Debye-like relaxation also exists in some strongly associating supramolecular polymer systems (Fig. 1.6).[112] The dielectric

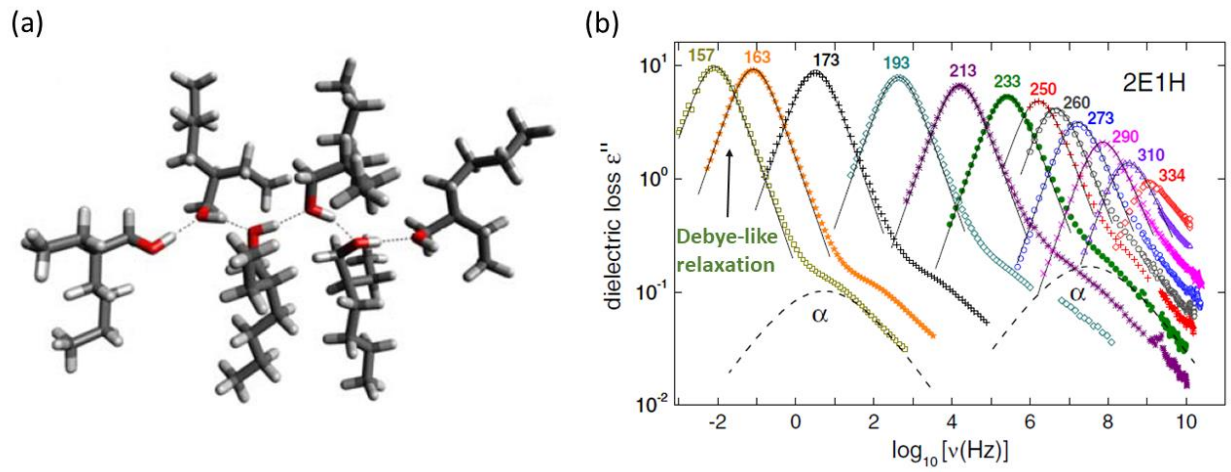

Figure 1. 5. (a) Illustration of the hydrogen-bonded supramolecular structure of 2-ethyl-1-hexanol (2E1H), a representative weakly associating simple liquid. (b) Dielectric spectra of 2E1H at a broad temperature range.[108]

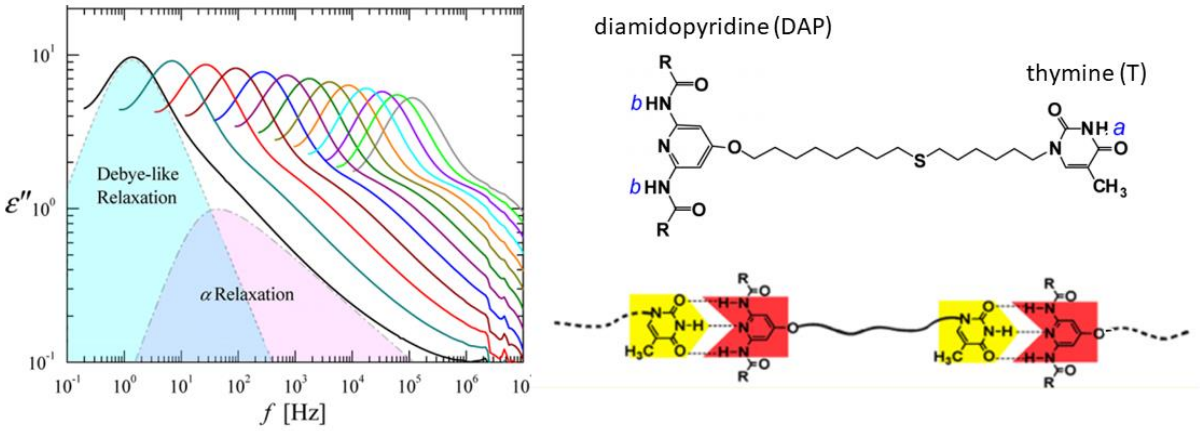

Figure 1. 6. Representative dielectric spectra of T-DAP9 on the left with a slow, clear Debye-like relaxation; Structure of T-DAP9 with triple hydrogen-bonding motifs on the right.[112]

spectrum shows a prominent ideal symmetric Debye-like relaxation and its dielectric strength decreases remarkably at elevated temperatures, resembling the peculiar features observed in simple hydrogen-bonding liquids (Fig. 1.5 b). While there's no corresponding mechanical relaxation found in mono-alcohols for the Debye-like process, a separate chain relaxation mode was observed in the T-DAP9 system in mechanical spectrum. It's worth pointing out that dielectric measurement has been employed as the main technique to study weakly hydrogen-bonded liquids, and the application of mechanical relaxation spectroscopy has only been included successfully recently. Meanwhile, rheological methods have been the main tool to investigate the dynamics and viscoelastic performance of strongly-hydrogen bonded supramolecular polymers and the use of dielectric spectroscopy is quite rare.

The understanding of the chain motions of supramolecular polymers in melts are still limited. It would be very promising to study the dynamics of both weakly and strongly associated polymers by a combination of dielectric and rheological methods, especially to explore the connection between the Debye-like relaxation and the chain relaxation.

1.4 Viscoelastic properties and diffusion in supramolecular polymers

The design and effective application of supramolecular polymer systems require precise description of relaxation mechanisms of polymer building blocks, understanding of the mechanical properties and the kinetics of reversible formation and breaking of reversible transient forces.[5] Therefore, it is of great importance to uncover how polymer backbone flexibility, molecular weight, the strength of associations and other molecular parameters affect the macroscopic rheological behavior of supramolecular polymers.

The dynamics of supramolecular polymers in solution are already well understood, since the association can be described via simple models, e.g. end-to-end association of telechelic polymers[79, 113] and reversible assembly of comb polymers.[114-116] While for concentrated solution (gels) and melts, the understanding is far from complete. In gels and melts, besides the association of two secondary groups, the transient active forces may associate strongly, pack collectively and form large aggregates (as shown in Fig. 1.7 a) and micelles, leading to macro-

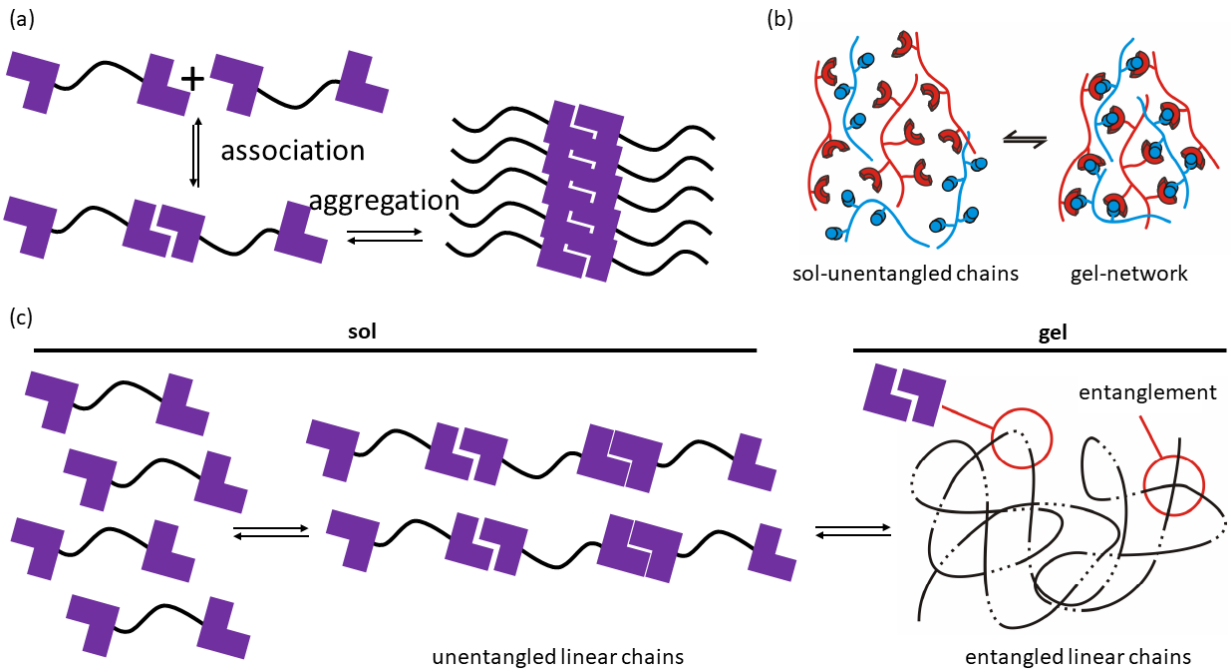

Figure 1. 7. a) Association of two supramolecular groups and their aggregation into larger aggregates; b) network formation of supramolecular polymers with secondary forces along the backbone chain; c) network formation of entangled linear chains with functional groups on chain ends.

phase separation. The "collective" packing association are mainly motivated by two factors: 1) surface tension reduction from the large difference of amphiphilicity or polarity between backbones and associating groups;[74, 117-119] 2) Gibbs free energy reduction by formation of transient interactions between supramolecular moieties.[120, 121] Upon percolation threshold, which is related to the formation of a physical network, solutions and melts exhibit reversible transition between the liquid-like (sol) and viscoelastic-like (gel) behaviors (Fig. 1.7 b & c).[118, 122-124]

There're several models developed to explain the rheological behavior and dynamics of supramolecular polymers, such as Cates's "living" reptation model,[125-127] sticky Rouse model[39, 41, 128-130] and sticky reptation model,[130-132] and other phenomenological theories of transient networks.[133-139] Each model has its limitations and only very few systems were reported to be described well. All theories presented didn't include the effects of aggregation, crystallization and phase separation, which are commonly observed in supramolecular systems especially in the melt state. The reduction of chain mobility and chain entanglements in the melt state make it even more challenging to relate experimental results to theoretical models. Furthermore, a detailed general model for the precise prediction of network formation and dynamics is still missing till now. Although the effort of connecting theory with experimental results and detailed mechanic spectra is far from sufficient, the existing theories are still enlightening to study the influence of molecular details on the mechanical and viscoelastic properties.

1.4.1 Cates's "living" reptation model

Cates's model[125] is one of the most remarkable theories that consider the presence of reversible secondary interactions, since it was found valid and applicable in various systems.[140-145] Cates's model, which is based on linear entangled polymeric chains in solution that can break and reconnect on experimental time scales, assumed that a chain can break with equal probability per unit time, length at all points along the chemical sequence and chains recombine at a rate proportional to the chain fragments' concentration.[125] In the view of this model, stress relaxation occurs via reptation mechanism that may be abetted by constant

reversible breaking and recombination at certain range of time and length scale. As depicted in Fig. 1.8, considering a linear end-functionalized transient polymeric chain that is trapped in a tube. Similar to conventional reptation model developed by de Gennes,[57] the tube can be regarded as movement restrictions according to the surrounding polymer matrix. When an associating bond breaks and the newly released chain ends can pass through the tube, the local movement becomes possible before these ends recombine. The available local movements can lead to the chain relaxation. Note that the released chain ends can combine with chain ends from the surrounding matrix as well.[125, 126]

After decades of study, the intrinsic nature of entanglement in high-molecular-weight polymers is still one of the greatest unsolved puzzles in polymer physics. It's generally accepted that entanglement is caused by the topological constraints long polymer chains impose on each other.[146] This problem becomes even more intriguing when it comes to supramolecular systems due to their transient nature. According to Cates, when the lifetime of the association is much shorter than the characteristic time for reptation, the rubbery plateau modulus of the "living" polymer should be similar to that of the conventional covalently-bonded polymer of the same backbone and the terminal relaxation should be dominated by a single Maxwell relaxation as shown in Fig. 1.9.[125] On the other hand, when reptation is much faster than the chain dissociation, the stress relaxation is non-exponential and deviates from Maxwell model.

The limitation of Cates's "living" reptation model is that it only discussed the kinetics of breaking and recombination, dynamics of stress relaxation of linear entangled transient chains in solution. It was later further developed by Granek and Cates,[147] Cates and Candau[148] and Cates himself.[149] Granek and Cates proposed a simplified Cates model by incorporating a stochastic hopping process instead of original exact reaction kinetics.[147] Cates and Candau refined Cates model for semidilute solutions of wormlike micelles and proposed scaling laws involving relaxation time, viscosity and the concentration of living building blocks.[148] Cates himself later extended the original model to describe non-linear behaviors applicable to systems under external deformation, which increase the average length of the confining tube thereby leading to a rapid retraction of the chain in its tube that is much faster than the reptation time.

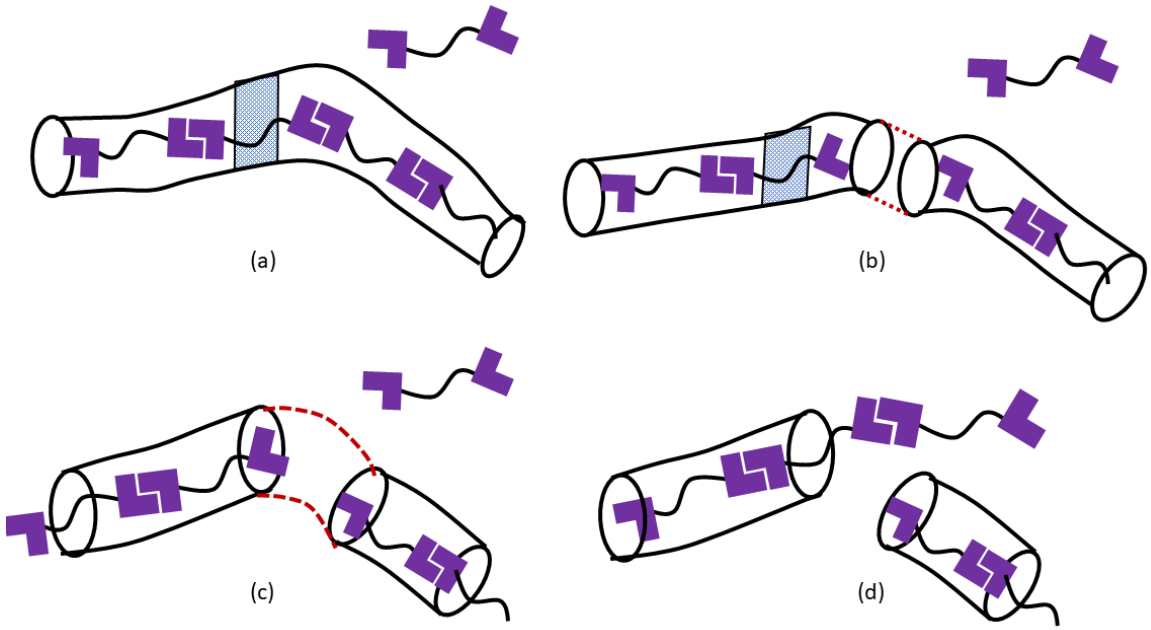

Figure 1. 8. Relaxation mechanisms presented by Cates's "living" reptation model. The shaded segment relaxes over the break which occurs within a certain distance along the chemical sequence (a); The break must be close enough that the newly released end can move through the shaded segment (b and c) before it recombines with a neighboring chain (d).

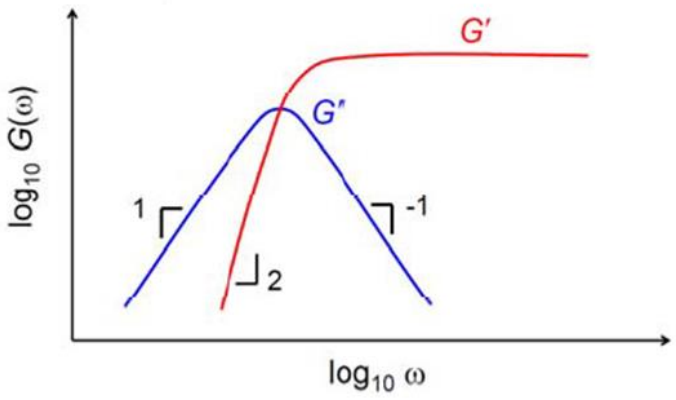

Figure 1. 9. Exponential stress relaxation with a single relaxation time (Maxwell-type mode).[125]

1.4.2 Sticky Rouse model

Sticky Rouse model is proposed mainly for unentangled solutions of associating polymers with many pairwise stickers per chain, corresponding to Rouse mode of segments between stickers before and after their dissociation.[39, 130]

Green and Tobolsky[133], Baxandall[150] have reported that when stress relaxation is governed by breaking and reassociation of reversible crosslinks/stickers, it's mainly Rouse-like[151] on time scales longer than the lifetime of association. For polymer melts, when Kuhn segments reach thermal equilibration, the whole chains can be seen as consisting of many flexible segments called Rouse segments. The Rouse segments normally have size similar to or slightly larger than Kuhn segments. For supramolecular polymers, the Rouse motion of segments between stickers prevails until the chain feels the constraints from the association or clusters. On lifetime shorter than the stickers' lifetime, the association behaves as a permanent crosslink. Thereby the chain relaxation on length scales larger than the distance between two nearby associations is controlled by the association lifetime, and meanwhile, the low order Rouse modes should be delayed.

Semenov and Rubinstein have investigated dynamics of entangled associating polymers with a high degree of stickers that can form large aggregates. In this situation, large aggregates and clusters yield reversible networks of interconnected micelles. They proposed two main mechanisms to release stress: polymer chain diffusion and positional rearrangement of the micelles.[130] The hopping of stickers take place by dissociating from one micellar core and associating with another as shown in Fig. 1.10. Different from the pairwise association systems,[129] the bond lifetime renormalization is regarded negligible when the sticker dissociation energy is in the range of $m^{1/2} \sim m^{4/3}$, in which m is the average aggregation of clusters. This assumption relies on the fact that the aggregate can hold a varying number of stickers and the estimated energy change before and after the sticker hopping is lower than the thermal energy $k_B T$.[130]

The strong interacted associations, such as ionic aggregates or multiple hydrogen bonding motifs, have a significant impact on the chain dynamics above T_g. Since the effective

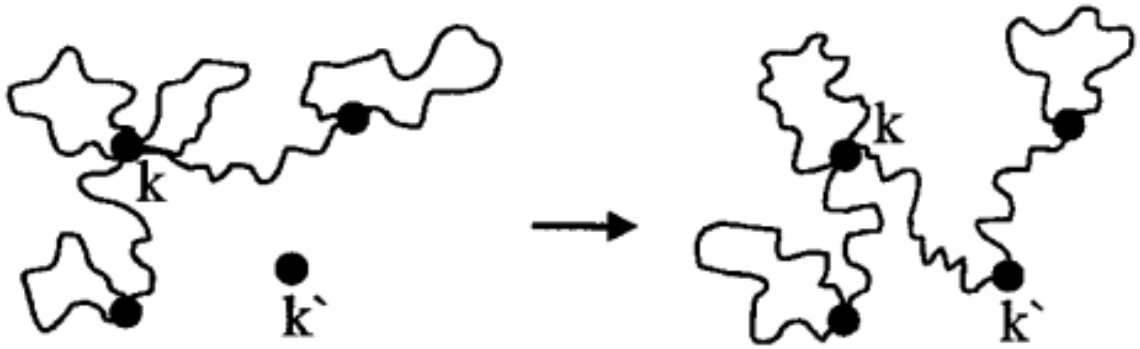

Figure 1. 10. Elementary step of the sticky Rouse motion for entangled associating polymers with large aggregates. A sticker dissociates from the core of an old partner (micelle k) and associates with another micelle k'. Black circles represent cores of micelles and only partial chain is shown for simplicity.[130]

friction grows dramatically, the global relaxation of the chains slows down prominently and thus a wide spectrum of stress relaxation modes can be observed. The sticky Rouse model especially captured these effects in unentangled systems and proposed that the friction is governed by the association lifetime.[39, 150]

Although there's qualitative agreements between experimental works and above-mentioned theoretical models on the diffusion, rheological and viscoelastic behaviors of certain supramolecular systems.[39, 152-154] It still remains a unfinished task to find microscopic evidence to validate the assumptions underlying in the theoretical models, such as the microscopic picture of the sticker hopping process and positional rearrangement of micelles.

1.4.3 Sticky reptation model

Another important theory extending de Gennes's classical reptation model[57] is Sticky reptation model, which is developed by Leibler, Rubinstein, and Colby for systems forming network through covalently jointed chains which are interconnected by reversible association of "sticky" side groups.[131]

The “sticky” reptation model is based on a concentrated solution or melt of linear flexible chains with several pairwise specific stickers (referring to associating units) attached along the backbone as side groups that can associate to form reversible cross-links. For a given chain, it has supramolecular tie-points with surrounding chains initially (Fig.1.11 a). These tie-points are dynamic, reversible and in a constant equilibrium between the open and closed state. When a tie-point is in the open state, the combination with other supramolecular groups from the surroundings is possible and therefore forms a new supramolecular tie-point (Fig. 1.11 b). Generally, the motion of chain building blocks is controlled by their conformation and topological constraints. In this theory, although temporary cross-links according to attraction among specific groups can lead to macroscopic phase separation or formation of aggregates or mesophases, the modification of chain conformation and topological state due to these attraction effects are presumably neglected. Since the associating groups distributed along the backbone, these sticky chains themselves do not break, thus possess fixed length, and the bonds between them can break, which makes chain reptation possible.

According to this model, on time scales shorter than the average lifetime of a cross-link, such networks behave as elastic rubbers (gels) that is not different from the one formed by covalently bonded polymers. At longer times, the successive breaking and recombination of a few cross-links allows the chain to diffuse along its confining tube and stress can relax. Therefore, the concentration and lifetime of tie points are decisive factors that control the motion of a chain in this hindered reptation model.

The “sticky” reptation model predicts the existence of two rubbery plateaus of the time-dependent relaxation moduli in reversible networks compromising linear chains with stickers (Fig. 1.12). One appears on time scales $\tau_e < t < \tau$ (τ_e is the Rouse time of an entanglement strand, τ is the average lifetime of a sticker in the associated state), which is similar to that observed in permanently cross-linked networks and has contributions from both transient crosslinks and “intrinsic” entanglements:

$$G_1 \cong cRT\left(\frac{p}{N_s} + \frac{1}{N_e}\right) \tag{1.8}$$

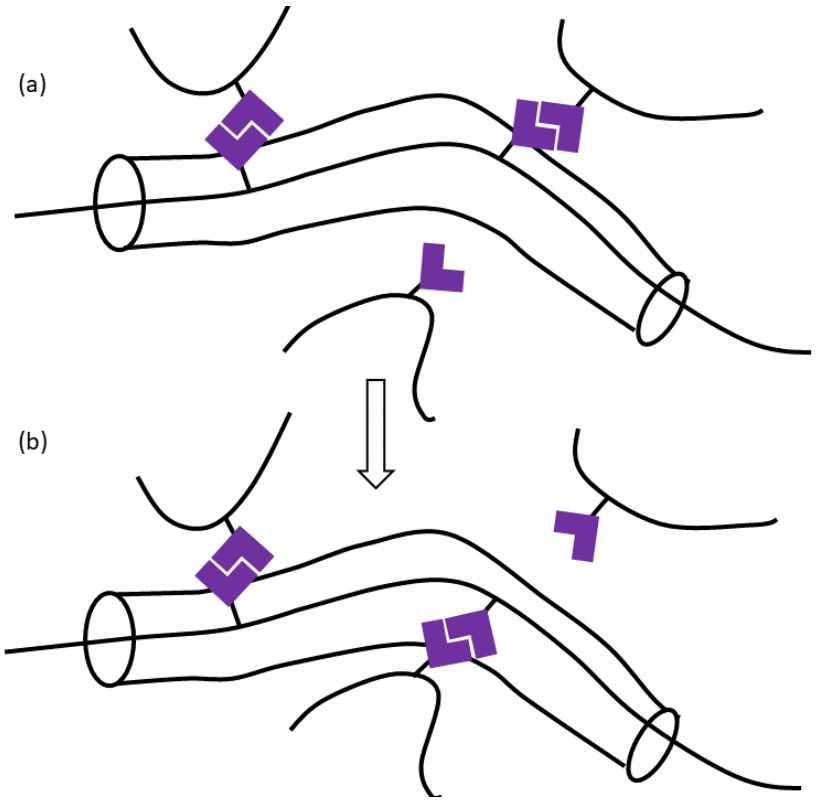

Figure 1. 11. Schematic representation of an elementary step of chain diffusion from "sticky" reptation model.[131] (a) The chain has several tie-points initially. (b) The sticker forms a new cross-link with another chain group from the surroundings. The dashed lines representing the tube confined by surrounding chains and stickers which are not shown specifically.

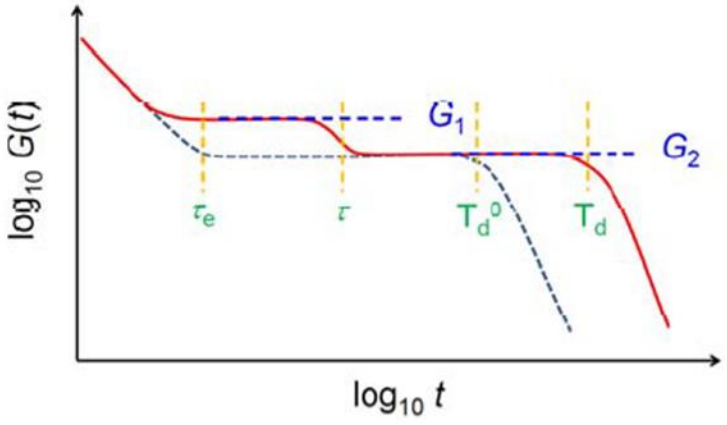

Figure 1. 12. Theoretical predictions of the time-dependent relaxation moduli from the "sticky" reptation model.[131] The solid line represents reversible networks consisting of linear chains with stickers and the dashed lines represents linear chains without stickers.

in which c is the number concentration of monomers, N_s is the average number of monomers along the chain between stickers, N_e is the average number of monomers in an entanglement strand and p is the average fraction of closed stickers. On time scale where the stickers open, $t > \tau$, due to stress relaxation by stickers dissociation, the modulus drops to that of the identical linear chain system without stickers:

$$G_2 \cong cRT(\frac{1}{N_e}) \tag{1.9}$$

Rubinstein and Semenov later extended the "sticky" reptation model for application to dilute, semi-dilute unentangled and semi-dilute entangled solutions.[155, 156] They discussed two important parameters that governs dynamic (but not static) properties: the effective energy of a bond between two stickers (also termed as binding energy, $\varepsilon k_B T$) , and the activation energy ($\varepsilon_a k_B T$), corresponding to the bond formation. The latter one, is an additional potential barrier that two stickers must overcome for association. In these works, they proposed that it's the effective bond lifetime τ_b* (named as renormalized bond lifetime in some literatures, denoting the characteristic time of structural reorganization of the network, *i.e*. the event when a sticker changes its bond partner), rather than bare bond lifetime τ_b ($\tau_b < \tau_b$*) of one specific supramolecular force (the characteristic time of sticker dissociation), that plays a decisive role on system's dynamics and properties. When there are several tie-points between two chains, the stress relaxation or network topology alteration can be done only when all tie-points are in the open state. If there's partial supramolecular groups still connected between two chains, it is impossible to find new partners to release applied stress and monitor the network (Fig. 1.13). In other words, the renormalization of bond lifetime stems from the fact that a sticker is supposed to go through many breaking and re-forming events with its old partner before associating with another open sticker.[130] Then, it is not difficult to conclude that the unbinding process is affected by both the mobility, rigidity of the polymer chains and the existence of adjacent tie-points. As a result, *e.g.*, in rheological behaviors, the onset of the terminal relaxation (crossover of G' and G'') should shift to lower frequencies (longer timescales).

In these works, Rubinstein and Semenov also predict the storage G' and loss G'' moduli as a function of frequency ω (Fig. 1.14).[156] They characterize the system by several relaxation

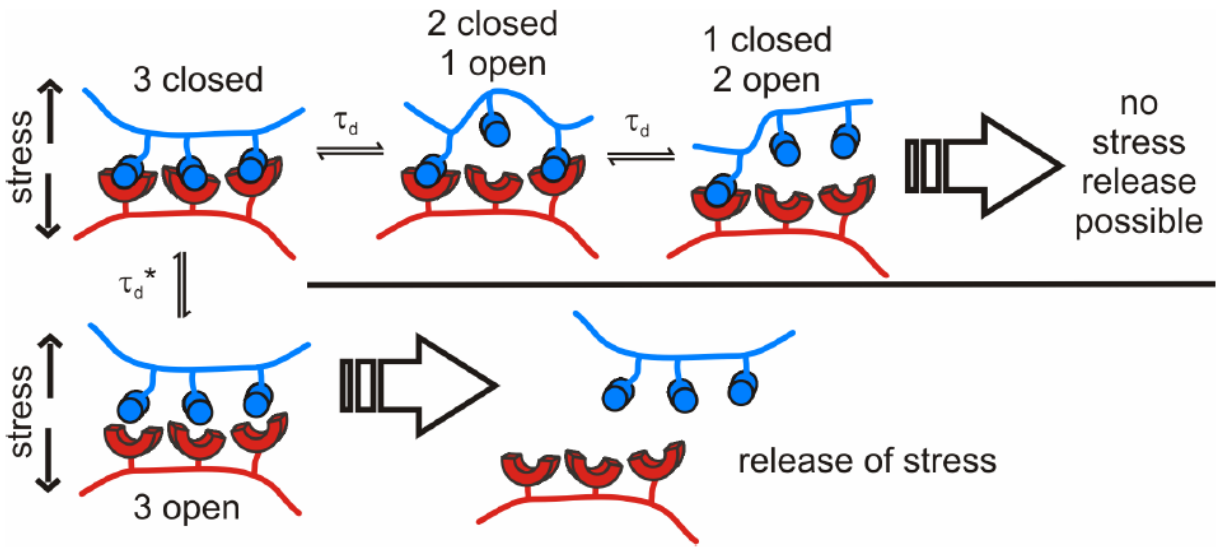

Figure 1. 13. Description of the renormalized tie-point lifetime, which is expressed by the effective bond lifetime.

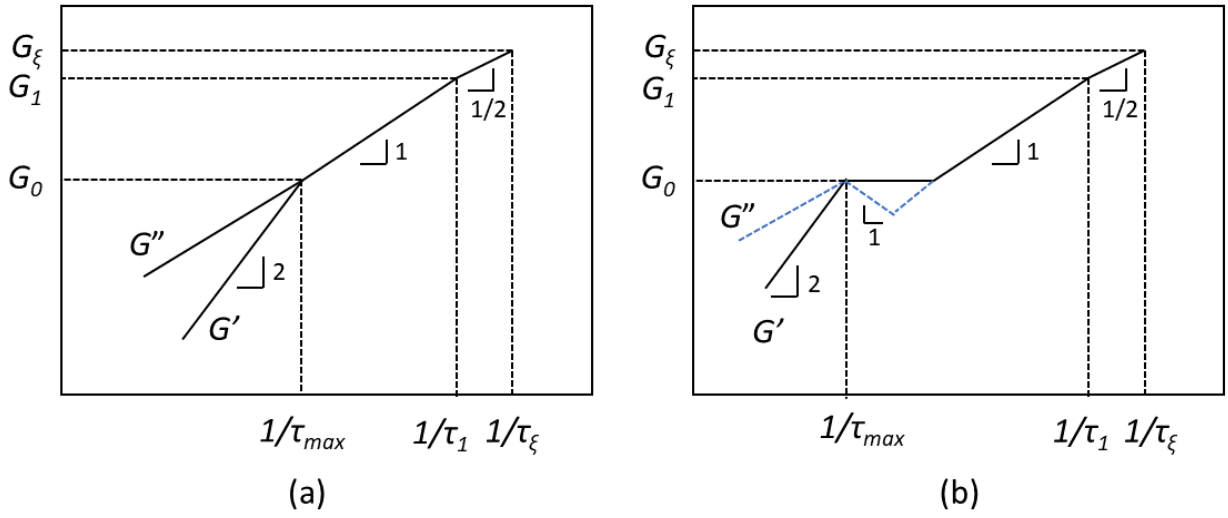

Figure 1. 14. Prediction of storage, *G*' and loss *G*" moduli as a function of frequency ω in log-log scale.[156]

times: the Zimm time of hydrodynamic blob τ_ξ, the single-chain relaxation time τ_1, the dynamical terminal time τ_{max} and the relaxation time of a network strand τ_{relax}, below (Fig. 1.14 a) and above (Fig. 1.14 b) the gel point. There are two relaxation processes contributing to the moduli above the gel point: (1) relaxation within the strands and free clusters on length scales smaller than the classical strand size; (2) the stress relaxation according to strands breakage. A recent refinement made by Semenov *et al*. lies on networks of binary associating, hetero-complementary polymers.[157] In this situation, the network strands comprise of collected chains in linear sequence. The diffusion mechanism is affected by an apparent activation energy which is much higher than the dissociation energy of a single pair of stickers. The terminal relaxation is further resisted by the randomly distributed side chain stickers, appearing as a typical non-Maxwellian behavior.

Rubinstein and Leibler lately further developed the concept of lifetime renormalization to study autonomic self-healing of unentangled polymer networks.[158] It differentiates between the actual lifetime of a bond τ_b and the renormalized bond lifetime τ_b*. The former produces a change in the dipole moment because each dissociation and association event change the dipole moment, and therefore is detected by dielectric spectroscopy. However, if the dissociated stickers re-associate back to their original partners, no stress relaxation occurs. Only the change of the partners, i.e. τ_b*, is relevant for mechanical stress relaxation.[159] The model predicts that only under certain conditions these two will be identical. The decisive parameter is the bond strength quantified by its activation energy E_a, and in the framework of the model, three regimes are discriminated: in the weak regime, $E_a < k_BT \ln N$ (N is the number of segments per telechelic chain), the association can be neglected while only in the strong regime, $E_a > 2\ k_BT \ln N$, bond dissociation and stress relaxation are approximately identical. For the intermediate regime, which is characterized by the condition $k_BT \ln N < E_a < 2\ k_BT \ln N$, a more complex relaxation mechanism is suggested with two relevant contributions to the renormalized bond lifetime[158]: i) after dissociation the sticker starts a random walk; since the walk is compact, there is a significant chance that the sticker returns to its former partner J times and remains associated with it for τ_b each time, before ii) the volume explored by the random walk is large enough for the sticker to encounter another free chain-end (sticker). This

model explains at least on a qualitative level why the terminal relaxation time from rheological measurements is often larger than the α^*-relaxation time deduced from dielectric data, which is observed in recent studies of entangled polyisoprene randomly functionalized with urazole goups.[160, 161]

1.4.4 Telechelic supramolecular polymers

Telechelic supramolecular polymers are linear polymers with secondary functional groups only at the end of the chain backbone. The morphology and dynamics of telechelic associating polymers are quite different from those of systems with stickers randomly distributed along the chain backbone. For example, when at low concentrations in solution, telechelic supramolecular polymers can form isolated flower-like micelles similar to the ones formed by block-copolymers, in which the chain-end stickers form the micellar core and the backbone forms corona (as shown in Fig. 1.15 a).[118] The inner structure of a supramolecular micelle is similar to that of star polymers.[162, 163] At elevated concentrations moderately above a certain threshold, the micelles cores are barely dispersed and the distance between cores are much larger than the size of the chain backbones. At this time the system often possesses dynamic features analogous to elastic network, e.g., plateau modulus that affected by dissociation of the chain ends, indicating that these micellar cores are connected. Thereby, it was reported that between cores, there are long, linear superbridges each formed by several chains, yielding the formation of transient gel network.[164, 165] Similarly, a fraction of the loops are consisting of the long sequence of linearly associated backbones that termed as superloop.[164, 165] While there's repellent between star polymers even in good solvents, possible bridges between telechelic "flowers" micelles can cause an attraction between micelles (Fig. 1.14 b).[166] The cores become even closer as concentration increases and the distance finally shrink to comparable size to the chain's. Therein, the network strands (termed as bridge) and the loops are mostly composed of a single chain backbone. As a result, in semi-dilute and concentrated solutions, the micelles may phase separate and collectively pack into dense "flowers" leading to reversible networks with supramolecular aggregates as junction points.

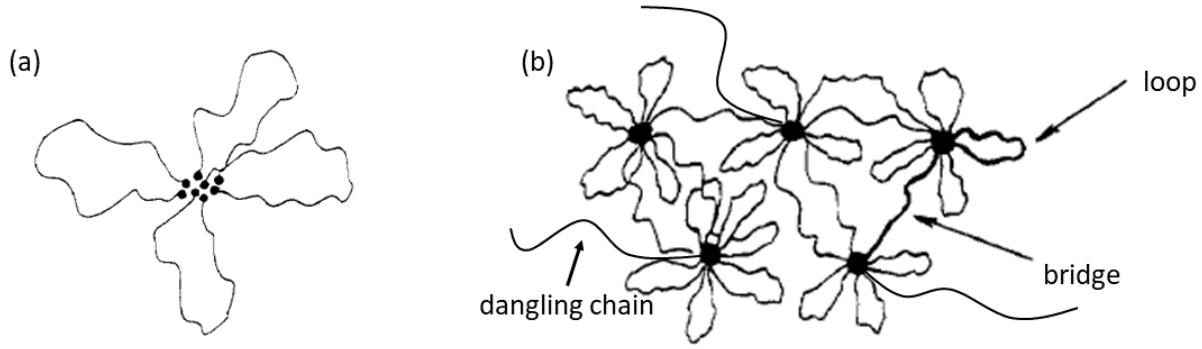

Figure 1. 15. a) A flower compromised of 4 loops, the core is an aggregate of several insoluble end groups; b) A reversible network of flowers connected by bridges.[130]

The possible flower-like micelles and large aggregates usually lead to rich rheological and viscoelastic behavior for associating polymers with stickers at their extremities.[34, 35, 47, 79, 112, 113, 164, 167-188] On time scales shorter than the lifetime of either bridge or superbridge, the telechelic supramolecular systems with gel network exhibit elastic properties and the corresponding plateau modulus can be expressed as[189]

$$G_N = \upsilon_{bridge} k_B T \tag{1.8}$$

where υ_{bridge} is the number density of elastically active bridges and superbridges, k_B is the Boltzmann constant. When there are two or more associative sites per chain, the intrinsic relaxation of the network strand between the transient crosslinks is usually much faster than the dissociation of associative sites. Therefore, the full relaxation of the transient network according to dissociation and the intrinsic relaxation of the strands can be observed as well-separated fast and slow processes.

The functionality, f of the stickers is another critical parameter that affect the structure of telechelic polymers. It's reported that telechelic associating polymers with functionality of f = 2 undergo head-to-tail associations and representative theoretical and simulation works can be found in ref [125, 190-194]. The minimum functionality required for percolated network formation is 3.[177, 195]

Yan *et al*. has reported telechelic polymers consisting of a poly(isobutylene) backbone and complementary triple hydrogen-bonding motifs on one or both chain ends in the melt state, one as thymine (Th) and the other as 2,6-diaminotriazine (Tr) as shown in Fig. 1.16 e.[181] Unspecific association between hydrogen-bonding moieties leads to formation of micelles, aggregation and microphase separation confirmed by Small-angle X-ray Scattering (SAXS) spectroscopy. For monofunctional samples, both pure PIB-Tr and mixtures of PIB-Tr and PIB-Th, ordering micelles were observed at lower temperatures and evolved into disordered micelles at increasing temperatures. Representative SAXS spectra of PIB-Tr are shown in Fig. 1.16 a and b and the depicted picture of micelles transition shown in Fig. 1.16 c. The rheological behaviors of those systems resemble the properties of a concentrated colloidal fluid or solid as shown in Fig. 1.16 d. For bifunctional polymers with complementary hydrogen-bonding groups, network formed by micellar aggregation. Solid-like properties induced by gelation were observed at low temperatures (Fig. 1.16 f).

Richter and coworkers studied the structure of telechelic polypropylene glycol (PPG) with either diaminotriazine (DAT) or thymine (Thy) motifs as end groups both in the melt and in dilute solution via small angle neutron scattering (SANS).[180] As shown in Fig. 1.17, the SANS data were quantitatively examined by using a random phase approximation (RPA) model, which is normally applied to pure polymer systems. It's concluded that linear association prevails in this system.

The self-healing materials can be achieved by incorporating noncovalent interactions and their strengths, healing times, together with mechanical and viscoelastic properties can be tuned subsequently with different chemistry design and external environments. The most critical feature of self-healing polymers is the auto-healing close to room temperature, instead of healing at elevated temperatures. It is quite challenging to achieve ideal healing properties without a fully understanding of the actual dynamics of the supramolecular polymers. Telechelic supramolecular polymers, as one of the simplest models of associating systems, are good candidates to study self-healing mechanisms arising from secondary forces.[196] Rubinstein and Leibler[158] have proposed a scaling theory based on systems with pairwise association and hopping diffusion of stickers to reveal the self-healing mechanisms of unentangled

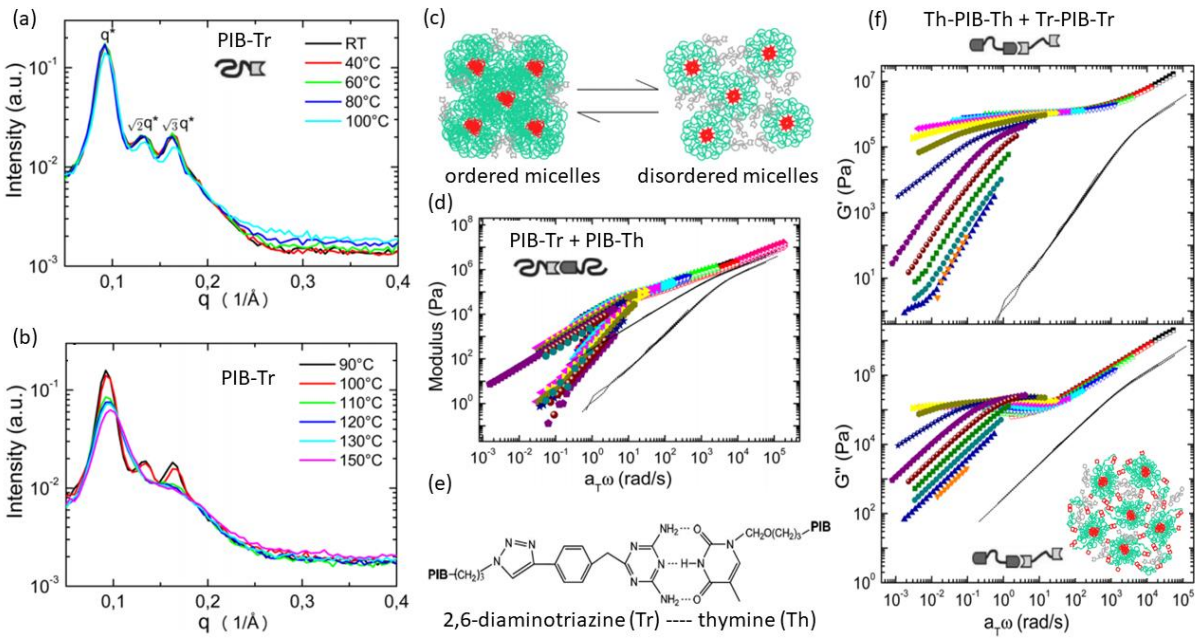

Figure 1. 16. a) and b) Scattering intensity at different temperatures of Tr-PIB in the melt state; c) a schematic picture of the phase transition from ordered micelles to disordered micelles. The red kernel represents the dense core formed by supramolecular groups, the green lines are the PIB corona chains and the light gray lines represent free chains matrix. d) Master curve from rheological measurements of PIB-Tr + PIB-Th with a clear breakdown of time-temperature superposition (TTS) indicating structural changes; e) structure of thymine and 2,6-diaminotriazine functionalized PIB; f) rheological master curve of Tr-PIB-Tr + Th-PIB-Th with a prominent plateau. Dashed lines represent data for the homopolymer.[181]

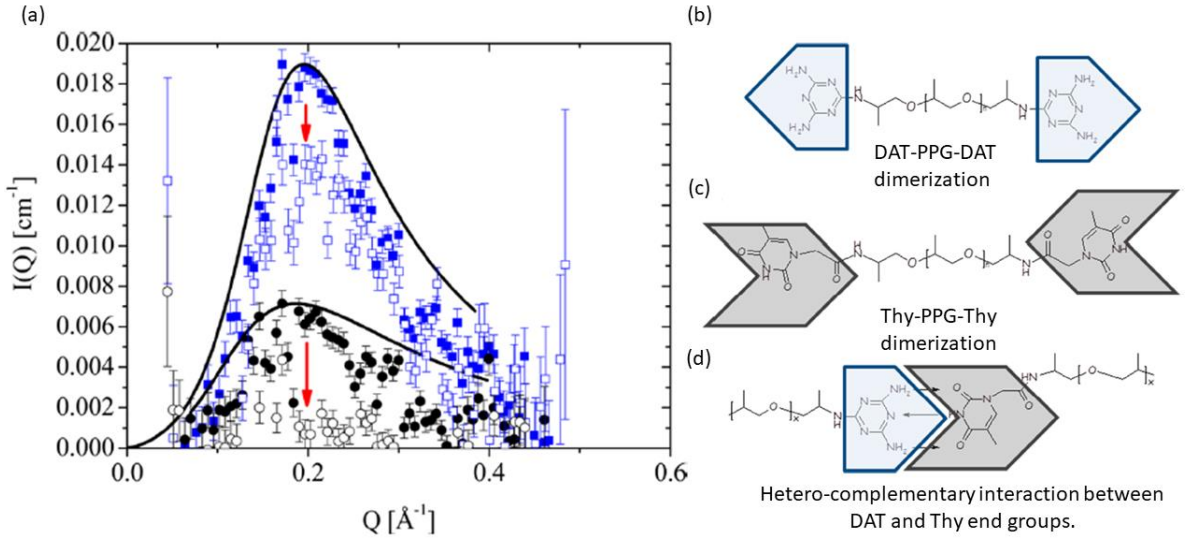

Figure 1. 17. a) SANS data of the pure hydrogeneous mixture 1:1 of nominally bifunctional oligomers (squares) and monofunctional ones (circles) in the melt state. Filled symbols refer to T = 298 K and open symbols refer to T=333 K. The solid lines are fits with the random phase approximation (RPA) equation at 298K. b) DAT-PPG-DAT; c) Thy-PPG-Thy; d) hetero-complementary interaction between DAT and Thy groups.[180]

supramolecular polymer networks. The most commonly used method to test the self-healing properties is to cut the sample into two parts, put them together for different times, and then perform tensile measurements to see how much time it needs to recover its mechanical and viscoelastic properties and to which extent. Thurn-Albrecht and coworkers have published a series of papers by employing Small-angle X-ray Scattering (SAXS) and both linear and nonlinear rheology to study the relations observations with structures and fundamental viscoelastic properties of the material.[65, 179, 196-198] They concluded that the terminal relaxation process is responsible for the self-healing kinetics in a reversible network of bi-functionalized PIB chains.

For the design of self-healing materials, a unified picture of chemical bonds' thermo-dynamical and kinetical behavior in different environments is still missing, especially considering the polarity difference according to the heterogeneity of the surrounding, and the strongly limited diffusion that affect the bond recombination.[65, 197, 199]

1.5 Binding energy and association/dissociation energy

It's generally accepted that the numerous dynamic behaviors of supramolecular polymers stem from different lifetimes, densities (concentrations) and positions of the interactive sites of the chain. Lifetime itself is usually correlated to the interaction energy. As shown in Fig. 1.18, binding energies of different secondary interactions as well as covalent bonds are ranging up to 1000 kJ/mol. Since the energy of covalent bonds is much higher than the thermal energy (kT = 2.5 kJ/mol at ambient temperature and pressure[200]), their formation of sol or gel are very stable at ambient pressure and temperature. For secondary interactions, the energy can be comparable to the thermal energy under certain conditions,[201-203] therefore making the bonding reversible at the timescale of experimental observation. By affecting the lifetime of stickers, the interaction energy can impede the relaxation and diffusion process of polymer chains.

Due to the nature of hydrogen bonding, its strength strongly depends on the polarity of the medium. According to the lower value of the dielectric constant when comparing to those solvent with high values, polymer systems usually enable hydrogen bonding to be much stronger. The highly polar hydrogen bonding groups (also termed stickers) can further aggregate, form micro phase separation and multifunctional crosslinks, thereby impede their dissociation. Additionally, besides the nature of donor and acceptor, the number and the arrangement of hydrogen bonding units play an important role on the association strength especially in the concentrated solutions and the melt state.[48, 120] Another significant factor is external stimulus, such as temperature. The association strength of hydrogen bonds can be largely reduced at elevating temperatures.

In summary, the activation energy of sticker dissociation is determined by several factors, such as the detailed structure and nature of the sticker, local environment, microstructure, which makes it difficult to estimate.[124, 131, 204-206]

From reported studies, activation energy can be calculated from the Arrhenius equation:[39, 124, 204, 205, 207, 208]

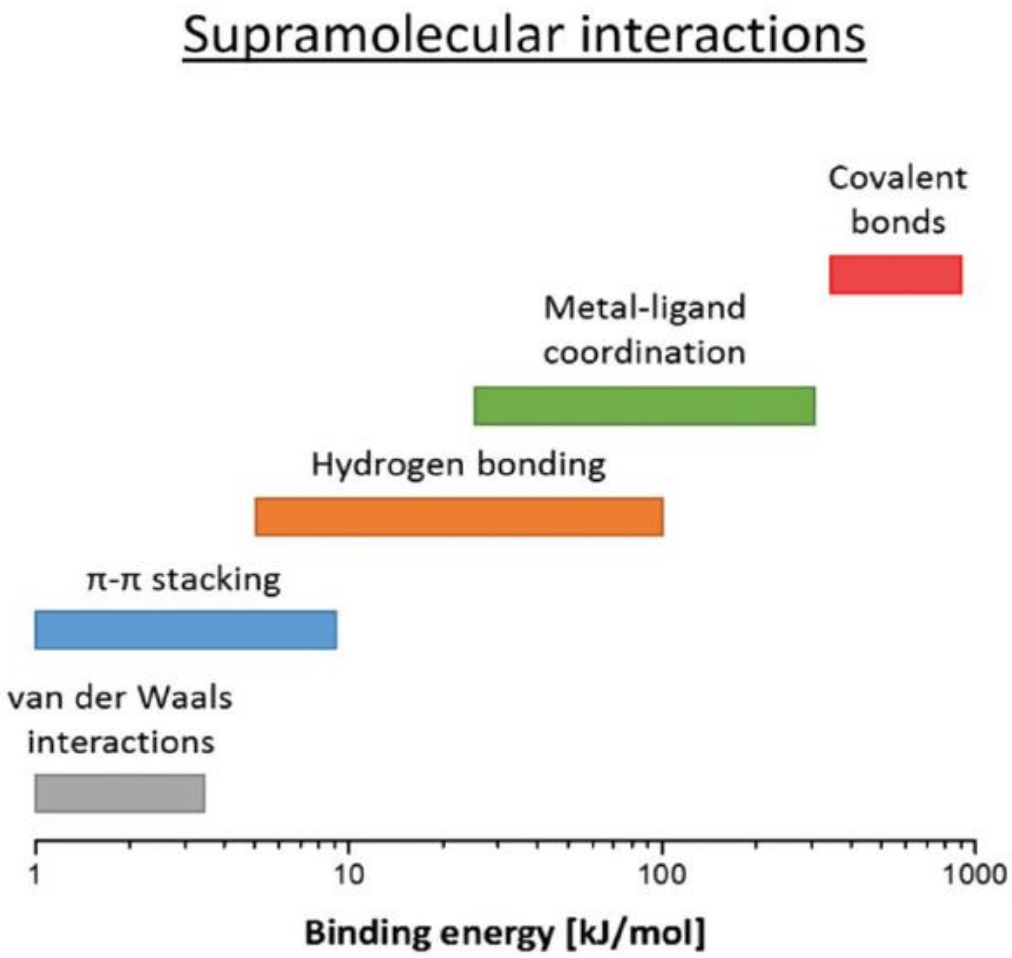

Figure 1. 18. Compare different interactions' energy range.[209]

$$\tau_s = \tau_0 \exp(\frac{E_a}{RT}) \quad (1.9)$$

in which τ_s is the sticker lifetime, τ_0 is the limiting relaxation time, in this situation is identified with segmental relaxation time τ_α and E_a is the activation energy for sticker dissociation which is expressed as a constant value at a specific temperature.

1.6 Research objectives

There are mainly three tasks in this work: 1) Establish the phenomenological foundation to describe the chain and structural dynamics in various types of associating polymers. Understand segmental and chain relaxations in associating polymers starting with bridging the fields of hydrogen-bonded small molecules and supramolecular polymers. Study the influence of association on glass transition and temperature dependence of segmental relaxation. 2) Provide experimental results and verifications of the existing theoretical models and explore a qualitative theoretical framework for description of supramolecular dynamics. Study the viscoelastic properties and diffusion in associating polymers, especially the stress relaxation mechanism and entanglement nature, by incorporating different molecular parameters such as backbone rigidity and polarity, molecular weight, association strength and lifetime of stickers. 3) Develop experimental techniques based on dielectric spectroscopy, differential scanning calorimetry, rheology and small angle X-ray spectroscopy for systematic analysis of local association-dissociation dynamics and reversible structural mechanisms. The research will rely on associating telechelic polymers in the melt state.

Chapter II

Experimental Techniques

2.1 Broadband Dielectric Spectroscopy (BDS)

2.1.1 Principles of dielectric spectroscopy

Broadband dielectric spectroscopy is a powerful technique to study molecular dynamics since it's sensitive to relaxation process in an extremely wide range of characteristic times (10^5-10^{-12} s). Dielectric Spectroscopy is about motions of permanent or induced dipoles in a system under external alternating electric field $E(\omega)$. As depicted in Fig. 2.1, when a sinusoidal external electric filed is applied to the sample, the inner dipoles will reorient, align with the applied field and reach a new equilibrium state. The neighboring dipoles, bonds and groups have to rearrange accordingly, thus different polarization process can be detected by dielectric spectroscopy. Generally, the system is polarized by the electric field and the polarization P depends on the electric field strength E. P characterizes the dielectric displacement D which stems from the influence of the external field on a material. For a small electric field, D can be expressed by Eq. 2.1, and P has a linear dependence on E, given by Eq. 2.2.

$$D = \varepsilon^* \varepsilon_0 E \tag{2.1}$$

$$P = D - D_0 = (\varepsilon^* - 1)\varepsilon_0 E = \chi^* \varepsilon_0 E \;\; with\, \chi^* = (\varepsilon^* - 1) \tag{2.2}$$

where ε_0 is the dielectric permittivity of vacuum, ε^* is the complex dielectric function or dielectric permittivity, D_0 is the dielectric displacement of vacuum and χ^* Is the dielectric susceptibility which represent how hard is it for a dipole to orient and relax under external electric field. The dielectric permittivity, also termed as dielectric constant, is independent of the field strength, whereas, dependent on the frequency of applied field, the temperature, the density (or the pressure) and the chemical composition of the system.

For a periodic electrical field $E(t) = E_0\exp(-i\omega t)$ (ω is the radial frequency):

$$\varepsilon^* = \varepsilon'(\omega) - i\varepsilon''(\omega) \tag{2.3}$$

in which $\varepsilon'(\omega)$ is the real part representing the dielectric energy stored reversibly. $\varepsilon''(\omega)$ is the imaginary part representing the energy dissipated per cycle.

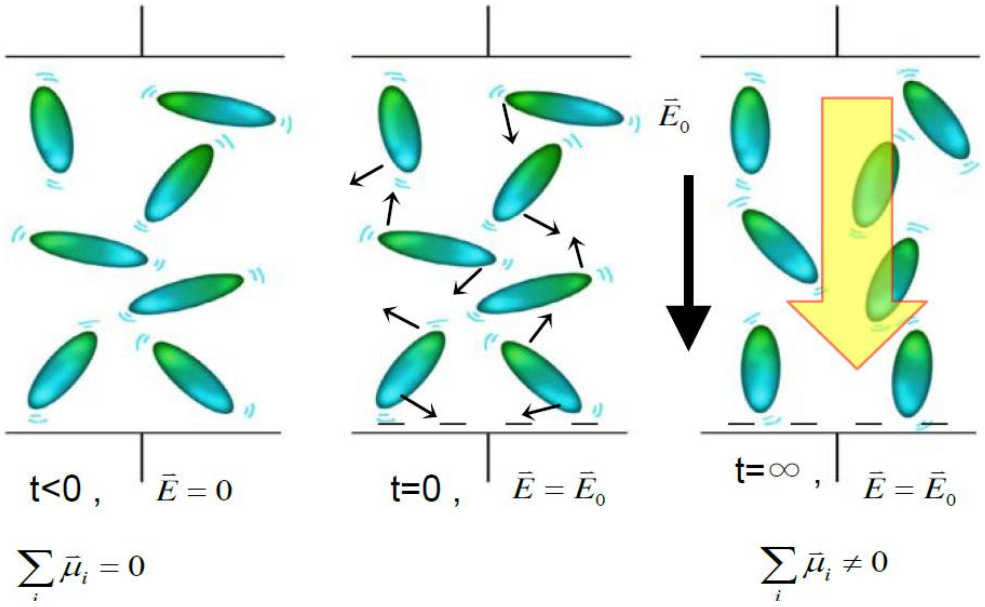

Figure 2. 1. Reorientation of dipoles on application of an external electric field.

2.1.2 Dipoles in polymers and relaxation modes

It is widely known that dielectric spectroscopy can be used as a powerful technique to study the conformation and dynamics of polymers due to the polarization effect. The conformational features can be reflected by the static dipole moments and the dynamic features can be investigated by the dielectric dispersion.

As shown in Fig. 2.2 a, the polymer dipoles are classified into three types: those aligned parallel to the backbone chain contour were called type-A; those aligned perpendicular to the contour were type-B; and those located on mobile side groups were termed as type-C. [111, 210]

As shown in Fig. 2.2 b, the total dipole moment along the backbone of a type-A polymer is proportional to the end-to-end vector *r* of the chain, so that the fluctuation and reorientation of the type-A dipoles reflects the global motion of the chains. Typical examples of type-A polymers are poly(cis-1,4-isoprene) and poly(propylene glycol). For polymers with type-B dipoles, the local motion of the backbone arises from conformational transitions, which reflects the segmental relaxation (also termed as *α*-relaxation) that is related to the glass transition

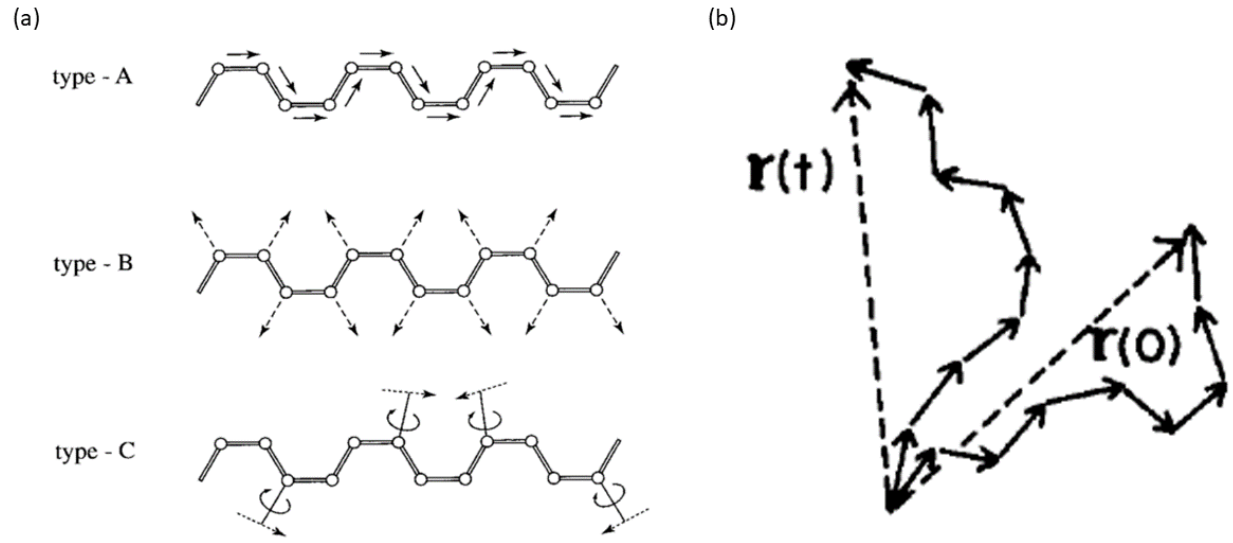

Figure 2. 2. (a) Schematic illustration classifying the dipoles of polymer chains.[210] (b) Schematic illustration of a type-A chain.[111]

temperature. The motion of type-C dipoles reflects the relaxation process of side groups which is commonly seen in the high frequency range. Examples of type-B polymers are poly(vinyl-chloride) and poly(styrene) and the example of type-C polymers is poly(n-alkyl methacrylate).

The fluctuation of the net dipole moments indicates many relaxation processes on different length scales and relaxation timescales. Localized motions which happen at very small length scales are referred as secondary relaxations. As shown in Fig 2.3, the higher frequency *β*-process and *γ*-process are secondary relaxations in PPG systems. On a relatively larger length scale including several repeating units, the segmental motion (*α*-relaxation) occurs. The activation energy of segmental relaxation correlates to the glass transition in polymers. On a much larger length scale, the motion of the whole chain occurs and this process appears as normal mode at low frequencies. Only polymers with type-A dipole moments have cumulative dipole moment along the backbone and exhibit normal mode that can be detected by dielectric spectroscopy.

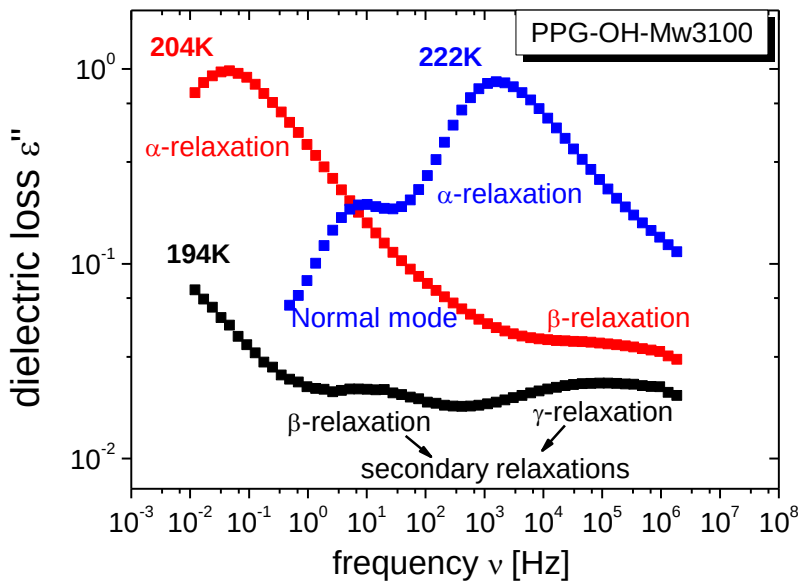

Figure 2. 3. Dielectric spectrum of PPG showing normal (chain) mode, segmental relaxation and secondary relaxations.

2.1.3 Analysis of the dielectric spectrum

Molecular relaxations stem from rotation and vibration of molecular dipoles. When the molecular dipole re-orientation times τ corresponds to the frequency of the external electric field, the relaxation processes are characterized by a peak in the imaginary part ε" and a step-like decrease of the real part ε' with increasing frequency. The shape of the loss peak indicates distribution of relaxation times. The dielectric strength $\Delta\varepsilon$ of a relaxation process can be obtained by either the area under the loss peak or the step in the real part.

There are several models employed to analyze the dielectric relaxation processes. Starting with the Debye function, the frequency dependent dielectric complex is:

$$\varepsilon^*(\omega) = \varepsilon_\infty + \frac{\Delta\varepsilon}{1+ i\omega\tau_D} \tag{2.4}$$

in which $\Delta\varepsilon = \varepsilon_s - \varepsilon_\infty$ is the dielectric relaxation strength with $\varepsilon_s = \lim_{\omega\tau\ll1} \varepsilon'(\omega)$ and $\varepsilon_\infty = \lim_{\omega\tau\gg1} \varepsilon'(\omega)$. The Debye relaxation time τ_D is related to the peak position of dielectric loss by

$1/\tau_D = 2\pi f_p = \omega_p$. In most real cases, the relaxations are non-Debye relaxations which appears much broader and usually asymmetric. Therefore, several empirical model functions have been developed to describe broadened and asymmetric dielectric loss peaks.

Cole/Cole-function (CC):

$$\varepsilon^*_{CC}(\omega) = \varepsilon_\infty + \frac{\Delta\varepsilon}{1+ (i\omega\tau_{CC})^\beta} \tag{2.5}$$

where *β* presents a symmetrical broadening of the peak.

Cole/Davidson function (CD):

$$\varepsilon^*_{CD}(\omega) = \varepsilon_\infty + \frac{\Delta\varepsilon}{(1+ i\omega\tau_{CD})^\gamma} \tag{2.6}$$

where *γ* describes the asymmetric broadening on the high frequency part.

With a combination of CC and CD functions, a more generalized model function was introduced by Havriliak and Negami (HN-function):

$$\varepsilon^*_{HN}(\omega) = \varepsilon_\infty + \frac{\Delta\varepsilon}{[1+(i\omega\tau_{HN})^\beta]^\gamma} \tag{2.7}$$

where shape parameters *β* and *γ* give the symmetric and asymmetric broadening of the complex dielectric function. Fig. 2.4 shows the dielectric spectra with different shape parameters from HN-function.

In real polymer systems, the complex dielectric permittivity is normally fitted by HN function and much information of the relaxation process can be obtained by extrapolating fitting parameters. Representative dielectric spectra of PPG with a molecular weight of 3100 g/mol at T=230 K are shown in Fig. 2.5. There are three major components in dielectric loss spectrum (Fig. 2.5 b) from high to low frequencies: (1) a dielectric relaxation process named as α-relaxation which correlates to glass transition, (2) a dielectric relaxation process named normal mode which indicating chain motions and (3) DC conductivity.

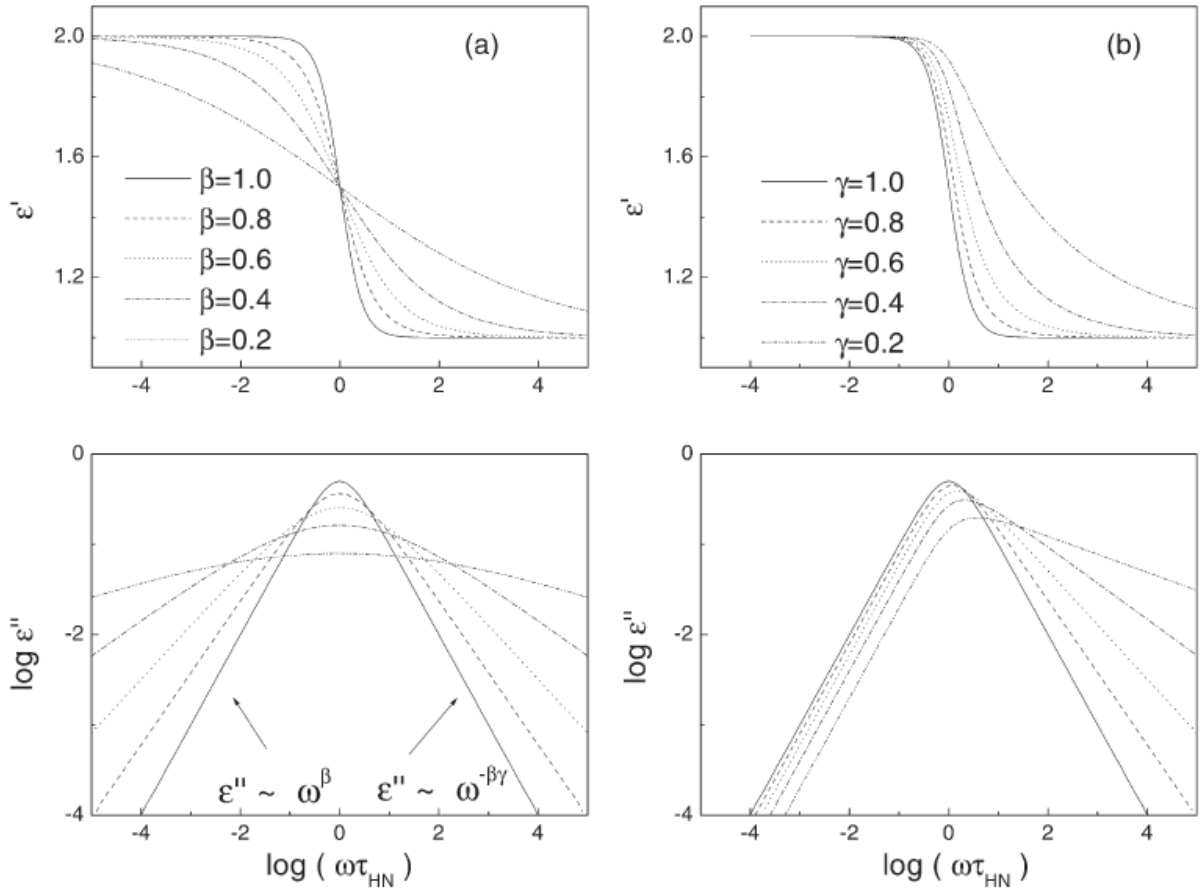

Figure 2. 4. Complex dielectric permittivity from the HN-function with fixed: (a) γ=1; (b) β=1 (ε_∞, $\Delta\varepsilon$ and τ_{HN} =1)[110]

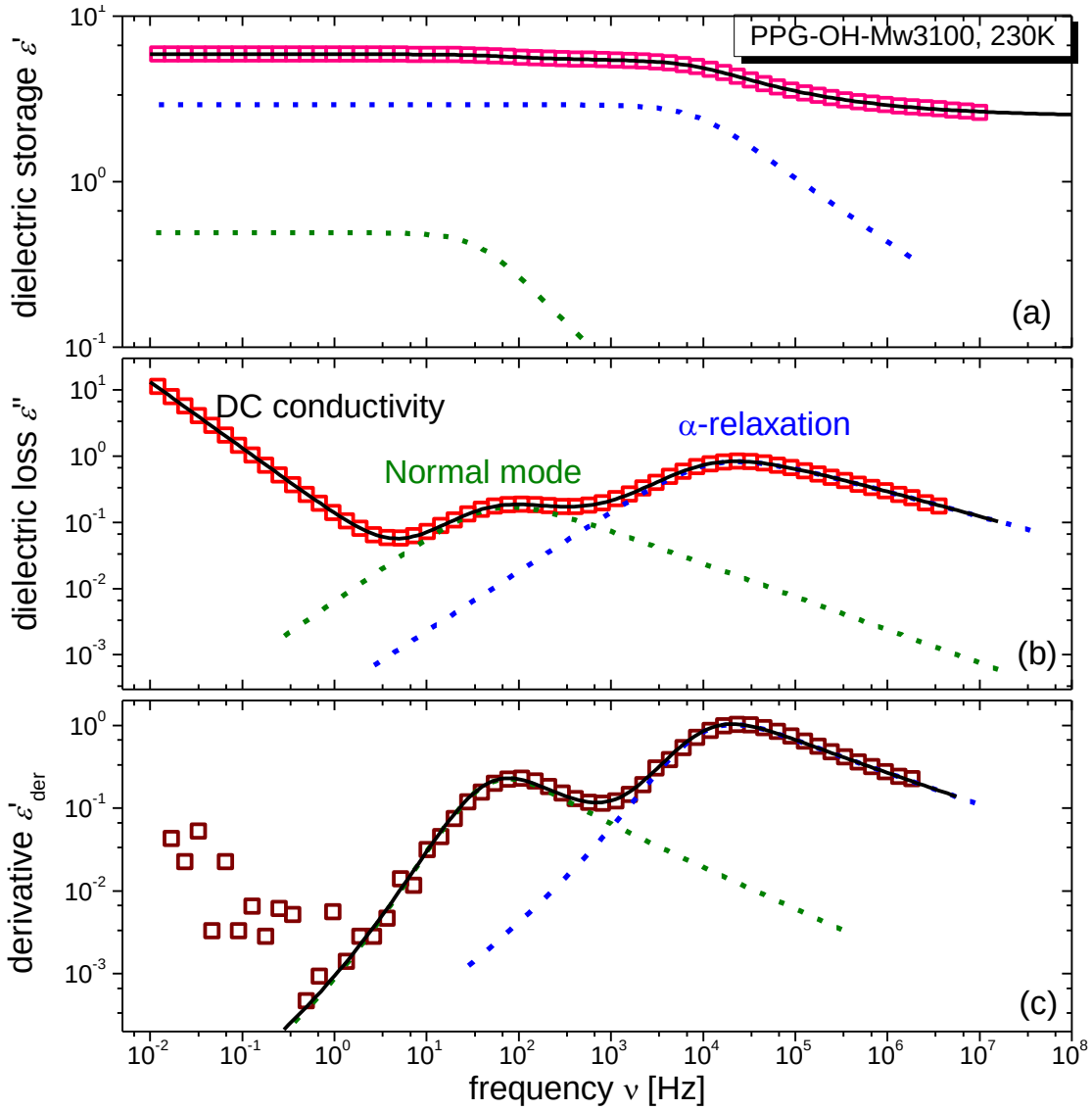

Figure 2. 5. Dielectric spectra of PPG with a molecular weight of 3100 g/mol at 230 K. (a) Dielectric storage ε', (b) dielectric loss ε'' and (c) derivative of the real part of permittivity ε'_{der} are presented. The black solid line represents the total fitting of all processes and the colored dash lines represent the fitting for each process from HN-function.

The derivative of the real part ε'_{der} is usually used to exclude the Ohmic conductivity influence on the relaxation peaks and assist a better analysis when processes overlapped in the loss spectra. It's calculated:

$$\varepsilon'_{der} = -\frac{\pi}{2}\frac{\partial \varepsilon\prime(\omega)}{\partial \ln \omega} \tag{2.8}$$

The relaxation processes estimated by the derivative spectra is shown in Fig. 2.5 c. To extract its characteristic relaxation time, the derivative can be fitted by a Havriliak-Negami function modified for the derivative representation[110, 211].

In a polymer system with several dielectric components in the spectra, the complex permittivity data can be fitted with a combination of several HN-functions and a dc conductivity term:

$$\varepsilon^*(\nu) = \varepsilon_\infty + \frac{\Delta\varepsilon_1}{[1+(i2\pi\nu\tau_1)^{\alpha 1}]^{\gamma_1}} + \frac{\Delta\varepsilon_2}{[1+(i2\pi\nu\tau_2)^{\alpha 2}]^{\gamma_2}} + \frac{\sigma}{2\pi i\nu\varepsilon_0} \tag{2.9}$$

Here, ε_∞ denotes the permittivity in the high frequency limit, $\Delta\varepsilon$ is the relaxation strength, τ is the HN relaxation time, $i = (-1)^{0.5}$ is the imaginary unit, the parameters α and γ describe the shape of the relaxation peak, σ corresponds to the DC conductivity and ε_0 is the permittivity of vacuum. The characteristic relaxation time that corresponds to the maximum position of the loss peak can be estimated from the HN relaxation time τ and the shape parameters α and γ:

$$\tau_{\max} = \tau\left[\sin\left(\frac{\alpha\pi}{2+2\gamma}\right)\right]^{-\frac{1}{\alpha}}\left[\sin\left(\frac{\alpha\gamma\pi}{2+2\gamma}\right)\right]^{\frac{1}{\alpha}} \tag{2.10}$$

2.1.4 Instrument and dielectric measurement set-up

Broadband dielectric measurements were carried out in the frequency domain using a Novocontrol Concept 80 broadband dielectric spectrometer with Alpha-A Impedance Analyzer and Quatro Cryosystem temperature control unit. The sample is held between two gold-plated electrodes or a parallel-plate dielectric cell made of sapphire and invar steel as shown in Fig. 2.6 forming a capacitor. Measurements were performed in the frequency range of 10^{-2}-10^7 Hz. A sinusoidal electric field is applied producing a resulting current with a phase lag depending on

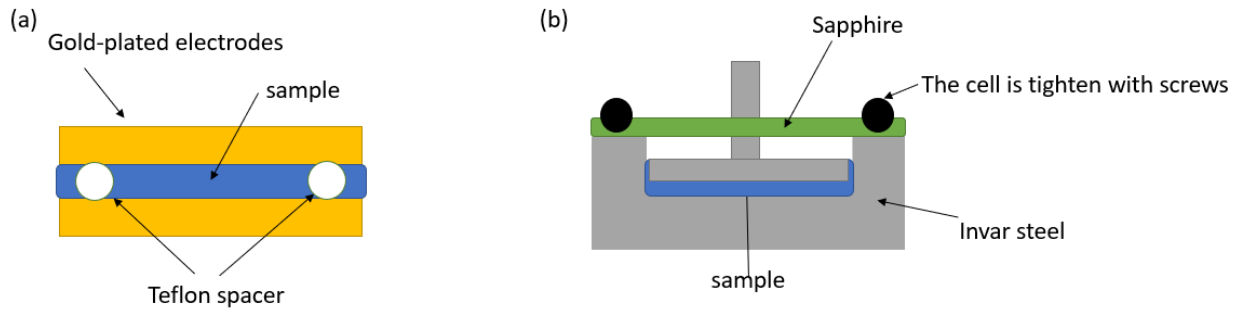

Figure 2. 6. Sample set-up: (a) Between gold-plated electrodes with Teflon spacer to guarantee the stability of the geometry of samples during experiments under different temperatures. (b) A parallel-plate dielectric cell made of sapphire and invar steel.

the impedance of the circuit (Fig. 2.7). The impedance of the sample is measured as $Z^* = U^*/I^*$. The impedance relies on the capacitance of the sample which is related to the complex dielectric permittivity of the sample. The capacitance of the electrode and sample assembly can be described as $C \propto \varepsilon^* A/d$, in which *A* is the surface area of the capacitor and *d* is the sample thickness. The relationship between capacitance and impedance is $C^* = 1/(i\omega Z^*)$.

2.2 Differential Scanning Calorimetry (DSC)

2.2.1 Principles of standard DSC

Differential Scanning Calorimetry (DSC) is used universally to study phase transitions, kinetic and thermodynamic properties, such as melting, crystallization, and glass transition of materials. In general, DSC monitors the heat flow of both the sample and reference as a function of time and temperature. Within the DSC instrument, when the sample is tested dynamically or kept isothermally under a certain temperature path, chemical reactions or physical transitions take place. The exothermic or endothermic processes produce generation or consumption of heat, which can be detected by the calorimeter as heat flow. The widespread use of DSC is based on its high sensitivity to both small and large energy fluctuations caused by phase transitions and structural changes of the sample.

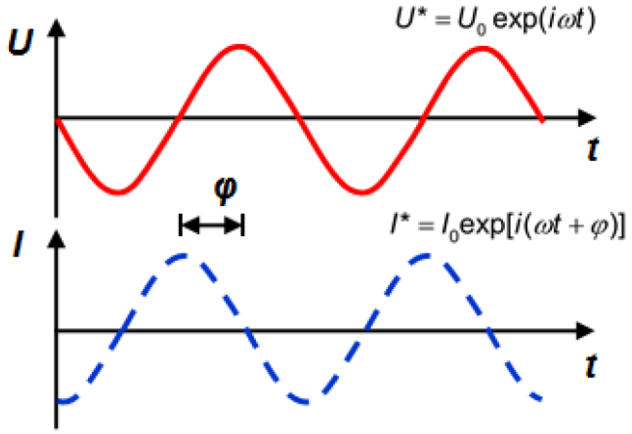

Figure 2. 7. A schematic representation of the phase difference between applied voltage and the resultant current in a dielectric spectrometer circuit.

Basically, there're two types of DSCs: the power compensation DSC and the heat flux DSC.[212, 213] Although there's difference in the design and measurement mechanisms between these two kinds of instruments, they both built on the same principle that the measured signal is proportional to the heat flow rate, Φ (J g^{-1} s^{-1}). Here use heat flux DSC with disk-type heat exchange path as an example to show how DSC instrument works. As shown in Fig. 2.8, the sample pan and an empty reference pan are held on the disk symmetrical to the center. During the measurement, both pans are heated at the same rate. When physical transformation, such as phase transition takes place in the sample pan, it will need more or less heat to maintain at the same temperature with the reference and a differential signal, Φ, is generated. The signal is proportional to the difference between the heat flow rate to the sample pan (Φ_S) and that to the reference pan (Φ_R), which is also the measured signal output by calorimeter:

$$\Phi = \Phi_S - \Phi_R = \frac{T_S - T_R}{R_{th}} = \frac{\Delta T}{R_{th}} \quad (2.11)$$

where T_S and T_R are temperatures of the sample and the reference, respectively. R_{th} is the thermal resistance of the sensor. The measured heat flow rate Φ is proportional to the true heat flow rate (Φ_{true}) with a proportionality factor K_Φ:

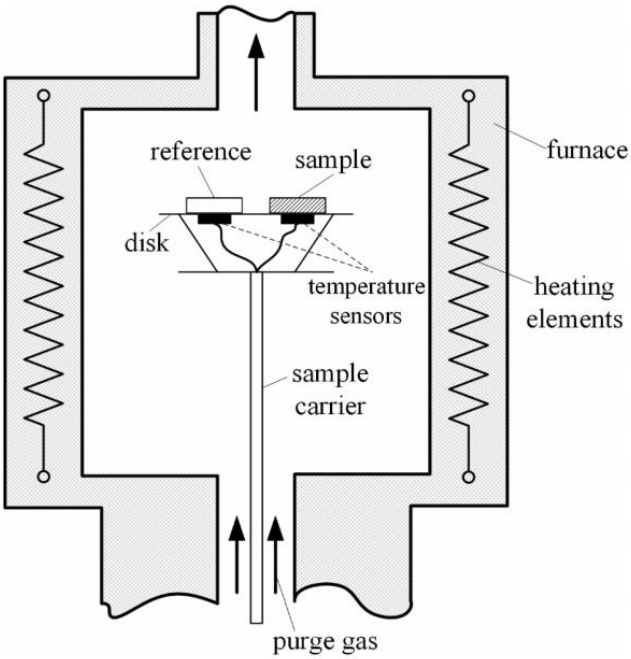

Figure 2. 8. Schematic diagram of heat flux DSC measurement furnace with disk-type heat exchange path.[214]

$$\Phi_{true} = K_{\Phi}\Phi \tag{2.12}$$

For the heat flow rate absorbed by the sample:

$$\Phi_{true} = C_p \cdot q \tag{2.13}$$

where C_p is heat capacity, which describes the heat absorbed by sample to increase temperature by one degree and $q = dT/dt$ is a constant scan rate. The DSC measurements can be conducted under air, nitrogen or argon, depending on the samples.

Fig. 2.9 is a schematic diagram for the DSC measurement result of a polymer. The glass transition appears as an endothermic step, since molecules have more accessible conformational states above T_g, thus higher entropy, which leads to an increase of the heat flow when the sample is heated crossing the glass transition. Crystallization shows up as an exothermic peak indicating a drop of heat flow. On the other side, melting process, as an endothermic process, appears as a peak with an increase of heat flow. Usually the

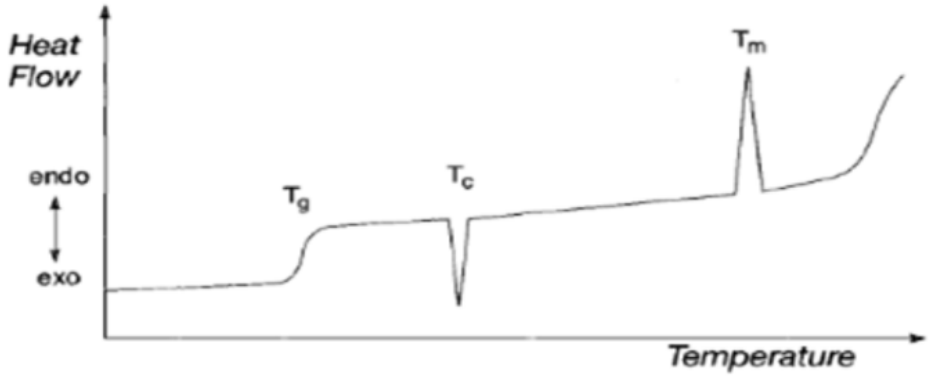

Figure 2. 9. Schematic diagram of DSC results. The y-axis and x-axis show the heat flow and the temperature, respectively. As temperature increases, the sample undergoes glass transition, crystallization and melting.

measurement is repeated several cycles to confirm the reproducibility. T_g is determined as the midpoint of the incline. In this work, all calorimetric T_g are taken as the midpoint of the step in the heat flow in the heating process. The observed value of T_g are different with the heating or cooling rate, and is affected by thermal history, mechanical history and measurement conditions, such as sample size and pre-treatment conditions.

It's worth noting that the glass transition is not a thermodynamic phase transition, but DSC measurements provide thermodynamic estimates of T_g. Since the configurational degrees of freedom are frozen in the glassy state, accordingly there's a sharp loss in second-order thermodynamic properties such as heat capacity and thermal expansion coefficient.[215] Such a thermodynamic consequence of this kinetic transition can be captured by DSC.

The standard DSC is a convenient and relatively fast technique. With a normal heating rate of 10 or 20 ^{0}C/min, a measurement with a temperature range of 300 ^{0}C can be finished within 30 minutes. However, when there's different overlapping transitions or the transition is very weak, the standard DSC cannot distinguish and detect the transitions very well since it measures the total heat flow.

2.2.2 Principles of temperature modulated-DSC

A more powerful and sophisticated technique, "temperature-modulated DSC (TMDSC)", has been developed to distinguish overlapping transitions and to detect secondary or weak transitions, since it can separate the heat capacity and kinetic components of the measurement signal. In TMDSC, the heat capacity is measured on dependence of modulation temperature, a small sinusoidal temperature oscillation is applied. The underlying foundation is to preserve linearity as well as small perturbations away from equilibrium (Fig. 2.10). The linearity produces total heat flow that is similar to standard DSC output. At the meantime, the modulated heating process produces reversing heat flow, which contains information about glass transition, melting, etc. The difference between total heat flow and reversing heat flow is called non-reversing heat flow, which is related to kinetic processes such as crystallization.

The average heating rate in TMDSC is relatively smaller compare to standard DSC, typically in the range from 1 to 10 ^{0}C/min. The modulation period is usually set between 30 and 120 seconds, and the modulation amplitude typically lies between ±0.1 and 2 ^{0}C.

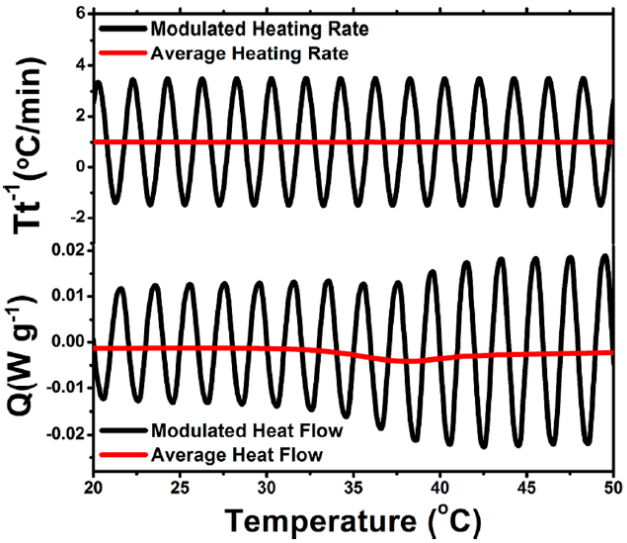

Figure 2. 10. On the top: modulated heating rate, Tt^{-1} (black curve) and temporal averages of the linear DSC heating rate (red line). On the bottom: the response function as modulated heat flow, Q (black curve) and temporal averages of the linear DSC heat flow (red line).[216]

2.2.3 Instrument and measurements

DSC measurements were performed using a Q-1000 differential scanning calorimeter (TA Instruments). The samples are loaded in aluminum hermetically sealed pans, which are designed for temperature range -180 to 600 ^{0}C and up to 300 kPa, especially ideal for materials in the liquid state, and an empty pan was placed in the same furnace as reference. All samples were dried in a vacuum oven at 313 K for 5 days before the experiment. For standard measurements, the samples were first equilibrated isothermally at 100 ^{0}C for 5 min, then scanned in the temperature range of -160 to 100 ^{0}C with a heating rate of 10 ^{0}C/min. The cooling and heating cycles were repeated twice to confirm the reproducibility of the results. The temperature-modulated measurements were performed according to following procedures: equilibrate at 100 ^{0}C, isothermal for 5 min, and then cool to -140 ^{0}C at 3 ^{0}C/min with a modulation of ±1 ^{0}C/min and heat back to 100 ^{0}C.

2.3 Rheology

Polymers are viscoelastic materials, i.e. they exhibit both viscous and elastic characteristics under deformation depending on the time scale of the applied force. When an external stress is applied, viscous materials resist shear flow and strain linearly with time. On the other hand, elastic materials strain and can recover to their original state once the stress is removed. For viscoelastic materials, they can store and recover the energy, release the deformation and recover to the initial state when the deformation applied on a short time scale. In this situation, they perform like an elastic solid. On the other hand, if the deformation is imposed on a longer and continuous time scale, they will have sufficient time to relax and fully release the external stress/strain. In this view, they behave like a viscous liquid that can dissipate energy by friction.

To study the viscoelastic properties of polymers, we start with the simple shear flow between two parallel plates which is shown in Fig. 2.11. The material is confined and fully filled the gap between parallel plates with the gap value d*y*. When one surface moved with a

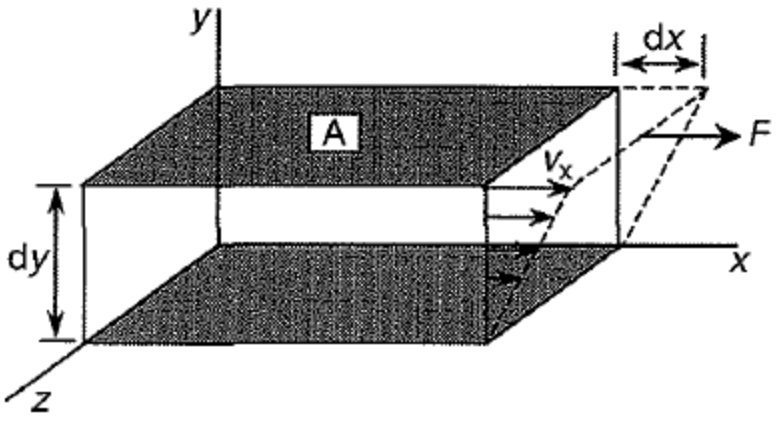

Figure 2. 11. A schematic illustration of simple shear deformation between two parallel plates.

distance d*x*, the material is subjected to a shear strain, $\gamma = dx/dy$. The strain rate (also termed as shear rate) is defined as:

$$\dot{\gamma} = \frac{d\gamma}{dt} = \frac{d(\frac{dx}{dy})}{dt} \tag{2.14}$$

The shear stress is defined as force per unit area:

$$\sigma = \frac{F}{A} \tag{2.15}$$

where *F* is the measured force and *A* is the area where plates get in contact with the sample.

Viscosity, modulus and compliance are the most important parameters to study viscoelasticity. Generally, viscosity is defined as the ratio of a stress to a strain rate and reflects the relative motion of molecules, where energy is dissipated by friction. In simple shear, it can be described as:

$$\eta = \frac{\sigma}{\dot{\gamma}} \tag{2.16}$$

Similarly, a modulus describing mechanics of elastic solids is defined as the ratio of a stress to a strain. In simple shear, the modulus is expressed as:

$$G = \frac{\sigma}{\gamma} \tag{2.17}$$

There's a linear viscoelastic regime when *G* is independent of the magnitude of *γ*. In the linear viscoelastic region, the observed viscoelastic properties, including modulus, viscosity and compliance, are independent of imposed stress or strain values. The linear region depends on frequency, temperature and state of the sample, i.e., solid or liquid. Therefore, it needs to be defined accurately. In this work, we focused on the study of viscoelasticity in linear region. The compliance, *J*, which can be defined as the ration of a strain to a stress:

$$J = \frac{\gamma}{\sigma} \tag{2.18}$$

When the time dependence is involved, there are two relaxation modes that can be tested: stress relaxation and creep. The sample undergoes creep when a certain stress is applied and held to and the resulting strain is detected as a function of time. The associated compliance is called the creep compliance:

$$J(t) = \frac{\gamma(t)}{\sigma} \tag{2.19}$$

On the other hand, the stress relaxation is tested by keeping the sample at a constant strain and the resulting stress is detected as a function of time. The associated modulus is called stress relaxation modulus:

$$G(t) = \frac{\sigma(t)}{\gamma} \tag{2.20}$$

When sample is tested under sinusoidally time-varying strain/stress at frequency ω, the resulting dynamic modulus, $G^*(\omega)$ is usually resolved into two dynamic moduli: storage modulus, G', which is in-phase with the strain and represents the elastic response; loss modulus, G'', which is in-phase with the strain rate and reflects the viscous response:

$$G^*(\omega) = G' + iG'' \tag{2.21}$$

2.3.1 Principles of rheology measurement

2.3.1.1 Creep measurement

In a creep test, a constant stress is applied to the sample and the resultant strain is detected as a function of time. The response of a typical viscoelastic material to creep measurement is shown in Fig. 2.12. After an instantaneous elastic strain, the strain increases over time with a decreasing strain rate and eventually a constant-strain steady state is reached where the strain increases linearly with time. Not all materials can reach such an obvious steady-state even after a long time. When the stress is released, there will be an elastic recovery of the fluid. This combination serves to illustrate the response of a viscoelastic liquid (the Maxwell model). The measured output in a creep measurement is usually presented in terms of the creep compliance $J(t)$. Although this measurement is applicable to all viscoelastic materials, it's mostly used to test viscoelastic solids and highly viscous viscoelastic liquids.

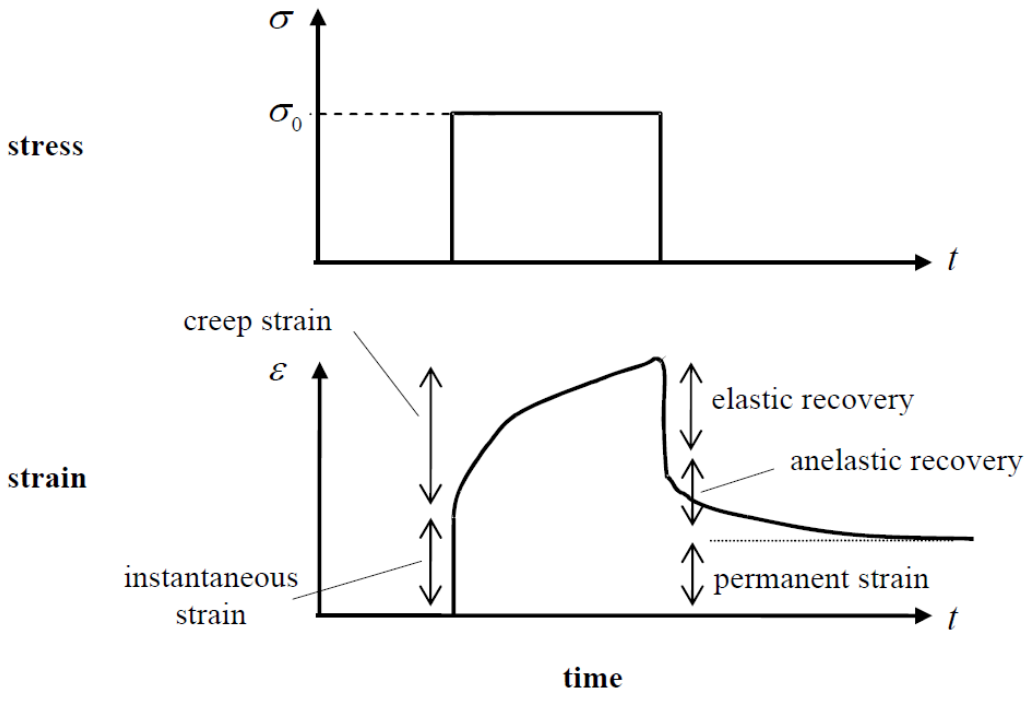

Figure 2. 12. Strain response of viscoelastic materials to the creep test.[217]

2.3.1.2 Small Amplitude Oscillation Shear (SAOS) measurement

The most common method to test viscoelastic properties is small amplitude oscillation shear (SAOS), where sample is tested under oscillatory time-varying strain/stress. In a strain-controlled SAOS measurement, the angular displacement is set and the requiring torque which need to be applied to the upper plate to give the displacement is measured (Fig. 2.13 a). Thus, the shear stress can be calculated. The oscillation strain is presented:

$$\gamma(t) = \gamma_0 \sin(\omega t) \tag{2.22}$$

where γ_0 is the amplitude of the oscillatory shear. The corresponding stress response is:

$$\sigma(t) = \sigma_0 \sin(\omega t + \delta) \tag{2.23}$$

Where δ is the phase angle.

For a purely elastic material in which stress is proportional to strain, the maximum stress occurs at the maximum strain (when deformation is greatest) and both stress and strain are in phase, therefore $\delta = 0$. For a purely viscous material in which stress is proportional to strain rate, the maximum stress occurs at the maximum strain rate (when flow rate is greatest). This time the stress and strain are out of phase and $\delta = 90^0$. For a viscoelastic material, $0 < \delta < 90^0$. This is illustrated in Fig. 2.13 b.

The response to the SAOS measurement is usually presented in terms of complex dynamic modulus:

$$G^*(\omega) = G'(\omega) + iG"(\omega) = \frac{\sigma(t)}{\gamma(t)} = \frac{\sigma_0}{\gamma_0}(\cos\delta + i\sin\delta) \tag{2.24}$$

For viscoelastic materials, both G' and $G"$ are significant. When $G' \gg G"$, the material is regarded as solid like. On the other hand, when $G" \gg G'$, the material is believed as liquid like. Phase angle is often described by the loss tangent, tan δ:

$$\tan\delta = \frac{G"}{G'} \tag{2.25}$$

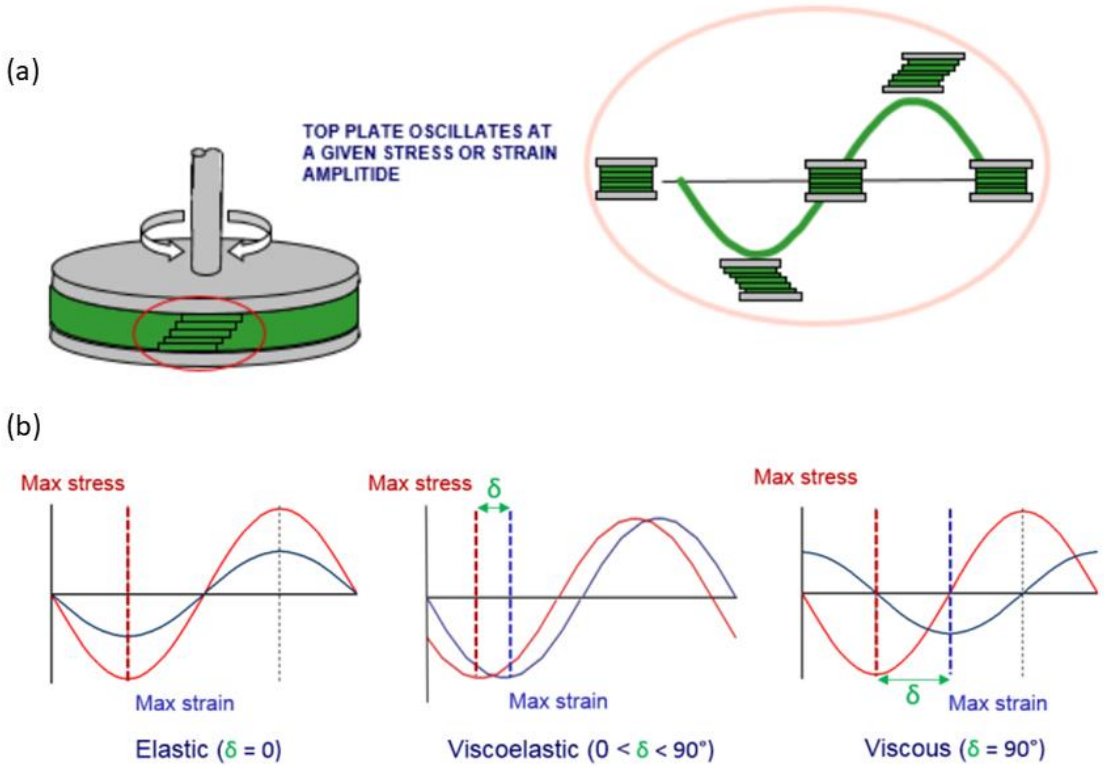

Figure 2. 13. (a) Sample loaded between parallel plates with an oscillatory shear applied. The height between two parallel plates is called gap (h) and the upper plate oscillated back and forth at a specific stress or strain and frequency. (b) Typical stress and strain curves for purely elastic, purely viscous and viscoelastic materials.

The viscoelastic response can also be presented in terms of a dynamic viscosity:

$$\eta^* = \eta' - \mathrm{i}\eta'' \tag{2.26}$$

The relationship between G^* and η^* is presented:

$$G^* = \mathrm{i}\omega\eta^* \tag{2.27}$$

$$G' = \omega\eta'' \tag{2.28}$$

$$G'' = \omega\eta' \tag{2.29}$$

Besides frequency sweep, the storage and loss shear modulus can be measured in many procedures, such as single point, temperature sweep (heating or cooling) and amplitude or time sweep.

In a stress-controlled SAOS measurement, an oscillatory torque is imposed on the upper plate and the resulting angular displacement is measured. Therefore, the strain can be calculated. The stress applied on the sample:

$$\sigma(t) = \sigma_0 \cos(\omega t) \tag{2.30}$$

where σ_0 is the amplitude of the oscillatory shear. The corresponding strain response is:

$$\gamma(t) = \sigma_0 |J^*(\omega)| \cos(\omega t + \delta) = \sigma_0 [J'(\omega) \sin \omega t + J''(\omega) \cos \omega t] \tag{2.31}$$

where J^* is the complex compliance, J' is the storage compliance and J'' is the loss compliance. The relationship between complex compliance and complex modulus is:

$$|G^*||J^*| = 1 \tag{2.32}$$

$$G' = \frac{J'}{J'^2 + J''^2} \tag{2.33}$$

$$G'' = \frac{J''}{J'^2 + J''^2} \tag{2.34}$$

2.3.1.3 Determine the linear viscoelastic region in polymers

In the linear viscoelastic region (LVER), microstructural properties can be estimated since the applied stress or strain are small and insufficient to cause structural breakdown (yielding) of the structure. In real world experiments, a measurable stress always needs a finite strain and whether the output falls in the linear viscoelastic region needs to be checked. In controlled stress rheology, there're two techniques to determining this region: creep and dynamic oscillation.

In Creep measurements, after extrapolating from strain and stress, a spectrum of creep compliance $J(t)$ under different stress level can be obtained. Creep compliance curves of a polymer sample under sequentially increased stress A, B and C are shown in Fig. 2.14 a. The overlapping curve under stress A and B indicating that they are within linear region while stress C is not.

In the dynamic oscillation measurements, the sample is tested under increasing levels of stress or strain at a constant frequency. As shown in Fig. 2.14 b and c, the onset where a dynamic viscoelastic function, such as G^* or η^*, deviates by more than 10% from a constant value indicates the end point of linear viscoelastic region.

In current work, we focused on the viscoelastic properties in the linear region and the linearity is confirmed by dynamic oscillation measurements in advance.

2.3.2 The viscoelastic spectrum of dynamic moduli and Time Temperature Superposition (TTS)

A typical viscoelastic spectrum in terms of dynamic moduli as a function of frequency for a low molecular weight polymer is shown in Fig. 2.15 (a). It possesses similar characteristics which are commonly observed for simple liquids.[58, 218] At the high frequency range, the plateau of G' and $G' \gg G''$ are typical characteristics for the elastic behavior and the material is in the glassy region with a modulus typical of a glass (10^9-10^{10} Pa). G'' exhibits a clear peak representing structural relaxation, where the material transits from elastic (at higher v) to viscous (at lower v) regime. The rheological characteristic time of structural relaxation is usually extracted from the crossover of G' and G''. Shortly after structural relaxation, terminal

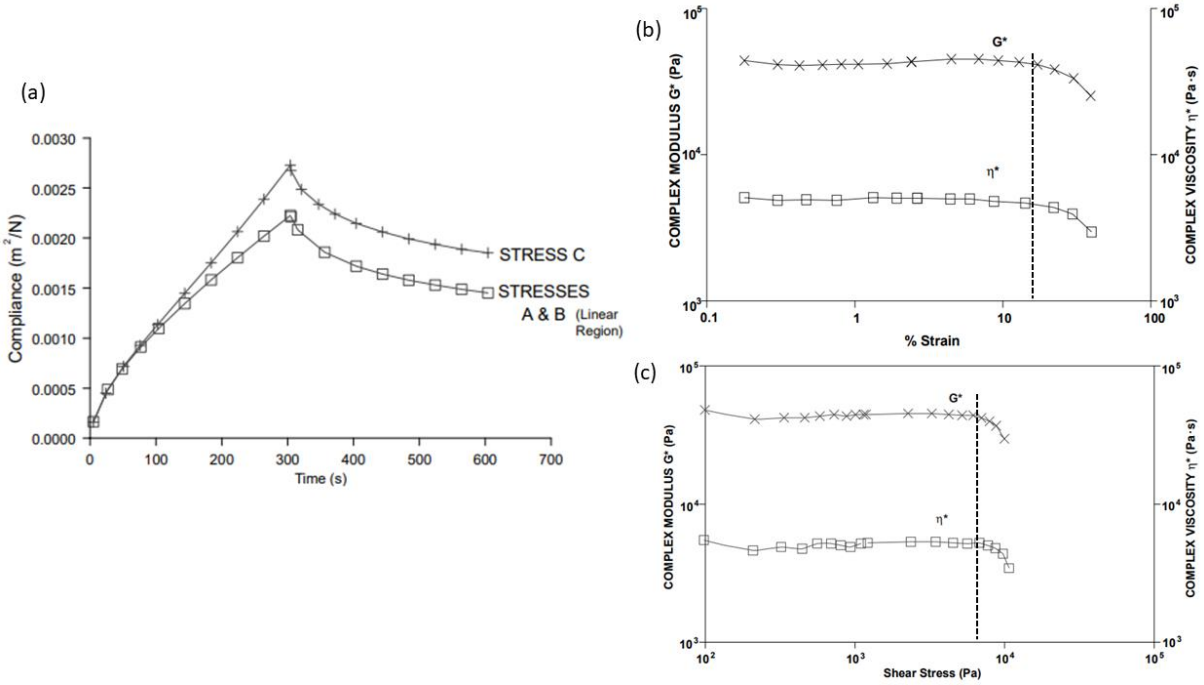

Figure 2. 14. Representative schematic spectra of a polymer in a) creep measurements under different stresses and dynamic oscillation measurements over b) strain percentage and c) shear stress. The vertical dashed line shows the onset where deviation from the linear region begins.

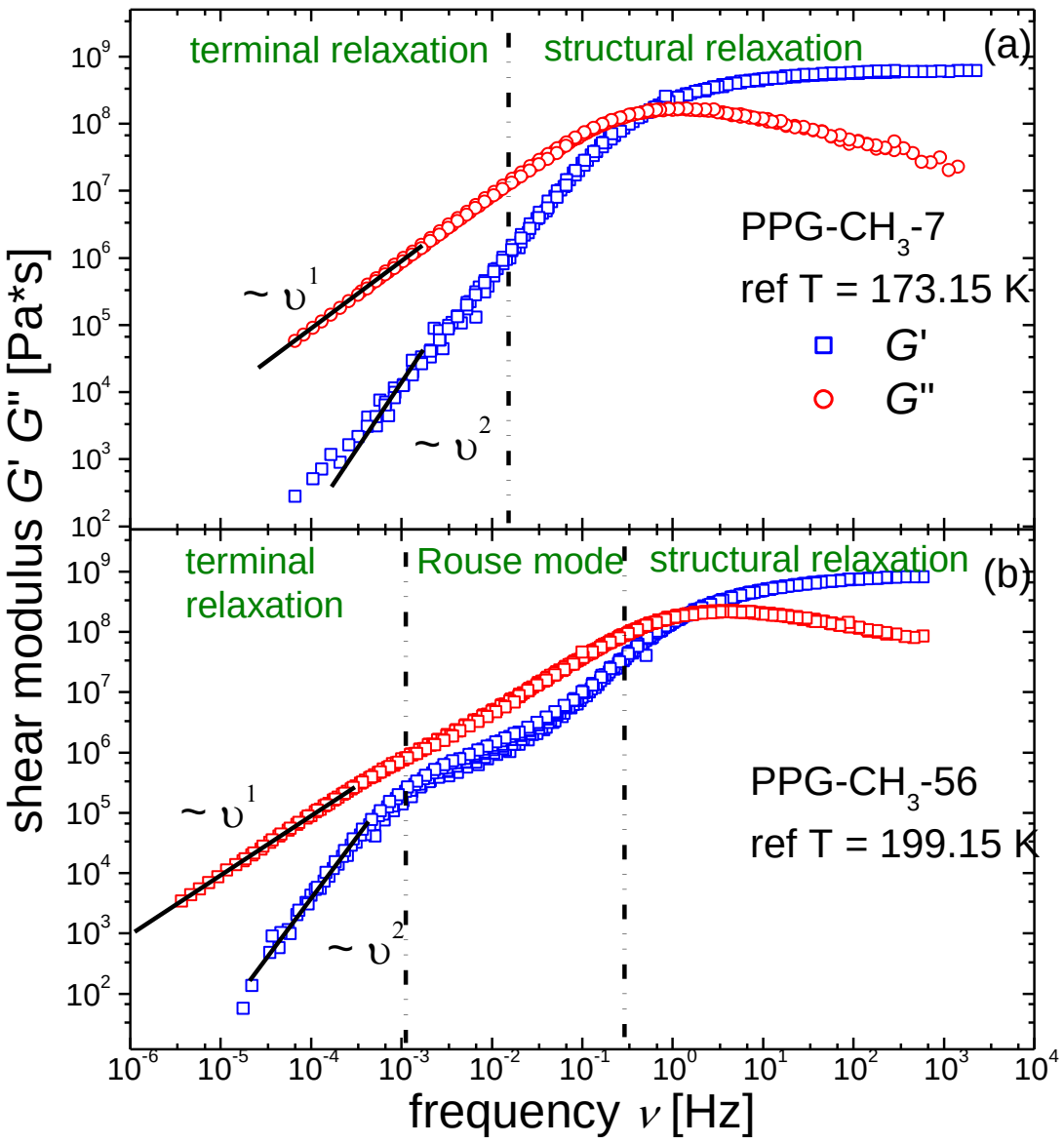

Figure 2. 15. Representative Shear modulus master curves constructed from linear viscoelastic spectra using TTS for PPG-CH_3 with (a) *DP*=7, (b) *DP*=56. The black lines display the typical slopes in the terminal regime as indicated.

relaxation ($G'(\omega) \sim \omega^2$, $G''(\omega) \sim \omega^1$ and $G'' \gg G'$) appears at the lower frequencies. In this regime, the stress is released, motions of entire molecules or large subsections come into action, and the material behaves like a viscoelastic liquid. Similarly, the rheological characteristic time of terminal relaxation can also be extracted from the crossover of G' and G''.

For systems with higher molecular weight (but still below the entanglement molecular weight), there's an intermediate zone between glassy regime and terminal regime, where Rouse modes appear (Fig.2.15 b). Recall one of the most important models to describe polymer chain dynamics, especially for the short, unentangled polymer melts – Rouse model, in which the single chain diffusion is represented by Brownian motion of beads connected by harmonic springs.[151] There are mainly three parameters: the monomeric friction ζ, chain connectivity (mean-squared bond length b^2 modeled through harmonic springs) and the degree of polymerization of the backbones N. The Rouse modes are defined as:[219]

$$\vec{X}_p = \sqrt{\frac{2}{N}} \sum_{i=1}^{N} \vec{r_i} \cos[\frac{p\pi}{N}(i - \frac{1}{2})] \tag{2.35}$$

in which the mode number p = 0, 1, 2, …, N-1. When p = 0, the Eq.2.35 describes the motion of the center-of-mass of the chain. When $p \geq 1$, the modes describe internal sub-chain relaxations with $\frac{N-1}{p}$ segments.

In an entangled polymer system (Fig. 2.16), besides the processes mentioned above, there's a signature rubbery plateau (where $G' \approx 10^5$-10^6 Pa) following rouse relaxation, which is characteristic of intermolecular entanglements. The modulus in the rubbery plateau region is called G_N:

$$M_e = \frac{\rho RT}{G_N} \tag{2.36}$$

in which M_e is the average molecular weight between entanglements, ρ is the density and R is the gas constant. The nature of entanglement in high molecular weight polymer systems remains one of the most intriguing and unsolved problems in polymer physics. Various models[220-225] have been proposed to explain the origin and mechanisms of entanglements on molecular scale, but the exact intrinsic nature is still left as elusive. It's commonly agreed that

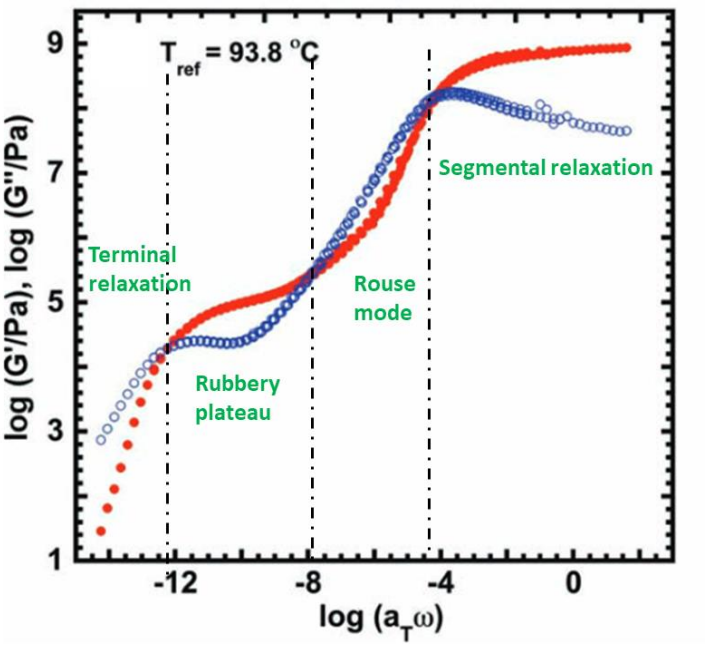

Figure 2. 16. A typical viscoelastic spectrum of dynamic moduli as a function of frequency (angular frequency) for an entangled polymer system. Data are from a star polystyrene at temperatures ranging from 95 to 170 ^{0}C.[226]

entanglement is generated by the topological constraints, which is produced by long polymer chains.[146] While for associating polymers, their entanglement behaviors are believed to be more complicated due to the transient nature of secondary interactions.

The terminal relaxation describes flow behavior of polymer systems. Fig. 2.17 shows modulus of polymers on dependence of temperature or time with varied molecular weights. The modulus magnitude of rubbery plateau reflects the value of cross-link density. As MW increase, longer chains exhibit longer terminal relaxation times, accordingly.

Due to the sensitivity of the rheometer, measurement conditions and the relaxation times of the sample, it is often to observe only a portion of these spectra.

Restricted by measurement limitations of normal rheometers, it can't cover a full frequency range at a certain temperature when testing via SAOS with frequency sweep. A so-called time-temperature superposition (TTS) principle is used to extend the relaxation spectrum to include long time relaxation processes. The TTS principle is applicable based on the

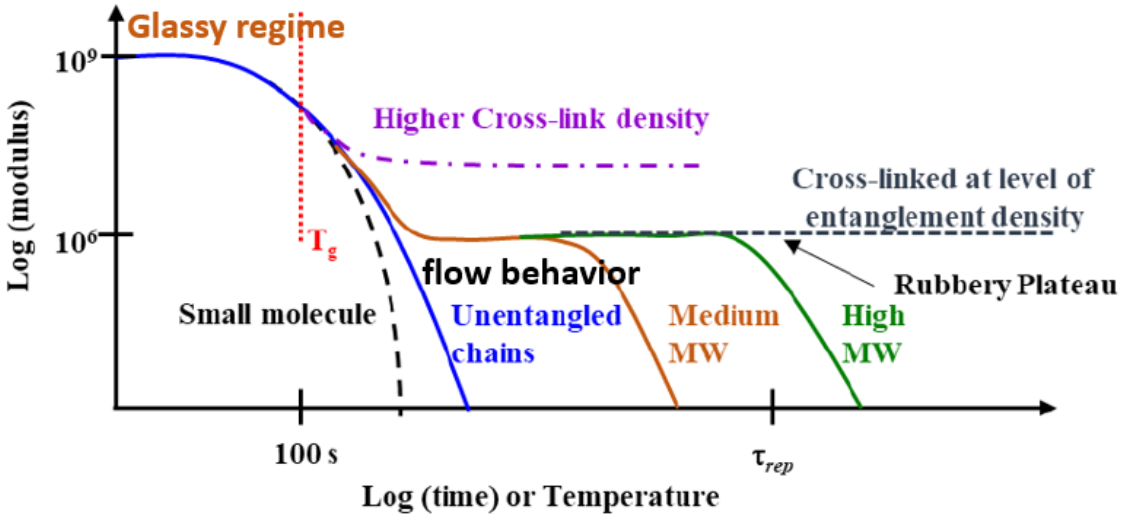

Figure 2. 17. Modulus of polymer systems with different MW in time or temperature domain.[227]

assumption that all relaxation processes have the same temperature dependence for viscoelastic materials over certain regions of behavior. In this way, measurements tested at higher temperatures can provide information of the lower frequency part in the full frequency range spectrum.

The SAOS with frequency sweep is usually carried out with several temperatures. After setting the data from one temperature as the reference, all others are shifted horizontally by the shift factor a_T and vertically by the shift factor b_T to overlap partially with each other. The resultant spectrum is called a master curve and is shown in Fig. 2.18.

Failure of TTS analysis has been reported in some cases. For example, when chain and segmental relaxation process are governed by different friction mechanisms, failure of TTS was observed in polystyrene system.[228] It's even more complicated in associating polymeric systems. Since the chain motion in a percolated transient network can be obtained only when the stickers are dissociated, the dynamics of such systems are divided into two regimes according to the lifetime of stickers. Therefore, there is a thermo-rheological complex behavior at intermediate frequency, where the stickers begin dissociating and re-associating. Accordingly, failure of TTS principle is observed both in unentangled and entangled associative

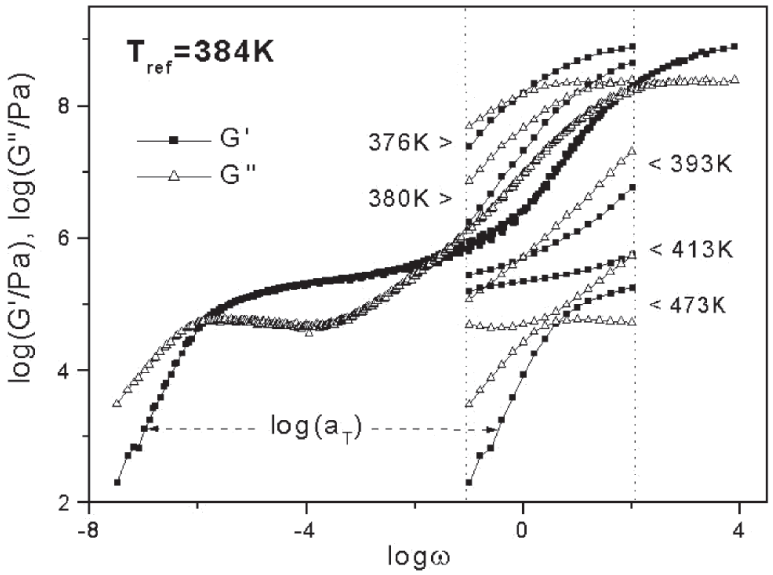

Figure 2. 18. Construction of a master curve of shear modulus on dependence of frequency for a polystyrene melt.[110]

systems.[206, 209] Although TTS principle fails in most associating systems, the master curve can still provide a general picture of the mechanical properties and relaxation processes.[179, 196, 229-232]

2.3.3 Zero-shear viscosity

The zero-shear viscosity η_0 is the viscosity obtained when shear rate approaching zero:

$$[\eta]_0 \equiv \lim_{\dot{\gamma}\to 0}[\eta] \tag{2.37}$$

The zero-shear viscosity is in the linear viscoelastic region. Relating to the terminal region of viscoelastic response, the zero-shear viscosity can be calculated:

$$\eta_0 \equiv \lim_{\omega\to 0}\frac{G''(\omega)}{\omega} \tag{2.38}$$

In practical, it is difficult to attain very low shear rate for many viscoelastic materials due to measurement conditions. In this situation, the zero-shear viscosity is tested at accessible shear

rate. The zero-shear viscosity depends strongly on the molecular weight of the polymer and temperature.

2.3.4 Instrument and measurement set-up

Experiments were performed by a stress-controlled AR2000ex rheometer from TA Instrument (Fig. 2.19 a). Small-angle oscillation measurements, creep and steady flow experiments were carried out. Two geometries: parallel plates and cone and plate were typically used for melts and employed in the rheology measurements in this work as shown in Fig. 2.19 b & c. The parallel plates are used for oscillation measurements in the linear-viscoelastic range and the cone and plate are mostly used in transient and steady test modes. The sample thickness is variable in parallel plates, and shear rate can be adjusted by changing gap or plate diameter. The cone and plate have homogeneous shear, shear rate and stress in the gap, but highly sensitive to the relative position (gap) of cone and plate. Sample loading for highly viscous samples in the cone and plate is quite difficult and they are not suitable for dispersions with solid particles. Both these geometries exhibit instabilities in shear field at high rates which may cause liquid loss, leading to inaccuracy in measurements.

Experiments were performed with liquid nitrogen to reach very low temperatures and under dry nitrogen above room temperature to avoid moisture and oxygen. The typical frequency range in SAOS frequency sweep for each temperature was set between 100 and 0.1 rad/s.

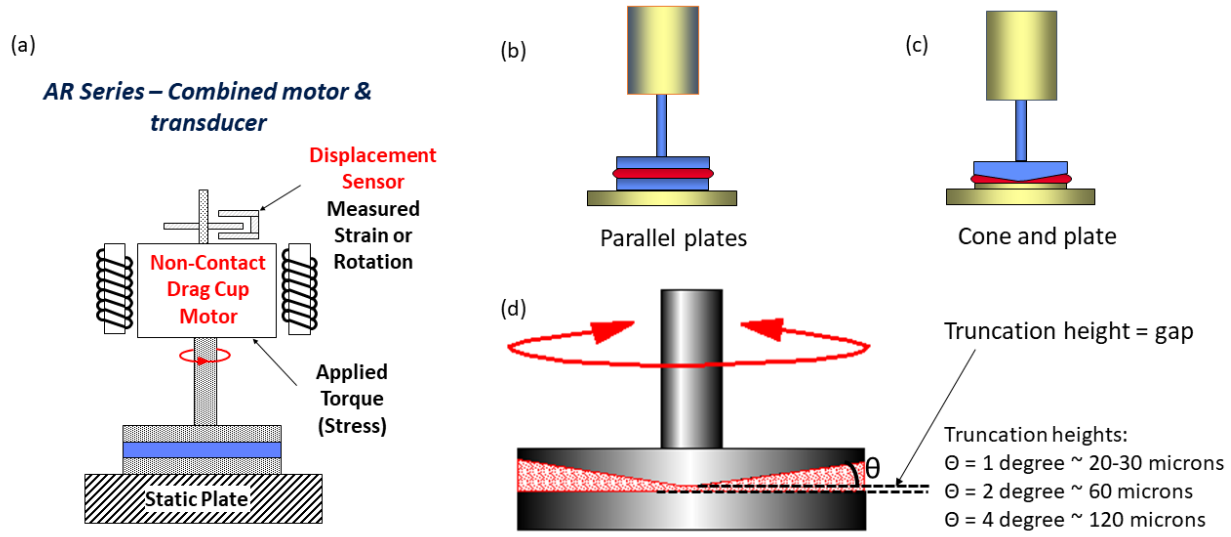

Figure 2. 19. (a) Rheology set-up of AR2000ex rheometer from TA Instrument. Two geometries: (b) parallel plates; (c) cone and plate are presented. The truncation height of cone and plate is the gap and several commercially available values are listed in (d).

Chapter III

Materials, Synthesis and Characterization

3.1 Telechelic Polydimethylsiloxane (PDMS) series

To study how H-bonding affect the dynamics and viscoelastic performance of associating polymers, we start from PDMS backbones. Well known for the remarkably flexible backbones and low glass transition temperature, PDMS is supposed to provide us with a very broad temperature window to investigate and would be relatively more sensitive to any additional mobility and packing restriction introduced by even weak secondary interactions. Moreover, PDMS is a well-developed commercially available polymers with abundant MW and different functional chain ends. The hydrogen-bonding end groups varied by strength from weakly associated hydrogel group (OH), amine group (NH_2) to moderate ones like carboxylic acid group (COOH) (Fig. 3.1). For the latter one, the linker group (-NHCO and -S) are found to play an important role in the materials performance. Non-associating PDMS were purchased as reference.

3.1.1 Commercial PDMS-H, PDMS-OH, PDMS-NH_2 and vinyl terminated PDMS (PDMS-V)

PDMS-OH with labeled MW of 400-700, 700-1500, 4200, 18000, and 139000 g/mol, PDMS-H with MW of 400-500, 1000-1100, and 4000-5000 g/mol, PDMS-NH2 with MW of 900-1000, 3000 and 5000 g/mol, vinyl terminated PDMS (PDMS-V) with MW of 800 and 6000 g/mol, respectively, were purchased from Gelest. For simplicity, we identify these samples using the above introduced abbreviation followed by the degree of polymerization (*DP*) (Table 3.1). The *DP* was specifically calculated by the end group analysis using the nuclear magnetic resonance (^{1}H NMR) spectra or the M_n characterized by GPC which will be described later in this chapter. All materials are liquids at room temperature and were used without further purification. To remove any undesired effects caused by water absorption the samples were dried in a vacuum (pressure bellow 0.01 bar) oven for at least 3 days prior the investigations. Note that although

Table 3. 1. Material Properties of the Investigated Polymers: Molecular Weight MW (labeled), Number Averaged Molecular Weight (M_n), Degree of Polymerization (*DP*), and Weight Fraction of End Groups (f_e). The weight fraction of end groups was estimated using the molecular weight of two end groups divided by the corresponding M_n. The molecular weight of the -NH2 and -NHCO-COOH end group is M_{end} = 58 g/mol and M_{end} = 158 g/mol, respectively. For PDMS-S-COOH, the molecular weight of each end group is M_{end} = 133 g/mol. The end group weight fraction was then estimated using the molecular weight of two end groups divided by the corresponding M_n.

Material	**labeled MW[g/mol]**	**M_n[g/mol]**	***DP***	**f_e[wt%]**
PDMS-OH-8	400-700	587	8[a]	5.8
PDMS-OH-13	700-1500	988	13[a]	3.4
PDMS-OH-75	4200	5600	75[a]	0.6
PDMS-OH-229	18000	17000	229[a]	
PDMS-OH-1094	139000	83000	1094[a]	
PDMS-H-9	400-500	668	9[b]	
PDMS-H-15	1000-1100	1112	15[b]	
PDMS-H-61	4000-5000	4516	61[b]	
PDMS-NH_2-22	900-1000	1744	22[b]	6.7
PDMS-NH_2-50	3000	3816	50[b]	3.0
PDMS-NH_2-74	5000	5592	74[b]	2.1
PDMS-NHCO-COOH-22		1944	22[c]	16.3
PDMS-NHCO-COOH-50		4016	50[c]	7.9
PDMS-NHCO-COOH-74		5792	74[c]	5.5
PDMS-V-13	800	1016	13[b]	5.3
PDMS-V-83	6000	6196	83[b]	0.9
PDMS-S-COOH-13		1228	13[c]	21.7
PDMS-S-COOH-83		6408	83[c]	4.2

[a]Determined from M_n obtained through GPC measurements.

[b]Determined from ^{1}H NMR measurements.

[c]The same with their starting materials which is determined from ^{1}H NMR measurements.

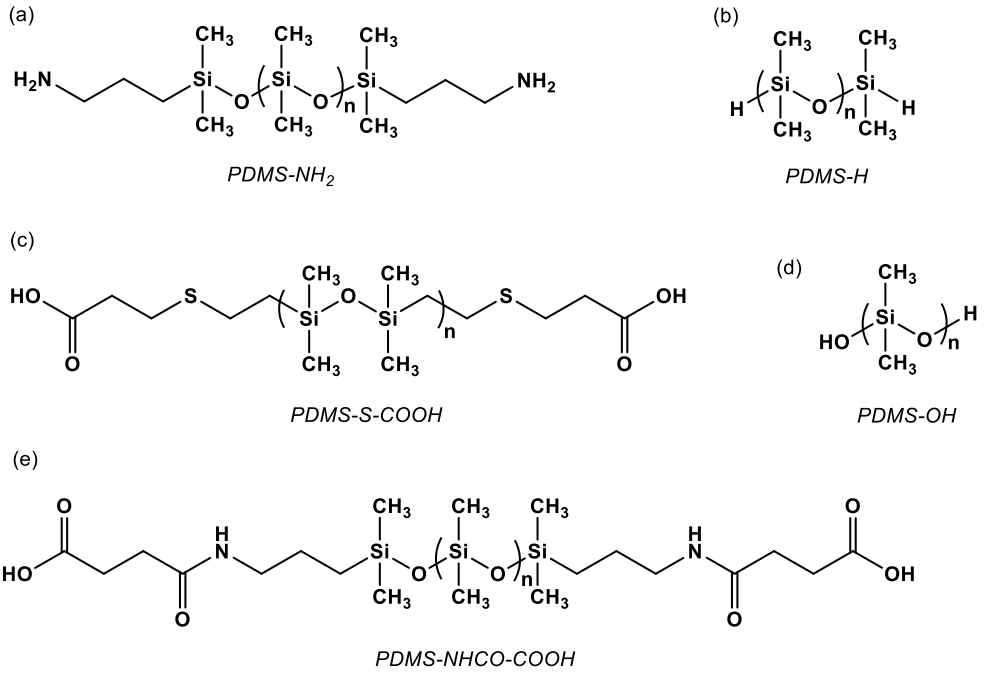

Figure 3. 1. Chemical structures of (a) PDMS-NH_2, (b) PDMS-H, (c) PDMS-S-COOH, (d) PDMS-OH, and (e) PDMS-NHCO-COOH[229, 233].

the abbreviated name only includes one end group for simplicity, the polymers are all functionalized on both chain ends.

3.1.2 Synthesis of amide-acid terminated PDMS (PDMS-NHCO-COOH)

The PDMS-NHCO-COOH was obtained by the reaction of PDMS-NH_2 and cyclic anhydride. Typical synthesis of PDMS-NHCO-COOH was performed as follows: PDMS-NH_2-22 (5 g, 5 mmol) and triethylamine (1.518 g, 15 mmol) were dissolved in 30 mL anhydrous tetrahydrofuran (THF). 4-(Dimethylamino) pyridine (0.611 g, 5 mmol) and succinic anhydride (2.001 g, 20 mmol) in 15 mL anhydrous THF were added to the PDMS solution. The reaction (Scheme 3.1) was performed at 40 ^{0}C for 2 days under the protection of a pure nitrogen atmosphere. After evaporating the organic solvent, hydrochloric acid solution (40 mL, 1 M) was added, and the mixture was stirred for 1 hour. DCM was used to extract the product (30 mL ×

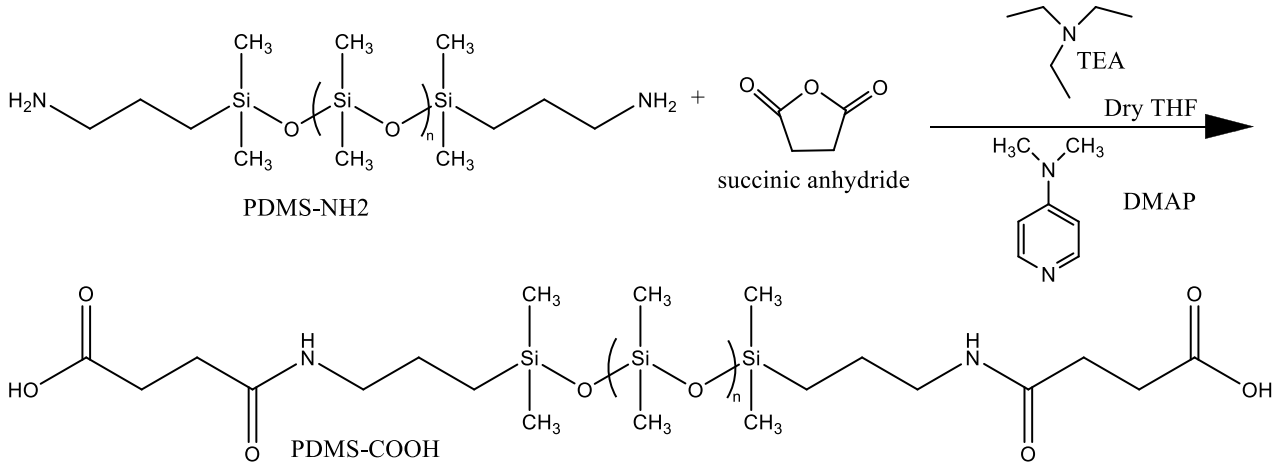

Scheme 3.1. Synthesis of amide-acid terminated (PDMS-NHCO-COOH) polydimethylsiloxane from the amine-terminated (PDMS-NH_2).

4). The organic layer was combined and dried with anhydrous sodium sulfate. After removing the solvent and drying in a vacuum oven for 3 days the pure product (around 2 g) was obtained.

As shown in Figure 3.2 b, the significant downfield shift of peak d and the appearance of the peaks e & f in the succinic acid after the reaction demonstrate the successful end group modification. Moreover, the comparative integration of the peaks e and f with peak b (the latter corresponding to the methylene group adjacent to the dimethyl-siloxane units) verified that more than 95% of the amine groups were substituted by the carboxylic acid groups. The NMR analysis has been applied to all the synthesized COOH terminated molecules, they will be denoted as PDMS-NHCO-COOH-n. The DP of the synthesized PDMS-COOH-n chain remains identical to the initial PDMS-NH_2-n chains, although the larger end groups increase total MW of these molecules.

3.1.3 Synthesis of sulfur-acid terminated PDMS (PDMS-S-COOH)

The PDMS-S-COOH was obtained by the reaction of vinyl terminated PDMS with 3-Mercaptopropionic acid. For example, vinyl terminated PDMS with MW of 6000 g/mol (3g,

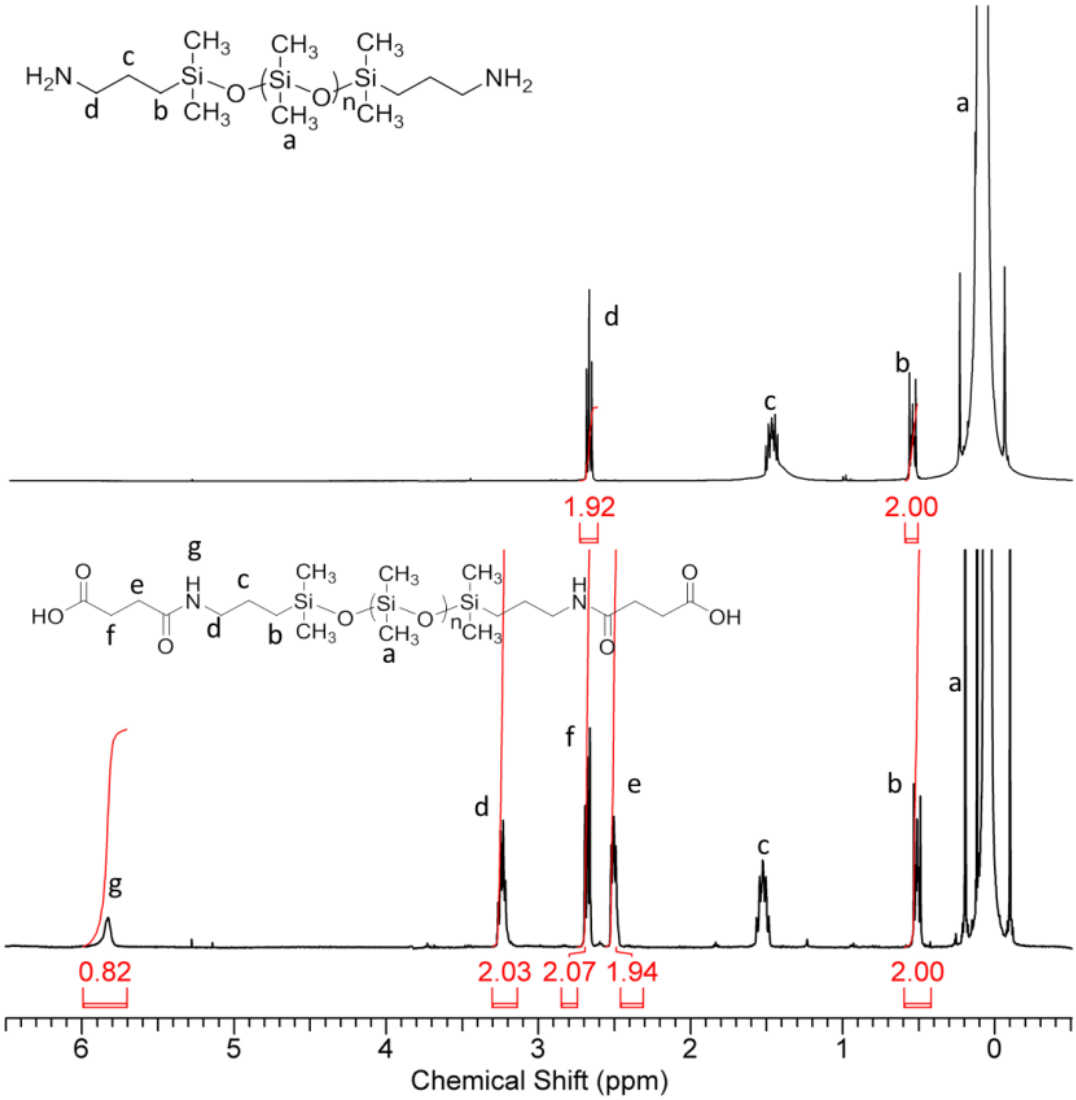

Figure 3. 2. ^{1}H NMR spectra of (a) PDMS-NH_2 and (b) PDMS-NHCO-COOH polymers with *DP* = 74.

0.5mmol) and 3-Mercaptopropionic acid (0.2123g, 2 mmol) were dissolved in 10 ml anhydrous toluene and purge Ar for half an hour. Then AIBN (0.041g, 0.25 mmol) in 3ml toluene was added to the polymer mixture. After purging Ar for another 10 min, the mixture was heated at 65 ^{0}C and reacted overnight (Scheme 3.2) under Ar atmosphere. After evaporating the organic solvent, dissolve product in hexane to remove the majority of AIBN. Then evaporating the hexane and dialysis in DCM (500 mL × 3) for 2 days. The structure of PDMS-S-COOH products were confirmed by ^{1}H NMR spectra as shown in Fig. 3.3.

3.1.4 Molecular characterization

The *DP* of PDMS-NH_2, PDMS-H and PDMS-V were specifically calculated by the end group analysis using the nuclear magnetic resonance (^{1}H NMR) spectra, i.e., for PDMS-NH_2, comparative integration of the peaks assigned to the methyl groups in the repeating units and methylene groups adjacent to amines (peak d and a, respectively, in Fig. 3.2 a). For PDMS-V, *DP* is calculated by comparative integration of the peaks assigned to the methyl groups in the repeating units and the vinyl groups near backbone (peaks d and c, respectively, in Figure. 3.3 a). The corresponding absolute number averaged molecular weight (M_n) of these materials were calculated from *DP* together with end groups molecular weight, 1.74 kg/mol (*DP* = 22), *i.e.* M_n of PDMS-NH_2 were 3.82 kg/mol (*DP* = 50) and 5.59 kg/mol (*DP* = 74), respectively. PDMS-S-COOH and PDMS-NHCO-COOH have the same *DP* with their starting material. The M_n of PDMS-OH was characterized by polystyrene (PS) standard GPC and the *DP* is calculated accordingly. All related information is included in Table 3.1.

3.2 Telechelic polypropylene glycol (PPG) series

PPG is a generally studied polymer with abundant commercial availability in MW and different chain ends. It makes a good comparison with PDMS backbone in terms of rigidity and polarity, thus presenting another good candidate for our research.

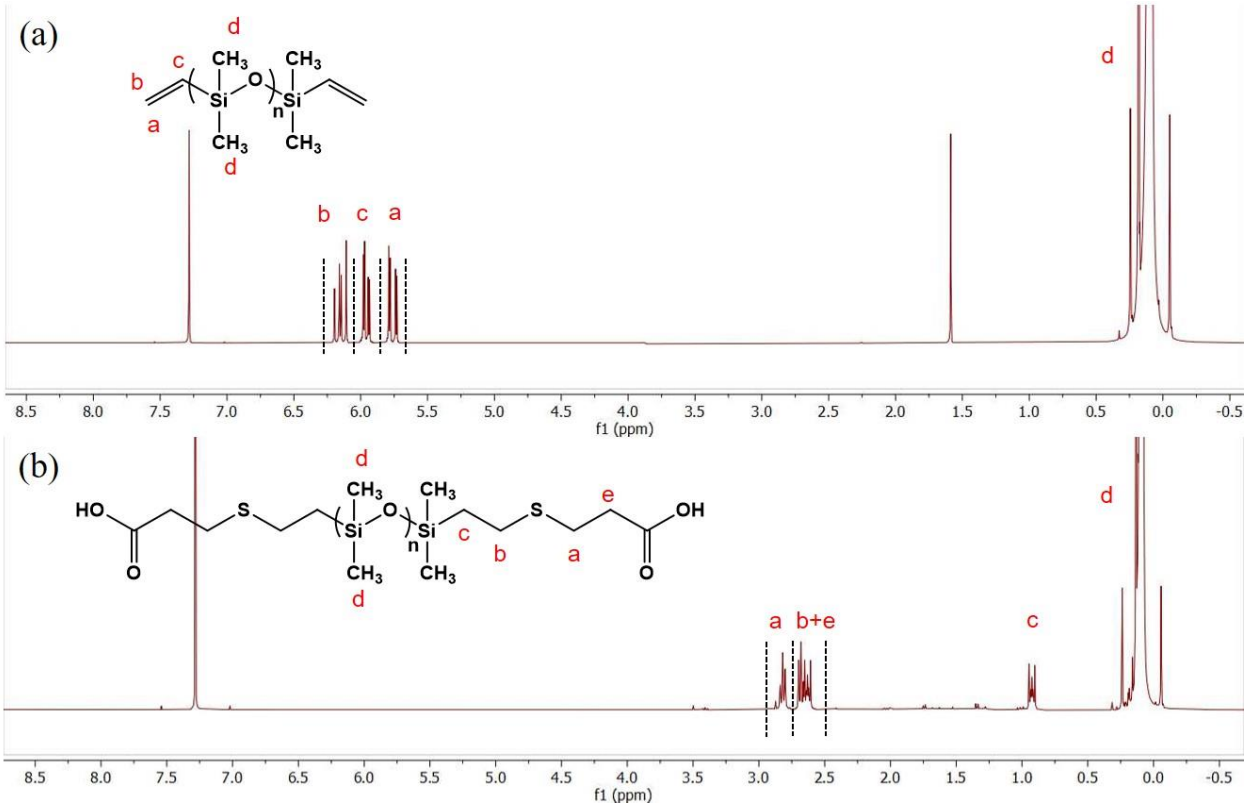

Figure 3. 3. ^{1}H NMR spectra of (a) PDMS-V-83 and (b) PDMS-S-COOH-83.

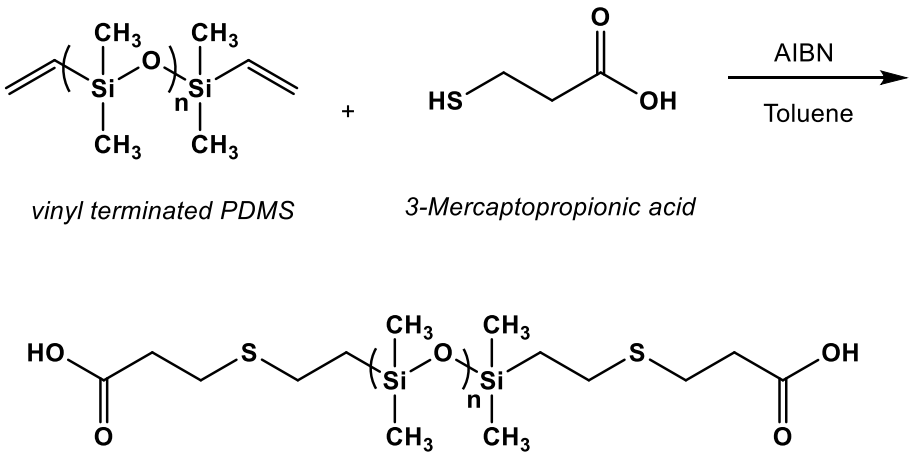

Scheme 3.2. Synthesis of sulfur-acid terminated poly(dimethylsiloxane) (PDMS-S-COOH) from the vinyl terminated poly(dimethylsiloxane).

3.2.1 Commercial PPG-OH, PPG-NH_2

Polypropylene glycol (PPG-OH) with number averaged molecular weights (M_n) of 440, 846, 1078, 2180, and 3282 g/mol was received from Scientific Polymer Products, Inc. PPG bis(2-aminopropyl ether) (PPG-NH_2) with M_n of 480, 2046 and 4018 g/mol was purchased from Sigma-Aldrich and used directly without further purification (all M_n values given here were determined by ^{1}H NMR, see below). The different types of H-bonding end groups vary significantly in their MW. In order to compare systems of the same main chain length, we use the degree of polymerization (*DP*) based on M_n of the main chain rather than the total molecular weight. The number at the end of the abbreviated polymer names presents the *DP* of the main chain, e.g. PPG-OH-7 is a hydroxyl terminated PPG consisting of 7 propylene glycol repeat units (i.e. a M_n of 440 g/mol, note that this value contains the MW of the end-groups which is not comprised in the *DP*). All information is included in Table 3.2.

3.2.2 Synthesis of amide-acid terminated polypropylene glycol PPG-NHCO-COOH

PPG-NH_2 of M_n = 480 g/mol (5.0 g, 12.5 mmol) and triethanolamine (5.23 mL, 37.5 mmol) were dissolved in 40 mL anhydrous tetrahydrofuran (THF). 4-(Dimethylamino) pyridine (1.527 g, 12.5 mmol) and succinic anhydride (5.0 g, 50 mmol) dissolved in 25 mL anhydrous THF were added to the PPG-NH_2 solution. The reaction (Scheme 3.3 a) was performed at 40 ^{0}C for 2 days under nitrogen atmosphere. After evaporating the organic solvent, hydrochloric acid solution (40 mL, 1 M) was added, and the mixture was stirred for 1.5 hours. DCM was used to extract the product (30 mL × 4). The organic layer was collected and dried with anhydrous sodium sulfate. Pure product (around 2 g) was obtained after removing the solvent by vacuum. The quantitative end group modification was checked by ^{1}H NMR (appearance of the characteristic peaks g, h in the succinic acid and the complete downfield shift of peak e after the reaction, Fig. 3.4).

Table 3. 2. Material properties of the investigated polymers: molecular weight MW* and *DP*.

Sample	*DP*	M_n [g/mol]
PPG-NH_2-6	6	480 [a]
PPG-NH_2-33	33	2046 [a]
PPG-NH_2-67	67	4018 [a]
PPG-COOH-6	6	680 [b]
PPG-COOH-33	33	2246 [b]
PPG-COOH-67	67	4218 [b]
PPG-OH-7	7	440 [b]
PPG-OH-14	14	846 [b]
PPG-OH-18	18	1078 [b]
PPG-OH-37	37	2180 [b]
PPG-OH-56	56	3282 [b]
PPG-CH_3-7	7	468 [c]
PPG-CH_3-14	14	874 [c]
PPG-CH_3-18	18	1106 [c]
PPG-CH_3-37	37	2208 [c]
PPG-CH_3-56	56	3310 [c]

[a] determined from H1 NMR measurements of PPG-COOH corrected for the end-group exchange

[b] determined from H1 NMR measurements

[c] determined from H1 NMR measurements of PPG-OH corrected for the end-group exchange

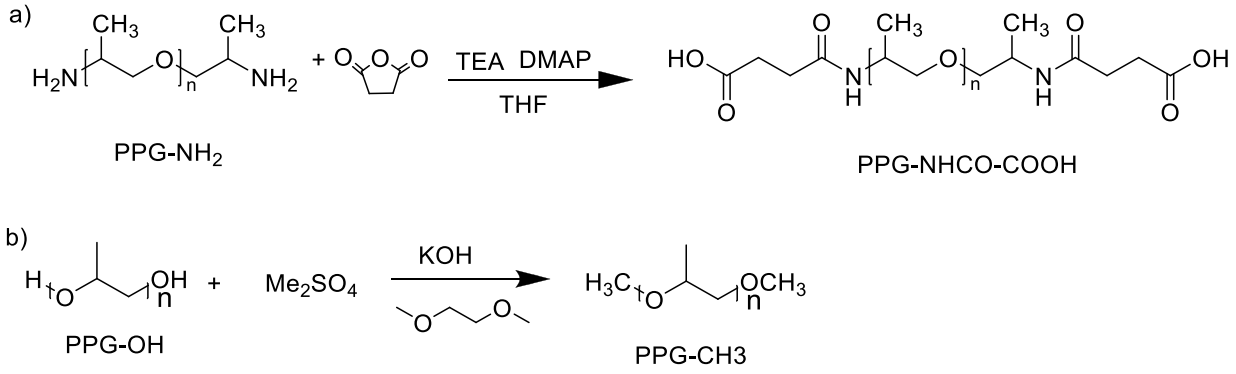

Scheme 3.3. (a) Synthesis of carboxylic acid-terminated polypropylene glycol (PPG-NHCO-COOH) from the amine terminated polypropylene glycol (PPG-NH_2); (b) Synthesis of methyl-terminated polypropylene glycol (PPG-CH_3) from the hydroxyl terminated (PPG-OH).

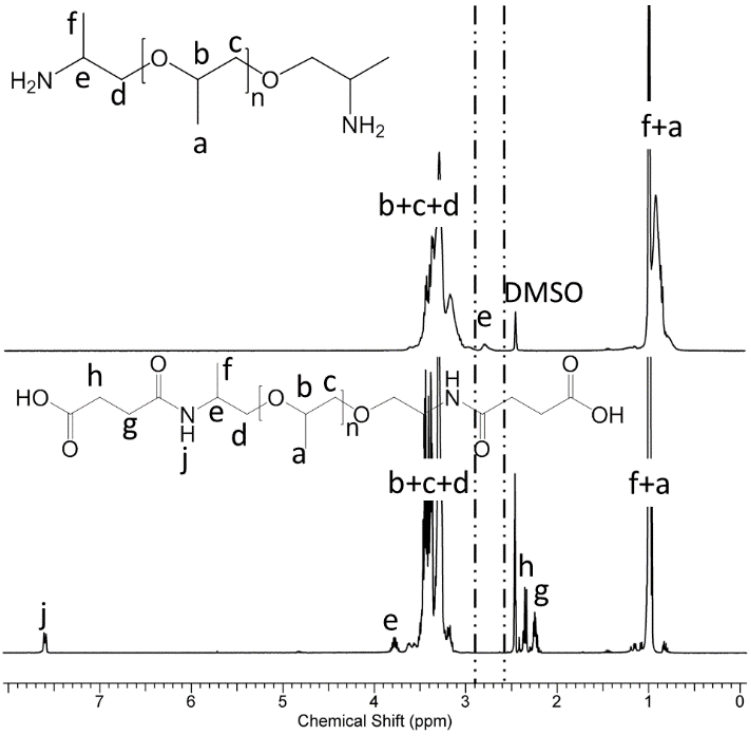

Figure 3. 4. ^{1}H NMR spectra and chemical structure of (a) PPG-NH_2 and (b) PPG-NHCO-COOH polymers with *DP* = 33 in DMSO. The dash-dotted lines indicate the region of peak e before the downfield shift corresponding to the end modification.

3.2.3 Synthesis of methyl terminated polypropylene glycol PPG-CH_3

Methylation of the PPG-OH was performed as follows[234, 235]: potassium hydroxide (KOH, 0.76 g, 13.6 mmol) was grinded into fine powder and dried in the vacuum oven before use. In a glove box, PPG-OH-7 (1.0 g, 2.27 mmol) was diluted with ethylene glycol dimethyl ether (12 mL). The KOH powder was slowly added into the PPG-OH solution while stirring until totally dissolved. Dimethyl sulfate (0.86 g, 6.81 mmol) was added to the mixture dropwise. The reaction (Scheme 3.3 b) was performed at room temperature for 2 weeks. The product mixture was transferred to the fume hood to evaporate the solvent (due to the toxicity of reagents). After the majority of the solvent was gone, hexane was added to wash the PPG-CH_3. The resulting polymer was dried under vacuum at room temperature for 3 days. ^{1}H NMR confirmed the complete methylation of the OH groups (complete shift of peak e which corresponds to the CH group adjacent to the terminal hydroxyl groups in the PPG-OH, Fig. 3.5).

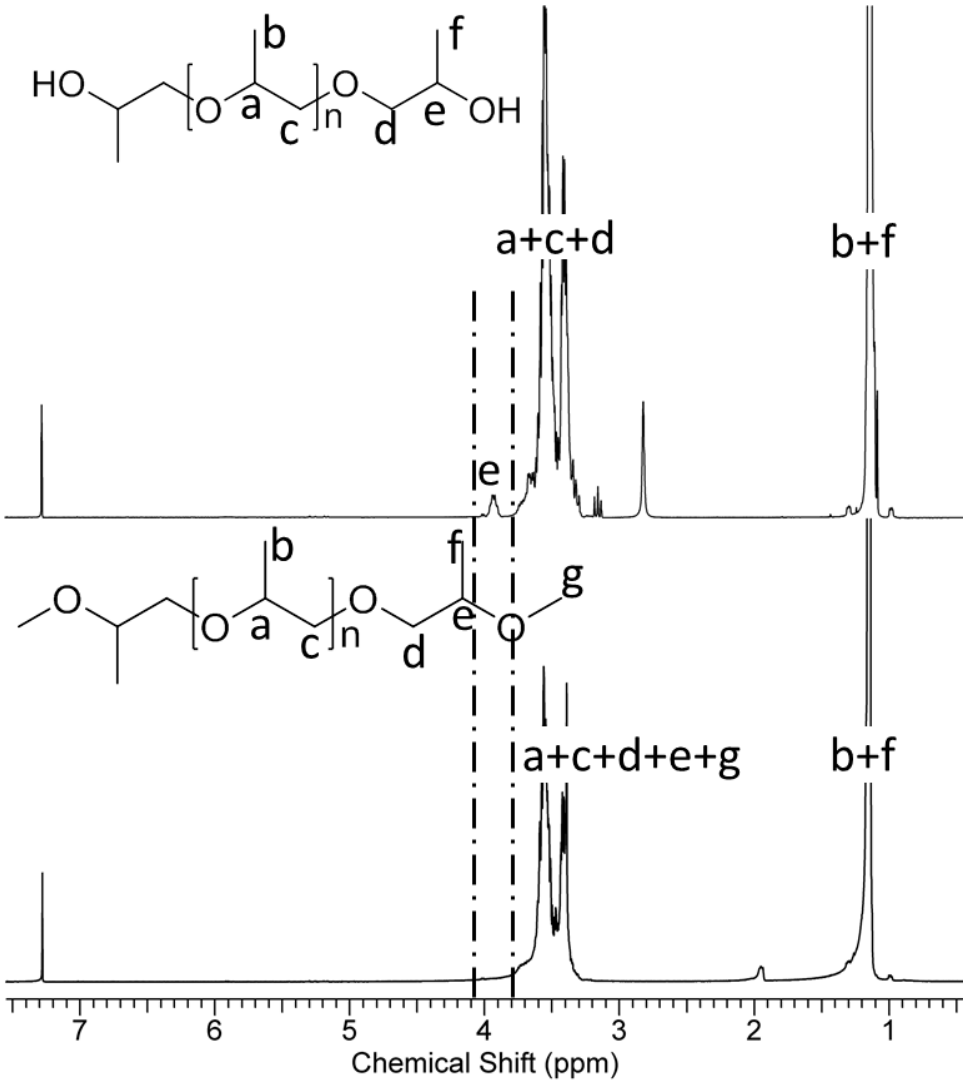

Figure 3. 5. ^{1}H NMR spectra of (a) PPG-OH and (b) PPG-CH_3 polymers with *DP* = 37 in $CDCl_3$.The dash-dotted lines indicate the region of peak e before the downfield shift corresponding to the end modification.

Chapter IV

Impact of Single Hydrogen-bonding Groups on Dynamics of Telechelic Associating Polydimethylsiloxane

Reproduced in part from: Kunyue Xing, Sabornie Chatterjee, Tomonori Saito, Catalin Gainaru and Alexei P. Sokolov. "Impact of hydrogen bonding on dynamics of hydroxyl-terminated polydimethylsiloxane" *Macromolecules* 2016, 49 (8), 3138-3147. Kunyue Xing contributed to BDS, DSC and rheology measurements, data analysis and writing. Catalin Gainaru contributed to data analysis and writing, Sabornie Chatterjee and Tomonori Saito helped with samples choice and preparation. Alexei Sokolov led the project, contributed to data analysis and writing.

4.1 Introduction

Hydrogen (H-) bonding is the most common interaction involved in the formation of supramolecular polymers due to its intrinsic directionality, cooperative nature, and variability of cohesive strength.[21, 22] The latter can be tuned, for example, by increasing the number of H-bonding centers attached to the molecular constituents, from a single to several (*e.g.*, triple[25-28], quadruple,[7, 8, 236] even sextuple[31]) units. Classical examples of molecules designed for sustaining multiple H-bonds include ureidopyrimidinone (UPy)[236, 237] and diaminopyridine-substituted isophthalamide and barbiturates.[31]

Not only the nature of secondary interactions but also the chemical structure of the units forming supramolecular aggregates can vary significantly, ranging from low molecular weight molecules[1] in the so-called associating liquids[107] to sizable covalently-bonded chains forming associating polymers.[118] Although an impressive progress was achieved regarding the synthesis of various associating polymers,[1, 2, 17, 51] the studies of their dynamics especially on segmental level in melts are rather limited. The work of Meijer and coworkers on UPy-terminated polydimethylsiloxane (PDMS)[142] revealed that a very strong secondary interaction mediated by the quadruple H-bonding end units could lead to an undesired structural

inhomogeneity, in this particular case with the UPy units forming microcrystalline domains embedded in the PDMS matrix. As a result, the PDMS-UPy system forms a network crosslinked by the microcrystalline domains. If the phase separation can be suppressed, the associating polymer can be investigated as a homogenous material that forms long supramolecular chains. This situation applies for the recent work of Lou *et al.* reporting a slow relaxation featured by dielectric and mechanical spectra of a self-complementary associating polymer with molecular terminal groups based on thymine and diamidopyridine triple H-bonding motifs.[112]

Here we present a combined study of segmental dynamics, glass transition, and rheological properties of hydroxyl terminated PDMS (PDMS-OH) with different molecular weights (MW). To unravel the role of chain end hydrogen bonding, we also studied hydride terminated PDMS (PDMS-H). We choose PDMS specifically due to its very low glass transition temperature T_g, with expectation that even single H-bonding group at the chain ends can have significant impact on dynamics at these low temperatures. Broadband dielectric spectroscopy, calorimetry and rheology were employed to characterize the relaxation behavior in these polymers. Our results indeed revealed a very strong change in segmental dynamics of PDMS induced by the chain end hydrogen bonding, especially at low MW. Surprisingly, the molecular weight dependence of T_g has been reversed in hydroxyl terminated chains: T_g decreases with increase in MW. Moreover, dielectric and mechanical relaxation spectra revealed the appearance of a low frequency mode in hydroxyl terminated PDMS, which does not exist in H-terminated and methyl terminated PDMS. We demonstrate that this mode can be ascribed to the so-called Debye process, well-known for mono-alcohols and some other small-molecule liquids.[107] Based on detailed analysis of the experimental data, we suggest that hydroxyl terminated PDMS may form chain-like or brush-like structures. In the latter case the terminal OH groups form a backbone and PDMS chains form brushes. Our estimates suggest that the formed supramolecular units include ~4-7 PDMS chains.

4.2 Materials

To compare with literature data of PDMS which is labeled with MW, we labeled hydroxyl terminated PDMS (PDMS-OH) and hydride terminated PDMS (PDMS-H) followed by its MW in this chapter. For the samples labeled with a MW range the *mean* value of this range is used. For example, hydroxyl terminated PDMS with molecular weight 400-700 g/mol is identified as PDMS-OH550, while hydride terminated PDMS with MW of 400-500 g/mol as PDMS-H450, respectively (Table 4.1). Note that in the following chapters in this work, these materials are named with degree of polymerization (*DP*) after its abbreviation for further analysis.

4.3 Methods

4.3.1 Differential Scanning Calorimetry (DSC)

The calorimetric measurements were performed using a Q1000 analyzer from TA Instruments. The samples were hermetically sealed in aluminum pans and an empty pan was used as reference. The probes were initially equilibrated at 363 K, then cooled down to 113 K and heated back to 363 K. The cycle of cooling and heating was performed with a rate of 10 K/min and repeated several times to insure the reproducibility of the results.

4.3.2 Dielectric spectroscopy

Dielectric spectra were acquired in the frequency range 10^{-3}-10^{6} Hz using a Novocontrol system that includes an Alpha-A impedance analyzer and a Quatro Cryosystem temperature control unit. The samples were placed in a parallel-plate dielectric cell made of sapphire and invar steel (Fig. 2.6 b), similar to the one described in Ref. [238]. The electrode separation of 100 µm yielded a geometrical capacitance of 20 pF. To prevent crystallization all samples were quenched from room temperature to about 113 K and reheated to 10 degrees below the glass-transition temperature T_g (estimated by DSC) prior the measurements upon further heating.

Table 4. 1. The parameters characterizing structural relaxation of PDMS-OH systems investigated in this work.

Material	MW(g/mol)	$T_{g,cal}$ (K)	$T_{g,diel}$ (K)	log(τ_0)	B (K)	T_0 (K)	m
PDMS-OH550	400-700	169	170	11.2	425	156	161
PDMS-OH1100	700-1500	157	154	13.5	677	135	133
PDMS-OH4200	4200	149	146	13.2	583	130	134
PDMS-OH18000	18000	148	145	13.8	642	128	130
PDMS-OH139000	139000	148	144	14.2	732	125	120

After each temperature increase the samples were equilibrated for at least 15 minutes to achieve a thermal stabilization within 0.2 K. Due to high tendency to crystallization we were able to measure PDMS-H450 only for few temperatures close to its T_g.

4.3.3 Shear rheology

Frequency dependent shear measurements were carried out with a stress-controlled AR2000ex rheometer from TA Instruments in a frequency range 10^{-1}-10^{2} Hz using a plate-plate geometry with a disk diameter of 4 mm. The samples were loaded between the two plates at room temperature, then cooled down to 10-15 K above the glass-transition temperature where the gap was slightly lowered to compensate for the thermal contraction of the sample and to insure the proper filling of the investigated volume. The adapted plate-plate distance was about 0.5 mm and kept constant for all the investigated temperatures. Before the acquisition of each shear spectrum (performed under zero normal force condition) the strain amplitude was adjusted to maintain linearity of the response. For all rheological measurements the temperature was stabilized within 0.2 K.

4.4 Results

4.4.1 Differential Scanning Calorimetry (DSC)

All the samples exhibit an endothermic step for temperatures $T > 140$ K associated with the glass transition (Fig. 4.1). Following previous work,[239] the *calorimetric* glass-transition temperature $T_{g,cal}$ was determined at the midpoint of this step and the corresponding values are listed in Table 4.1. $T_{g,cal}$ is practically independent of polymer size for MW ≥ 4200 g/mol (Fig. 4.1). At higher temperatures, the samples with MW ≥ 4200 g/mol show an exothermic transition indicating that crystallization process occurs upon heating. No signs of crystallization were observed in samples of PDMS-OH550 and PDMS-OH1100.

4.4.2. Dielectric spectroscopy

The dielectric loss ε" spectra of hydroxyl terminated PDMS with different MW are shown in Fig. 4.2. Here only the relaxation component of the spectra is displayed, as the DC conductivity contribution, largely controlled by the amount of impurities in the samples and dominating the low-frequency side of the spectra, is not shown for clarity reasons.

For the system with MW of 18000 g/mol (not included in Fig. 4.2) the relaxation pattern is practically indistinguishable from the ones displayed by PDMS-OH4200 (Fig. 4.2 c) or PDMS-OH139000 (Fig. 4.2 d): The dielectric loss is dominated by the structural relaxation (α-) peak that enters the investigated frequency window from the high-frequency side at temperatures close to 160 K. By lowering temperature, the characteristic frequency of the α-peak shifts to lower values as the overall dynamics slow down. A high-frequency tail of the α-peak is visible in spectra recorded in the deeply supercooled state. The presence of this so-called "excess wing"[240] was previously reported for the methyl terminated PDMS.[241] Regarding slow dynamics, for all samples with MW ≥ 4200 g/mol a weak spectral feature occurs on the low-frequency flank of the main peak. One example is given by the spectrum recorded at 158 K (Fig. 4.2 c). Such low-frequency processes were previously reported for PDMS and polystyrene[241] and were attributed to impurities. Please note that both PDMS and polystyrene are classified as type-B

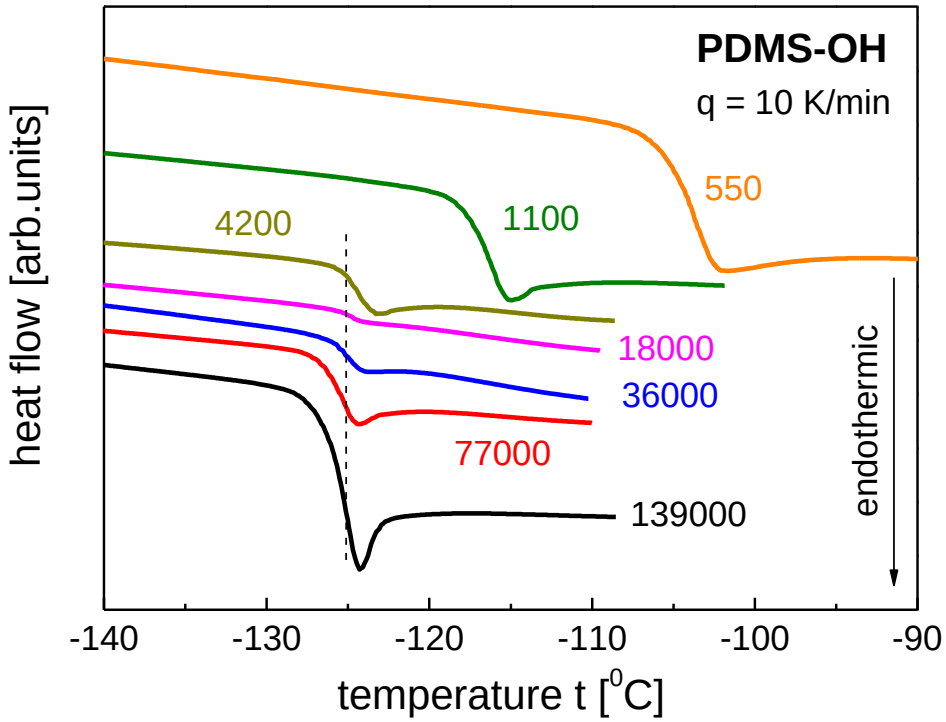

Figure 4. 1. Calorimetric curves recorded on heating of PDMS-OH with a constant rate q = 10 K/min. The numbers represent MW in g/mol. The original curves have been shifted vertically for clarity. The dashed vertical line indicates that T_g does not vary much for the samples with 4200 g/mol ≤ MW ≤ 139000 g/mol.

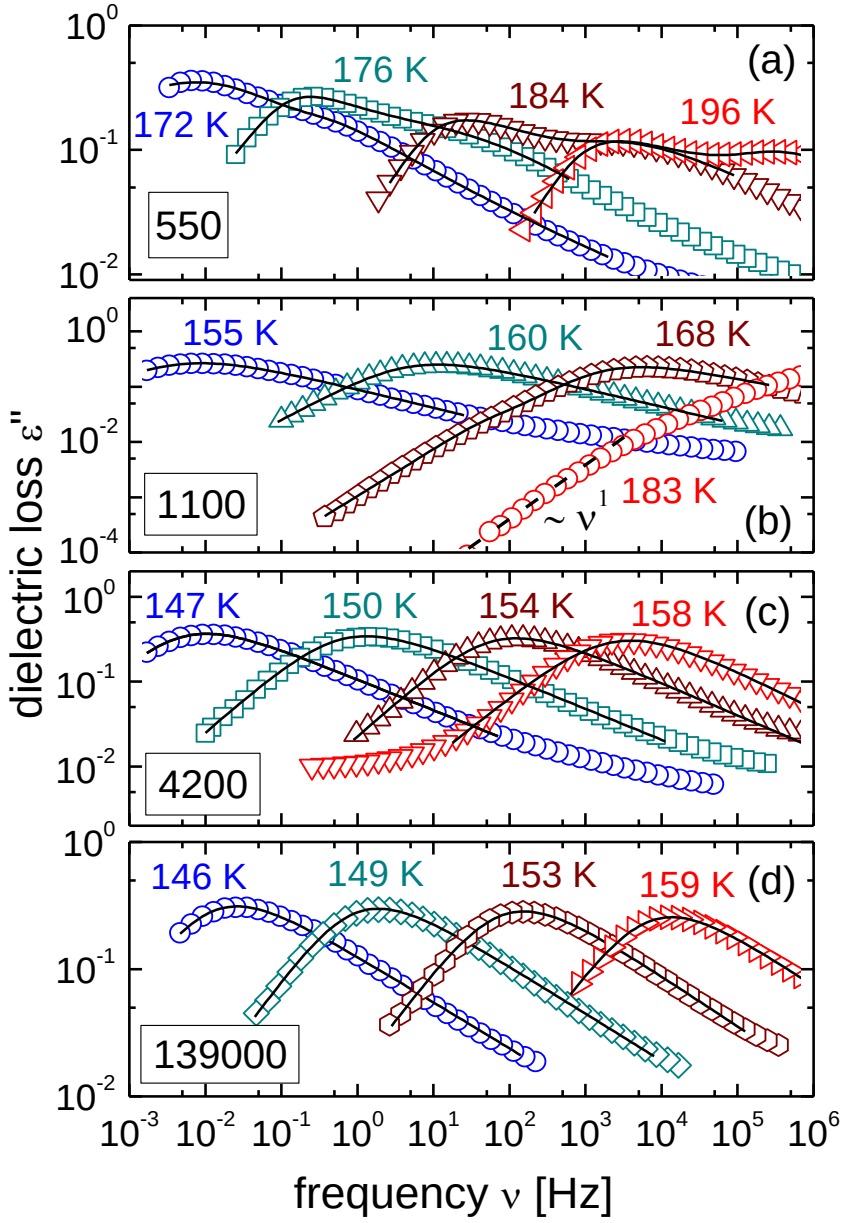

Figure 4. 2. Dielectric loss ε" spectra at several investigated temperatures for PDMS-OH with molecular weight of (a) 550 g/mol, (b) 1100 g/mol, (c) 4200 g/mol, and (d) 139000 g/mol, as indicated on the bottom left corner of each frame. The results of the fitting procedure employing Eq. 4.1 are shown as solid lines. The dashed line in (b) indicates the presence of the terminal relaxation mode characterized by $\varepsilon'' \propto \nu^1$.

polymers[110] which do not possess an end-to-end dipole moment, and the chain modes don't appear in dielectric spectra of these polymers.

These impurity-related processes are not affecting the dielectric response of PDMS-OH1100. Nevertheless, another relaxation feature emerges on the low-frequency side of the structural relaxation peak of this sample at 183 K and 168 K (Fig. 4.2 b). In the frequency range below this slow shoulder the spectrum can be described by a power-law $\varepsilon'' \propto \nu^{\lambda}$ with an exponent λ = 1 which indicates the low-frequency end of the relaxation processes. The dielectric response becomes even more complex for PDMS-OH550, as the spectra reveal two well distinguishable loss peaks (Fig. 4.2 a). For temperatures close to 200 K the two processes have similar strength and are separated in frequency by two orders. Upon cooling the slower process increases in amplitude, largely covering the contribution of the faster process close to T_g.

To parameterize such spectra a common approach is to employ a superposition of two Havriliak-Negami (HN) functions[242] accounting for the contribution of two relaxation processes. We indicate by the indices "I" the slow process and "II" the fast one:

$$\varepsilon''(\nu) = \mathrm{Im}\left\{ \frac{\Delta\varepsilon_{\mathrm{I}}}{\left[1+\left(2\pi i\nu\tau_{\mathrm{I}}\right)^{\alpha_I}\right]^{\gamma_1}} + \frac{\Delta\varepsilon_{\mathrm{II}}}{\left[1+\left(2\pi i\nu\tau_{\mathrm{II}}\right)^{\alpha_{II}}\right]^{\gamma_{II}}} \right\}. \tag{4.1}$$

Here $\Delta\varepsilon$ denotes the relaxation strength, τ the characteristic time, ν the measuring frequency, and the parameters α and γ describe the shape of the relaxation peak: for α = 1 and γ < 1 the terms in the right hand side of Eq. 4.1 reduce to Cole-Davidson[243] functions, for α < 1 and γ = 1 to Cole-Cole functions,[110] while for α = γ = 1 a Debye relaxation (a single exponential relaxation) is recovered. The time constant that corresponds to the maximum of the loss peak can be estimated using the Eq 2.10.[242] For PDMS-OH550 and PDMS-OH1100 at high temperatures the fitting procedure involved two HN functions, while for the systems with MW ≥ 4200 g/mol a single term ($\Delta\varepsilon_I$ was fixed to zero in Eq. 4.1) is sufficient to fit the loss peak close to its maximum (Figs. 4.2 c, d).

For PDMS-OH550 $\alpha_I \approx \alpha_{II} \approx 1$holds, while γ_{II} displays a weak temperature dependence and stays below 0.6 in the entire investigated temperature range. On the other hand, γ_I is about 0.2 at T = 200 K and monotonically increases up to 1 down to T = 172 K.

4.4.3. Shear rheology

Small-amplitude shear oscillation experiments were performed to investigate the influence of H-bonding on the mechanical behavior of low-MW PDMS-OH. We were not able to find literature data on the mechanical response of short PDMS in its supercooled regime. So, to reveal the role of H-bonding in mechanical processes we measure and compare the shear behavior of PDMS-OH and of PDMS-H450.

The rheological response of PDMS-H450 (Fig. 4.3 a) shares many characteristics usual for simple liquids[218, 244]: Deep in the supercooled regime the loss modulus is dominated by the structural peak with the frequency of the maximum marking the transition from elastic (at higher ν) to viscous (at lower ν) regime. A terminal relaxation[245, 246] characterized by the relation $G''(T,\nu) = A(T)\nu^{\lambda}$ with $\lambda = 1$ sets in at frequencies below the peak maximum (Fig. 4.3 a). Using the trivial relation between viscosity and modulus $G^*(\nu) = i2\pi\nu\eta^*(\nu)$ one can easily demonstrate that the proportionality constant $A(T)$ determines the value of the static viscosity η_0 characterizing the macroscopic flow:

$$\eta_0(T) = \left.\frac{G''(T,\nu)}{2\pi\nu}\right|_{\nu\to 0} = \frac{A(T)}{2\pi}. \qquad (4.2)$$

Comparing the results for PDMS-H450 and PDMS-OH550 (Figs. 4.3, 4.4) one could directly observe the influence of the end groups on the mechanical response. First of all, the large temperature shifts (Fig. 4.3) indicate that H-bonding leads to a tremendous slowing down of the segmental dynamics. Moreover, the degree of separation between the loss maximum and the onset of terminal mode becomes significantly larger for PDMS-OH550 (Fig. 4.4), suggesting the emergence of additional spectral contributions at intermediate frequencies. The

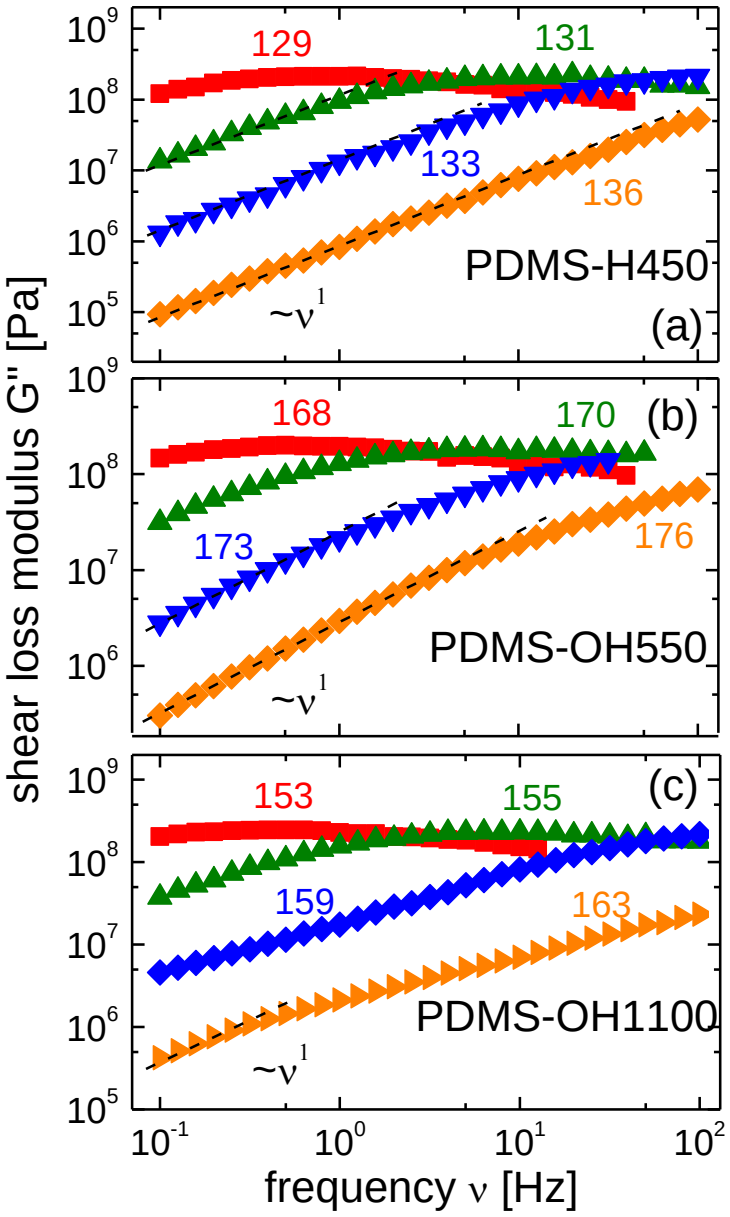

Figure 4. 3. Frequency dependent shear loss modulus *G*”(*v*) measured for (a) PDMS-H450, (b) PDMS-OH550, and (c) PDMS-OH1100 at several selected temperatures indicated by the numbers (in Kelvin units). The dashed lines represent a linear increase of *G*” with frequency, as expected for the terminal relaxation mode.

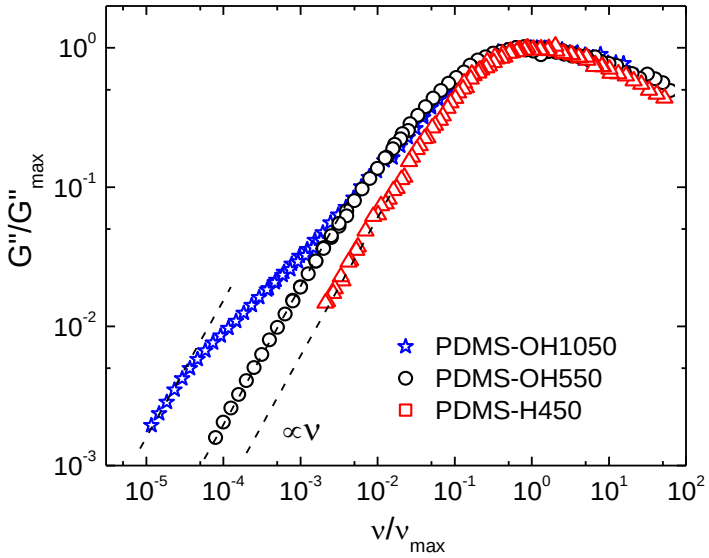

Figure 4. 4. Mechanical relaxation spectra obtained using time-temperature superposition for OH- and H-terminated samples. An additional low-frequency mode is obvious in OH-terminated PDMS. The dashed lines show the terminal relaxation end of the spectra.

separation between structural relaxation and the low-frequency terminal region becomes even more prominent for PDMS-OH1100 (Fig. 4.4).

4.5 Discussion

4.5.1. Influence of H-bonding on segmental dynamics

To reveal the role of end-chain hydrogen bonding we compare our dielectric relaxation time data to literature data on methyl terminated PDMS.[241] Analysis of the data revealed tremendous slowdown of structural relaxation due to H-bonding, especially in low-MW samples (Fig. 4.5). The effect of H-bonding decreases strongly with increase in MW and essentially disappears for PDMS with MW>3000-4000 g/mol. It is interesting that segmental dynamics of OH terminated PDMS slows down with decrease in MW, in contrast to usual acceleration of dynamics, as observed e.g. for methyl terminated PDMS (Fig. 4.5).

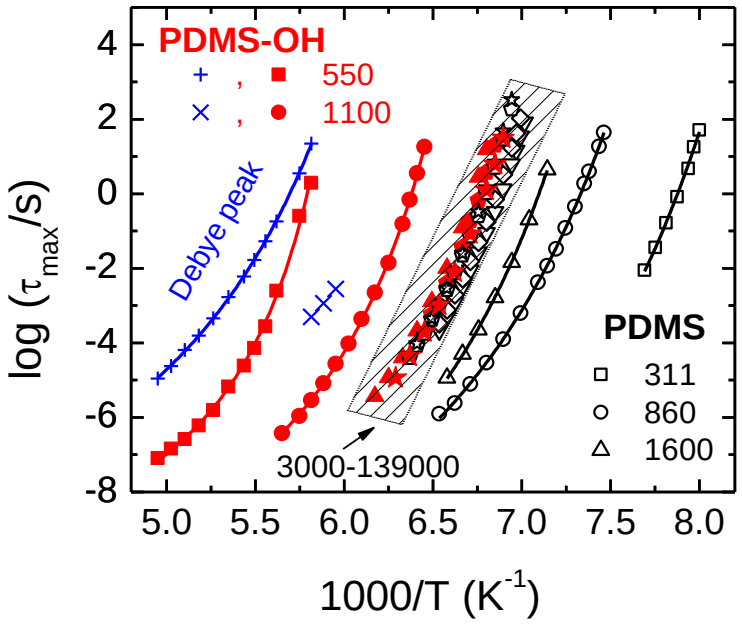

Figure 4. 5. Arrhenius plot of the dielectric time constants corresponding to the α-process for PDMS-OH (red, filled symbols, this work) and methyl terminated PDMS (black, open symbols, taken from Ref. [241]). The time constants of Debye peak for PDMS-OH550 and PDMS-OH1100 are also included as blue crosses. The numbers represent MW in g/mol units. The dashed area marks the data obtained for all PDMS-OH and PDMS systems with MW in the range 3000–139000 g/mol. Solid lines are the VFT fits (Eq. 1.2).

To quantify the temperature dependence of τ_{max} we fit the data in Fig. 4.5 using the Vogel-Fulcher-Tammann (VFT) relation (Eq. 1.2). The VFT parameters τ_0, B, and T_0 obtained from the fits are included in the Table 4.1. By extrapolating the VFT to τ_{max} = 100 s we extracted the dielectric glass-transition temperature $T_{g,diel} = T\big|_{\tau_{max}=100s}$ (Table 4.1). The results for $T_{g,diel}$ are very similar to those obtained for $T_{g,cal}$ from DSC measurements (Fig. 4.6).

The molecular weight dependence of T_g for hydroxyl-terminated PDMS is compared with earlier data for methyl terminated PDMS[241, 247, 248] in Fig. 4.6 a. As the degree of polymerization increases, T_g of methyl terminated PDMS increases and saturates at high MW. This behavior is usual for polymers. In contrast, T_g of hydroxyl terminated PDMS increases strongly as MW decreases. It is interesting that the molecular weight dependence of T_g seems to be saturated

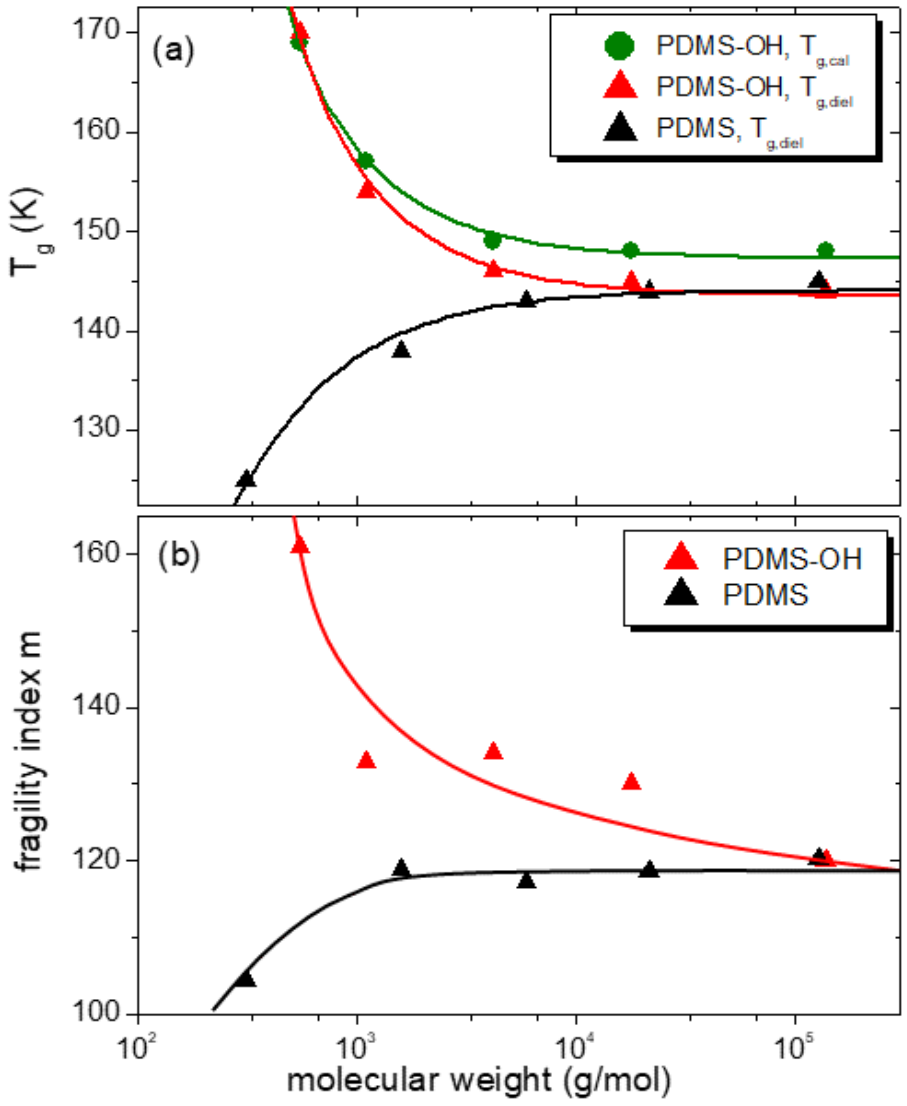

Figure 4. 6. Molecular weight dependence of T_g (a) and fragility index *m* (b) in methyl terminated PDMS (black filled triangles, data from Ref. [241]), and in PDMS-OH (red triangles – dielectrics, green circles – DSC). Lines are guides for the eye.

at the same MW, regardless of the end groups. Moreover, the effect of H-bonding disappears at the same MW (Fig. 4.6 a).

Such an abnormal MW dependence is also displayed by the fragility index *m* that quantifies the steepness of the temperature dependence of the structural relaxation time at T_g.[249] This parameter can be estimated using the results obtained from the VFT fit according to Eq. 1.3 and 1.4. The fragility index increases with MW for methyl terminated PDMS (Fig. 4.6 b), following the usual trend for polymers.[98] In contrast, fragility of the hydroxyl terminated PDMS decreases with MW (Table 4.1, Fig. 4.6 b). According to the generalized entropy theory,[250] fragility of segmental relaxation can be ascribed to frustration in molecular packing. Apparently, chain end hydrogen bonding frustrates the packing of PDMS, especially for short chains that might be pinned by the chain ends.

Segmental dynamics in low-MW OH-terminated PDMS is significantly slower than the dynamics in high-MW PDMS (Fig. 4.5). Apparently, hydrogen bonding plays much larger role in slowing down dynamics at lower temperatures (T_g of PDMS is significantly lower than its counterpart for PPG). Another reason for the larger effect in PDMS can be a *micro*phase separation (see also the discussion below). Polar OH groups most probably separate from hydrophobic PDMS chains, forming small clusters. This might additionally restrict segmental motion in short PDMS chains. In contrast, no significant chain end segregation is expected in PPG.

4.5.2 Dielectric Debye process in low-MW PDMS-OH

Hydroxyl chain ends in low-MW PDMS not only affect T_g and fragility, but they also affect the low-frequency regime in both dielectric and mechanical relaxation spectra (Fig. 4.2, 4.3). From the viscoelastic perspective, this slower process could be ascribed to a chain-like relaxation in associating PDMS molecules. However, this explanation is inconsistent with the dielectric data. There are type A polymers[110, 111] (e.g. PPG, polyisoprene) where the dipole moment accumulates along the chain and the chain relaxation (normal mode) is visible in the dielectric spectra. PDMS does not belong to this class of polymers, and the chain modes are not

dielectrically active. Thus, the slow dielectric relaxation mode cannot be ascribed to the chain modes of associated PDMS.

There are several groups of low molecular weight H-bonding liquids that exhibit in their dielectric spectra a process slower than structural relaxation. These systems include monoalcohols (MA),[107] secondary amides,[106, 251] several pharmaceuticals[252-254] and protic ionic liquids.[255, 256] This process has a Debye-like shape and is widely accepted to be a signature of polarization fluctuations attributed to the transient supramolecular structures formed by H-bonding in these liquids. Largely supported by the results of computer simulations[257-261] and scattering experiments[262-266] another general agreement emerges that, at least for MA and secondary amides[267-269] these supramolecular aggregates have a quasi-linear structure, with the polar groups associating into a polymer-like backbone surrounded by the non-polar parts of the molecules radiating outwards.

Among all H-bonding liquids investigated so far, the Debye-like process was reported for systems formed by molecules with a singular H-bonding center, and to our knowledge has never been reported for polyalcohols. For example, this process dominates the dielectric response of *n*-propanol, but is absent for propylene glycol or glycerol. For the systems considered in the present study, even the lowest molecular weight sample PDMS-OH550 has hydroxyl end groups separated by about 7 monomers. This exceeds the persistence length of PDMS,[222] and thus may be considered as a relatively large distance. Is it possible that the slow dielectric process is the same Debye-like process formed by hydroxyl end groups association? The composite spectra displayed in Fig. 4.2 a suggests that this is indeed the case. Actually, the dielectric response of PDMS-OH550 is in many aspects very similar with the one observed for associating MAs such as 4-methyl-3-heptanol[270] or 2-buthyl-1-octanol.[271]

Analysis of the dielectric spectra reveals that the slow process gains amplitude and approaches the faster process as temperature decreases. The ratio of their relaxation strengths and of their relaxation times vary from $\Delta\varepsilon_I/\Delta\varepsilon_{II} \approx 3.5$ and $\tau_{max,I}/\tau_{max,II} \approx 135$ at $T = 212$ K to $\Delta\varepsilon_I/\Delta\varepsilon_{II} \approx 5.3$ and $\tau_{max,I}/\tau_{max,II} \approx 109$ at $T = 172$ K, respectively. This tendency of merging for the two processes and the increase in the amplitude of the slowest relaxation mode upon cooling

are reported in many works analyzing the dielectric characteristics of Debye liquids.[107] The fit of the spectra to the Eq. 4.1 indicates that for PDMS-OH550 both processes have Cole-Davidson spectral shapes ($\alpha_{\mathrm{I}} \approx \alpha_{\mathrm{II}} \approx 1$) in the entire investigated temperature range. The Cole-Davidson stretching parameter for the fast process γ_{II} has weak temperature dependence and stays below 0.6 in the entire investigated T range. On the other hand, for the slow process γ_{I} is about 0.2 at temperatures around 200 K and increases strongly with lowering T, reaching a value close to 1 for T = 172 K. Besides the overall evolution of the entire spectra, the Debye-like shape of the slow process close to T_g indicates that this relaxation is indeed similar in nature with the Debye process observed for MAs.

In the absence of H-bonding, the dielectric spectra of PDMS-H450 exhibit a single Cole-Davidson peak associated with the structural relaxation (Fig. 4.7 a). Comparison of this spectrum to the spectra of PDMS-OH550 (Fig. 4.7 a, for clarity the frequency axis for PDMS-H450 was multiplied by 133 and the y-axis was divided by 7.3) support our assignment of the faster process to structural relaxation, and the slow mode to the relaxation of H-bonded networks. Interestingly, a non-negligible contribution of the Debye process persists even when the concentration of hydroxyl groups is reduced by about half by increasing PDMS molecular weight from ~550 to 1100 (Fig. 4.7). To emphasize the influence of hydrogen bonding, we compared in Fig. 4.7 b the spectrum of PDMS-OH1100 measured at 172 K with two other spectra taken from literature[241, 272] for methyl-terminated PDMS with similar MW, namely 800 g/mol (PDMS800) and 1600 g/mol (PDMS1600). For these two systems the spectra were chosen so that the characteristic frequencies of the α-peaks are in proximity of the maximum for the dielectric loss of PDMS-OH1100. To match the peak maxima, the frequency axis and the loss axis for PDMS800 were multiplied by the factors 3 and 1.25, respectively, while for PDMS800 a multiplication of the γ-axis with 1.4 was applied. Clearly, an additional relaxation process appears at lower frequencies in hydroxyl terminated PDMS. A *free fitting* strategy based on the eight parameters of Eq. 4.1 did not converge, as the contribution of the slow process overlaps strongly with the structural peak. However, a good fit is obtained by assuming Debye spectral shape ($\alpha_{\mathrm{I}} = \gamma_{\mathrm{II}} = 1$) for the slow process (Fig. 4.7b). In that case, however, the amplitude of the Debye peak relative to the segmental relaxation peak drops to $\Delta\varepsilon_{\mathrm{I}}/\Delta\varepsilon_{\mathrm{II}} \approx 0.02$, i.e. more than

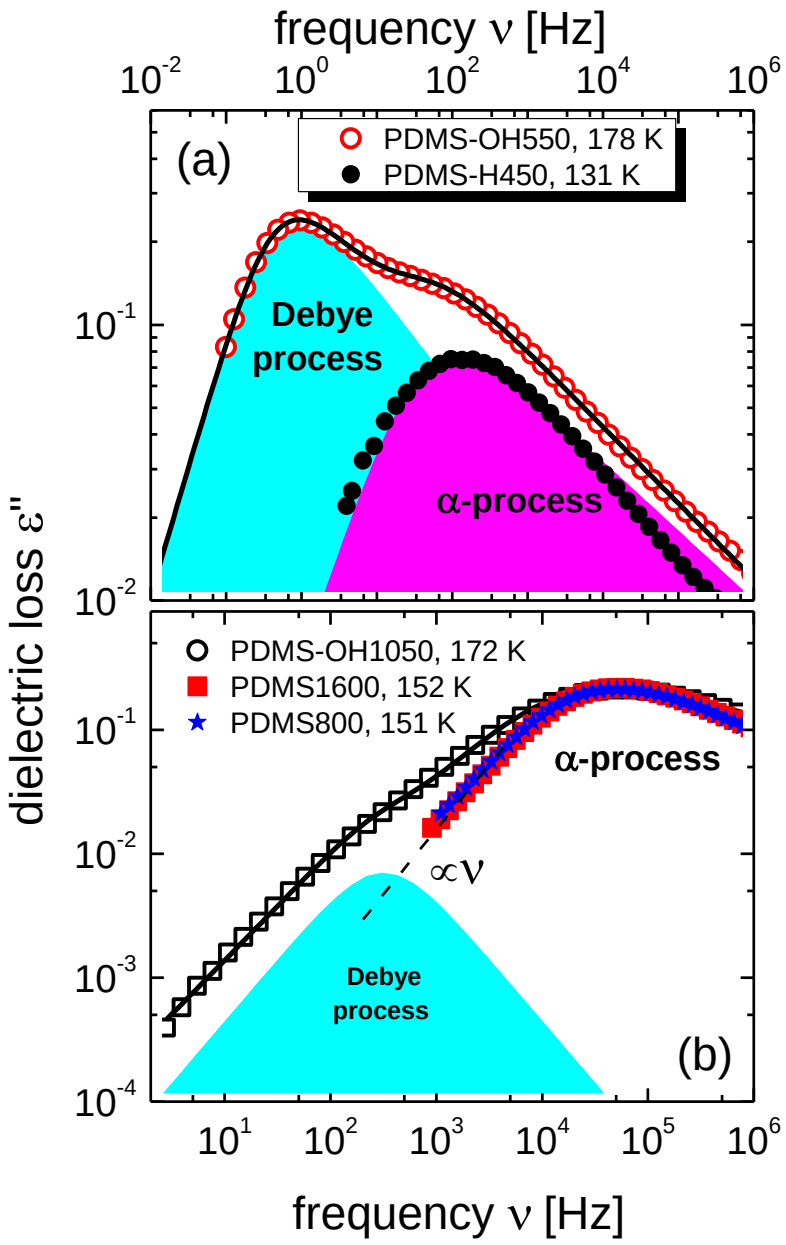

Figure 4. 7. (a) Dielectric loss ε'' spectrum of PDMS-OH550 at 178 K (open red circles) and its fit to the Eq. 4.1 (solid line). The individual contributions of the two processes obtained from the fit are highlighted by the colored areas. The loss spectrum of PDMS-H450 at 131 K is included (solid circles) for comparison. (b) Dielectric spectrum of PDMS-OH1100 (open squares) with its corresponding fit (solid line) is compared with those taken from literature for PDMS with MW of 800 g/mol (filled blue triangles) and 1600 g/mol (filled red squares). The individual contribution of the Debye peak of PDMS-OH1100 is highlighted. For comparison reasons the raw PDMS spectra were slightly shifted so the position and amplitude of the relaxation maxima match that of PDMS-OH1100. The dashed line marks the terminal relaxation region $\varepsilon''(\nu) \propto \nu$.

100 times relative to PDMS with MW=550, by far exceeding the decrease in fraction of hydroxyl groups. On the other hand, the ratio of the Debye relaxation time to the segmental relaxation time is $\tau_{max,I}/\tau_{max,II} \approx 130$ at $T = 172$ K, i.e. about the same for the longer and shorter PDMS-OH.

The performed analysis provides hints to what kinds of structures are formed in hydroxyl terminated PDMS. The H-bonding groups of PDMS-OH are located at the two ends of molecules. One possibility is formation of linear supramolecular structures with the oligomers regarded as segments in the backbone of the associated polymer (Fig. 4.8 a). Alternatively, several OH-units may phase separate and connect in a fashion similar to that of MA. In this second case the backbone is formed by the OH-groups, see Fig. 4.8 b, and the architecture of supramolecular aggregates resembles that of polymer brushes.[273] The absence of a significantly large dipole moment accumulating along the chain in the first situation (Fig. 4.8 a) and the strong analogy with the behavior of the Debye process in mono-alcohols suggest that at least for PDMS-HO550 the second structural motifs (Fig. 4.8 b) will be consistent with the results from dielectric spectroscopy.

One important conclusion of this study is that the Debye process, previously reported for systems with only one H-bonding group per molecule, can be also identified in dielectric spectra of *di*hydroxy PDMS molecules. It is important to emphasize that PDMS chains are highly flexible, with short persistence length, so double-OH terminated molecules might also form "head-to-tail" *intra*molecular H-bonds, reducing the effective number of relaxing OH-units. This could explain why the dielectric strength for these low-MW materials containing a significant amount of OH-groups is relatively low. If one OH-unit becomes part of a given associated backbone as proposed in Fig. 4.8 b, the terminal group at the other chain end could also be included in an adjacent H-bonded cluster. The stiffness of the oligomer located between these two groups can lead to a correlated motion of neighboring clusters, a situation that could also affect the amplitude of the dielectric Debye process. To better elucidate the structural foundation for such slow relaxation in associating oligomers, our dielectric results call for additional investigations with complementary techniques such as nuclear magnetic resonance[109, 274-276] or infrared spectroscopy.[107, 277]

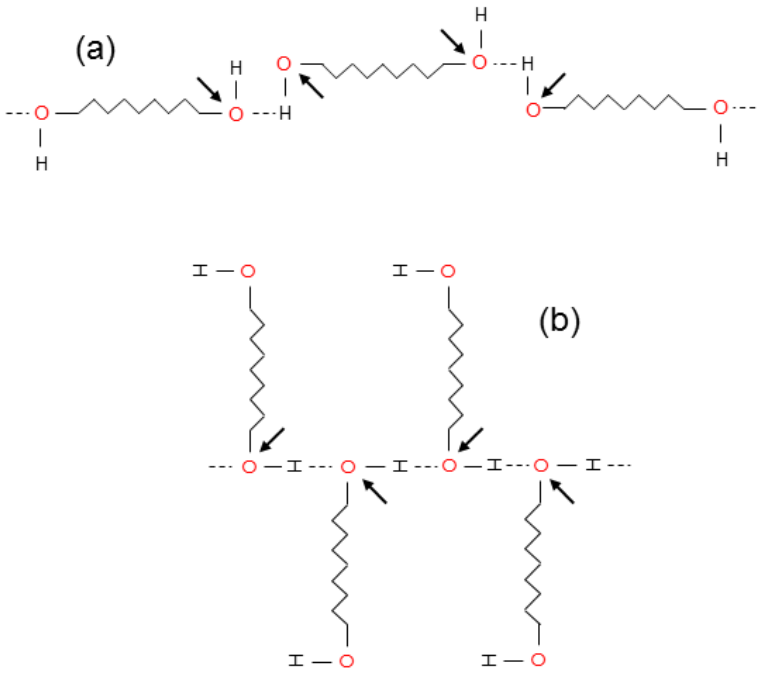

Figure 4. 8. Sketched (a) chain-like versus (b) brush-like association of PDMS-OH molecules via H-bonding (represented as dashed line) of terminal groups. The zigzags represent the PDMS chains. The arrows represent the individual dipole moments located in the proximity of the hydroxyl units.

4.5.3. Rheological signature of the H-bond associated networks in PDMS-OH

The master curves for the shear relaxation spectra (Fig. 4.9) show the so-called "glassy regime" at higher frequency, where the storage component *G*' reaches plateau values of about 10^9 Pa and the loss component *G*" is dominated by the structural relaxation peak. One important observation is that the position of the shear loss peak is close to the one of the fast dielectric processes, supporting our previous assignment that the latter is to be regarded as the α-process. At lower frequencies the shear spectra show expected terminal regime.[245, 246] The rheology data reveal that the structural relaxation peak is separated from the terminal relaxation by about two orders of magnitude for PDMS-OH550 and about four orders of magnitude for PDMS-OH1100 (Fig. 4.9).

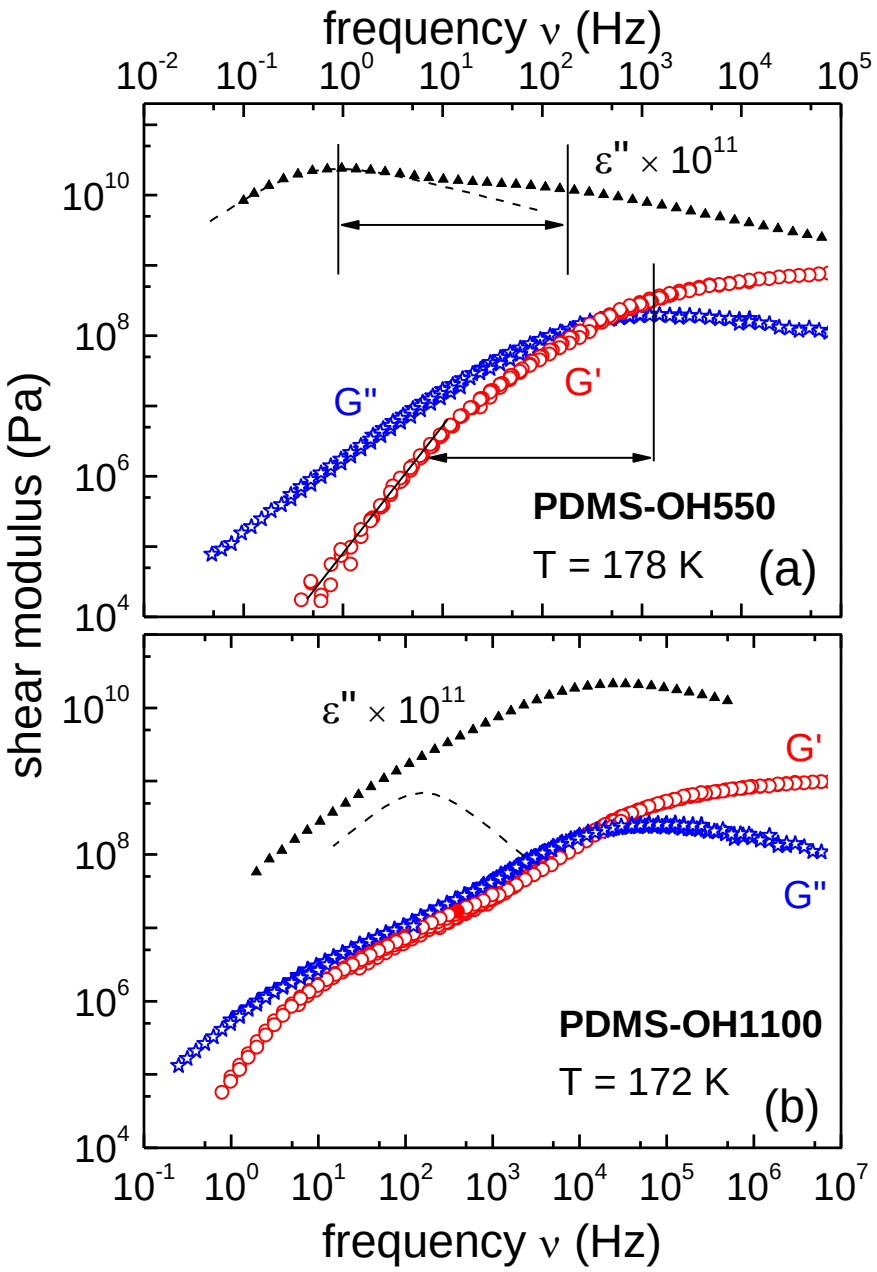

Figure 4. 9. Master curves obtained for mechanical relaxation spectra using time-temperature superposition, and dielectric loss spectra for two short hydroxyl-terminated PDMS. The dielectric contribution of the Debye modes is indicated by the dashed lines. The low-frequency mode appears in both viscoelastic and dielectric spectra at (a) approximately the same distance from the structural relaxation for PDMS-OH550 and (b) at larger separation for the first with respect to the latter for PDMS-OH1100.

It is tempting to ascribe the low frequency mode to the chain relaxation. However, as we discussed above the dielectric data exclude this possibility for PDMS-OH550, where the low-frequency mode appears to be similar in both dielectric and mechanical spectra (Figs. 4.9a). Apparently, the slow rheological mode, similar to the dielectric Debye process, reflects the same supramolecular relaxation. Indeed, recently it was demonstrated that the Debye process in small H-bonding liquids is not merely a dielectric feature, but can be also detected by other experimental methods including light scattering[255] and rheology.[255, 278] Similar to dielectric spectroscopy, the response probed by these complementary techniques reveals the presence of additional relaxations at frequencies lower than those corresponding to the structural relaxation. In MAs, for example, it was demonstrated that this supra-molecular rheological contribution is comparable to that of short-chain polymers and that the H-bonding in these liquids enhances viscosity up to a tenfold.[278] Analyzing the values of the macroscopic viscosity in terms of, *e.g.*, Rouse model one is able to estimate the *effective* molecular weight of the transient H-bonded clusters, which for MAs can comprise about ten molecules close to the glassy state.[255, 278]

On the other hand, Fig. 4.9 b reveals that for PDMS-OH1100 the terminal mechanical relaxation is much slower than the dipolar Debye process. The presence of this slow mode in the dielectric spectra indicates that brush-like structures (Fig. 4.8 b) may still form. However, its low amplitude suggests that the amount of such structures is very low for this oligomer. At the same time, the shear spectra (Fig 4.9 b) show much lower frequency of the terminal mode, suggesting formation of linear aggregates (Fig. 4.8 a) for PDMS-OH1100. To estimate the *effective* molecular weight M_{eff} of chain-like structures in PDMS-OH1100, we followed previous considerations[255, 278] and used the Rouse model[245, 246] as the simplest theoretical approach. This model connects M_{eff} with the values for steady shear viscosity η_0 and characteristic frequency of the terminal mode ν_R via the relation:

$$M_{eff} = \frac{\pi \rho RT}{12 \nu_R \eta_0} \tag{4.3}$$

where ρ is the mass density, R the ideal gas constant, and T the temperature. For our analysis we determined η_0 and ν_R using raw (unscaled) viscosity data $\eta'(\nu) = G''(\nu)/(2\pi\nu)$ recorded at 166 K for PDMS-OH1100 (Fig. 4.10). As indicated by the dashed lines in Fig. 4.10, η_0 represents the low-frequency plateau of viscosity, while ν_R is the frequency at which the ν-dependence sets in. With ρ = 965 kg/m^3, $\eta_0 = 1.47 \times 10^5$ Pas and ν_R = 0.32 Hz, one obtains by employing Eq. 4.3 $M_{eff} \approx$ 7500 g/mol. Based on this estimate we may conclude that close to T_g the supramolecular linear polymers include about 7 PDMS-OH1100 repeating units.

Based on the above results, we propose the following picture. Relatively high concentration of hydroxyl groups in the melt of short hydroxyl-terminated PDMS chains (MW~550) leads to a microphase separation and formation of brush-like structures (Fig. 4.8 b). Their presence is obvious from the low-frequency Debye-like mode in the dielectric spectra (Fig. 4.7). This low-frequency mode decreases in amplitude (relative to the segmental mode) and is getting broader with temperature increase, suggesting a decrease in the number of these brush-like structures and broadening distribution of the number of associated molecules in these structures. This is consistent with both the decrease of H-bonding effects with temperature increase and an increase in miscibility of hydroxyl groups at high T. In contrast, the Debye-like process appears very weak in the melt of hydroxyl-terminated PDMS with MW~1100, suggesting almost 100 times lower concentration of the brush-like structures. At the same time rheological data suggest formation of transient linear supramolecular structures with ~7 molecules at temperatures close to T_g in melts of PDMS-OH1100. Apparently, a decrease in microphase separation in longer chains favors formation of long transient chains (Fig. 4.8 a), instead of brush-like structures.

4.6 Conclusions

In this work we studied the influence of chain end hydrogen bonding on dynamics of PDMS. Our analysis reveals that hydrogen bonding leads to an inversion of the classical molecular weight dependence of segmental relaxation and T_g: segmental dynamics of hydroxyl-terminated PDMS slows down and T_g increases with decrease in MW. This is a surprising result

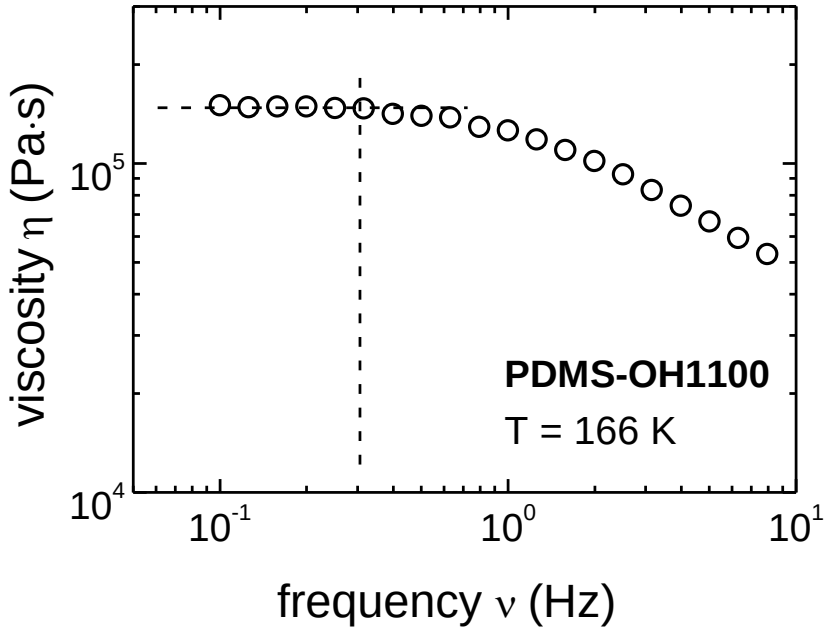

Figure 4. 10. Frequency dependent viscosity used for the estimation of the effective size of H-bonded structures in PDMS-OH1100. Horizontal and vertical dotted lines correspond to static viscosity η_0 and the terminal characteristic frequency ν_R, respectively, see text for details.

because hydrogen bonding in PPG leads to essentially molecular weight independent segmental dynamics. Apparently, H-bonding plays a significantly stronger role in PDMS. This might be also related to a microphase separation of hydroxyl groups in this system. In addition, hydrogen bonding in shorter PDMS affects both dielectric and mechanical relaxation spectra. Detailed analysis of the dielectric relaxation spectra suggest that the slow process has similar microscopic origins as the Debye process discussed for small molecular H-bonding liquids. This suggests formation of brush-like structures in the melt of short OH-terminated PDMS chains. Our results demonstrate that hydroxyl terminated PDMS oligomers can be added to the already large family of Debye systems. The comparison between the dielectric and mechanical spectra reveals an interesting change in architecture of H-bonded clusters: they change from brush-like at low MW to chain-like with increasing the MW of associating oligomers. Analyzing the shear

terminal mode, we estimate that close to the glass transition the chain-like structures include about 7 oligomers in the melt of PDMS-OH1100. Our results suggest that by changing molecular weight various architectures of supramolecular assemblies can be achieved.

Chapter V

Hydrogen-bond Strength Changes Network Dynamics in Associating Telechelic PDMS

Reproduced in part from: Kunyue Xing, Martin Tress, Pengfei Cao, Shiwang Cheng, Tomonori Saito, Vladimir N Novikov, Alexei P. Sokolov. "Hydrogen-bond strength changes network dynamics in associating telechelic PDMS" *Soft Matter* 2018, 14 (7), 1235-1246. Kunyue Xing contributed to material design and synthesis, BDS, DSC and rheology measurements, data analysis and writing. Pengfei Cao and Tomonori Saito contributed to material design, Martin Tress, Shiwang Cheng and Vladimir Novikov contributed to data analysis and writing. Alexei Sokolov led the project, contributed to data analysis and writing.

5.1 Introduction

To efficiently design functional materials of supramolecular polymers with specific application, it is important to understand its dynamics at two levels that are defined by 1) the lifetime of the sticker association and 2) the segmental relaxation time of the transient or permanent polymer backbones. There are several factors that affect the dynamics of supramolecular polymer systems: the lifetime, strength, number density and the distribution (whether located at chain ends or along the polymer chain) of associating motifs, the states of the supramolecular polymer systems (*e.g.* in melts, dilute solutions, or concentrated solutions), the molar mass of the precursor polymer and whether it's above or below the entanglement MW. Although there's various models developed as introduced in Chapter 1, the systematic investigation of the segmental and chain relaxation, and glass transition temperature of supramolecular system in melts is quite rare. To fill this gap, we designed PDMS based telechelic supramolecular systems with varied H-bonding end groups and different chain molecular weight (all below entanglement MW) in melt state.

Here, we combined mechanical and dielectric spectroscopy to study the macroscopic and molecular dynamics in telechelic poly(dimethylsiloxane) (PDMS) of several chain lengths forming supramolecular networks. Two different end groups, i.e. amine-terminated PDMS (PDMS-NH_2) and amide acid terminated PDMS (PDMS-NHCO-COOH), were investigated and also compared with previous results of methyl terminated[241] and OH-terminated[233] PDMS. Despite their similarities in main chain length and chemistry, these systems exhibit some qualitative differences in their supramolecular network formation. Particularly the PDMS-NHCO-COOH reveals an outstanding feature: though consisting of only one species of terminal group its characteristics resemble a dual network with two types of connections, namely transient (temporary) and effectively permanent bonds. This unique behavior seems to be enabled by strong phase segregation of most of the end groups which form the effectively permanent associates while a certain fraction remains in rather loose, non-segregated associates (possibly dimers) which can perform transient stress relaxation.

5.2 Methods

5.2.1 Differential Scanning Calorimetry (DSC)

DSC measurements were performed using the Q-1000 DSC calorimeter from TA Instruments. All samples were dried in a vacuum oven at 313 K for 5 days before the experiment, then were hermetically sealed in aluminum pans with an empty pan as reference. For the DSC measurements, samples were equilibrated isothermally at 363 K for 5 min, and cooled down to 113 K, then heated back to 363 K with a scan rate of 10 K/min. The cooling and heating cycles were repeated twice to confirm the reproducibility of the results. Generally, T_g was taken as the midpoint of the heat flow step in the heating cycle.

5.2.2 Broadband Dielectric Spectroscopy (BDS)

BDS in the frequency range 10^{-2}–10^{7} Hz was employed using a Novocontrol system that includes an Alpha-A impedance analyzer and a Quatro Cryosystem temperature control unit. The samples of PDMS-NH_2 were placed in a parallel-plate dielectric cell made of sapphire and

invar steel with an electrode diameter of 12 mm (as shown in Fig. 2.6 b). A capacitance of 20 pF was obtained for the empty cell which yields an electrode separation of 49 µm. Further information on this cell can be found elsewhere[238]. The samples of PDMS-NHCO-COOH were placed between two gold-plated electrodes separated by a Teflon spacer of 34.4 µm thickness (as shown in Fig. 2.6 a). To prevent crystallization all samples were quenched from room temperature to about 113 K and reheated to 10 K below the glass-transition temperature T_g prior to the measurements. After each temperature increase the samples were equilibrated for at least 15 minutes to achieve a thermal stabilization within 0.2 K.

5.2.3 Shear rheology

Linear viscoelastic properties were measured by an AR2000ex rheometer (TA instrument) through small amplitude oscillatory shear measurements in stress-controlled regime. Three different geometries were involved depending on the level of the shear modulus. For glassy modulus and glassy dynamics, we use a pair of parallel plates of 4 mm in diameter while parallel plates of 8 mm in diameter were employed for the rubbery plateau and the onset of terminal relaxation. The gaps for parallel plate geometries were fixed to 500 µm. In the glassy regime, a strain amplitude of 0.03 % corresponding to an angular displacement of 150 mrad was used, which is larger than the rheometer resolution of 25 nrad. Checks of the stress and strain wave functions verified a sinusoidal shape during the frequency sweeps. For the measurements of the terminal regime, we used a conical plate of 25 mm in diameter with a cone angle of 2° and a truncation of 58 m. Before each measurement, a thermal stabilization of 10 minutes was performed to assure thermal equilibrium. For all linear viscoelastic measurements, the temperature was stabilized within 0.2 K.

Temperature sweep tests in oscillatory shear mode were employed to study mechanical transitions with respect to temperature in the range of 147 K to 243 K with a temperature ramping rate of 1 K/min and an angular frequency of 1 rad/s. Parallel plates of 4 mm and 8 mm in diameter were employed for measurements from 147 K to 173 K and from 165 K to 233 K, respectively. A cone-plate of 25 mm in diameter, 2° in cone angle, and 58 µm in truncation was applied for measurements from 173 K to 243 K. The amplitude of oscillation is set to be close to

0.05 % at temperatures close to 147 K, and gradually increased to 1 % at temperatures above 223 K.

5.3 Results & discussion

5.3.1 Differential Scanning Calorimetry (DSC)

The PDMS-NH_2 samples exhibit a clear step at about 150 K associated with the glass transition (Fig. 5.1 a). Pronounced signs of crystallization appear in the PDMS-NH_2-74 sample on heating at ~210 K, followed by a melting peak at ~230 K. The latter agrees with PDMS T_m. Crystallization was more obvious in BDS and rheological measurements due to slower heating rate in these cases. DSC data of the PDMS-NHCO-COOH samples revealed two steps (Fig. 5.1 b): one around 150 K, and the other one around 200 K. The existence of two T_g's indicates phase separation in these samples. No signs of crystallization were observed in the DSC data of all three PDMS-NHCO-COOH samples (Fig. 5.1 b). For both PDMS-NH_2 and PDMS-NHCO-COOH, T_g increases slightly with decrease of *DP* (Table 5.1), a trend we also observed in our previous studies on PDMS-OH[233] as reported in Chapter 4 (Fig. 5.1 c). Remarkably, these three different end groups associated with different hydrogen bond strengths yield practically the same T_g in telechelic PDMS of the same molecular weight. This indicates that at T_g, the end group associations are effectively permanent compared to the structural relaxation, i.e. their life time is much longer.

5.3.2 Shear rheology

The temperature sweep tests of the storage and loss part of the shear modulus, *G*' and *G*'', respectively, between 147 K to 243 K (Fig. 5.2) reveal two steps in *G*' at around 150 K and 200 K, respectively, for PDMS-NHCO-COOH-22, indicating the activation of two major dissipative modes upon heating. The dissipative mode at low temperature of around 150 K is the glass-to-rubber transition of the PDMS as supported by the value of the modulus as well as the collapse with the calorimetric T_g. The dissipative mode at high temperature of around 200 K is consistent with the 2nd T_g observed in the DSC measurements of PDMS-NHCO-COOH-22

Table 5. 1. Total molecular weight M_n, degree of polymerization *DP*, weight fraction of end groups f_e, calorimetric (DSC) and dielectric (BDS) T_g, activation energy determined from Eq.5.3 as well as VFT parameters and fragility index *m* from the dielectric measurements of PDMS-NH_2 and PDMS-NHCO-COOH systems. The molecular weight of the -NH_2 and -NHCO-COOH end group is M_{end} = 58 g/mol and M_{end} = 158 g/mol, respectively. M_n was calculated from the *DP* and the end group molecular weight. The end group weight fraction was then estimated using the molecular weight of two end groups divided by the corresponding M_n.

Material	M_n [kg/ mol]	*DP*	f_e [wt%]	T_g (DSC) [K]	T_g (BDS) [K]	log (τ_0 [s])	*B* [K]	T_0 [K]	*m*	E_a [kJ/mol]
PDMS-NH_2	**1.74**	**22**	**6.7**	**153**	**151**	**-12.1**	**516**	**135**	**132**	**9.1 (±1)**
	3.82	**50**	**3.0**	**150**	**147.5**	**-13.5**	**657**	**129**	**125**	**7.6 (±1)**
	5.59	**74**	**2.1**	**149**	**146.5**	**-13.8**	**688**	**127**	**123**	**9.3 (±1)**
PDMS-NHCO-COOH α relaxation	**1.94**	**22**	**16.3**	**154**	**151**	**-11.8**	**484**	**136**	**137**	**13.5 (±1)**
	4.02	**50**	**7.9**	**152**	**148**	**-13.4**	**642**	**130**	**125**	**15.4 (±1)**
	5.79	**74**	**5.5**	**149**	**146**	**-13.7**	**692**	**127**	**121**	**13.7 (±1)**
PDMS-NHCO-COOH 2nd T_g	**1.94**	**22**	**16.3**	**196.5**	**193.5**	**-12.4**	**2093**	**130**	**44**	
	4.02	**50**	**7.9**	**197**	**186.5**	**-12.6**	**1905**	**130**	**48**	
	5.79	**74**	**5.5**	**193.5**	**190**	**-11.1**	**1111**	**153**	**68**	

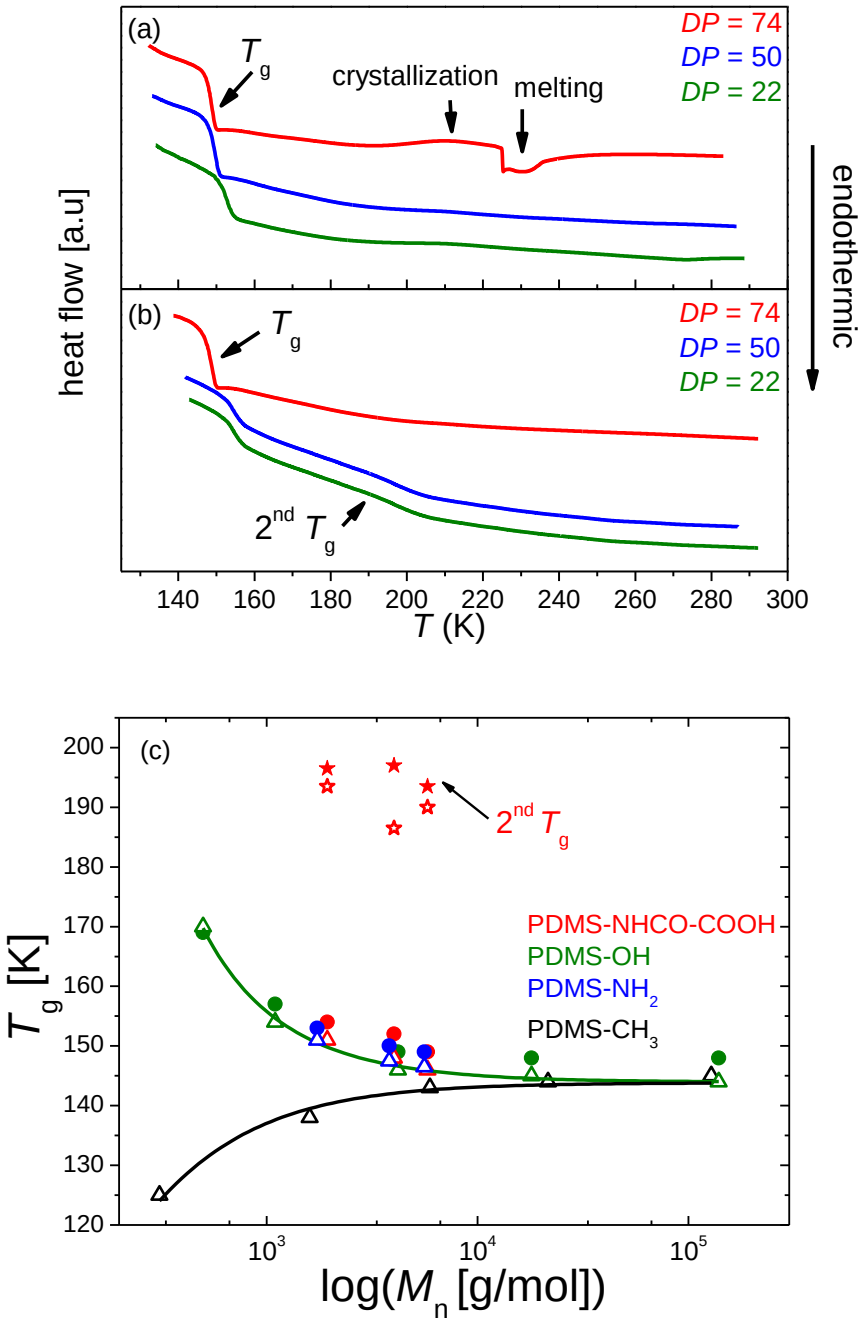

Figure 5. 1. Calorimetric heat flow curves of (a) PDMS-NH_2 and (b) PDMS-NHCO-COOH with a constant heating rate q = 10 K/min for different *DP* as indicated. The curves are vertically shifted for clarity. (c) Calorimetric and dielectric T_g (closed and open symbols, respectively) *vs* total number averaged molecular weight M_n (including end groups) in methyl-terminated (PDMS-CH_3), hydroxyl-terminated (PDMS-OH), amine-terminated (PDMS-NH_2) and amide acid terminated (PDMS-NHCO-COOH) PDMS. Dielectric T_g values were obtained by interpolating VFT fits of the segmental mean relaxation time to τ = 100 s. The green and black line in (c) are fits of the PDMS-OH[233] and the PDMS-CH_3 data[241], respectively, to the Fox-Flory equation.[279]

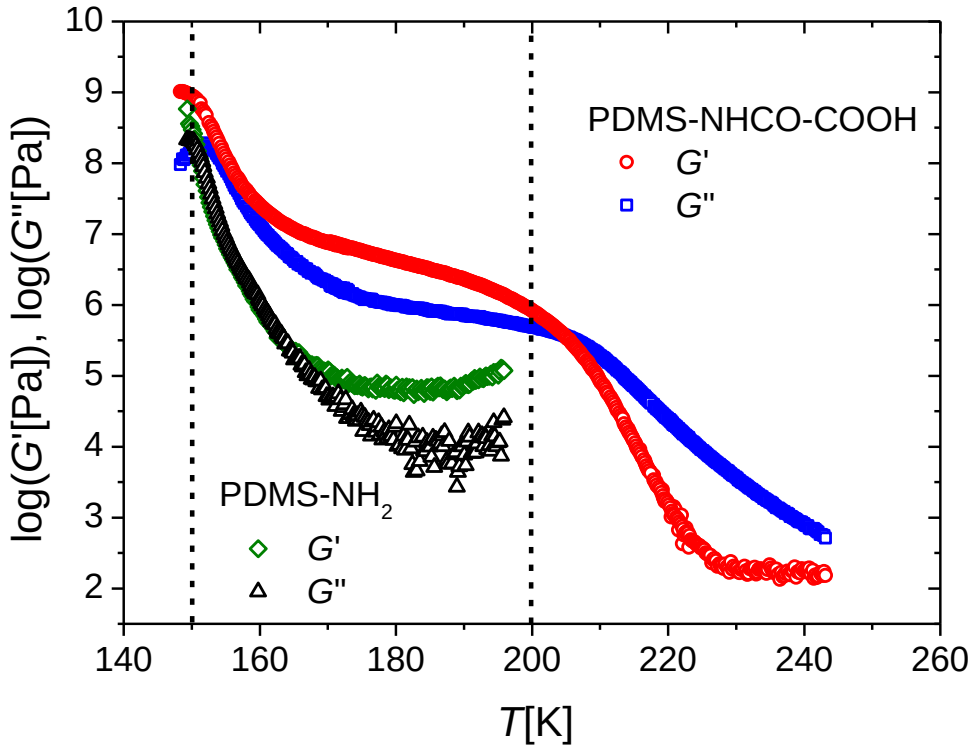

Figure 5. 2. Temperature sweep tests of the shear modulus in PDMS-NH_2-22 and PDMS-NHCO-COOH-22. Two major dissipation modes appear in the system: one starts at ~150 K and the other at ~200 K as indicated by the dashed lines. The increase in *G*′ and *G*′′ with increasing temperature at T > 180 K in PDMS-NH_2 is most likely caused by crystallization of this material.

supporting the existence of phase separation in this system. We note that the relatively high modulus of PDMS-NH_2-22 after the dissipative mode, and especially its increase with increasing temperature is most likely a result of crystallization in that system. The fact that in the DSC this barely shows up in the shorter PDMS-NH_2 samples may be due to the faster heating rate used in the DSC measurements, and also due to stress induced crystallization in the shear modulus measurements.

The shear modulus master curves of both the PDMS-NH_2 and PDMS-NHCO-COOH samples were constructed from the linear viscoelastic spectra using time-temperature superposition (TTS) (Fig. 5.3). Although TTS may not be valid due to several phenomena discussed in the following, we analyze the master curves to qualitatively deduce features of the long-time flow behavior. For all PDMS-NH_2 samples, the typical features of polymers are observed (Fig. 5.3): i) a nominal crossover of $G'(\omega)$ and $G''(\omega)$ at high frequencies with a modulus in the GPa range signifying the segmental relaxation, ii) Rouse modes following at lower frequencies, and iii) indications of a terminal relaxation. Unfortunately crystallization of these materials in the relevant temperature range limits the lower frequency data, and the characteristic signature of the terminal regime ($G'(\omega) \sim \omega^2$ and $G''(\omega) \sim \omega^1$) is obscured. Nevertheless, the transition from Rouse modes to terminal modes is evident in the master curves of all PDMS-NH_2 samples (Fig. 5.3). This onset is ~4 decades separated from the segmental relaxation which is much larger than expected for such short chains and, thus, suggests that the chains associate, forming effectively longer chains.

In contrast to this, the master curves of PDMS-NHCO-COOH show pronounced long-chain polymer behavior (Fig. 5.3): i) the crossover of $G'(\omega)$ and $G''(\omega)$ (modulus ~1 GPa, segmental relaxation), and ii) Rouse modes are followed by (iii) a lengthened rubbery plateau, and finally (iv) a terminal relaxation with clear scaling of $G'(\omega) \sim \omega^2$ and $G''(\omega) \sim \omega^1$. Clearly visible in PDMS-NHCO-COOH-50 and PDMS-NHCO-COOH-22, the additional extended rubbery plateau separates the terminal relaxation from the segmental dynamics by ~11 and ~13 orders, respectively; in case of PDMS-NHCO-COOH-74, crystallization prevents the observation of the terminal relaxation (like in the short PDMS-NH_2 samples, this may be a shear induced

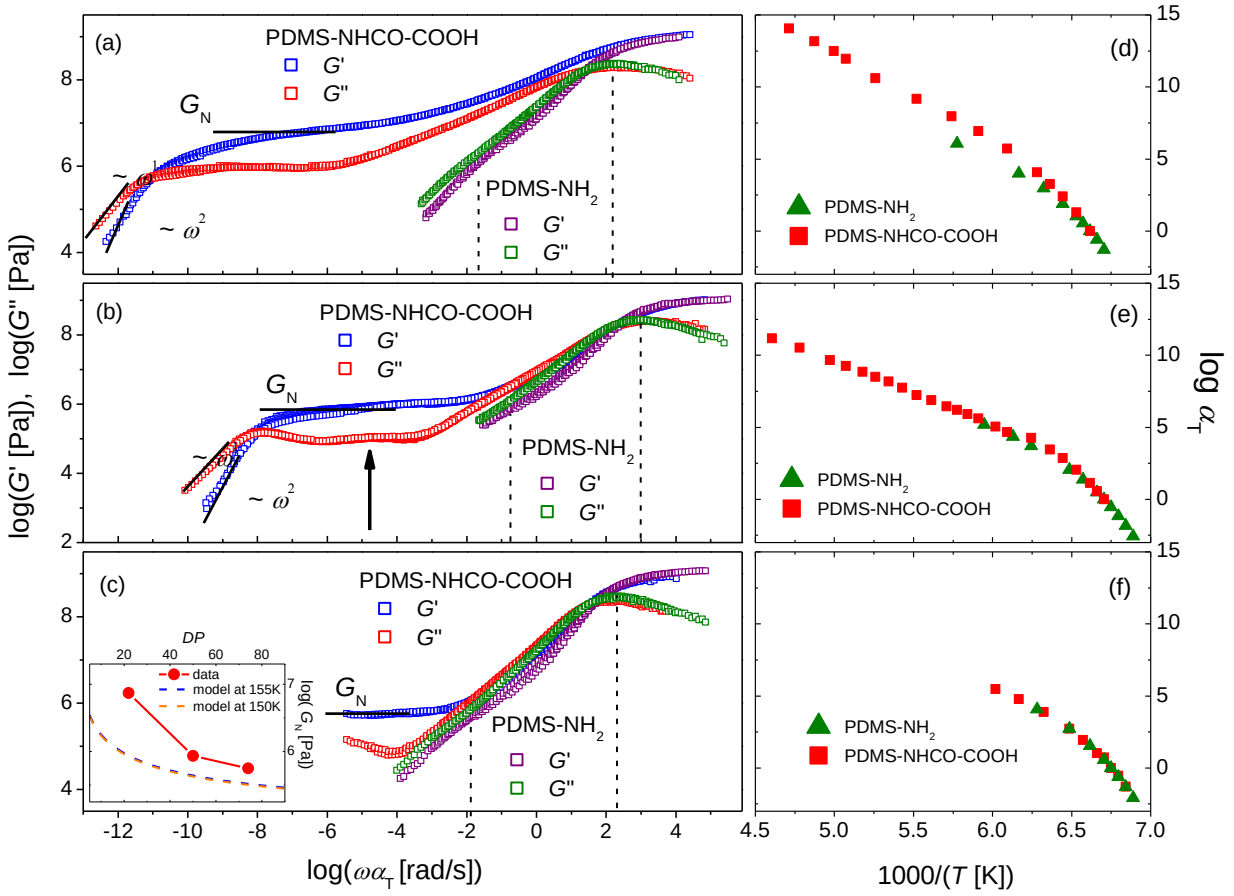

Figure 5. 3. Master curves constructed from linear viscoelastic spectra using TTS for PDMS-NH_2 and PDMS-NHCO-COOH with (a) *DP* = 22 (T_{ref} = 155 K for PDMS-NHCO-COOH and 151 K for PDMS-NH_2), (b) *DP* = 50 (T_{ref} = 153 K for PDMS-NHCO-COOH and 149 K for PDMS-NH_2), (c) *DP* = 74 (T_{ref} = 150K for PDMS-NHCO-COOH and 148 K for PDMS-NH_2). The master curves were shifted horizontally to match their α-relaxation peak positions. For PDMS-NH_2 the curves were cut at low frequencies due to the onset of crystallization. The inset in (c) shows the dependence of the plateau modulus G_N of PDMS-NHCO-COOH on the degree of polymerization (*DP*), and its comparison to the model expectations. The temperature dependence of the horizontal shift factors α_T employed for the TTS is given for both materials for (d) *DP* = 22, (e) *DP* = 50 and (f) *DP* = 74. The shift factors of the PDMS-NHCO-COOH are rescaled to have the same reference temperature as the PDMS-NH_2.

crystallization since it is not evident in the DSC curve). This additional feature indicates already a qualitative change in the chain association, possibly suggesting some kind of network forming structure.

To illustrate this, we compare the extracted rubbery plateau values G_N with the prediction of a network model considering entanglements, and physical crosslinks due to the end-association (inset Fig. 5.3 c). G_N is defined as the value of the storage modulus $G'(\omega)$ at the frequency where the loss modulus $G''(\omega)$ exhibits a minimum (Fig. 5.3).[245] It is related to the molecular weight between entanglements M_e and between the physical crosslinks M_c by the relation:[195]

$$G_N = \rho RT \left(\frac{1}{M_e} + \frac{1}{M_c}\right) \tag{5.1}$$

where R is the ideal gas constant, and ρ is the mass density of PDMS. Using the density of pure PDMS ρ = 965 kg/m^3, the known entanglement molecular weight M_e ~12 kg/mol, and the PDMS molecular weight as M_c, we estimated the values for G_N at T ~155 K. The model predictions (Eq. 5.1) provides reasonable agreement for the sample with DP = 74, but differs by ~10 times for the shortest chains (DP = 22) (Fig. 5.3 c inset). Hence, the latter value is too high to be caused by entanglement or physical crosslinking alone, and most probably reflects an additional reinforcement due to the hard, glassy phase of the phase-separated end groups, especially pronounced in PDMS-NHCO-COOH-22.

A rather subtle feature, which corroborates this conjecture, is a small peak in the loss modulus in the rubbery plateau region of PDMS-NHCO-COOH. Most pronounced in the sample with DP = 50 and to a little extent in that one with DP = 22 (in PDMS-NHCO-COOH-74, crystallization dominates the relevant temperatures, thus preventing its detection), it resembles a peak reported in polybutadiene transient networks containing physical crosslinks.[280] In that system, it is assigned to the dissociation and re-association of transient bonds according to the sticky reptation model.[131] It must be emphasized that this mechanically determined process probes the timescale of a linker group to dissociate from its counterpart and establish a new bond to a different linker group. This procedure may involve several

dissociation/association events with the initial counterpart before bonding to the new one, hence it is expected to take place at much longer timescale than the pure association/dissociation between identical linker groups.[158, 160]

5.3.3 Dielectric spectroscopy

BDS spectra of all PDMS-NH_2 samples show two distinct loss peaks (Fig. 5.4) separated by slightly more than 3 decades. To analyze these spectra we fit them by a superposition of two Havriliak-Negami (HN) functions (Eq. 2.9).[110] The characteristic relaxation time that corresponds to the maximum position of the loss peak can be calculated using the Eq. 2.12. [110]

Three relaxation modes are clearly visible in the dielectric relaxation spectra of PDMS-NHCO-COOH-50 and PDMS-NHCO-COOH-74, while only two of them, those at high and low temperatures are clearly visible in the spectra of PDMS-NHCO-COOH-22 (Figs. 5.5). However, the intermediate process also exists in PDMS-NHCO-COOH-22, but it is covered by the wings of the other two processes, primarily caused by an increase of the relaxation strength of the high temperature process (Fig. 5.5 a). Consequently, the low-temperature spectra of the latter system were fit to Eq. 2.9 with the added high frequency contribution of the third process estimated from the fit of high temperature spectra (see below). At such elevated temperatures, the slowest relaxation process is well separated from other two and can be fit by a single HN function (Fig. 5.5). Due to the proximity of the conductivity contribution, a respective term has been added to the fit function in this case:[110]

$$\varepsilon^*(\nu) = \varepsilon_\infty + \frac{\Delta\varepsilon}{[1+(2\pi i f\tau)^\alpha]^\gamma} + \frac{\sigma}{2\pi i f \varepsilon_0} \quad (5.2)$$

Where σ corresponds to the DC conductivity and ε_0 is the permittivity of vacuum. The symbols in the first term are similar to those used in Eq. 2.9 without indices. Due to crystallization of PDMS-NHCO-COOH-74, the slowest process could be accessed only at temperatures above the melting point (like the rheology measurements, also the dielectric experiments are probably more prone to crystallization than the DSC because of the much slower heating rate, on average 0.01-0.07 K/min).

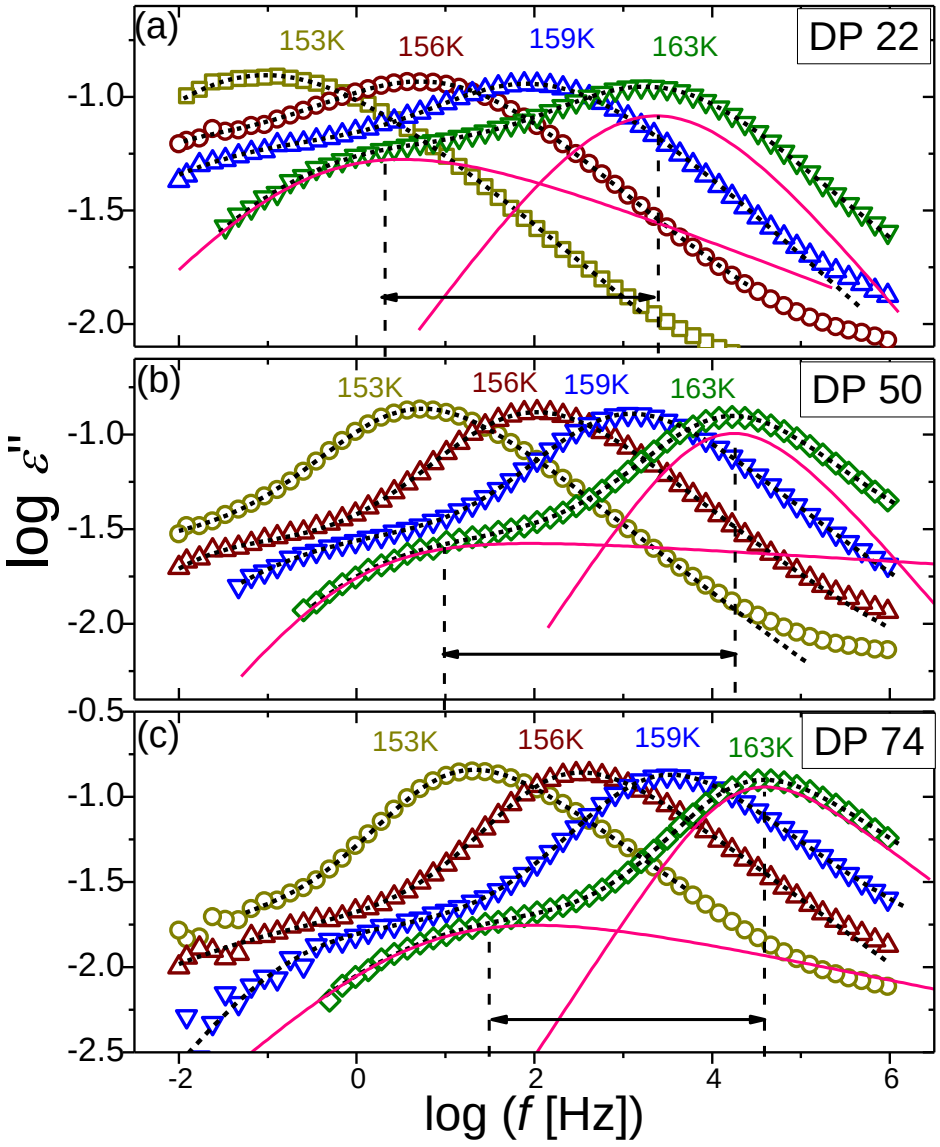

Figure 5. 4. Dielectric loss spectra ε"(*f*) (symbols) at several temperatures as indicated of PDMS-NH_2 with a *DP* of 22 (a), 50 (b) and 74 (c). The solid lines are fits of two HN functions (Eq. 2.9) and the dotted lines represent the individual contribution of each process. The vertical dashed lines illustrate the separation of the two modes.

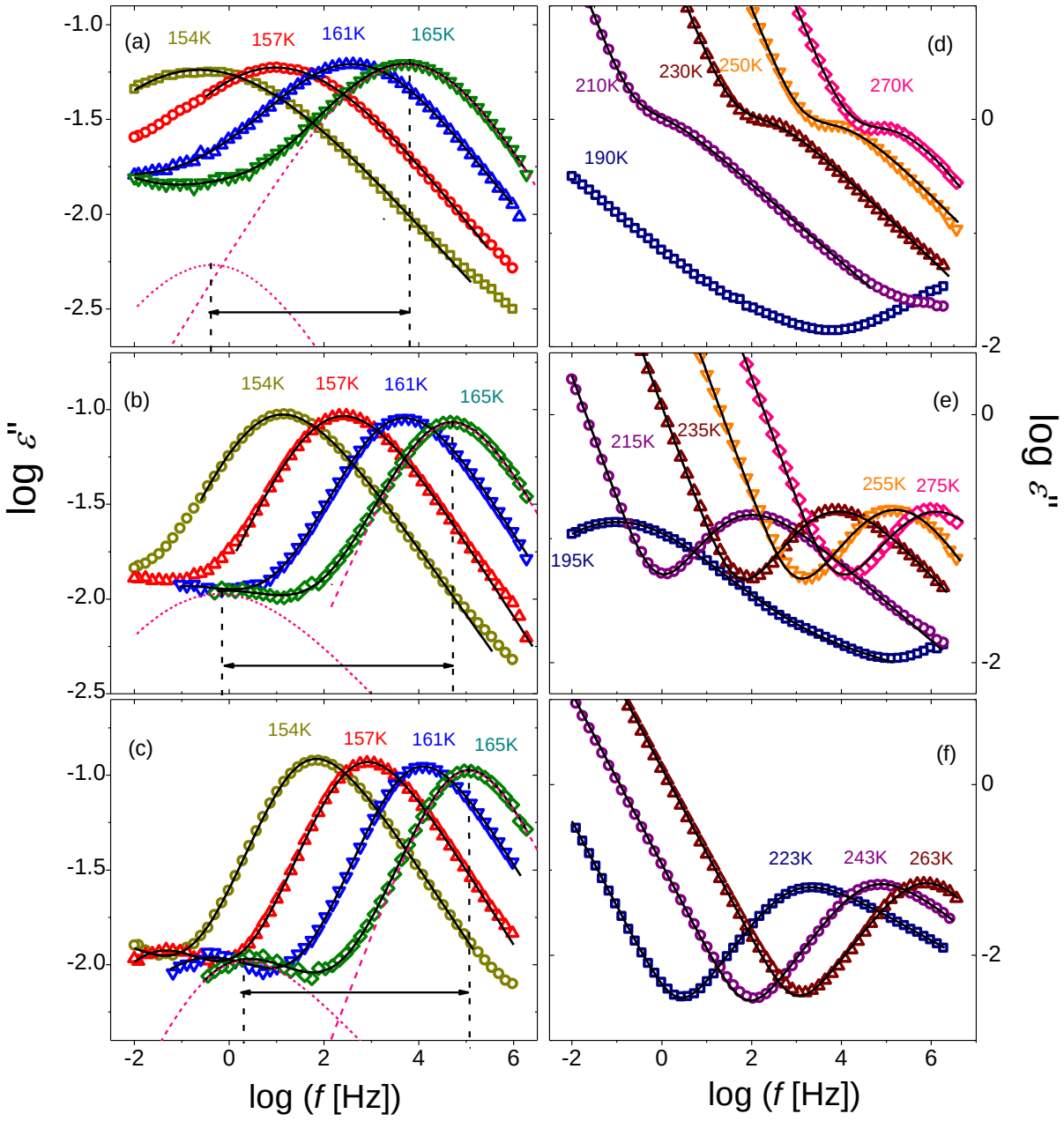

Figure 5. 5**.** Dielectric loss spectra ε"(*f*) (symbols) at several temperatures as indicated of PDMS-NHCO-COOH samples with *DP* = 22 (a & d), 50 (b & e) and 74 (c & f). The solid lines are fits of (a-c) two HN functions (Eq. 2.9), and (d-f) one HN function and a conductivity contribution (Eq. 5.2). The dotted lines (a-c) represent the individual contribution of each process and the vertical dashed lines illustrate their separation.

The fastest dielectric relaxation mode in all samples can be assigned to the segmental or α-relaxation because its extrapolation to $\tau \approx 100$s coincides with the T_g from the DSC measurements (Fig. 5.6, Table 5.1). This process slows down as DP decreases, consistent with the increase in T_g, due to the increased number of associating chain ends. As expected, the temperature dependence of the mean relaxation time τ_{max} of this process follows a Vogel-Fulcher-Tamman (VFT) equation (Eq. 1.2) in all samples (Fig. 5.6):[281-283]

Furthermore, the α-relaxation exhibits an increased broadening with decreasing *DP* (Fig. 5.7) which typically indicates a dynamical constraint and frustrated packing. This trend is very similar for both systems suggesting that the increasing end group content of both NH_2 and COOH impacts the segmental motion in an analogous way. Apparently, the associated end groups form some moiety which induces a packing frustration and, by that, imposes a dynamical constraint on the segments in their vicinity. Remarkably, this effect is independent of the involved association strength.

The second relaxation in the NH_2-terminated PDMS also exhibits a VFT-like temperature dependence. Since it is roughly in parallel to the segmental relaxation with a separation of ~3 decades (Fig. 5.6 a), we presume an interrelation between the two and refer to this process as *α**-relaxation. Its relaxation strength (which is proportional to the amount of participating dipoles) scales linearly with the weight fraction of the chain ends (Fig. 5.8) which confirms that this process is related to the end groups. Two mechanisms seem plausible to explain the *α**-process. First, it could reflect the life-time of the association/dissociation process of the H-bonds established between the NH_2 groups, i.e. a chemical relaxation[284, 285] that will generate dielectric response by changing the combined dipole moments. Second, it could present the orientational motion of the associated chain end dimers, i.e. a kind of structural relaxation of associated chain ends. The fact that the separation between the *α*- and the *α**-process in the dielectric spectra (Fig. 5.4) is roughly comparable to the separation between segmental and terminal modes (the onset of the latter) in the mechanical relaxation spectra (Fig. 5.3) may be in accord with either explanation since both resemble a stress release mechanism.

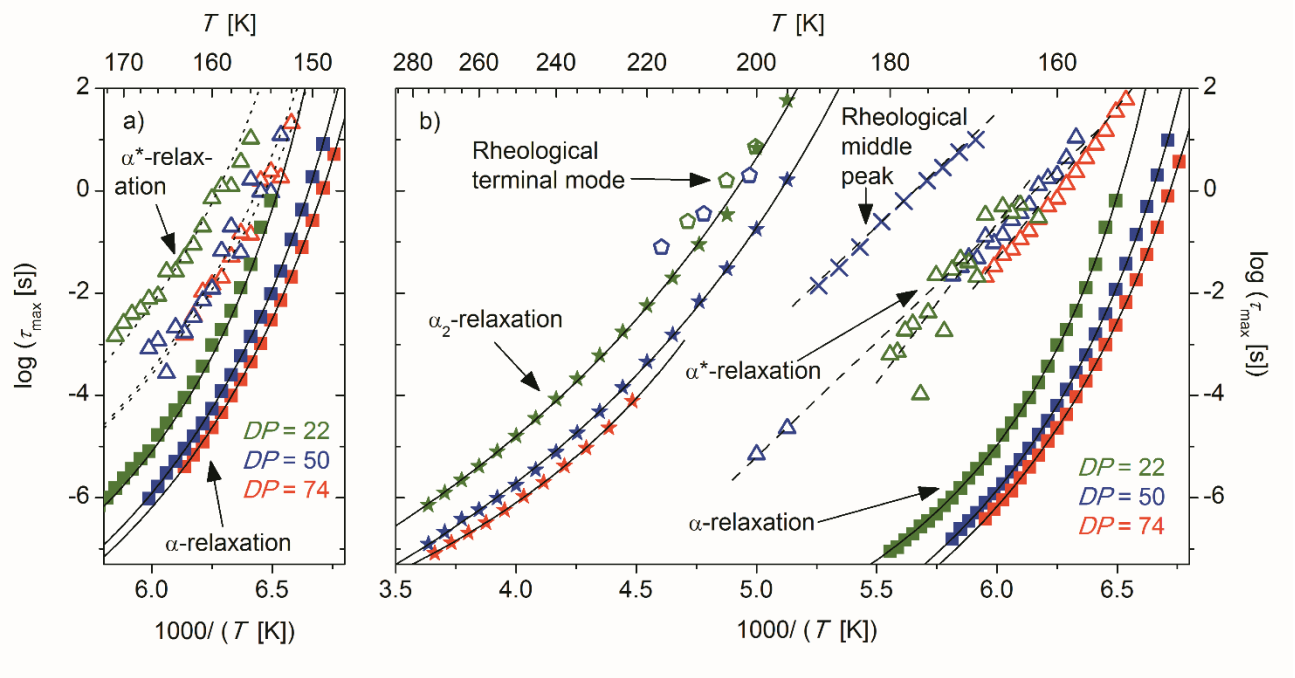

Figure 5. 6. (a) Arrhenius plot of the dielectric mean relaxation time of the α-relaxation (solid squares) and the α*-relaxation (open triangles) for PDMS-NH_2 of different *DP* as indicated. The solid lines are VFT fits to the α-relaxation, and the dotted lines represent products of exactly these VFT equations describing the α-relaxation and an Arrhenius type factor yielding the activation energy corresponding to the separation from the α-relaxation (see text for details). (b) Arrhenius plot of the dielectric mean relaxation times of the α-relaxation (squares), the α*-relaxation (open triangles), the α_2-relaxation (stars), the rheological relaxation time of the middle peak in the sample with *DP* = 50 (crosses), and the rheological terminal mode (open pentagons) for PDMS-NHCO-COOH systems of different *DP* as indicated. Solid lines are fits to the data by the VFT equation (Eq.1.2).

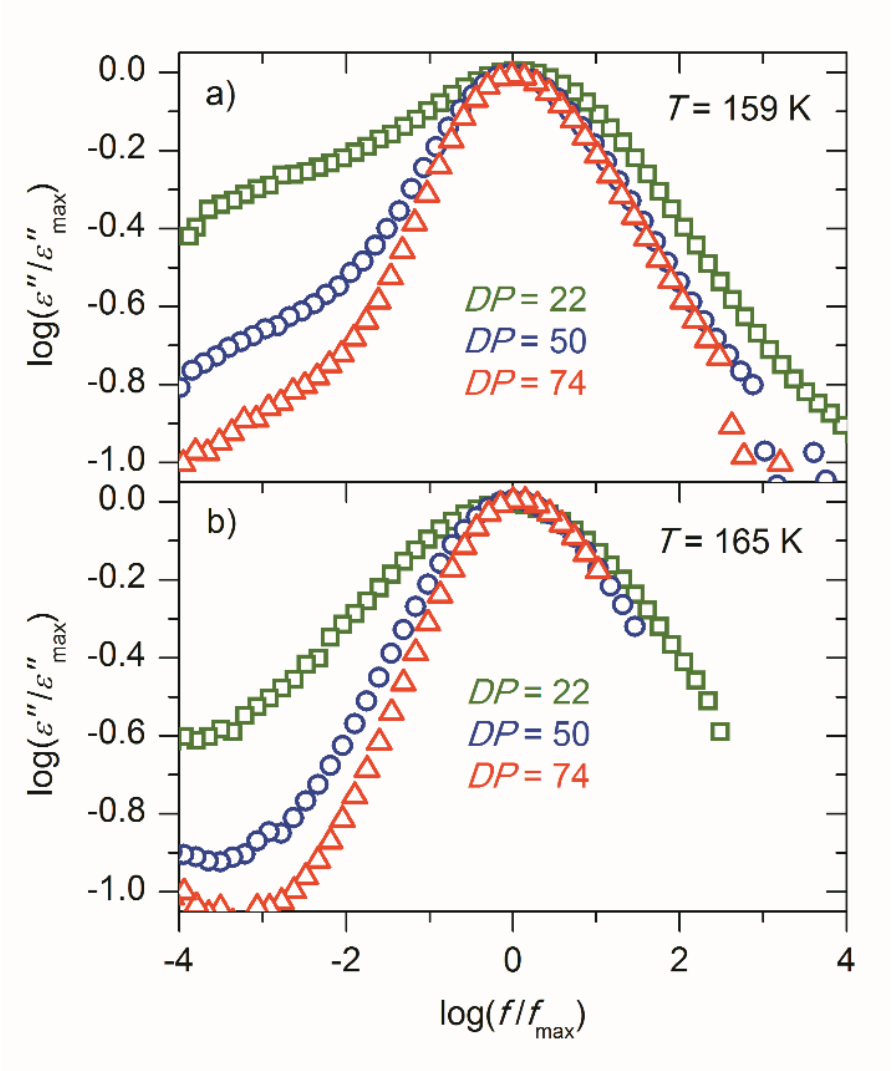

Figure 5. 7. Normalized dielectric loss ε'' *vs* normalized frequency of the α-relaxation of (a) PDMS-NH_2 and (b) PDMS-NHCO-COOH for samples of different *DP* as indicated at a temperature of 159 K and 165 K, respectively.

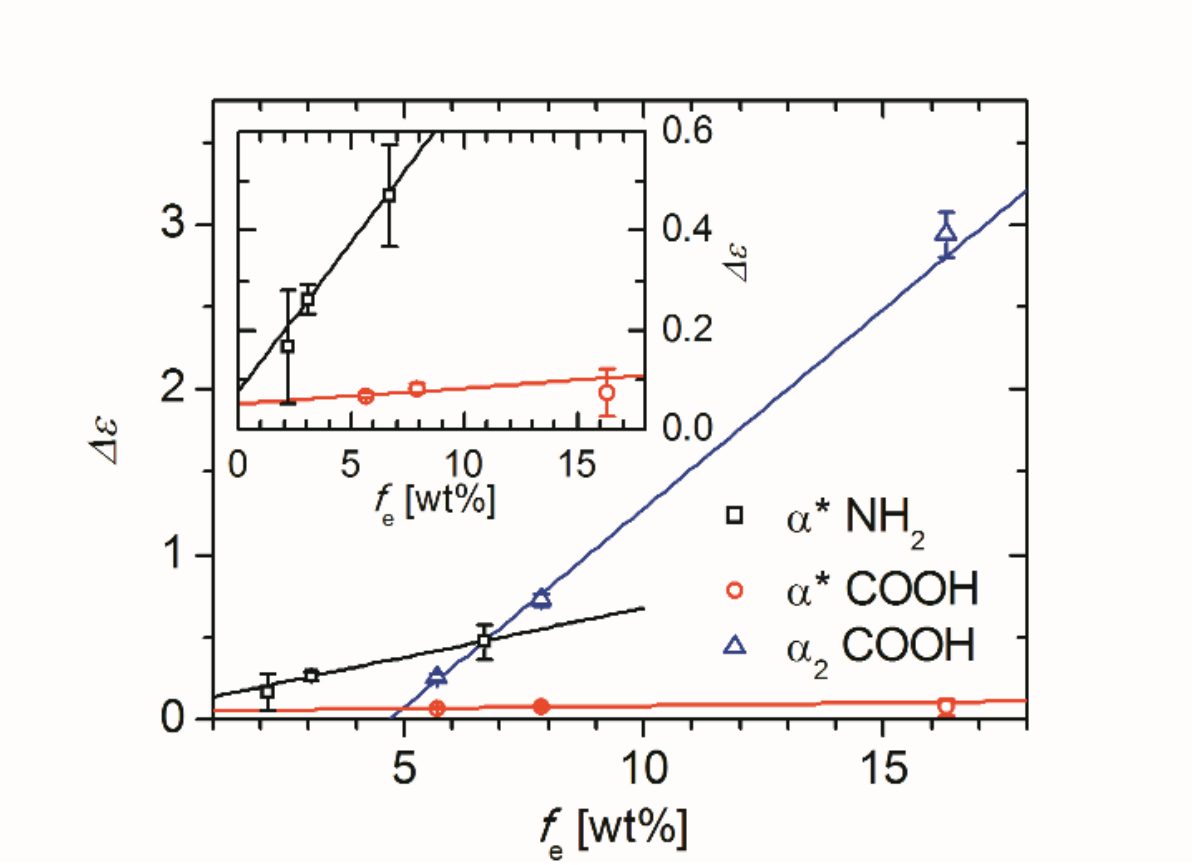

Figure 5. 8. Dependence of the dielectric relaxation strengths $\Delta\varepsilon$ on the weight fraction of chain ends f_e: for different relaxations in PDMS-NH_2 and PDMS-NHCO-COOH as indicated. The amplitudes of the peaks were averaged over several temperatures in the range where the peaks are well within the measured spectral window (156-159 K and 161-168 K for the α*-relaxation in PDMS-NH_2 and PDMS-NHCO-COOH, respectively, and 225-275 K for the α_2-relaxation of the latter). The inset shows the data of the α*-relaxations at an enlarged scale. The solid lines are linear fits to the data.

If the α*-relaxation reflects the association/dissociation life-time of the end-groups as proposed by previous studies,[115, 160, 161, 284, 285] a close connection to the rheological terminal relaxation of the melt is expected[158] since both processes relate to the transition from virtually long chains due to association to the constituting short chains. Recent work suggests that despite this connection the respective relaxations in dielectric and rheological experiments take place on different timescales because the former probes each association/dissociation event between functional groups while the latter only senses those involving an exchange of the counterpart.[160] Hence, the relaxation time probed by rheology will be much larger than the dielectric one. This is in accord with our observation of the α*-relaxation being ~3 decades slower than the segmental motion whereas that separation amounts to more than ~4 decades for the rheological terminal relaxation.

In this scenario, the segmental melt dynamics (friction) controls the dissociation rate of the end groups and the difference in time scale between the α- and the α*-relaxation is related to the activation energy E_a required for the dissociation of the bond between stickers.[115, 160, 161] It's basically agreed that the structural relaxation time τ_α (segmental relaxation time in polymers) is the pre-factor in an Arrhenius type equation describing the temperature dependence of the characteristic dissociation time $\tau_{\alpha*}$ of supramolecular network:

$$\tau_{\alpha*}(T) = \tau_\alpha(T)\exp\left(\frac{E_a}{RT}\right) \tag{5.3}$$

where R is the universal gas constant. Using the VFT fit parameters of the respective α-relaxation to fix τ (T), and keeping E_a as the only free parameter in the Eq. 5.3, the activation energies of the α*-relaxation of PDMS-NH_2 is estimated as 9.1 (±1) kJ mol^{-1}, 7.6 (±1) kJ mol^{-1}, 9.3 (±1) kJ mol^{-1} with DP of 22, 50 and 74, accordingly. This is close to the dissociation energy of the NH-N hydrogen bond E_a ≈ 10-12 kJ/mol.[286]

The amide acid terminated PDMS (PDMS-NHCO-COOH) samples also exhibit some type of α*-relaxation which is partially superimposed by the close-by α-relaxation. However, it differs in several characteristics from its counterpart in PDMS-NH_2. We estimated the activation energies of the α*-relaxation to be 13.5 (±1) kJ mol^{-1}, 15.4 (±1) kJ mol^{-1}and 13.7 (±1) kJ mol^{-1} for

PDMS-NHCO-COOH with *DP* of 22, 50 and 74, respectively (Fig. 5.6). Crystallization of the sample with *DP*=74 limited analysis of the α*-process in this sample.

We want to emphasize that the estimated values of the COOH dissociation energy is much smaller than the dissociation energies reported for carboxylic acid terminated polyisoprene in solution (~100-130 kJ/mol[287]). The difference is that in the latter case, the apparent activation energy (the slope in the Arrhenius plot) was identified as the dissociation energy. This is not correct, however, because the temperature dependence of the dissociation process is additionally affected by the temperature dependence of segmental relaxation (Eq. 5.3). It's worth mention that authors of Ref[287] actually discussed that the estimated activation energy is affected by two factors, segmental mobility and by re-association of dissociated chain ends. The latter emphasizes that the mechanical relaxation time does not reflect the dissociation time, while former essentially agrees with the Eq. 5.3. Thus, one needs to take the temperature dependence of segmental dynamics explicitly into account for accurate estimates of the dissociation energy barrier specifically imposed by the H-bonds.

In resemblance to PDMS-NH_2, the α*-relaxation in PDMS-NHCO-COOH shares a feature in the mechanical relaxation spectra. In this case, however, the signature in the loss part of the shear modulus is a peak (Fig. 5.3) which can be ascribed to a (partial) mechanical stress release due to bond partner exchange.[280] In this case, a difference of the absolute values of the mean relaxation time between the dielectric α*-relaxation and the shear modulus loss peak is ~2 decades (Fig. 5.6). The difference between the chain end dissociation time and the time of switching to another chain has been discussed in several theoretical and experimental studies.[158, 160, 280] This difference reflects the probability of the dissociated chain ends to associate back vs connecting to different chains. Thus, the dielectric α*-relaxation might be ascribed the association/dissociation rate of any two end groups while the shear modulus loss peak reflects the time until the end group switches to another chain.[160] Our analysis suggests that for PDMS-NHCO-COOH-50 chain ends dissociate/re-associate ~100 times before they exchange with other chains.

The above discussion suggests that the α*-relaxation could be assigned to the association/dissociation of COOH chain ends. However, this picture fails to explain why the relaxation strength $\Delta\varepsilon$ of this process is much lower compared to its counterpart in PDMS-NH_2 (Fig. 5.8), in contrasts to the fact that COOH possess a larger dipole moment than NH_2 (1.74 D[288] vs. 1.5 D[289]). Moreover, the values of $\Delta\varepsilon$ are similar in all PDMS-NHCO-COOH samples (Fig. 5.8), i.e. it does not scale with the weight fraction of chain ends. Meanwhile, the terminal group of PDMS-NHCO-COOH comprises an additional amide group which provides the possibility of further hydrogen bonds and thus may complicate the interaction. Hence, the identification of the origin of this process is not as clear as it may appear, and poses a challenge; both chemical or structural relaxations may still be considered.

At elevated temperatures, an additional, well separated process appears which is only present in PDMS-NHCO-COOH (Fig. 5.5). Its extrapolation matches with the second glass transition observed in these systems (Fig. 5.6, Table 5.1) Because of this we refer to it as α_2-process; since it follows a VFT temperature dependence, the assignment to a structural relaxation in this second phase seems plausible. Like the T_g, it shifts to higher temperatures for samples of smaller *DP*. The relaxation strength of this process increases linearly with the fraction of end groups in the system (Fig. 5.8) which supports the view that these end groups form a segregated phase. Further, an extrapolation of this linear scaling to $\Delta\varepsilon = 0$ yields an end group fraction of ~5 %. This indicates that PDMS-NHCO-COOH with a lower end group content (i.e. longer PDMS chains) are not expected to form this type of segregated phase. We speculate, that – possibly due to some solubility threshold – chain ends up to a fraction of ~5 % form merely smaller associates contributing to the α-relaxation; and only if the system contains more end groups, the excessive fraction segregates into a separate phase giving rise to the α_2-relaxation.

A related phenomenon occurred in our previous study of telechelic polymers:[233] for $M_W \approx 500$ g/mol, PDMS-OH chains phase separate while $M_W \approx 1100$ g/mol did not show signs of phase segregation. This is consistent with our finding of the existence of such a threshold M_W (or *DP*, respectively) in PDMS-NHCO-COOH, and also with the absence of phase separation in PDMS-NH_2 with M_W larger than ~1500 g/mol (or an end group fraction lower than ~7-10 wt%).

A major difference between the α- and the α_2-process is unraveled by the fragility index m which quantifies the steepness of the temperature dependence of the relaxation time at T_g. It can be estimated using the VFT fit parameters according to Eq. 1.3 and Eq. 1.4.

The fragility index of the α-relaxation in both PDMS-NH_2 and PDMS-NHCO-COOH takes values of 120-140 and increases with decreasing M_W or *DP*, respectively (Fig. 5.9). This is in accord with our previous work on hydroxyl terminated PDMS and opposes the common trend in polymers as we demonstrate for methyl terminated PDMS (Fig. 5.9).[97, 290, 291] According to the generalized entropy theory,[100, 250] the fragility of the segmental relaxation can be ascribed to frustration in molecular packing. Apparently, the chain end associations frustrate the packing of PDMS segments which matches the increased broadening of the relaxation (Fig. 5.7).

In contrast, the fragility of the α_2-relaxation in PDMS-NHCO-COOH has much lower values of 45-50 and decreases with decreasing M_W or *DP*, respectively. Such low values are characteristic for H-bonding systems which is consistent with our assignment to a structural relaxation of a phase consisting of (H-bond rich) chain ends. The decrease in fragility with decreasing M_W (*DP*) may even indicate reduced packing frustration suggesting larger associations in smaller *DP* samples. This may also explain the increase of the mean relaxation time (and T_g) of the α_2-relaxation with decreasing *DP* since larger aggregates will be affected less by the highly mobile PDMS environment.

Furthermore, also the α_2-process seems to be connected to a feature in the mechanical relaxation spectra, namely the apparent terminal relaxation time which basically indicates the transition from the rubber to the melt regime. For PDMS-NHCO-COOH-22, both processes almost coincide while in the case of PDMS-NHCO-COOH-50, the mechanical relaxation is ~10 times slower than the α_2-relaxation (Fig. 5.6). Due to the different timescales of the α_2-relaxations, the two rheological terminal modes nearly coincide. Additionally, they seem to follow a VFT dependence with a slightly lower thermal activation than the α_2-relaxations. Qualitatively, these features attributed to the α_2-relaxation and its relation to the other processes can match the picture of a second type of network formed by more stable phase

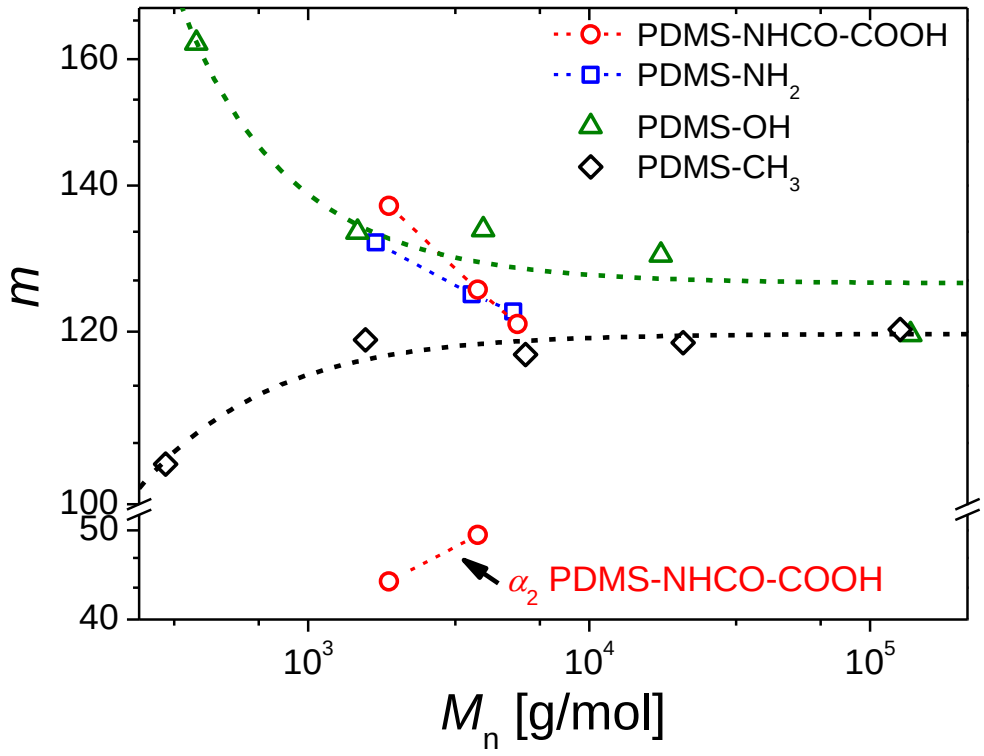

Figure 5. 9. Fragility index *m vs* total number averaged molecular weight M_n (including end groups) of the α-relaxation in methyl-terminated (PDMS-CH_3),[241] hydroxyl-terminated (PDMS-OH),[233] amine-terminated (PDMS-NH_2) and amide acid terminated (PDMS-NHCO-COOH) PDMS and the α_2-relaxation in PDMS-NHCO-COOH. Crystallization prevents a reasonable determination of the fragility of the α_2-process in PDMS-NHCO-COOH-74. The dotted lines are guides to the eye.

segregated associates[292], but quantitatively, the details of certain characteristics still require further investigation.

It is remarkable that, although we find indications that the α*-relaxation reflects the lifetime of end group association in both systems, in the case of PDMS-NH_2 this process determines the transition to the melt regime while PDMS-NHCO-COOH exhibits only a slight reduction of its elasticity in the rubbery state. Following the concept of a dual network, two types of bonds seem to exist in the latter[280] (Fig. 5.10): i) Some type of transient bonds which release stress by a transient network mechanism controlled by the characteristic times of association/dissociation between pairs of end groups and an average number of such association/dissociation events until these pairs exchange their counterpart[158, 160]. Such transient bonds may be just dimeric associates, i.e. contacts involving just two chain ends. ii) This is complemented by some sort of much more stable type of bond or associate which requires elevated temperatures to be dissociated.[292] Below the second T_g, these will appear effectively permanent on the timescale of the transient bond exchange. Our results indicate a second phase formed by a fraction of the end groups which apparently provides these features. However, it remains unclear why the same type of end group should form two types of associates having such big qualitative differences, and which role the specific composition of the end group plays. The former may be related to some kind of solubility threshold of the polar end group dimers in the non-polar PDMS matrix before it segregates to separate phases at higher concentrations while the latter requires more investigations on systems with systematically altered chemistry.

5.4 Conclusions

In the present study, we combine dielectric and mechanical spectroscopy to unravel the impact of different types of H-bonding end groups in telechelic PDMS on segmental dynamics and rheological properties of the material. Surprisingly, significant change in the association energy between NH_2 and COOH groups does not affect the segmental dynamics and the glass transition temperature in PDMS-based chains. The molecular weight dependence of segmental

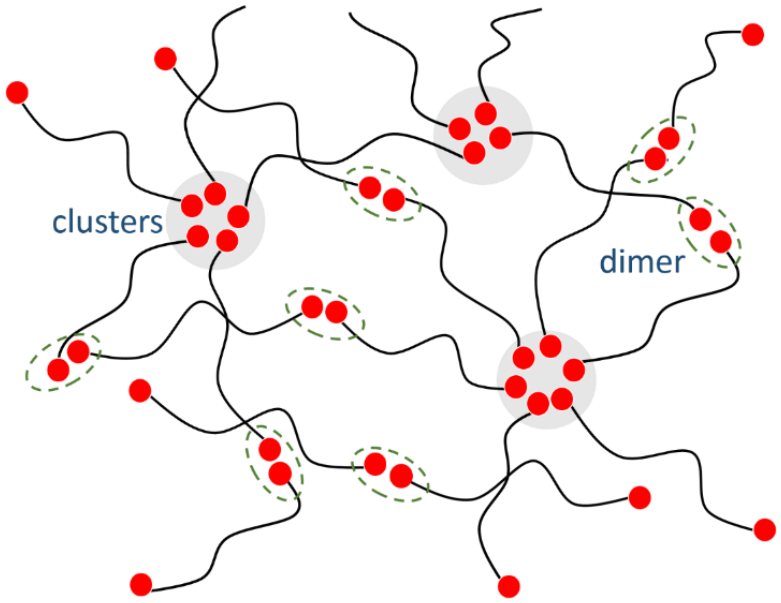

Figure 5. 10. Schematic illustration of the association structure of PDMS-NHCO-COOH samples with small transient bonds, presumably *dimers*, and larger effectively permanent bonds, here denoted as *clusters*.

dynamics in these chains appears to be the same as in PDMS-OH systems[233] and differs strongly from the behavior of methyl terminated[241] PDMS. In contrast, the different types of end groups significantly affect the rheological properties of these melts and can even induce phase separation. No signs of phase separation have been detected in the case of studied PDMS-NH_2 molecules, while all PDMS-NHCO-COOH samples show phase separation and a slow dielectric process ascribed to structural relaxation and glass transition in these phase-separated regions. Based on the analysis of rheological and dielectric spectroscopy data we suggest that the viscoelastic properties of the PDMS-NH_2 samples are controlled by the energy of H-bond dissociation. At the same time, a qualitatively different picture emerges for the structure and dynamics of the PDMS-NHCO-COOH melts. It is characterized by the interplay between small associations, possibly dimers, and phase separated domains with the fraction of the latter strongly increasing with decrease of PDMS chain length. These phase-separated clusters form physical cross-links in the PDMS network and result in extended rubbery-like plateau in the rheological spectra. The characteristic relaxation time in these phase-separated regions seems

to define the terminal relaxation time in PDMS-NHCO-COOH samples which occurs at temperatures above their second T_g. Remarkably, these two very different types of connections, i.e. small associates and clusters, are formed by the same species of end group establishing dual network behavior. Due to the reversibility of the cluster association, the studied PDMS-NHCO-COOH systems combine viscoelastic properties of short chains at high T, and those of crosslinked rubber below the second T_g. This suggests a promising route to combine easy processability of low M_W liquids with the desired mechanical performance of high M_W polymers and even crosslinked networks.

Chapter VI

The Role of Chain-end Association Life Time in Segmental and Chain Dynamics of Telechelic Polymers

Reproduced in part from: Kunyue Xing, Martin Tress, Peng-Fei Cao, Fei Fan, Shiwang Cheng, Tomonori Saito, Alexei P. Sokolov. "The role of chain-end association lifetime in segmental and chain dynamics of telechelic polymers" *Macromolecules* 2018, 51 (21), 8561-8573. Kunyue Xing contributed to material design and synthesis, BDS, DSC and rheology measurements, data analysis and writing. Pengfei Cao and Tomonori Saito contributed to material design, Shiwang Cheng contributed to data analysis, Fei Fan contributed to material synthesis of PPG-CH_3, Martin Tress contributed to analysis and writing. Alexei Sokolov led the project, contributed to data analysis and writing.

6.1 Introduction

In the previous chapters, we studied the role of chain ends on the dynamics of supramolecular polymer systems. The peculiar characteristics of the backbone (*e.g*. polarity and rigidity) and the interplay between the chain ends and backbones are also significant factors that affect the glass transition, fragility and mechanical performance of the systems. Till now, there's not much research covering this region, especially in the melt state.

Polypropylene glycol (PPG) is a common glass forming polymer that has been studied by different techniques such as dielectric spectroscopy[293-300], calorimetry[301], nuclear magnetic resonance (NMR)[302], mechanical experiments[303-305], neutron scattering[306] and various light scattering methods[307-309]. It is known that the glass transition temperature (T_g) of PPG with hydroxyl groups at both chain ends is almost independent of molecular weight[310]. On the contrary, Engberg et al.[308] found that the structural relaxation dynamics of methyl-terminated PPG exhibits a pronounced molecular weight dependence. Richter and coworkers[180] studied the association of heterocomplementary telechelic PPG, bearing either diaminotriazine (DAT) or

thymine (Thy) stickers as end-groups that can produce 3 H-bonds each. From small angle neutron scattering (SANS), they concluded that linear association prevails in this system. Leibler and coworkers[79] presented results of telechelic supramolecular polymers based on PPG with DAT/Thy functionalities on both ends (DAT-PPG-DAT, Thy-PPG-Thy). By comparing Thy/DAT self-association and complementary association, they concluded that complementary interactions can suppress mesoscopic order[75], thus leading to a counterintuitive change in material properties. The tendency of crystallization of the Thy and resulting phase segregation of the chain-ends makes the system more complicated. While these results reveal many details about the dynamics and network structures of PPG with different associating chain-ends, there is rather limited discussion of segmental dynamics in telechelic polymers and its role in the formation of supramolecular networks.

Here we present a combined study of segmental dynamics, glass transition and rheological properties of telechelic PPG with different strength of chain end interactions: methyl-terminated (PPG-CH_3), hydroxyl-terminated (PPG-OH), amine-terminated (PPG-NH_2) and amide-carboxylic acid terminated (PPG-NHCO-COOH). Analysis of the data revealed significant influence of the chain end interaction strength on T_g at relatively low molecular weight. At the same time, viscosity appears to be almost independent of the chain-end interactions once the shift of T_g is accounted for (presented vs temperatures scaled by T_g). These results are in strong contrast to earlier studies of telechelic PDMS with the same set of chain ends (as discussed in Chapter 5).[229, 233] In the case of telechelic PDMS the increase in T_g is independent of the strength of the chain-end H-bonding, while viscosity varies drastically (even plotted vs T/T_g). Based on these contrasting results, we propose a qualitative explanation considering the lifetime of chain-end dissociation in comparison to the characteristic chain and segmental relaxation time. If the dissociation time is much longer than the segmental time, T_g appears to reach some limiting value with no significant dependence on the strength of the chain end association. However, if the dissociation time is shorter than the chain relaxation time, no significant influence on viscosity is expected. Thus, the ratio of characteristic time scales should be considered in the design of associating polymers in order to achieve the desired properties.

6.2 Methods

6.2.1 Differential Scanning Calorimetry (DSC)

DSC measurements were performed using a Q-1000 differential scanning calorimeter (TA Instruments). Samples were dried in a vacuum oven for several days before each measurement to remove any remaining solvents and moisture. In all measurements, the samples were sealed in aluminum hermetic pans and went through the same temperature range of 150 – 350 K at a scan rate of 10 K/min. The cooling and heating cycles were repeated twice to confirm the reproducibility of the results. The glass transition temperature (T_g) was determined from the midpoint of the heat flow step during the 2nd heating via the TA Universal Analysis 2000 software.

6.2.2 Broadband Dielectric Spectroscopy (BDS)

BDS measurements in the frequency range 10^{-2} – 10^{7} Hz were carried out using a Novocontrol Concept-80 system with an Alpha-A impedance analyzer and a Quatro Cryosystem temperature controller. Prior to the measurement, the samples were dried in the same way as described in the DSC protocol. The PPG-OH, PPG-NHCO-COOH and PPG-NH_2 samples were placed in a parallel-plate dielectric cell made of sapphire and invar steel, similar to the one described in ref [238]. The empty cell, with an electrode diameter of 12 mm and electrode separation of 49 µm, had a capacitance of 20 pF. The PPG-CH_3 samples were placed between two gold-plated electrodes with a diameter of 10 mm separated by a Teflon spacer of 50 µm thickness. The experiments proceeded from high to low temperatures. The samples were stabilized at each temperature within 0.2 K for at least 10 min to achieve a thermal equilibrium before each sweep.

6.2.3 Shear rheology

Prior to all rheological measurement the samples were dried in the same way as described above. Small-amplitude oscillatory shear (SAOS) measurements were performed with a stress-controlled mode of the AR2000ex (TA Instruments) in an angular frequency range 10^{-1}-

10^2 rad/s using parallel plate geometry, with a disk diameter of 4 mm and 8 mm according to the magnitude of the shear modulus. The gap between plates was about 0.5 mm and kept constant for all the investigated temperatures. A strain sweep measurement was performed at each temperature to ensure that the SAOS response was within the linear regime. Before each rheological measurement, a thermal stabilization of 10 minutes was performed to assure thermal equilibrium. Temperature was stabilized within 0.2 K for all measurements. Zero shear viscosity measurements for the $\eta_0 < 10^5$ Pa*s (temperature range from 220 K to 300 K) were conducted using the same AR2000ex rheometer in continuous ramp measurements with a shear rate of 10 s^{-1}. We used a conical plate of 25 mm in diameter with a cone angle of 2^0 and a truncation of 58 µm. Zero shear viscosity $\eta_0 > 10^5$ Pa*s ($T < 220$ K) were estimated using terminal relaxation mode in SAOS measurement $\eta_0 = \lim_{\omega \to 0} G''/\omega$.

6.3 Results

6.3.1 Differential Scanning Calorimetry

The heat flow data for all studied PPG samples exhibit a clear endothermic step (Fig. 6.1) associated with their glass transition (Table 6.1). For PPG-CH_3, T_g decreases with decrease of MW, following the normal trend for polymers[98] (Fig. 6.2 a). In case of PPG-NH_2 and PPG-OH, T_g is almost independent of MW with only a slight reduction for small MW, as has been found by other researchers for PPG-OH before[311]. In contrast, T_g of PPG-NHCO-COOH increases strongly with decrease in MW. The observed behavior of T_g is consistent with known increase in the glass transition temperature of linear associating polymers with intermolecular H-bonds.[48, 229, 231, 233, 312] Stronger H-bond strength significantly alters the MW dependence of T_g at low molecular weights[311].

These results (Fig. 6.2 a) are in strong contrast to earlier studies of telechelic PDMS with the same set of chain ends, where no influence of chain end association strength on T_g has been found[229] (Fig 6.2 b). We emphasize that special care was taken to avoid influence of crystallization on measured T_g in the case of telechelic PDMS studies (for details see ref [229]).

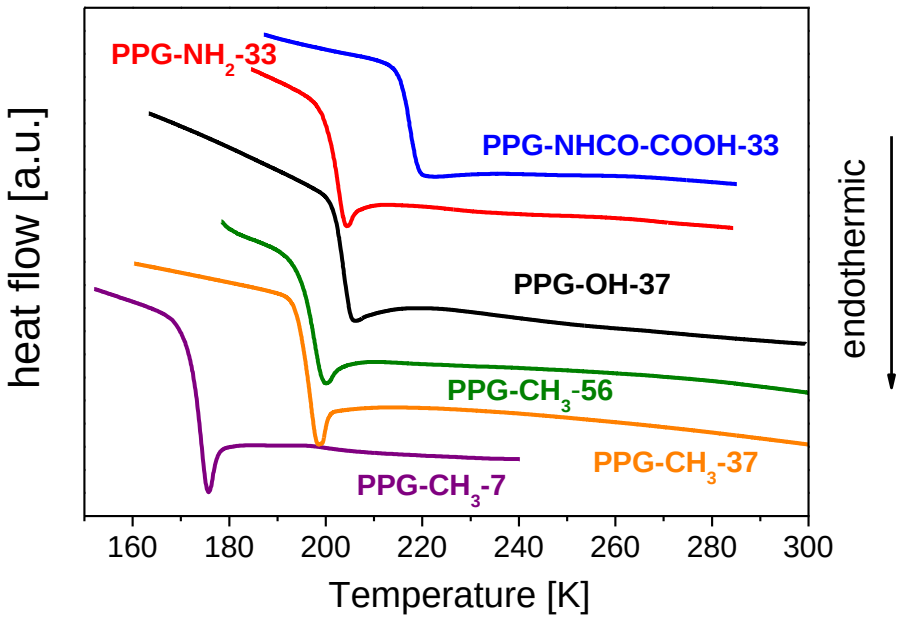

Figure 6. 1. Calorimetric heat flow curves of PPG-COOH, PPG-NH_2, PPG-OH and PPG-CH_3 measured with a constant heating rate q = 10 K/min for different *DP,* as indicated. For clarity, the original curves are shifted vertically.

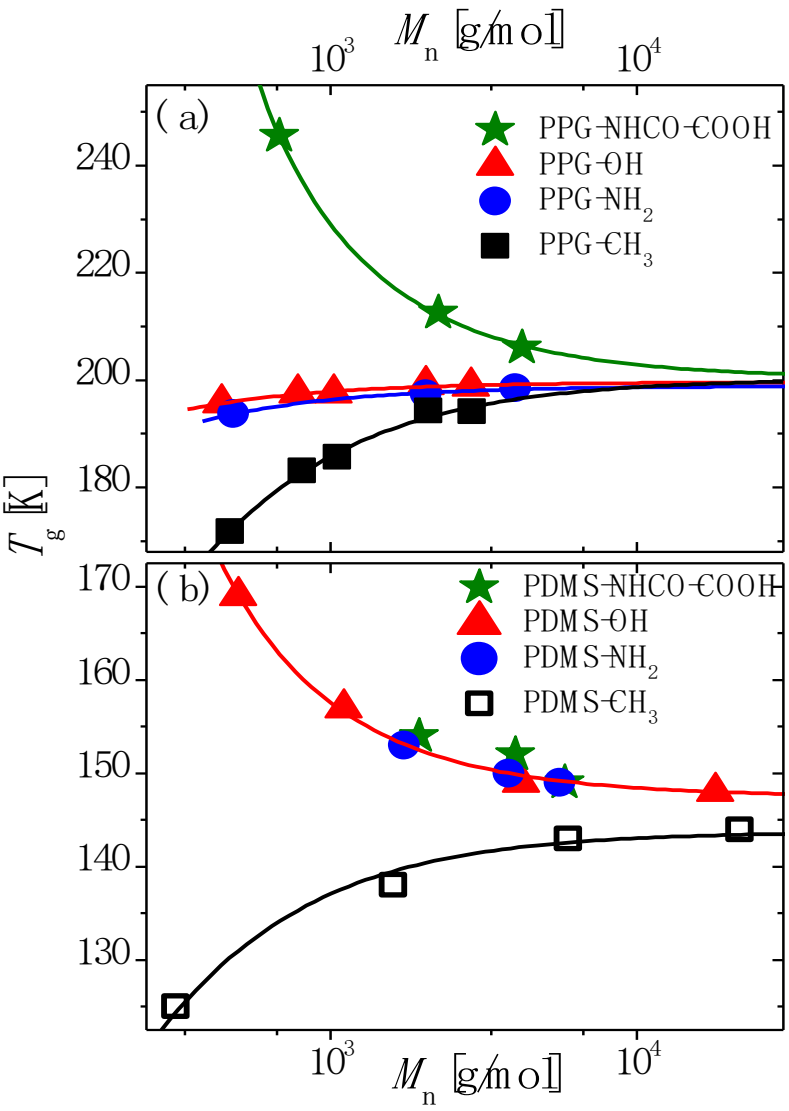

Figure 6. 2. Calorimetric T_g (solid symbols) *vs* total molecular weight M_n (including end groups) in telechelic PPG (a) and PDMS[229, 233] (b) with different end-groups, as indicated. The PDMS-CH_3 data are dielectric T_g values taken from ref[241]. The lines are fits to the Fox-Flory equation[279].

Table 6. 1. Material properties of the investigated polymers: molecular weight MW*, glass transition temperature as determined by DSC and BDS $T_{g,cal}$, $T_{g,diel}$, respectively.

Sample	*DP*	M_n [g/mol]	$T_{g,cal}$, [K]	$T_{g,diel}$, [K]
PPG-NH_2-6	6	480 [a]	193.7	192.3
PPG-NH_2-33	33	2046 [a]	197.4	198.8
PPG-NH_2-67	67	4018 [a]	198.5	200
PPG-NHCO-COOH-6	6	680 [b]	245.5	248.8
PPG-NHCO-COOH-33	33	2246 [b]	212.6	213.6
PPG-NHCO-COOH-67	67	4218 [b]	206.1	205.3
PPG-OH-7	7	440 [b]	195.7	196.8
PPG-OH-14	14	846 [b]	197.5	198.8
PPG-OH-18	18	1078 [b]	197.6	200.1
PPG-OH-37	37	2180 [b]	199.1	200.8
PPG-OH-56	56	3282 [b]	198.9	200.8
PPG-CH_3-7	7	468 [c]	171.8	172.9
PPG-CH_3-14	14	874 [c]	183.1	182.5
PPG-CH_3-18	18	1106 [c]	185.7	186.7
PPG-CH_3-37	37	2208 [c]	194.3	193.3
PPG-CH_3-56	56	3310 [c]	194.2	195.4

[a] determined from H1 NMR measurements of PPG-NHCO-COOH corrected for the end-group exchange
[b] determined from H1 NMR measurements
[c] determined from H1 NMR measurements of PPG-OH corrected for the end-group exchange

6.3.2 Dielectric spectroscopy

The dielectric loss spectra of regular PPG show two relaxation processes which is characteristic for type-A[110, 111, 313] polymers: i) the dielectric α-relaxation at high frequencies that represents segmental relaxation, and ii) the normal mode at lower frequency that represents the end-to-end relaxation (chain modes). The loss spectra of PPG-CH_3-7, PPG-NH_2-6, PPG-OH-7, PPG-NHCO-COOH-6, PPG-OH-14 and PPG-CH_3-14 exhibit only one process, while the spectra of all other samples exhibit two relaxation peaks (Fig. 6.3). The dielectric loss spectra of PPG-OH and PPG-CH_3 are basically similar to those of PPG-NH_2 (all are presented in Fig. 6.4) and are consistent with literature reports [110, 293, 294, 296, 300, 302, 311, 314-319].

The spectra of PPG-NHCO-COOH-33 and PPG-NHCO-COOH-67 also show two relaxation processes (Fig. 6.3 e and 6.3 f), but these are much closer in frequency than in the other systems with similar MW (see *e.g*. Fig. 6.3 b and 6.3 c). Moreover, the normal mode amplitude is lower than the segmental peak amplitude in the spectra of CH_3-, OH- and NH_2-terminated PPG, while in the spectra of the amide-acid terminated PPG the lower frequency peak is stronger, and the higher frequency peak appears as a shoulder. To analyze the spectra, we fit them using two Havriliak-Negami (HN) functions (with indices 1 and 2, respectively) and a conductivity contribution (Eq. 2.9).[110] For the fits of the spectra which exhibit only one clear relaxation peak (the low MW samples), the relaxation strength of one of the HN functions is fixed to zero. In the PPG-NHCO-COOH-33 spectra, the low-frequency process overlaps with the high-frequency peak which appears only as a shoulder, so its low-frequency wing is not visible. Consequently, the respective parameter α describing the slope of this wing is fixed to the value 0.864 (as obtained from the average of α in NH_2-, OH- and CH_3-terminated PPG). The characteristic relaxation time that corresponds to the maximum position of the loss peak can be calculated using the expression (Eq. 2.12).[110]

The temperature dependence of τ_{max} is non-Arrhenius and can be fitted by the Vogel-Fulcher-Tamman (VFT)[110, 281-283] equation (Eq. 1.2) in all samples (Fig. 6.5). From these parameters, also the fragility index m can be calculated by Eq. 1.3 and Eq. 1.4, which indicates the steepness of the temperature dependence of the relaxation time at T_g, and is considered to reflect the frustration in molecular packing[100, 250] (Table 6.2).

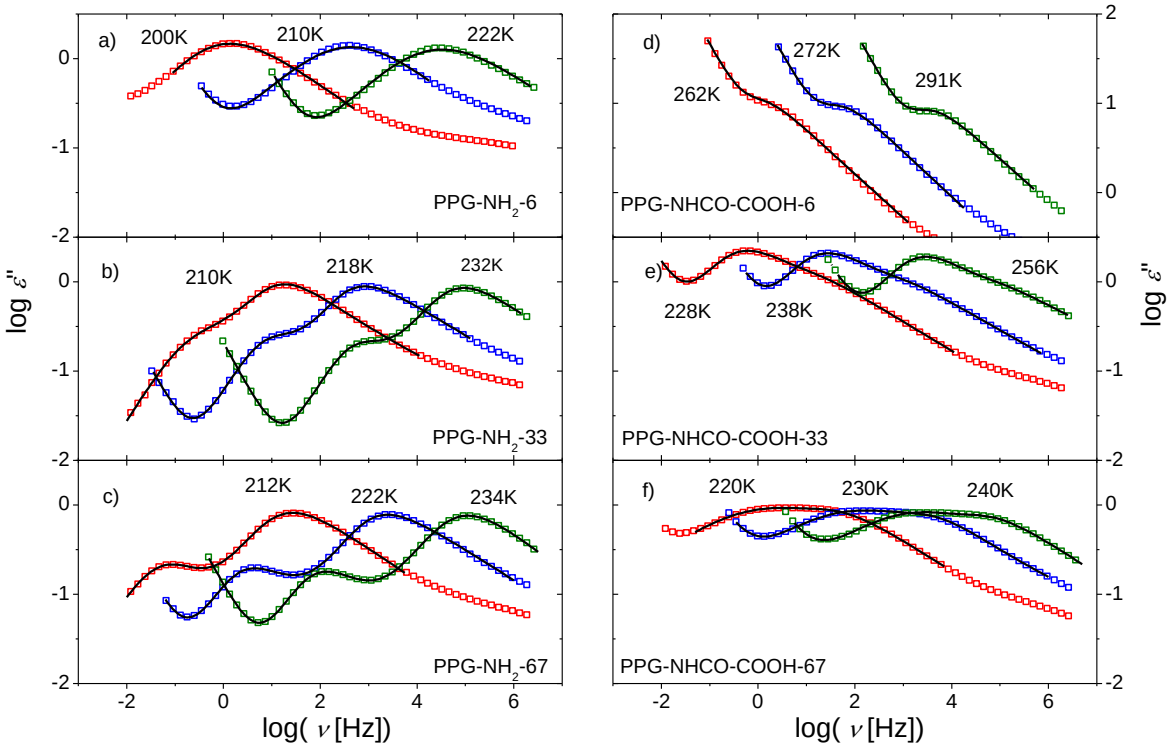

Figure 6. 3. Dielectric loss spectra $\varepsilon''(\nu)$ (symbols) at several temperatures as indicated of PPG-NH_2 with *DP* of 6 (a), 33 (b) and 67 (c) and PPG-COOH with *DP* of 6 (d), 33 (e) and 67 (f). The solid lines are fits to functions consisting of one/two HN functions and a conductivity contribution (Eq. 2.9).

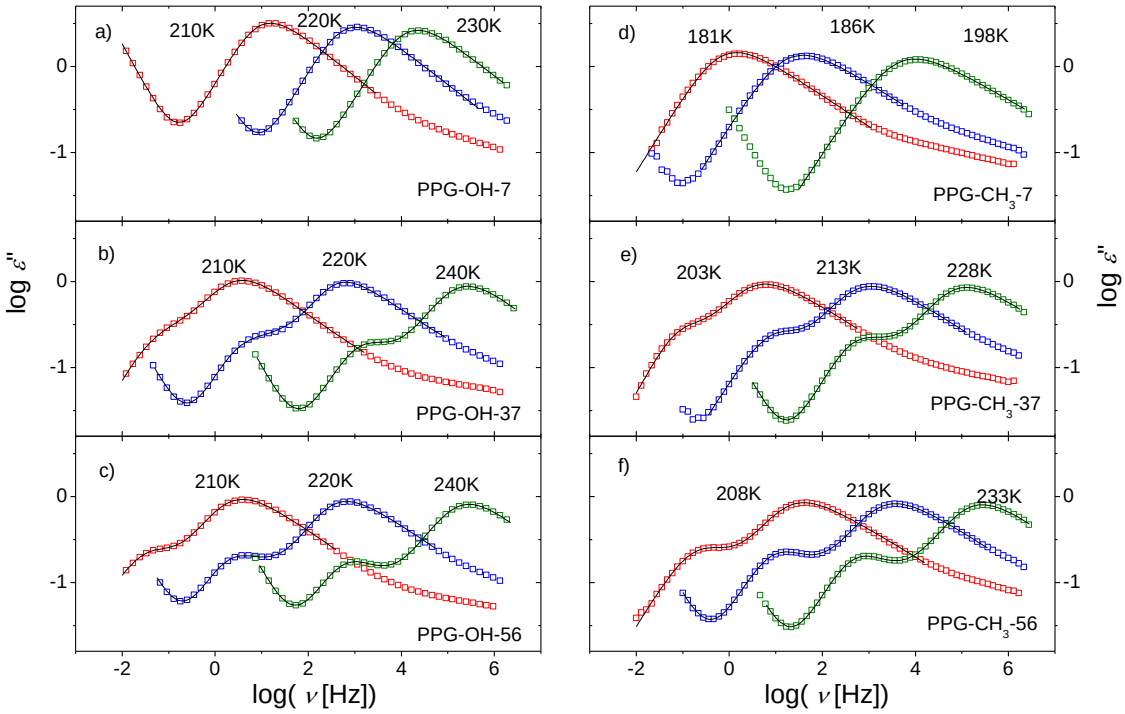

Figure 6. 4. Dielectric loss spectra $\varepsilon''(\nu)$ (symbols) at several temperatures as indicated of PPG- OH with *DP* of 7 (a), 37 (b) and 56 (c) and PPG-CH_3 with *DP* of 7 (d), 37 (e) and 56 (f). The solid lines are fits to functions consisting of one/two HN functions and a conductivity contribution (Eq. 2.9).

Table 6. 2. VFT parameters (Eq. 1.2) and fragility index *m* of the dielectric relaxations of PPG terminated with different chain ends.

	Fast process				**Slow process**			
Sample	log(τ_0 [s])	B [K]	T_0 [K]	m	log(τ_0 [s])	B [K]	T_0 [K]	m
PPG-NH_2-6	-13.2	1128	160	92	-	-	-	-
PPG-NH_2-33	-12.7	1002	169	99	-11.4	1383	155	60
PPG-NH_2-67	-12.8	1022	170	98	-10.3	1244	162	58
PPG-COOH-6	-	-	-	-	-11.5	1405	204	74
PPG-COOH-33	-12.6	1129	180	93	-11.5	1403	172	65
PPG-COOH-67	-13.9	1303	170	91	-12.6	1473	165	69
PPG-OH-7	-13.1	1270	160	81	-	-	-	-
PPG-OH-14	-13.1	1206	164	87	-	-	-	-
PPG-OH-18	-12.8	1079	168	94	-	-	-	-
PPG-OH-37	-12.7	1052	170	95	-11.8	1554	153	57
PPG-OH-56	-12.7	1044	170	96	-11.5	1500	156	57
PPG-CH_3-7	-13.5	1161	141	83	-	-	-	-
PPG-CH_3-14	-12.6	965	154	93	-	-	-	-
PPG-CH_3-18	-13.0	1045	156	98	-	-	-	-
PPG-CH_3-37	-12.8	1032	163	95	-11.4	1327	153	61
PPG-CH_3-56	-12.1	874	168	102	-10.8	1276	156	59

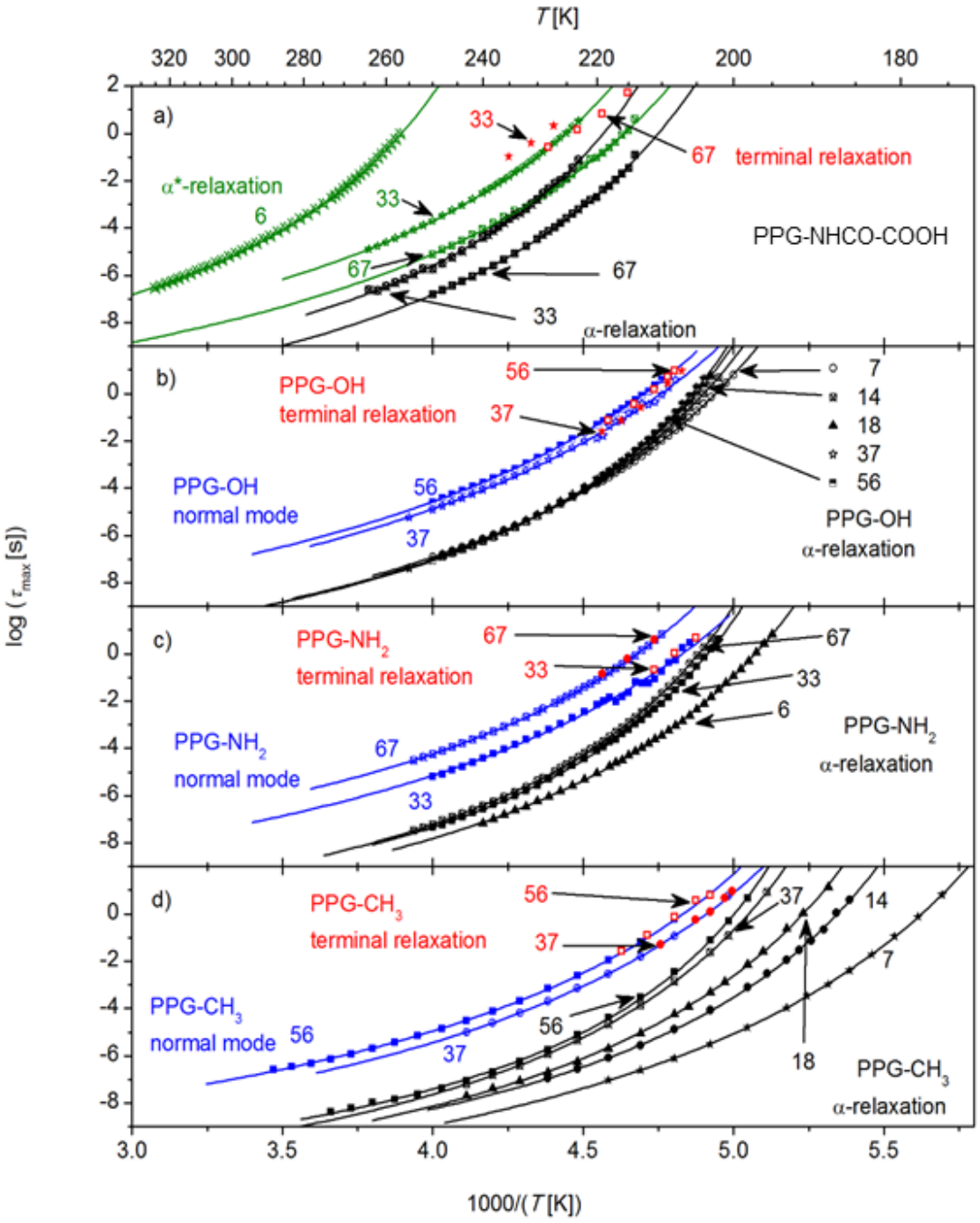

Figure 6. 5. Arrhenius plot of the mean relaxation time of dielectric relaxations for (a) PPG-NHCO-COOH, (b) PPG-OH, (c) PPG-NH_2 and (d) PPG-CH_3 with different *DP* as indicated by the numbers. The solid lines are fits to the VFT equation (Eq. 1.2). Additionally, the relaxation times of the terminal relaxation as determined from the shear modulus spectra are shown; we note that the rheological segmental relaxation times (not shown for clarity) are significantly slower than the dielectric α-relaxation times.

Since in PPG-NHCO-COOH spectra the normal mode is not visible (its amplitude is significantly smaller than the segmental peak), we also analyzed the derivative of the real part of the permittivity (Eq. 2.8).[211] This representation can help to unravel relaxation processes which are obscured by Ohmic conductivity or adjacent processes in the loss spectra. The derivative spectra of PPG-NHCO-COOH-67 indeed reveal a third relaxation process which appears as a shoulder at the low-frequency wing of the slower process (Fig. 6.6). In order to extract its characteristic relaxation time, we fitted the data to a Havriliak-Negami function modified for the derivative representation (see ref[211]).

6.3.3 Shear rheology and viscosity

The shear modulus master curves of all measured PPG samples were constructed by horizontal shifting of the shear modulus loss spectra until a best match with the spectra of the respective previous temperature scan was achieved. Although the underlying assumption of time-temperature superposition (tTS) may not be accurate in our case, the master curves can still provide a general picture of the mechanical properties and unravel distinctive processes of stress relaxation[229]. The shear modulus spectra (examples of telechelic PPG-NHCO-COOH are presented in Fig. 6.7) show the typical polymer features: i) at high frequencies, the value G_∞ is found in the GPa range common for segmental dynamics and G''(ω) exhibits a peak of segmental relaxation; ii) Rouse modes follow at lower frequencies, and iii) terminal relaxation ($G'(\omega) \sim \omega^2$ and $G''(\omega) \sim \omega^1$) appears at lowest frequencies. The separation between segmental relaxation and terminal mode becomes larger with increasing MW. In order to extract the respective timescales, the data sets have been fit to a function composed of a generic peak function[110] to account for contributions of segmental and chain dynamics:

$$G' = \frac{A}{[(\omega\tau_s)^{b1}+(\omega\tau_s)^{b2}]} + G_e \frac{\omega^2\tau_c^2}{1+\omega^2\tau_c^2} \quad (6.1\text{ a})$$

$$G'' = \frac{A}{[(\omega\tau_s)^{c1}+(\omega\tau_s)^{c2}]} + G_e \frac{\omega\tau_c}{1+\omega^2\tau_c^2} \quad (6.1\text{ b})$$

Where ω is the angular frequency, A and G_e represent the plateau moduli in the glassy and terminal regime, respectively, and τ_s and τ_c are the characteristic relaxation times of the

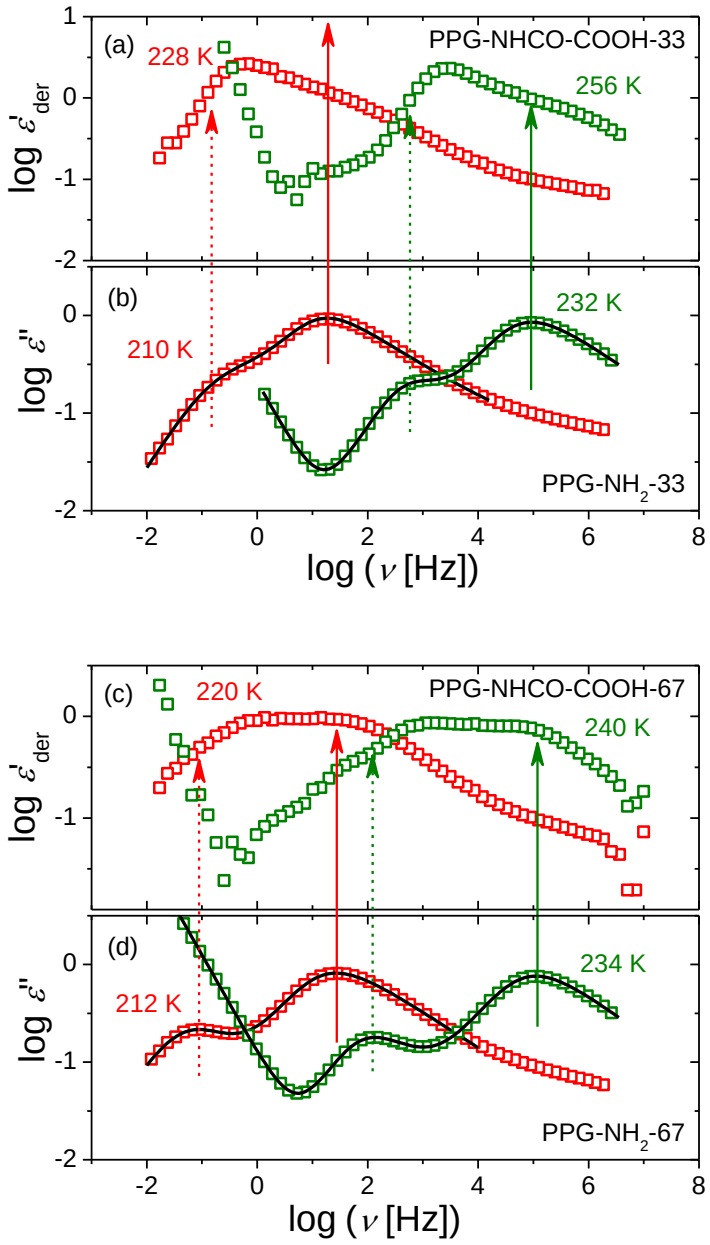

Figure 6. 6. a) and c) Spectra of ε'_{der} of PPG-NHCO-COOH with *DP* of 33 and 67, respectively, at several temperatures as indicated, as well as b) and d) the dielectric loss spectra ε'' of the corresponding PPG-NH_2. The temperatures of the latter were chosen to roughly match the α-relaxation peaks with the PPG-NHCO-COOH of the same *DP* in order to compensate the difference in T_g. The solid lines are fits to eq. 2.9.

segmental and terminal relaxation, respectively. The parameters b_1 and b_2 as well as c_1 and c_2 are the low and high frequency slopes of the G' and G'' curves, respectively. We note that this is a very rough approximation of the complex rheological spectra, and its generic shape includes the contribution of additional dynamics like Rouse modes which are very difficult to fit separately. Moreover, the first term in G' and G'' does not satisfy Kramers-Kronig relationship which is known to be valid for linear viscoelastic regime. Thus the approximation[110] is not valid for rigorous analysis of the relaxation spectra. However, this approximation is sufficient to estimate the characteristic relaxation times of segmental and terminal modes. The obtained relaxation times refer to the reference temperature. However, if the two processes have different temperature dependence, the constructed master curve will suffer from a corresponding distortion. Failure of tTS in our case is reflected in the slight difference in the temperature dependencies of the shift parameter a_T and the dielectric α-relaxation (Fig. 6.7). To obtain the terminal relaxation times at those temperature where they were actually measured (and not at the reference T) we divided the characteristic relaxation time obtained from the master curve by the shift factor at the respective temperature.

Normalized shear modulus master curves G' (ν/ν_{max}) / G_∞ and G'' (ν/ν_{max}) / G''_{max} (here G_∞ is the high frequency plateau value of G', and G''_{max} and ν_{max} represent the glassy relaxation peak maximum and position in G'') of PPG with similar molecular weight clearly reveal the impact of the different end groups (Fig. 6.8). The terminal relaxation for all OH-, NH_2- and amide-acid terminated PPG shifts to lower frequencies in comparison to that of non-associating PPG-CH_3. The separation between the loss maximum and the onset of (an apparent) terminal mode becomes significantly larger for PPG-NHCO-COOH. Since similar molecular weights are compared, this shift in terminal relaxation must be a consequence of the chain end association.

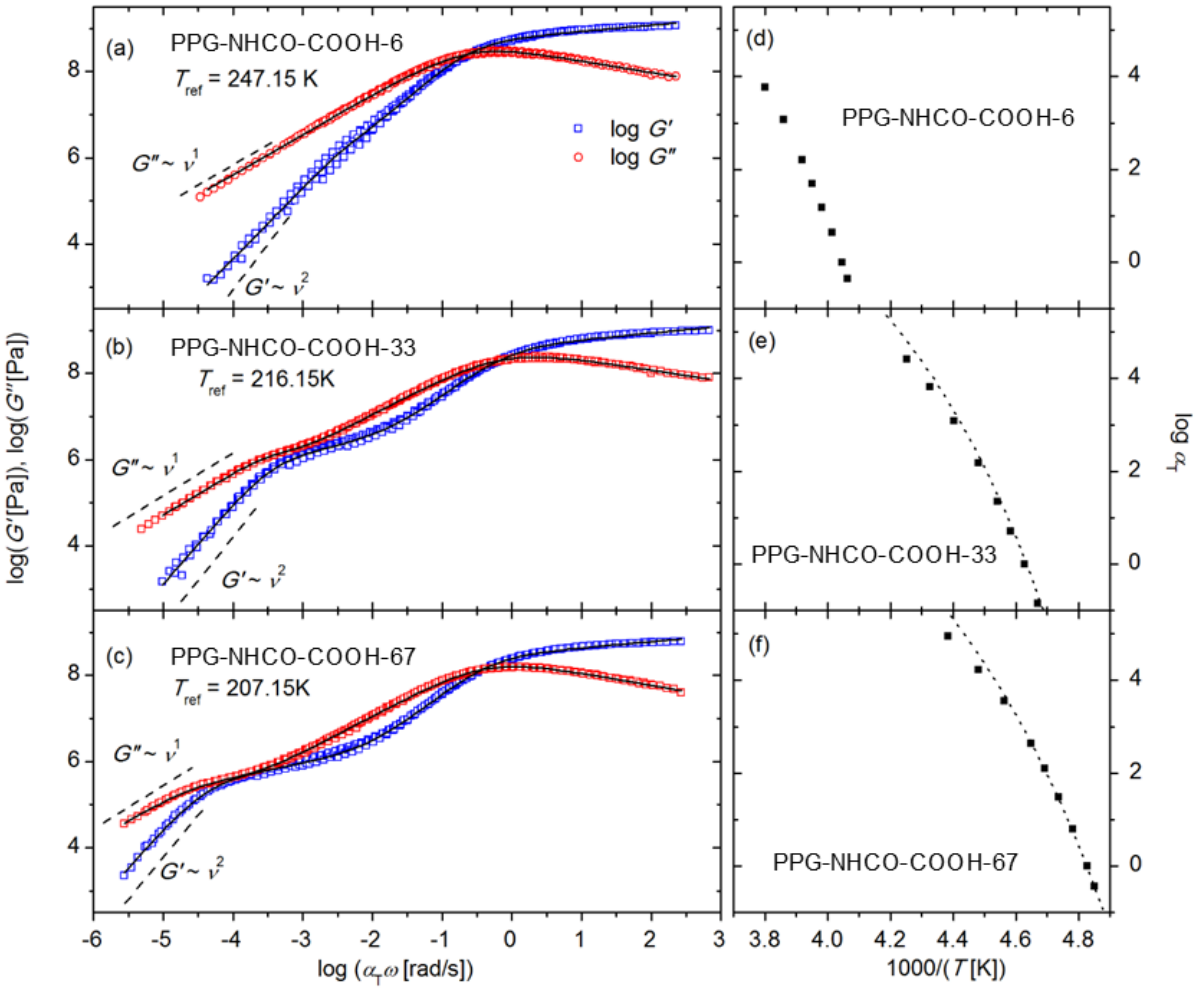

Figure 6. 7. Shear modulus master curves constructed from linear viscoelastic spectra using tTS for PPG-COOH with (a) *DP* = 6, (b) *DP* = 33 and (c) *DP* = 67, and the respective shift parameters (d-f). The solid lines are fits to Eq. 6.1, the dashed lines display the typical slopes in the terminal regime as indicated, and the dotted lines represent the temperature dependence of the dielectric α-relaxation time.

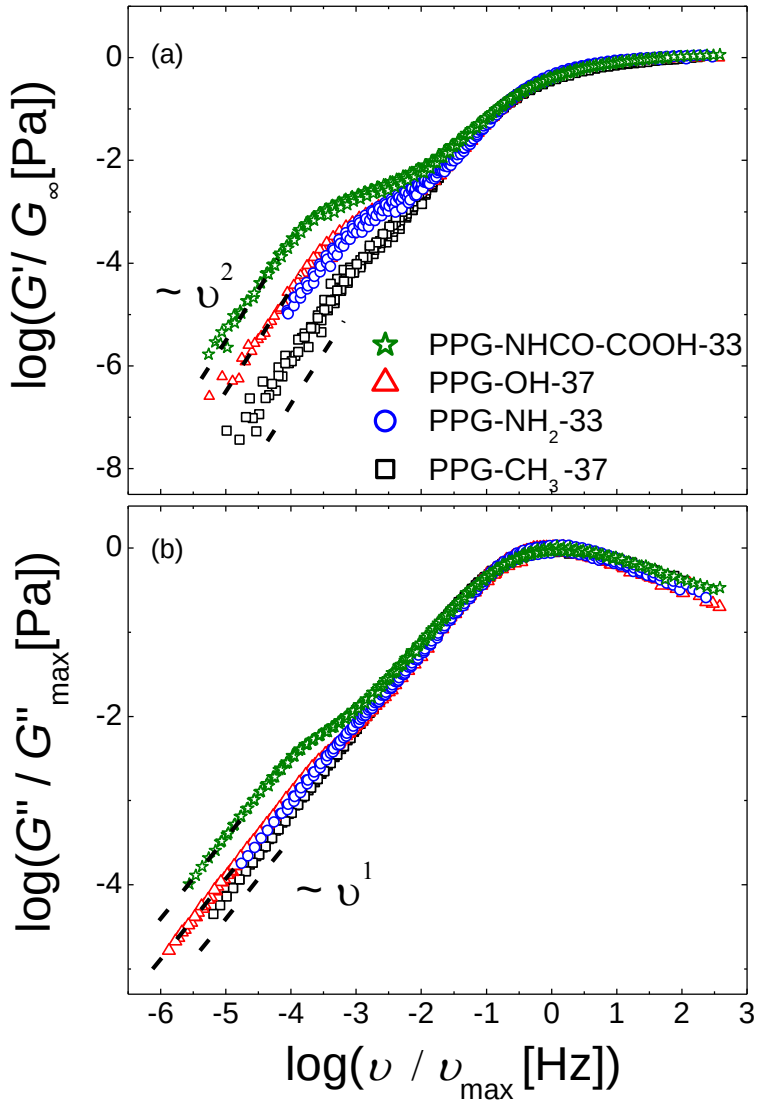

Figure 6. 8. Storage (a) and loss part (b) of the shear modulus master curves normalized with respect to the respective maxima G' (ν/ν_{max}) / G_∞ and G'' (ν/ν_{max}) / G''_{max} as well as the frequency position ν_{max} of G''_{max} obtained using tTS for PPG of different end-groups as indicated and similar *DP*. The dashed lines indicate the terminal end of the spectra.

To compensate for the impact of the difference in segmental dynamics, we present the zero-shear viscosity of different telechelic PPG vs T_g-scaled temperature (Fig. 6.9). The viscosities vs T_g/T for the NH_2 and OH terminated PPG differ only slightly from the viscosity of the CH_3 terminated system, while the viscosity increases by almost one decade for the amide-acid terminated PPG. A similar analysis of the viscosity has been performed for telechelic PDMS with the same set of chain ends[229]. In that case, a significant alteration in the viscosity, even after scaling out the role of T_g, was found for amide-acid terminated chains, while only a weak effect was observed for OH and NH_2 terminated PDMS (Fig. 6.9 b).

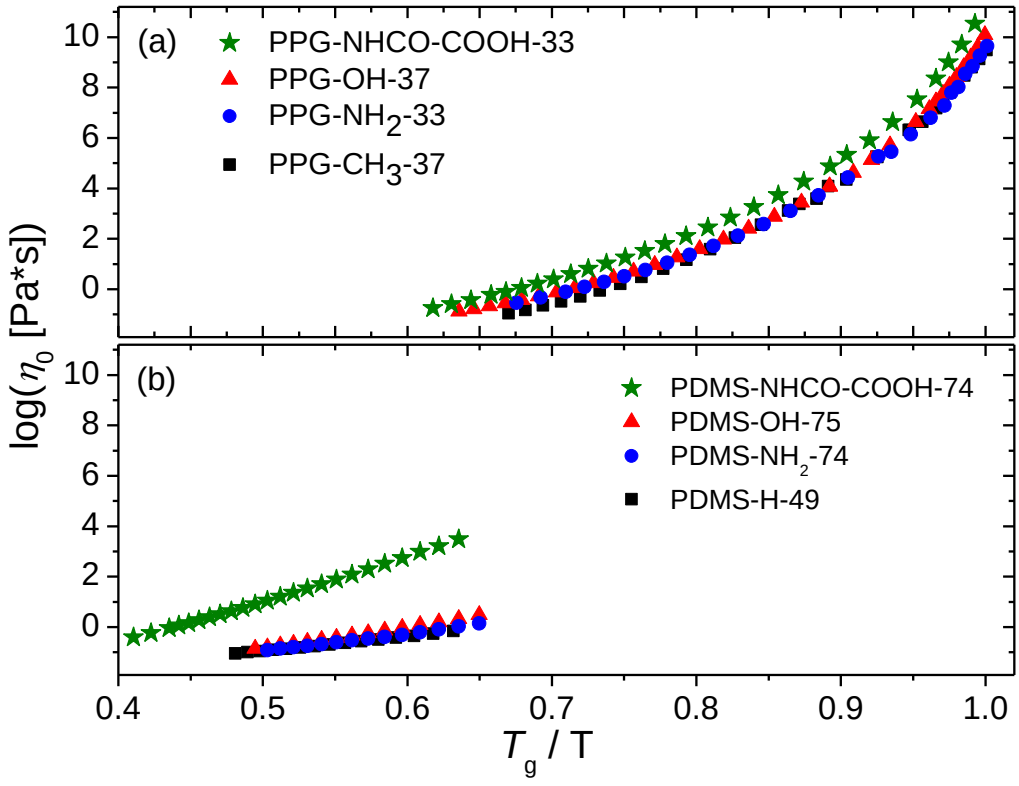

Figure 6. 9. Zero shear viscosity η_0 vs T_g/T for telechelic PPG (a) and PDMS (from continuous ramp measurements[320]). (b) with different end-groups as indicated with *DP* of 33-37 and 75, respectively.

6.4 Discussion

6.4.1 Impact of associating end-groups on T_g

One peculiar observation is the very different dependence of T_g (segmental dynamics) and viscosity (chain dynamics) on the strength of H-bonding end-groups association in the PPG systems. T_g increases significantly with increasing interaction strength, especially at lower MW (Fig. 6.2 a). However, once the shift in T_g is accounted for (by scaling the temperature by T_g), the viscosity shows only a very small increase with increase in strength of the chain end interaction strength (Fig. 6.9 a). This means, that beyond the increase of T_g, viscosity does not undergo any significant enhancement. This result strongly contrasts our previous findings in telechelic PDMS terminated with the same end-groups[229, 233]. In this more flexible backbone, the increase in T_g is similar for all three H-bonding end-groups independent of the interaction strength (Fig. 6.2 b). However, the T_g-scaled viscosity of PDMS-NHCO-COOH is enhanced by about 2-3 orders of magnitude compared to the chains with weaker or non-H-bonding end-groups (Fig. 6.9 b). These trends suggest that the difference in the backbone flexibility might play a significant role for the consequences chain-end association has on the system properties. We would like to note that larger effects seen in amide-acid terminated PDMS chains compared to the other two H-bonding systems may be due to the additional amide group[229]. In similar systems, urea and urethane groups were found to establish additional lateral H-bonds reinforcing the supramolecular structure[321]. Moreover, this end group seems to have the tendency to phase separate in PDMS, as evidenced from two T_g's observed in DSC data of PDMS-NHCO-COOH systems[229].

The most surprising result is that T_g in the telechelic PDMS is essentially independent of the H-bond strength, while it changes strongly for telechelic PPG with different end-groups (Fig. 6.2). We speculate that the chain end association in telechelic PDMS even in the weaker OH and NH_2 terminated chains essentially freezes the motions of the chain end segments at temperatures below ~180 K. In a simple picture, the end-groups and the adjacent segments may be considered as the high-T_g component of a miscible polymer blend or a co-polymer. An increase in molecular weight leads to a decrease of the volume fraction of this high-T_g component, and the measured T_g approaches the T_g of non-associating chains (Fig. 6.2).

However, at higher temperatures, e.g. T_g of PPG ~200K, the structural relaxation of the chain ends of OH and NH_2 terminated PPG becomes comparable to the segmental relaxation of long PPG chains. This would result in an essentially molecular weight independent T_g (Fig. 6.2 a). In contrast, the stronger NHCO-COOH association still freezes the PPG end segments even at T ~250K. This leads to the significant increase in T_g with decrease in MW for amide-acid terminated PPG (Fig. 6.2 a). Thus, the main difference in the behavior of segmental dynamics in these telechelic PDMS and telechelic PPG is the temperature range defined by their backbone flexibility. The much lower T_g of PDMS (~145K) makes even weaker H-bonding end-groups (e.g. NH_2 and OH) form strong enough associations which slow down the chain-ends and adjacent segments significantly. In contrast, at the higher T_g of PPG (~200K) these associations are weaker, resulting in structural relation times of the end segments with OH and NH_2 groups which are comparable to the segmental dynamics of the main chain. Only the end segments with -NHCO-COOH groups remain significantly slower leading to an increase of the overall T_g with decrease in MW.

6.4.2 Assignment of dielectric relaxations

For all the samples exhibiting two dielectric relaxations, the extrapolation of the VFT fits of the faster process to a mean relaxation time of 100 s yields a temperature that agrees well with the calorimetric $T_{g,cal}$ (Table 6.1). Consequently, we can identify the high-frequency process with the dielectric alpha-relaxation (segmental mode) and refer to the extrapolated temperature as the dielectric glass transition temperature $T_{g,\,diel}$. Also, the rather large fragility index *m* of this process (Table 6.2) is indicative for segmental relaxation. These characteristics hold also for the single relaxation observed in PPG-CH3-7, PPG-NH_2-6 and PPG-OH-7, and thus this process can also be assigned to the segmental relaxation. Only for the PPG-NHCO-COOH-6, $T_{g,\,diel}$ is more than 3K higher than $T_{g,cal}$, and the respective process has a much lower fragility index (Table 6.2); a point which will be discussed below.

The separation of the slower relaxation peak from the segmental peak in the spectra of CH_3, NH_2 and OH terminated samples decreases with decreasing MW, as is expected for the

normal mode.[110] There is no normal mode in the spectra of the smallest *DP* (~7 repeat units). Good agreement between the relaxation time of the slow dielectric mode and of the terminal relaxation time (Fig. 6.5) supports the assignment of the slow dielectric process in CH_3, NH_2 and OH terminated PPG to the normal mode.

In contrast, the slower process in the loss spectra of amide-acid terminated PPG exhibits approximately the same separation from the segmental relaxation, in all molecular weights where the two can be separated (Fig. 6.5 a). Furthermore, its relaxation strength by far exceeds that of the normal mode observed in other PPG samples of similar MW, and it grows drastically with decreasing MW (Fig. 6.10). In fact, the relaxation strength of this process exhibits linear dependence on inverse *DP* (inset Fig. 6.10). Finally, in the derivative spectra of the permittivity of PPG-NHCO-COOH-67 the normal mode relaxation can be observed precisely where it is expected based on the PPG-NH_2-67 data (Fig. 6.6). All these observations suggest that the slower process in the dielectric loss spectra of amide-acid terminated PPG is not the chain mode; instead, it reflects apparently a phenomenon which happens at the chain ends. Since it follows a VFT-like temperature dependence that is roughly parallel to the segmental relaxation with a separation of ~2 decades, a relation between these two processes can be assumed. Most likely, the slower process is related to the chain-end association/dissociation, as has been found in several other H-bonding supramolecular polymers[115, 160, 161, 229, 285], and we refer to it as the α*-relaxation. We assume that in PPG-NHCO-COOH-6, the α*-relaxation dominates the spectra and the segmental relaxation is hidden in its high frequency wing. This explains the largest difference between $T_{g,\,diel}$ and $T_{g,cal}$ observed for this sample (Table 6.1).

The α*-relaxations have been also observed in our earlier studies of NH_2 terminated telechelic PDMS[229] at frequencies lower than the segmental relaxation. However, in the cases of PPG-NH_2 and PPG-OH no such contribution is visible; the only process present in the low frequency region of the spectra is plausibly identified as the normal mode (Fig. 6.11). Our previous results on PDMS suggest that the dielectric relaxation strength of the α*-process of these end-groups is significantly lower than $\varepsilon''(\omega) < 0.1$[229], and is too weak to be detectable in the PPG samples where the low frequency range is dominated by their normal mode relaxations with the amplitude $\varepsilon''(\omega) > 0.2$ (Fig. 6.11).

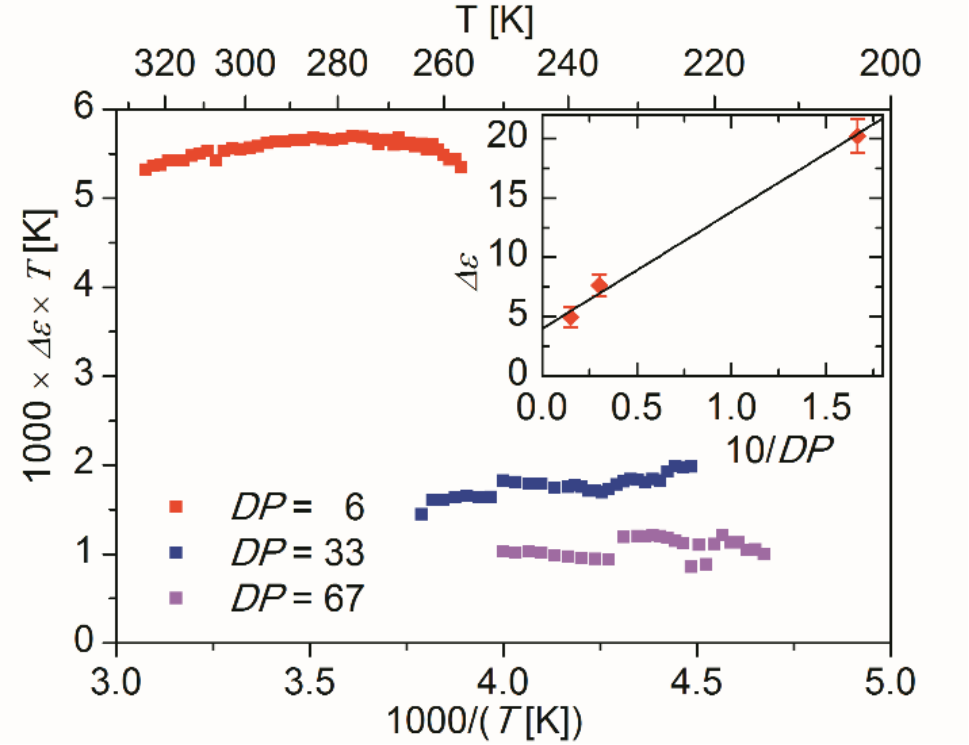

Figure 6. 10. Temperature dependence of the product of dielectric relaxation strength with temperature $\Delta\varepsilon T$ of the slower process of PPG-COOH with *DP* as indicated. Inset: dependence of the dielectric relaxation strengths of the slower process of PPG-COOH on the inverse of *DP*. The amplitudes of the peaks were averaged over several temperatures in the range where the peaks are well within the measured spectral window (266 – 297 K for PPG-COOH-6, 225 – 248 K for PPG-COOH-33 and 214 – 232 K for PPG-COOH-67).

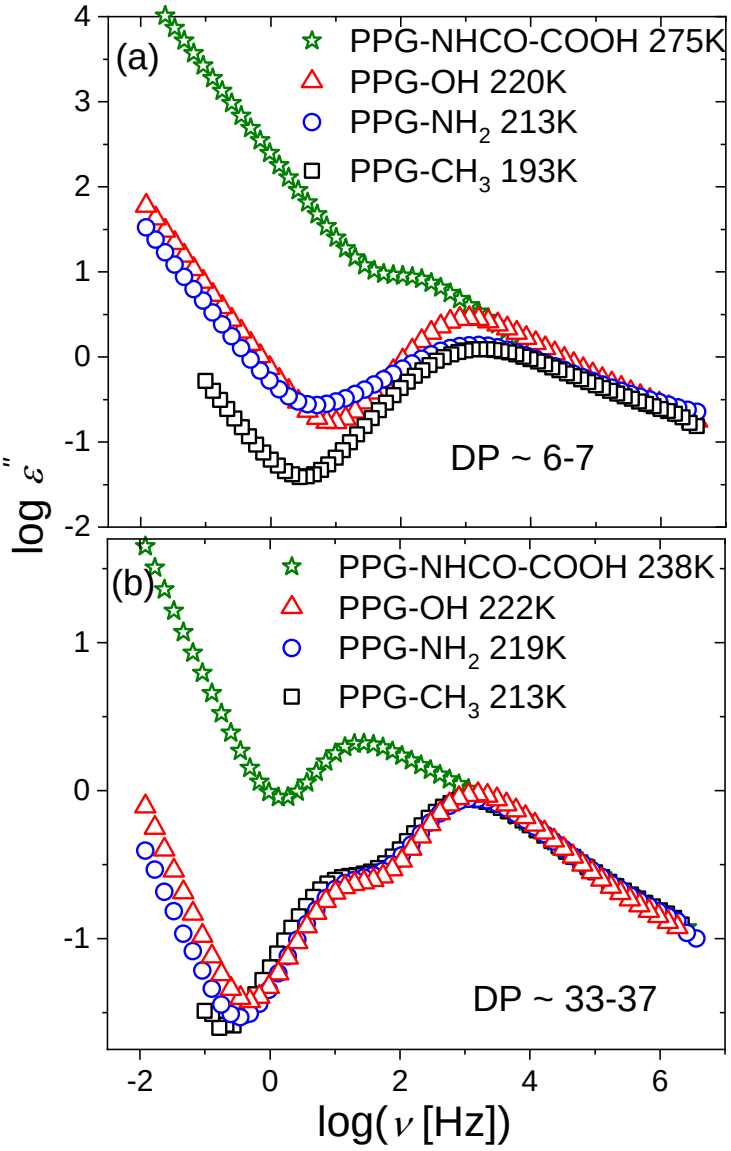

Figure 6. 11. Dielectric loss spectra $\varepsilon''(\nu)$ of PPG with different end-groups as indicated and *DP* of (a) 6-7 and (b) 33-35. Note that the curves are not normalized; to account for the change in T_g, different temperatures were chosen as indicated to match the α-relaxations.

6.4.3 Activation energies of the chain-end association

To estimate the characteristic chain-end dissociation energy E_a, we follow the recently proposed consideration that the segmental dynamics defines the attempting dissociation rate, and E_a can be obtained from the difference in relaxation time between the α- and the α*-relaxation:[39, 115, 160, 161]

$$\tau_{\alpha*}(T) = \tau_{\alpha}(T)\exp\left(\frac{E_a}{RT}\right) \quad (6.2)$$

where R is the universal gas constant. Using the VFT fit parameters of the respective α-relaxation to fix τ (T), and keeping E_a as the only free parameter in the Eq. 6.2, we estimated the activation energies of the α*-relaxation to be 8.5 (±1) kJ mol^{-1} and 7.2 (±1) kJ mol^{-1} for PPG-NHCO-COOH with *DP* of 33 and 67, respectively (Fig. 6.12). For the single process observed in the dielectric spectra of PPG-NHCO-COOH-6 we have several indications that it is the same chain-end dissociation process: its estimated T_g is significantly higher than that obtained from DSC, meaning that it seems to be slower than the α-relaxation. Also, its fragility index m is close to that of the α*-relaxations (Table 6.2). Based on this assignment, we can estimate $\tau_\alpha(T)$ in this sample using Eq. 6.2 and assuming an activation energy of 8 kJ/mol. The obtained temperature dependence of the segmental relaxation is presented as the dashed-dotted line in the Fig. 6.12, and its extrapolation to τ_α = 100 s provides an estimate of $T_{g,\,diel}$ somewhat closer to the calorimetric T_g, which further supports our assignment of the major process (Fig. 6.5 a) to the chain-end dissociation process.

Additionally, the polarity of the medium where the dissociation of chain ends occurs might play a role. In the case of PPG, the dissociation energy for H-bonding end groups might be significantly smaller than in PDMS (~15 kJ/mol, as discussed in Chapter 5), because these groups will have some attractive interactions with hydrophilic PPG, but not with hydrophobic PDMS.

Since in the shear modulus master curves we observed a trend of increasing separation between segmental and terminal relaxation with increasing association strength of the end-group (Fig. 6.8), one might be inclined to presume the same mechanism behind the prolonged

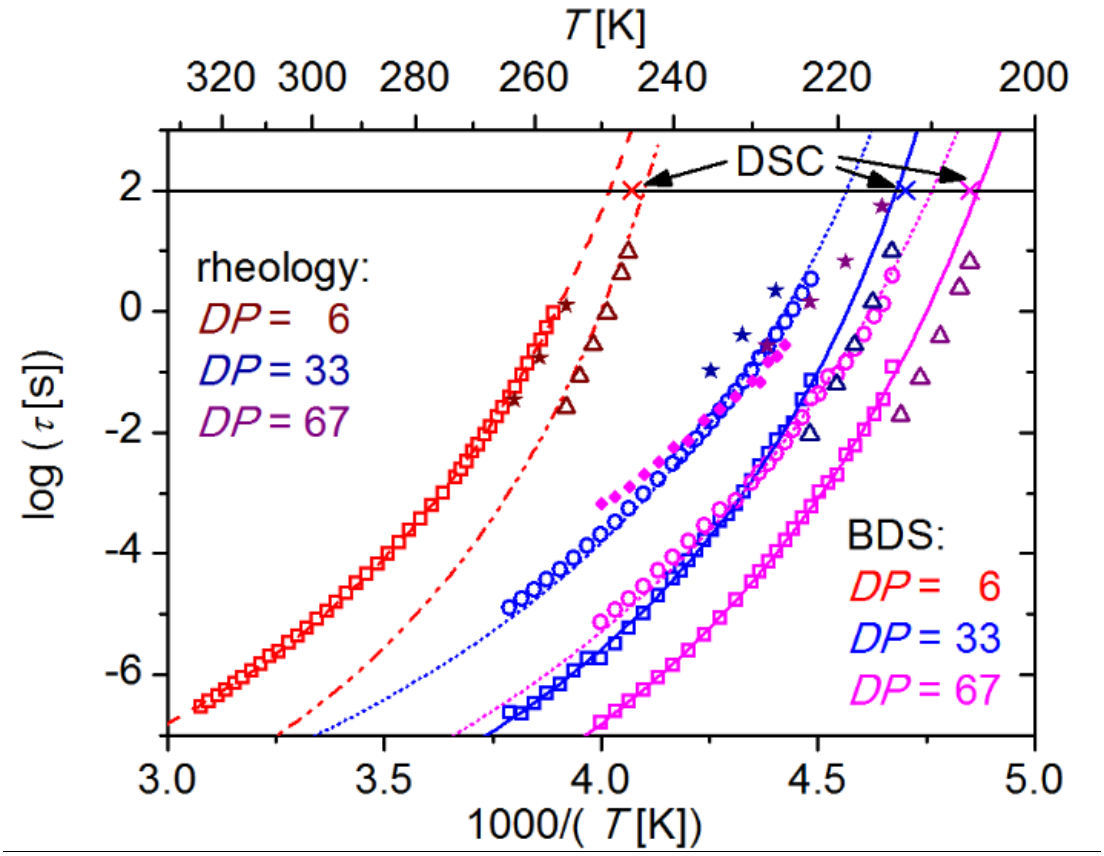

Figure 6. 12. Arrhenius plot of the dielectric mean relaxation time of the α-relaxation (open squares) and the α*-relaxation (open circles) obtained from the ε'' spectra, as well as the normal mode (solid diamonds) obtained from the ε'_{der} spectra, the calorimetric T_g (crosses), and the rheological segmental relaxation (open triangles) and terminal relaxation (solid stars) for PPG-NHCO-COOH with different *DP* as indicated. The solid and dashed lines are VFT fits, and the dotted lines are fits to Eq. 6.2 where the VFT parameters were fixed to the values obtained for the α-relaxation (see text for details). The dash-dotted line represents the estimated temperature dependence of the α-relaxation in PPG-NHCO-COOH-6 sample, assuming E_a = 8 kJ/mol and that the dielectric relaxation process presents the chain-end dissociation.

terminal relaxation and the α^*-relaxation from the dielectric spectra. However, the analysis of the characteristic times of these two processes (Fig. 6.12) reveals, that in PPG-NHCO-COOH of *DP* 33 and 67 the separation between the rheological terminal and segmental relaxations is significantly larger than between the dielectric α^*- and α-relaxations. This difference originates from the fact that these two processes seem to reflect different molecular mechanisms in the chain end disscociation[39, 115, 160, 161]. The dielectric relaxation represents the rate of the chain end dissociation since this process involves a change in a dipole moment, which happens every time the chain ends associate or dissociate. In contrast, the process in shear modulus reflects a macroscopic stress relaxation which requires a switch of the associated chain-end from one partner chain to another[115, 160, 161]. Dissociation and reassociation with the same bond partner will not provide stress relaxation, but will appear in the dielectric spectra. It means that mechanical relaxation probes the rate of partner exchange which depends not only on the dissociation rate, but also on the probability to find another associating chain-end relative to the probability to reconnect to the same initial chain-end. It has been proposed[115, 160, 161] that the rheologically detectable timescale τ_r comprises a certain number *n* of dissociation and reassociation events with the same partner, and additionally the time of chain end diffusion, before a new partner can be reached. Thus, the mechanical relaxation does not provide direct estimates of the dissociation energy. At that point we will not go deeper into an analysis of these results because it requires relatively long discussion and complex data analysis, and this is not the major focus of the current manuscript.

6.4.4 Interplay of end-group association, segmental dynamics and shear viscosity

The above discussion demonstrates the complex interrelation of segmental dynamics, chain dynamics and the end-group association. Segmental dynamics is affected by any associating end-groups as reflected by the increase in T_g compared to non-associating reference systems. This increase is large for short chains and diminishes with increasing MW (Fig. 6.2). For strong associations there seems to be a limit in the T_g increase while intermediate interaction strengths can yield, depending on their dissociation energy, any T_g shift between this limit and

the behavior of the reference. Additionally, the strength of the chain-end association depends on temperature; the same OH and NH_2 end-groups provide strong association for PDMS at its characteristic T_g ~145, while they have only intermediate association strength in PPG with T_g ~200K (Fig. 6.2). Consequently, the chain flexibility strongly affects the chain-end association simply through the relationship of the association energy to T_g that controls the characteristic chain-end dissociation time.

Furthermore, we suspect that the possibility of the end-groups to form H-bonds with the PPG backbone additionally reduces the energy barrier for dissociation of H-bonding end groups in this polymer. Thus, we expect that the dissociation time of the H-bonding chain-ends is additionally reduced in PPG relative to the case of PDMS. In fact, PDMS-NHCO-COOH exhibits a larger separation of α*- and α-relaxation than PPG-NHCO-COOH which supports the view that apparently the polarity of the surrounding medium is important as well.

A different relation to the end-group association is found for the macroscopic mechanical properties, e.g. terminal relaxation and viscosity, because these are governed primarily by the relaxation of the whole chain. Several timescales are involved: i) the local dissociation time, governed by the segmental relaxation time and activation energy of dissociation (Eq. 2.10); ii) the time it takes a chain-end to switch its association partner (i.e. partner-exchange time), defined by the probability for the dissociated chain end to find another chain, which should vary strongly with MW; and iii) the longest relaxation time of a similar chain without association (i.e. normal chain relaxation). If the partner-exchange time is of the same order or longer than the normal chain relaxation, both zero shear viscosity and terminal relaxation time will increase compared to the reference system with non-H-bonding end-groups (even after scaling out the effect of T_g). However, if the normal chain relaxation time is much longer than the partner-exchange time, the terminal relaxation time and viscosity will be defined by this normal chain relaxation time, i.e. these will be similar to the behavior of non-associating chains.

In particular, the partner-exchange time in the PDMS based systems apparently exceeds the normal chain relaxation only in case of amide-acid end-groups, while for OH and NH_2 chain-

ends it is shorter than the chain relaxation time, resulting in the strong increase of viscosity in the former and no significant change in the latter two (Fig. 6.9 b). In contrast, in the PPG based systems the temperature is higher (larger T_g) and the matrix is more polar, both of which result in weaker associations for the same end-groups. As a result, even in the case of PPG-NHCO-COOH the dissociation time appears to be significantly shorter than the chain relaxation time (Fig. 6.12). This leads to the partner-exchange time also being shorter than or comparable to the normal chain relaxation time in PPG. This explains similar behavior of viscosity (scaled by T_g) in all PPG samples regardless of their chain-ends (Fig. 6.9 a).

In more general terms, for the design of materials with enhanced mechanical properties based on associating functional groups, just considering the activation energy for dissociation of those groups is insufficient. Instead, the ratio of dissociation time to the segmental and chain relaxation times as well as the probability to find a new partner available for association (i.e. chain length) must be taken into account.

6.5 Conclusion

We studied the impact of H-bonding interaction strength and molecular weight in telechelic PPG using DSC, dielectric spectroscopy and linear rheology. As expected, the chain-end interactions lead to a slowdown of segmental dynamics, an increase in T_g, and both effects are larger for smaller MW. However, the magnitude of this increase in PPG strongly depends on the chain-end interaction strength. This is in contrast to our previous results on telechelic PDMS where the T_g shift was essentially independent of the strength of the chain-end H-bonding[233]. At the same time, zero shear viscosity corrected for the shift in T_g is almost independent of the type of end-group in telechelic PPG, while large differences were found in telechelic PDMS with the same set of end-groups. We explain these observations by the differences in chain-end dissociation time relative to the timescale of the respective structural motion (faster segmental relaxation – T_g vs. slower chain relaxation – viscosity). In telechelic PPG, these chain-end dissociation times, as measured by dielectric spectroscopy, do not exceed the normal chain relaxation even for the end-group with the strongest interactions studied here (amide-acid).

Consequently, viscosity is barely affected in strong contrast to the case of PDMS in our previous study where the viscosity of the amide-acid terminated chains exhibits a pronounced increase. In this system, the dissociation of the end-groups is much slower, partially due to the lower temperature at which the relaxations take place in this material.

We would like to emphasize that the segmental relaxation rate plays a fundamental role in defining the timescale of the dissociation process. This means that the activation energy of the functional groups alone is not sufficient to describe their impact on the macroscopic mechanical properties. Instead, we should consider the rate of dissociation which is based on both the segmental relaxation and activation energy for dissociation. Furthermore, to realize a mechanical relaxation of the system, also the probability for a dissociated-chain end to switch from its current partner to another one must be considered. Comparing this partner exchange rate with the chain relaxation rate eventually allows predictions for the resulting macroscopic viscoelastic properties. In other words, the associating groups must be selected particularly for a specific polymer to ensure that, in combination with segmental relaxation and partner exchange probability, the chain relaxation can be matched accordingly to achieve the desired properties.

Chapter VII

Interplay of Structure, Dynamics and Viscoelastic Properties in Supramolecular Networks of Telechelic Polymers

Reproduced in part from: Martin Tress, Kunyue Xing, Sirui Ge, Pengfei Cao, Tomonori Saito, Alexei P. Sokolov. "What dielectric spectroscopy can tell us about supramolecular networks" *Eur. Phys. J. E* 2019, 42, 133. Kunyue Xing contributed to material synthesis, BDS, DSC and rheology measurements, data analysis and writing. Sirui Ge contributed to data analysis, Pengfei Cao and Tomonori Saito contributed to material design. Martin Tress contributed to data analysis and writing. Alexei Sokolov led the project, contributed to data analysis and writing.

And Sirui Ge, Martin Tress, Kunyue Xing, Pengfei Cao, Tomonori Saito, Alexei P. Sokolov. "Viscoelasticity in associating oligomers and polymers: experimental test of the bond lifetime renormalization model", accepted by *Soft Matter*. Kunyue Xing contributed to material synthesis, BDS, DSC and rheology measurements, data analysis and writing. Sirui Ge and Martin Tress contributed to data analysis and writing. Pengfei Cao and Tomonori Saito contributed to material design. Alexei Sokolov led the project, contributed to data analysis and writing.

The Small-angle X-ray (SAXS) experiments were done by Dr. Halie Martin.

7.1 Introduction

Besides the interchain reversible associations, the properties of the polymeric backbones, *e.g.*, rigidity, and chain entanglements, another important factor that plays a decisive role in the properties and functions of supramolecular polymer networks is nano- or micro-phase separation of the associating groups. These nano or microscopic phase separations are normally driven by the difference between the polarity of the transient associative motifs and the polymer backbones. There are several systems reported with associating groups

densely or collectively packed and phase segregated into aggregates, clusters or assemblies,[39-41, 50, 79, 113, 181, 285, 322-328] but the understanding of how phase morphology and chain structures affect the performance of supramolecular polymers on molecular or microscopic scale is still far from complete.

Since the structure and dynamics can change according to microphase separation in polymer melts, even relatively weak secondary interactions (H-bonding) can exert significant influence on the performance of the transient networks.[326, 329-331] Thurn-Albrecht *and coworkers* had conducted a series of research based on telechelic polyisobutylenes (PIB) with triple H-bonding motifs (self-complementary barbituric acid groups, hetero-complementary thymine and 2,6-diaminotriazine groups) and varied molecular weight.[179, 181, 196] By employing detailed structural analysis by SAXS (Small-angle X-ray Spectroscopy), the authors claimed that the mechanical properties possess a sensitive dependence on chain association as well as on aggregation and self-assembly phenomena.[181] They also reported that the temperature dependence of the terminal relaxation time is governed by the functional groups, not by chain dynamics, and meanwhile, the terminal relaxation time is weakly correlated to molecular weight. Thus, it's concluded that it's possible to independently tune the elastic properties and terminal flow behavior of telechelic networks by the molecular weight of the backbones and the functional groups respectively.[179] Alegria *and coworkers* have reported that monocarboxydecyl-terminated dimethylsiloxane (DMS-DCOOH) oligomer, roughly 14 monomeric units per molecule, developed well-ordered regular mesostructure below 230 K and a hexagonally packed cylinders appear below 200 K, and the latter one provided rubber-like properties to the material. They summarized that the H-bonding interactions (carboxylic acid group) plays a decisive role in its properties below room temperature, tending to form small size regular nanostructures and meanwhile, preventing the development of long-range atomic order. It's amazing that for short PDMS backbone, even mono-associating chain end which could only provide double H-bonding can give rise to nano-scale phase separation below room temperature. Although there's several investigations taken up on how structure and chain length of the backbones influence the viscoelastic and mechanical properties of associating

telechelic systems, detailed systematic research including different end-groups and phase separation, besides the former mentions factors, is rather limited.

Here, we investigated telechelic poly(dimethylsiloxane) (PDMS) with different hydrogen-bonding end-groups and varying chain length in the melt state by means of broadband dielectric spectroscopy (BDS), differential scanning calorimetry (DSC), rheology and small-angle X-ray scattering (SAXS) to study the influence of phase segregation driven by hydrogen-bondings on the macroscopic and molecular dynamics in unentangled associating telechelic systems. Depending on the type of hydrogen-bonding end group, -NH_2, -OH, -S-COOH, or -NHCO-COOH, we observe characteristic similarities and differences in structure, dynamics and viscoelastic properties of these associating polymers. All systems exhibit an increase of the glass transition temperature T_g with decreasing M_W. Only in the amide-acid (NHCO-COOH) terminated system, a 2nd T_g is found which indicates phase separation of chain ends. This is corroborated by the SAXS measurements and also the BDS experiments. As a result, the shear viscosity of PDMS-NHCO-COOH is significantly higher than for the systems with other end groups, even after scaling with T_g. Additionally, the shear modulus exhibits an extended rubbery plateau of high magnitude in the -NHCO-COOH terminated systems. In contrast, PDMS-S-COOH shows only a short rubbery plateau. This suggests, that not just the end-group (-COOH in both case) but also the linker group (-NHCO- vs. -S-) plays an important role. Only the -NHCO-COOH groups aggregate strongly, leading to a pronounced phase separation as evident from the SAXS measurements. The absence of higher order peaks in SAXS suggests that the spatial arrangement of the aggregates is not highly ordered. Our analysis clearly demonstrates that phase separation affects viscoelastic properties stronger than the strength of the chain ends interactions.

7.2. Methods

7.2.1 Different Scanning Calorimetry (DSC)

The calorimetric measurements were performed by TA Instrument DSC 2500. Samples were all dried in the vacuum oven at 313 K for 5 days before use. In all measurements, the

samples were sealed in Tzero pans, weight between 7-11 mg, stabilized at 378K for 5 min and went through the same temperature range of 100-293 K at a scan rate of 10 K/min. The cooling and heating cycles were repeated twice to confirm the reproducibility of the results. The glass transition temperature (T_g) was determined from the midpoint of the heat flow step during the 2nd heating by the TA Universal Analysis 2000 software.

7.2.2 Broadband Dielectric Spectroscopy (BDS)

Dielectric spectra in the frequency range 10^{-2}-10^{7} Hz were performed using a Novocontrol system that includes an Alpha-A impedance analyzer and a Quatro Cryosystem temperature control unit. Samples were dried in the vacuum oven at 313 K for 5 days before use, placed in a parallel-plate dielectric cell made of sapphire and invar steel (Fig. 2.6 b), similar to the one described in ref[238]. The empty cell, with an electrode diameter of 12 mm and electrode separation of 49 μm, had a capacitance of 20 pF. To avoid crystallization, all samples were quenched from room temperature to about 113 K and reheated to 5 K below the calorimetric glass transition temperature (T_g) prior to the measurements upon further heating. Samples were equilibrated for at least 15 min to maintain a thermal stabilization within 0.2 K.

7.2.3 Shear rheology

Prior to all rheological measurement the samples were dried in the same way as described above. Linear viscoelastic properties were performed with the AR2000ex (TA Instruments). Small-amplitude oscillatory shear (SAOS) measurements were carried out in an angular frequency range 10^{-1}-10^{2} rad/s using parallel plate geometry, with a disk diameter of 4 mm and 8 mm according to the magnitude of the shear modulus. The samples were loaded at room temperature and fast cooled down to calorimetric glass transition temperature (T_g). The strain amplitude was adjusted to maintain linearity of the shear modulus response in each sweep. Before each rheological measurement, a thermal stabilization of 10 minutes was performed to assure thermal equilibrium. Temperature was stabilized within 0.2 K for all measurements. Zero shear viscosity measurements for the $\eta^0 < 10^5$ Pa*s (temperature range

from 220 K to 300 K) were conducted in continuous ramp measurements with a shear rate of 1-10 s^{-1}. We used a conical plate of 25 mm in diameter with a cone angle of 20 and a truncation of 58 µm. Zero shear viscosity $\eta_0 > 10^5$ Pa*s ($T < 220$ K) were estimated using terminal relaxation mode in SAOS measurement $\eta_0 = \lim_{\omega \to 0} G''/\omega$.

7.3 Results and discussion

7.3.1 Different Scanning Calorimetry and glass transition temperature

The two samples both exhibit an endothermic step for temperatures $T > 150$ K associated with the glass transition in the heating process (Fig. 7.1 a). The calorimetric glass transition temperature $T_{g,cal}$ was determined at the midpoint of this step, which is shown in Table 7.1. An exothermic transition at ~ 185 K indicates the crystallization process in PDMS-S-COOH-83 upon heating, followed by melting processes among 210- 240 K. Crystallization of PDMS-S-COOH-83 also take place in BDS and rheological measurements. No signs of crystallization appear in PDMS-S-COOH-13.

To compare T_g of PDMS with different chain-end association strength, we plotted T_g of PDMS-S-COOH together with PDMS-OH (chapter 4), PDMS-NH_2, PDMS-NHCO-COOH and PDMS-CH_3 (chapter 5) on dependence of M_n (Fig. 7.1 b). PDMS-S-COOH possesses similar trend to PDMS-OH, PDMS-NH_2 and PDMS-NHCO-COOH, that their T_g increases with a decrease of M_n. On the contrary to the normal polymers, this trend is captured in several associating polymers with intermolecular H-bonds[48, 229-231, 233, 332]. As we proposed in chapter 6, although they have functional end motifs with different strength, the similar MW dependence of the glass transition in telechelic PDMS with different chain ends (-OH, -NH_2, -NHCO-COOH) is a result of their relatively longer lifetime of the associating chain ends, comparing to the structural relaxation time of the backbone, that they all behave as permanent interactions on segmental motion scale. Surprisingly, the T_g of PDMS-S-COOH-13 is much higher than that of PDMS-NHCO-COOH-13, and we leave it as an open question in this manuscript.

Noted that for PDMS-NHCO-COOH, we have observed a 2nd T_g of all three molecular weights indicating phase separation in these materials which is also confirmed in rheological

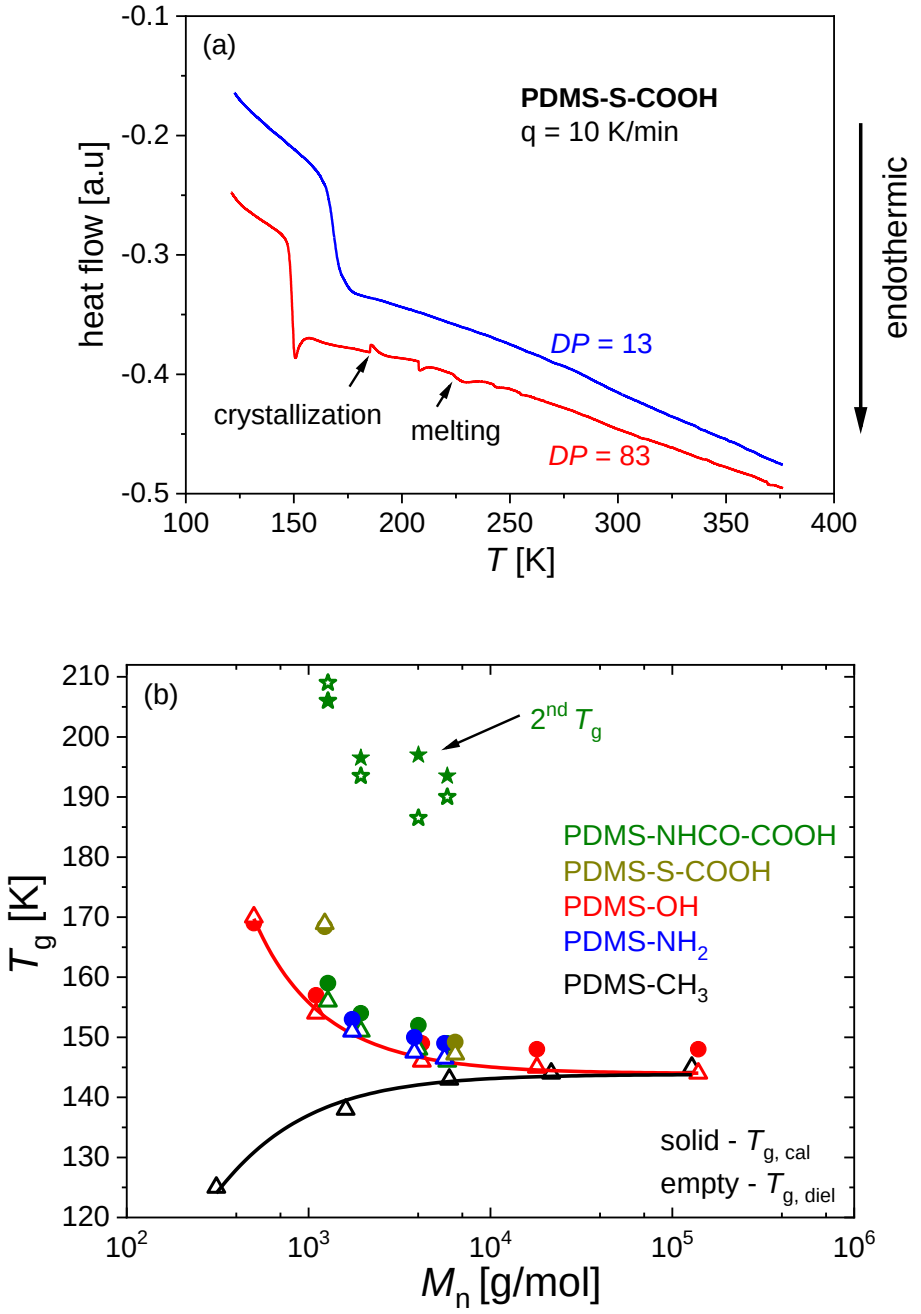

Figure 7. 1. (a) Calorimetric curves recorded on heating of PDMS-S-COOH with a constant heating rate q= 10 K/mol. The curves are vertically shifted for clarity. (b) Calorimetric and dielectric T_g (solid and open symbols, respectively) vs. number averaged molecular weight M_n (including end groups) in PDMS-OH[233], PDMS-CH_3[241], PDMS-NH_2[229], PDMS-NHCO-COOH[229] and PDMS-S-COOH. Lines are fits of the PDMS-OH and the PDMS-CH_3 data to the Fox-Flory equation[279]. X axis is in logarithmic scale.

and BDS results (Chapter 5). While for PDMS-S-COOH, with similar carboxylic acid chain ends but without the linker group (-NHCO-) that could produce extra H-bonding, there's only one T_g appeared in DSC results.

7.3.2 Small-angle X-ray Scattering (SAXS)

To study aggregation phenomena and phase structure, samples can be characterized by Small-angle X-ray Scattering (SAXS). The detailed analysis of the SAXS features of selected PDMS-H, PDMS-NH_2, PDMS-NHCO-COOH and PDMS-S-COOH at different temperatures was done after subtraction of a background signal (Fig. 7.2). The peak at 0.85 $Å^{-1}$ is related to spatial correlations between chain segments of PDMS[333]. A well-defined peak at a scattering vector q^* is visible in PDMS-NHCO-COOH-22, 50, 74 and PDMS-S-COOH-13 both at 200 K and room temperature, showing the existence of aggregation in these systems.

The average distance between the clusters' centers d can be estimated by $2\pi/q^*$ (4~6nm) and its dependence on chain end volume fraction Φ_v (Table 7.1) at varied temperatures is shown in Fig. 7.3 a. At a certain temperature, the mean distance between the aggregates drops as chain end volume fraction increases (namely, shorter chain backbones). For PDMS-NHCO-COOH-22, -50, as temperature increases, q^* shift to higher values, accordingly the mean distance between the aggregates becomes smaller and their number density becomes larger. As expected, the H-bonding becomes less stable at elevated temperatures and less chain end motifs tend to aggregate into one cluster. Therefore, there will be more clusters with smaller size per unit volume and the mean distance between clusters becomes smaller, correspondingly.

The peak in spectra of all samples becomes broader as temperature increases (Fig. 7.2), suggesting increase of the distribution of the distance between clusters. Furthermore, to compare the intensity of the characteristic peak at the low q^*, they were normalized by the intensity of the peak at 0.85 $Å^{-1}$ which is related to spatial correlations between chain segments of PDMS. For each temperature, the normalized peak intensity of PDMS-NHCO-COOH drops as

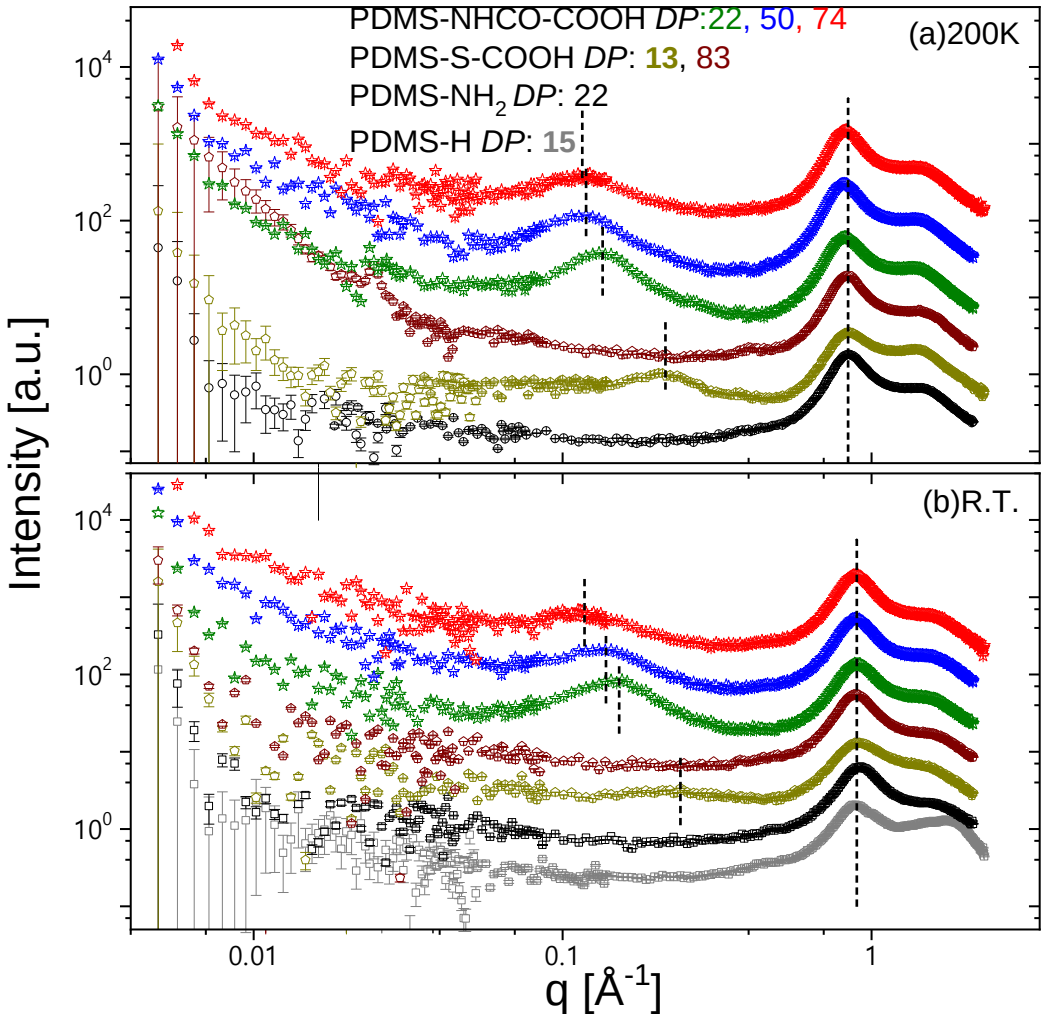

Figure 7. 2. SAXS patterns of PDMS-NHCO-COOH, PDMS-S-COOH, PDMS-NH_2 and non-associated PDMS-H (from top to bottom) with different *DP* at 200 K (a) and room temperature (b). The curves are shifted vertically, subtract with background signal and plot in logarithmic scale.

Table 7. 1. Total molecular weight M_n, degree of polymerization (*DP*), weight fraction of end groups f_e, volume fraction of end groups Φ_v, activation energy E_a, calorimetric (DSC) and dielectric (BDS) T_g. The volume of the backbone and end group is calculated by $V_m = M/\rho N$A. The PDMS density is 0.965 g/cm^3. Since the end group structure is similar to 3-ethylsulfanylpropanoic acid, we use the density of the latter one, 1.121 g/cm^3, as the end group's density. The volume fraction of the end groups is estimated using the volume of end groups divided by the total volume of end groups and backbone.

Material	M_n[g/mol]	*DP*	f_e[wt%]	Φ_v[%]	$T_{g,cal}$[K]	$T_{g,diel}$[K]	E_a[kJ/mol]
PDMS-S-COOH-13	1228	13	21.7	19.2	168.4	168.9	8.2±1
PDMS-S-COOH-83	6408	83	4.2	3.6	149.2	147.2	8.1±1

weight fraction of chain ends decreases, suggesting formation of less aggregates. For PDMS-S-COOH-13 and PDMS-NHCO-COOH-74, the peak becomes weaker in intensity (Fig. 7.2 and Fig. 7.3 b) at the higher temperature. We expect that this indicates a diminishing number of the aggregates with increasing temperature. Namely, there are more chains with chain ends not bounded to the clusters at the high temperature.

The similar phenomena has been reported in other telechelic associating polymer systems with multi-hydrogen bonding motifs[179, 181, 196] and it's proposed that the telechelic polymers can be regarded as asymmetric triblock copolymers[334, 335], in our case, with nonpolar PDMS middle block and polar carboxylic acid end blocks. The end blocks possibly tend to assemble and form spherical-like clusters and the PDMS chains will form a brush-like configuration from the surface of these clusters (Fig. 7.4 a). Because no higher order peaks appear in Fig. 7.2, the spatial arrangement of the aggregates is not an ordered state.

Upon the simple picture drawn above, we can roughly estimate the chain length that connecting adjacent clusters. Taking a unit volume *V* with radius equals to *d*/2, the volume of clusters V_0 is proportional to the unit volume with a factor that equals to the chain ends volume fraction (eq. 7.1), since we assume that the clusters mostly consist of the chain end motifs. The average radius of the clusters, R_1 can be estimated accordingly (listed in Table. 7.2) :

$$V_0 = \frac{4\pi}{3}(R_1)^3 = V * \Phi_v = \frac{4\pi}{3}(\frac{d}{2})^3 * \Phi_v \quad (7.1)$$

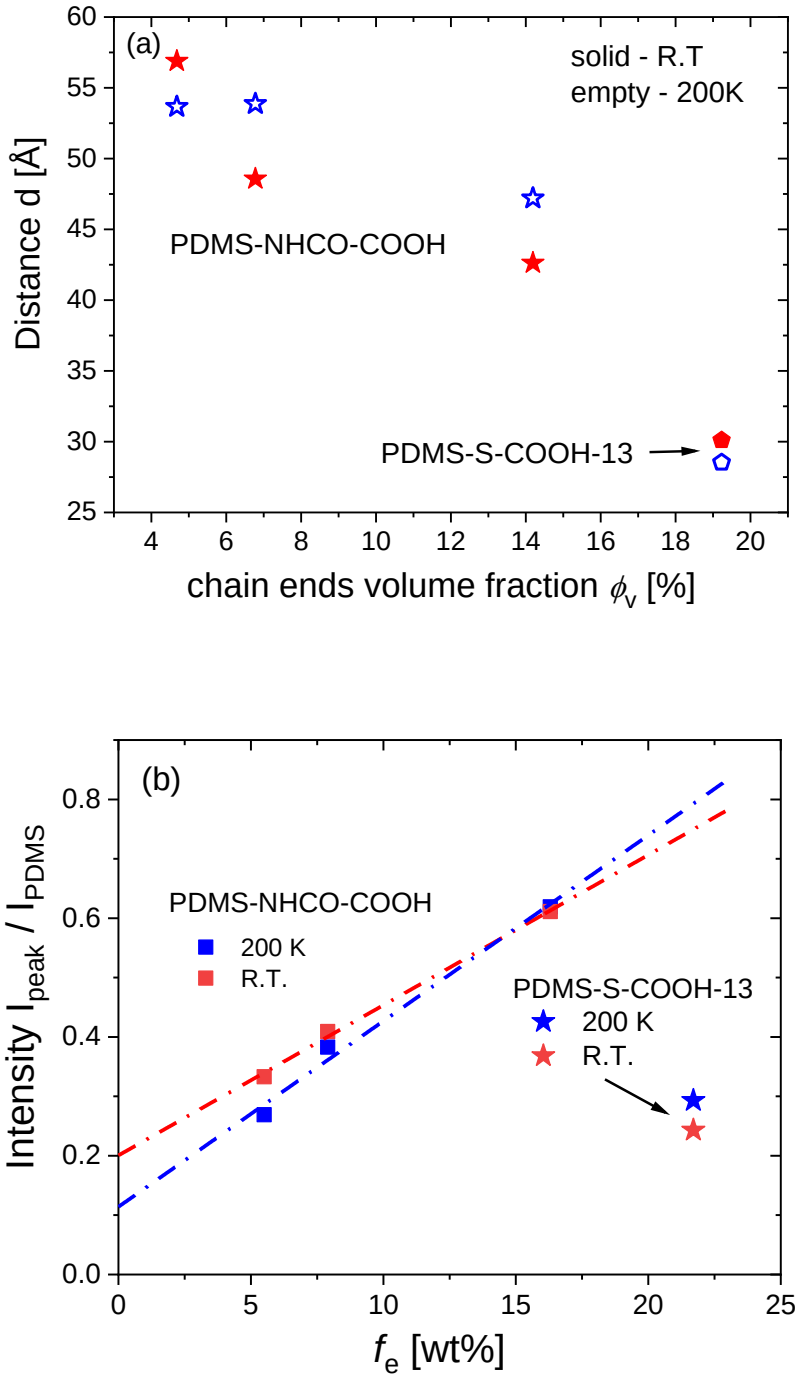

Figure 7. 3. (a) The mean distance between the centers of aggregates on dependence of chain ends volume fraction at different temperatures for PDMS-NHCO-COOH and PDMS-S-COOH. (b) The normalized peak intensity is plotted on dependence of weight fractions of end groups at both 200 K and room temperature (R.T).

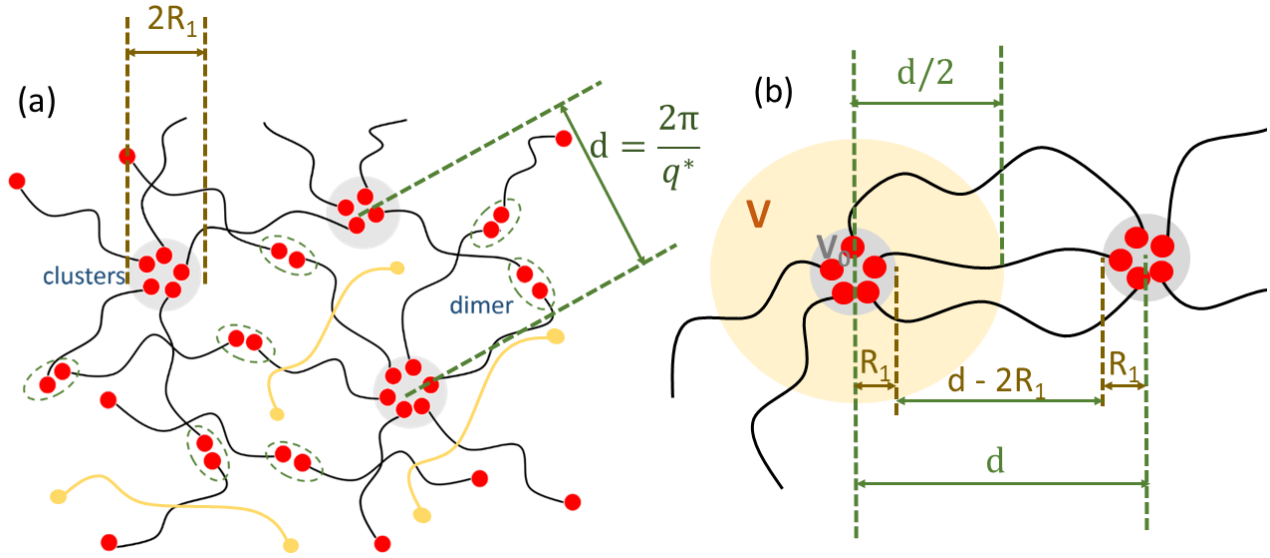

Figure 7. 4. (a) Schematic illustration of the association structure of PDMS-NHCO-COOH samples with small transient bonds, presumably dimers, and larger effectively permanent bonds, denoted here as clusters (Chapter 5) and corresponded to the characteristic peak at the lower q^* in SAXS. The shaded spheres are the aggregates(clusters) formed by associating chain ends and the black lines are the polymer precursor PDMS. The yellow lines represent free telechelic PDMS-NHCO-COOH. d represents the averaged distance between the centers of clusters and R_1 is the radius of the aggregates. (b) The d - $2R_1$ represents the mean shortest distance between 2 nearby clusters. V_o represents the volume of clusters and a unit volume V with radius = $d/2$.

Table 7. 2. The average radius of the clusters, R_1 of PDMS-NHCO-COOH and PDMS-S-COOH-13 at different temperatures calculated by Eq. 7.1.

Materials	***DP***	**R_1 at 200 K [Å]**	**R_1 at R.T. [Å]**
PDMS-NHCO-COOH	22	12.3	11.1
	50	11.0	9.9
	74	9.7	10.3
PDMS-S-COOH	13	8.2	8.7

Based on the assumption that the bridging chains are most probably located on the surface that close to each other, the chain length of the joint chains between nearby clusters would be distributed in the range between $d - 2R_1$ and d (Fig. 7.4 b). Assuming $d - R_1$ as the average dsitance, Fig. 7.5 presents the estimated average chain end distance of the joint chains between clusters for various MW of backbone. We plotted it together with the end-to-end distance of a Gaussian chain R_{EE} as a function of the chain molecular weight (Fig. 7.5). R_{EE} can be estimated by :

$$R_{EE} = \sqrt{nC_\infty {l_0}^2} \tag{7.2}$$

in which n is the number of atomic bonds in backbones, C_∞ is the characteristic ratio and l_0 is the bond length of Si-O. For PDMS, $n = 2 * DP$, $C_\infty = 6.3$[336] and $l_0 = 1.64$ Å.[337] As shown in Fig. 7.5, the average chain length of the joint chains between nearby clusters, $d - R_1$ of all PDMS-NHCO-COOH and PDMS-S-COOH-13 is comparable to R_{EE} at both temperatures. Here, we expect bridging chains in the system, together with free chains, dangling chains, and loop chains.

7.3.3 Dielectric spectroscopy

The dielectric loss ε" spectra of PDMS-S-COOH with different *DP* are shown in Fig 7.6. Two processes are observed in PDMS-S-COOH-13 with a separation of ~3 decades. In PDMS-S-COOH-83, three processes are clearly visible in the dielectric relaxation spectra. Please note that PDMS is classified as type-B polymer which do not possess dipole moment along the main chain[110], thus no chain modes are supposed to appear in the dielectric spectra[111]. To analyze the spectra, we fit them using three Havriliak-Nagami (HN) functions (with indices 1, 2 and 3) and a conductivity contribution:

$$\varepsilon^*(\nu) = \varepsilon_\infty + \frac{\Delta\varepsilon_1}{[1+(i2\pi\nu\tau_1)^{\alpha 1}]^{\gamma_1}} + \frac{\Delta\varepsilon_2}{[1+(i2\pi\nu\tau_2)^{\alpha 2}]^{\gamma_2}} + \frac{\Delta\varepsilon_3}{[1+(i2\pi\nu\tau_3)^{\alpha 3}]^{\gamma_3}} + \frac{\sigma}{2\pi i\nu\varepsilon_0} \tag{7.3}$$

Here, ε_∞ denotes the permittivity in the high frequency limit, $\Delta\varepsilon$ *is* the relaxation strength, τ is the HN relaxation time, $i = (-1)^{0.5}$ is the imaginary unit, the parameters α and γ describe the shape of the relaxation peak, σ corresponds to the DC conductivity and ε_0 is the permittivity of

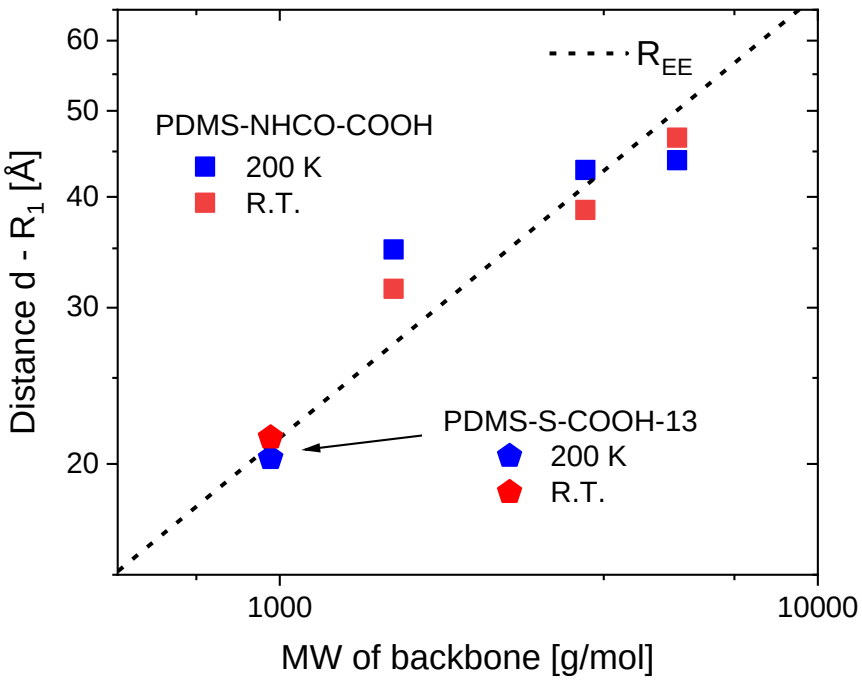

Figure 7. 5. The average chain length of the bridging chains between adjacent clusters is plotted on dependence of MW of polymer backbones. The dashed line represents the end to end distance of a Gaussian chain. Both axes are in logarithmic scale.

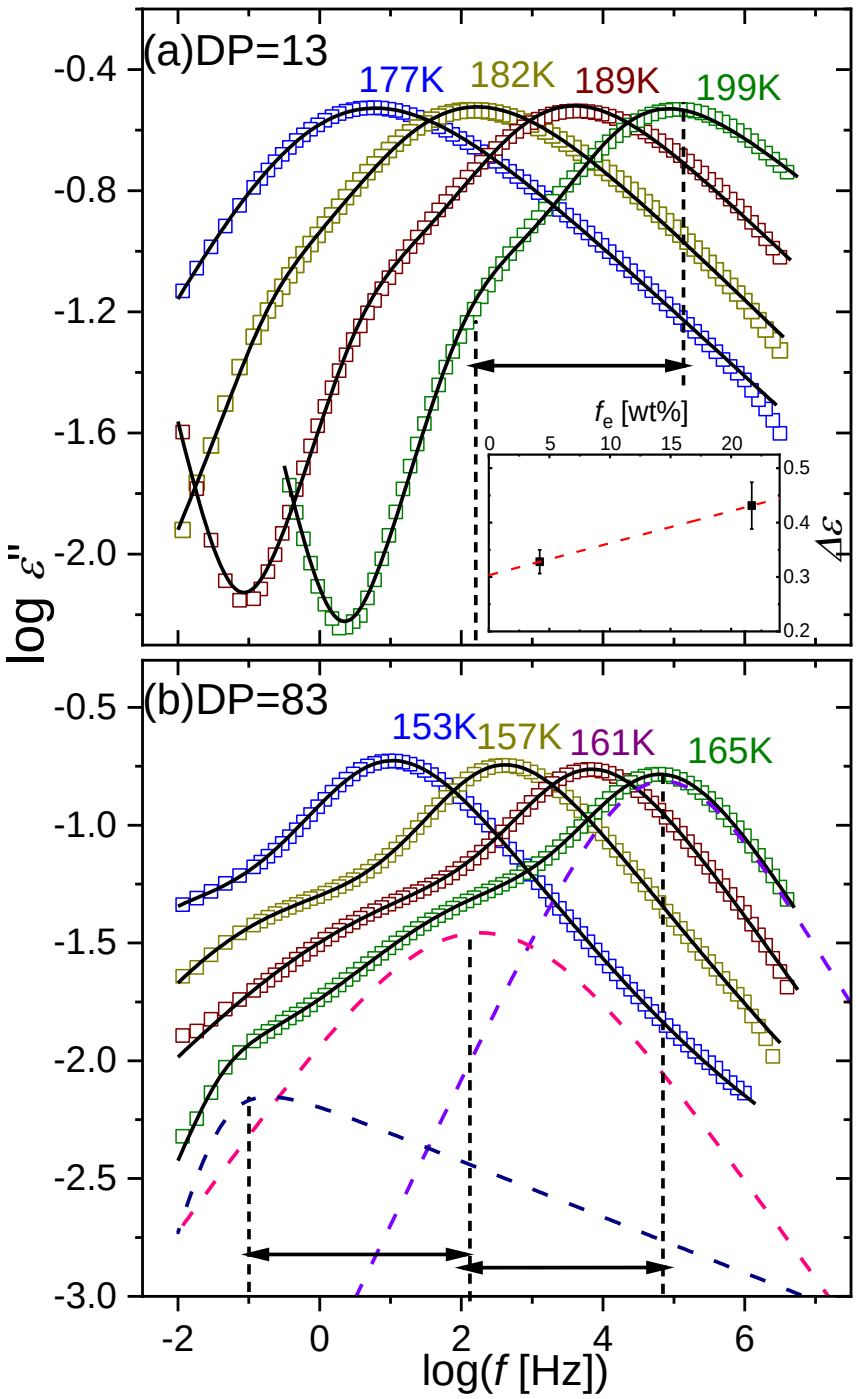

Figure 7. 6. Dielectric loss ε'' spectra at several investigated temperatures for PDMS-S-COOH with *DP* of (a) 13, (b) 83. At the higher temperatures the spectra of PDMS-S-COOH-13 exhibit a conductivity contribution at low frequencies while in PDMS-S-COOH-83 no such contribution was detected at the depicted frequencies and selected temperatures shown in the graph. The solid lines are fits employing equation (7.3). The dashed lines in (b) represent the individual contribution of each process and the vertical dashed lines illustrate their separation. The inset shows the dielectric strength of the α*-relaxation as a function of weight fraction of chain ends f_e. The temperature range of estimation was chosen as 185-211 K for *DP*=13 and 152-162 K for *DP*=83. The dashed lines are linear fits to the data and guides for the eye.

vacuum. For the fits of PDMS-S-COOH-13 which exhibit only two clear relaxation processes, the relaxation strength of one of the HN functions is fixed to zero. The characteristic relaxation time that corresponds to the maximum position of the loss peak can be calculated using the Eq. 2.12 (Fig. 7.7).[110]

The temperature dependence of τ_{max} is non-Arrhenius and can be fitted by the Vogel-Fulcher-Tammann (VFT)[110, 281-283] equation (Eq. 1.2) in all samples (Fig. 7.7 b). The VFT fit parameters for all samples are summarized in Table 7.3. For the process that appears at the lowest temperatures and highest frequencies in both *DP* = 13 and 83, the extrapolation of the fitted curve to a relaxation time of τ=100 s is consistent with the calorimetric T_g (Table 7.1), indicating that this faster process represents the segmental relaxation. The second relaxation which is separated ~3 decades in frequency from the α-relaxation peak, exhibits a dielectric relaxation strength which increases slightly with weight fraction of chain ends f_e (Fig. 7.6 a, inset). This is pretty similar to what we had for the intermediate dielectric process in PDMS-NHCO-COOH (α*-relaxation, as discussed in Chapter 6), and we ascribe it to the chain end dissociation α*-relaxation of PDMS-S-COOH as well.[229] The α*-relaxation usually appears a few decades slower than the segmental relaxation and possesses a similar temperature dependence. It corresponds to the dissociation process of H-bonds; this leads to a change of dipole moment due to the change in the distance between the partial charges of the H-bond donor and acceptor atoms (similar process was also found in our previously investigated systems PDMS-NHCO-COOH, PDMS-NH_2, PPG-NH_2 and PPG-NHCO-COOH, as discussed in Chapter 5 and 6).[200, 230, 280, 284, 285, 338]

The activation energy E_a of the H-bond dissociation can be estimated according to:

$$\tau_{\alpha^*}(T) = \tau_{\alpha}(T)\exp(\frac{E_a}{RT}) \quad (7.4)$$

in which *R* is the universal gas constant. By employing the eq. 7.4, we got the activation energies of the α*-relaxation to be 8.2±1 and 8.1±1 for PDMS-S-COOH-13, 83, respectively (Table 7.1). We would like to emphasize that Eq. 7.4 directly implies that the activation energy in these materials is given by the spectral separation of the α*-relaxation from the α-relaxation.

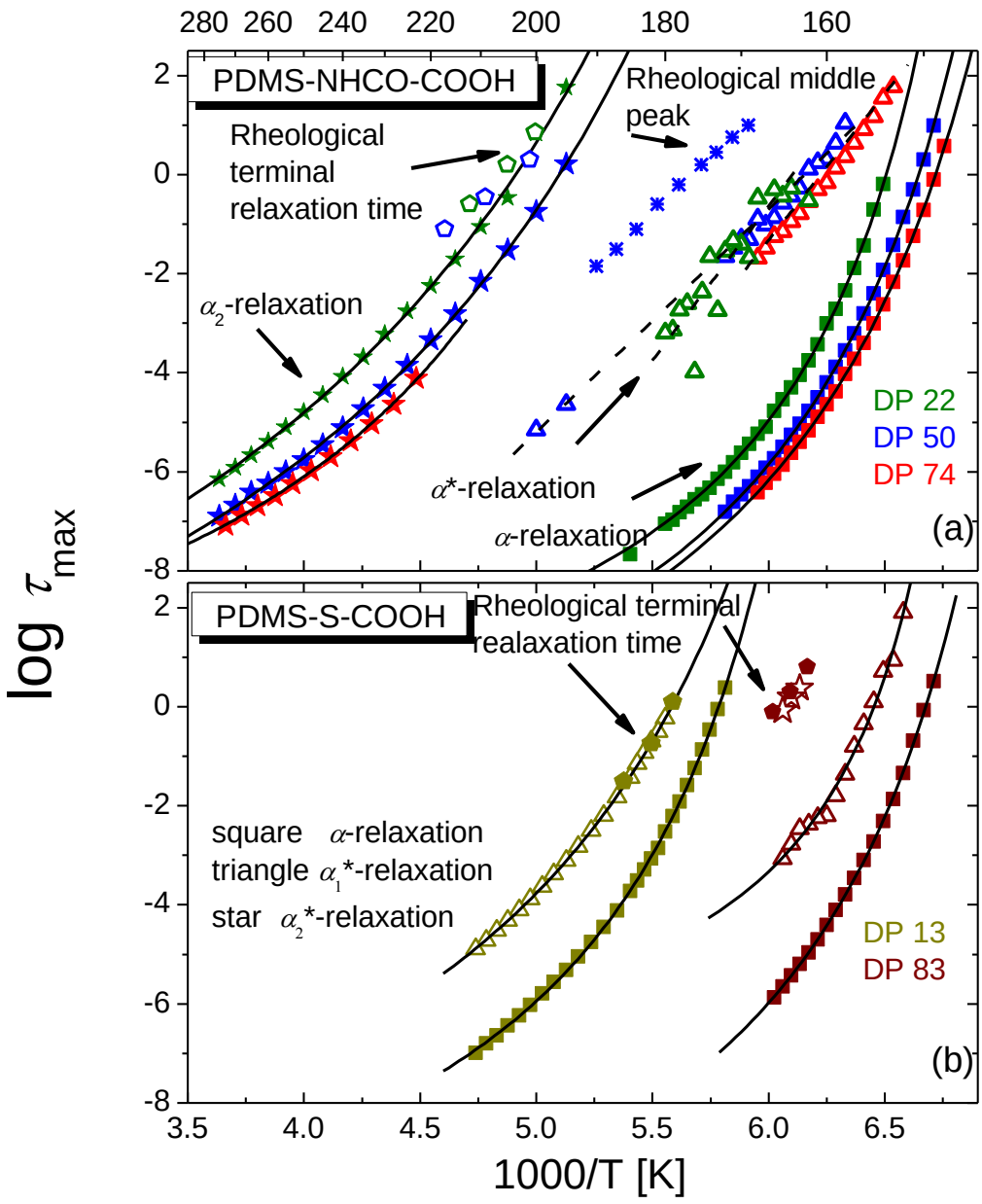

Figure 7. 7. (a) Previously reported[229] (chapter 5) Arrhenius plot of the dielectric mean relaxation times of the α-relaxation (squares), the α*-relaxation (open triangles), the α_2-relaxation (stars), the rheological relaxation time of the middle peak in the sample with DP = 50 (crosses), and the rheological terminal mode (open pentagons) for PDMS-NHCO-COOH systems of different DP as indicated. Solid and dashed lines are fits to the data by the VFT and Arrhenius equation, respectively. (b) Arrhenius plot of the dielectric mean relaxation times of the α-relaxation (squares), the α*-relaxation (α^*_1 in open triangles and α^*_2 in solid stars) and the rheological terminal mode (closed pentagons) for PDMS-S-COOH systems of different DP as indicated. The rheological terminal relaxation time were estimated directly from the crossing point of G'(ω) and G''(ω). Solid lines are fits to the data by the VFT equation (Eq. 1.2).

Table 7. 3. VFT parameters (Eq. 1.2) from the dielectric measurements of PDMS-S-COOH.

Materials	**PDMS-S-COOH-13**			**PDMS-S-COOH-83**		
VFT parameter	$\log(\tau_0[s])$	B[K]	T_0[K]	$\log(\tau_0[s])$	B[K]	T_0[K]
α-relaxation	-11.5	700	147	-13.6	679	128
α*-relaxation	-11.1	1041	138	-7.6	259	140
third process				-8.9*	-1122*	110*

*Since there are only limited points for the third process in PDMS-S-COOH-83. Its VFT fitting cannot converge and has relatively large error.

It is not the slop in the activation plot as has been employed in some earlier investigations.[208, 229]

The third relaxation process found at high temperatures in PDMS-S-COOH-83 can only be fitted with limited temperatures, since it is mostly covered by the conductivity at elevated temperatures and crystallization happens at lower T. Thus, the molecular assignment of this process is unclear and left as an open question.

In PDMS-NHCO-COOH, as discussed in Chapter 5, the dielectric spectra reveal a third relaxation at elevated temperatures (Fig 5.5 d-f) and its characteristic times also exhibits a VFT dependence (Fig. 7.7 a). Similar to the α-relaxation, the extrapolation of the fitted VFT functions to a timescale of about 100 s coincides with the 2nd glass transition which was observed in DSC measurements. This suggests that these samples phase separate and the phase separation is confirmed with SAXS results above. Although we have observed a characteristic peak in SAXS corresponding to phase separation in PDMS-S-COOH-13, no prominent process appears in BDS that can be assigned to aggregates. A possible explanation would be that the dielectric process is significantly slow and superimposed by conductivity that can't be solved by any fitting methods. It's worth noting that we also just observed only one glass transition in DSC measurements of this system.

7.3.4 Shear rheology

The shear modulus master curves were constructed from linear viscoelastic spectra using time-temperature superposition (TTS) (Fig. 7.8). In theory, valid TTS requires a homogeneous system where all the relaxation modes possess the same temperature dependence[58]. Although it failed in most associating polymer systems due to intermolecular interactions, the master curve can still provide a general picture of the mechanical properties and relaxation processes[179, 196, 229-232]. The first process occurs at high frequencies (corresponding to temperatures near T_g) and exhibits storage modulus values ~ 1 GPa; consequently, it is assigned to the segmental relaxation. The crossover of G' and G" is used to determine the corresponding segmental relaxation time. In both investigated polymers a second process appears at lower frequencies, i.e. higher temperatures, although it is demanding to separate it from the segmental relaxation in the samples with short chains. At even lower frequencies the distinctive slopes of 2 and 1 in G' and G", respectively, are present in the double-logarithmic presentation. These slopes are characteristic for the terminal relaxation, usually related to the motion of whole chains. In these materials, however, the terminal relaxation occurs at times much longer than expected for their molecular weight. This indicates that it reflects the mechanical enhancement due to the formation of a supramolecular network. To estimate the corresponding characteristic relaxation times we employed a simplified model function to fit the master curves:[110]

$$G' = \frac{A}{(\omega\tau_1)^{b_1}+(\omega\tau_1)^{-b_2}} + G_e \frac{\omega^2{\tau_2}^2}{\omega^2{\tau_2}^2+1} \quad (7.5\ a)$$

$$G'' = \frac{A}{(\omega\tau_1)^{c_1}+(\omega\tau_1)^{-c_2}} + G_e \frac{\omega\tau_2}{\omega^2{\tau_2}^2+1} \quad (7.5\ b)$$

The first term phenomenologically describes the segmental relaxation with the constant *A* reflecting the level of *G'* (glassy modulus) and the area under *G"*, the characteristic relaxation time τ_1 which indicates the segmental relaxation time and the parameters b_1 and $-b_2$ as well as c_1 and $-c_2$ for the slopes of the high and low frequency wings of G' and G", respectively. Even though, in general, this term does not fulfill the Kramers-Kronig relation, it provides a sufficiently accurate approximation to estimate the characteristic segmental relaxation time.

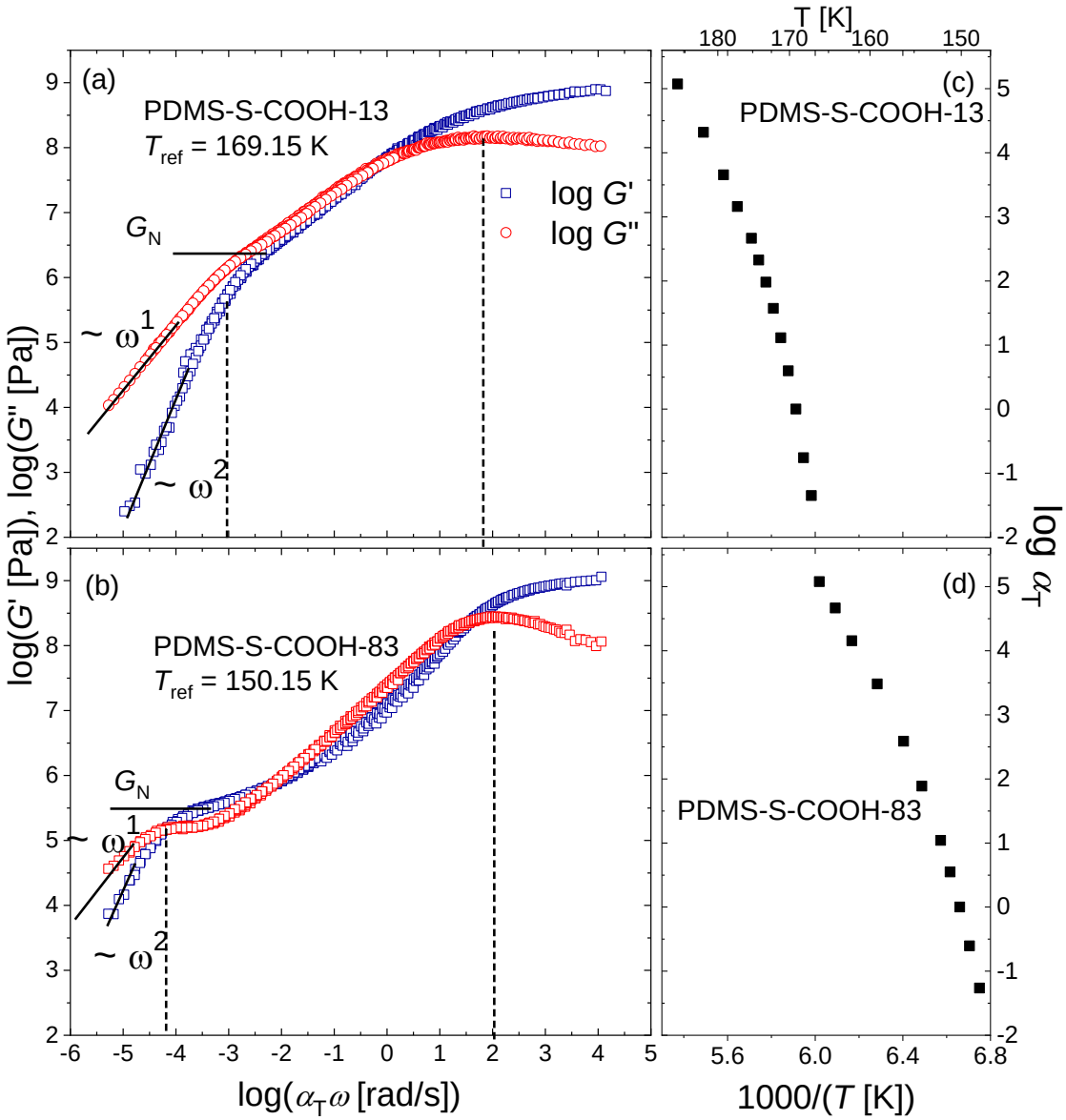

Figure 7. 8. Master curves constructed from linear viscoelastic spectra using TTS for PDMS-S-COOH with *DP* of (a) 13 and (b) 83, and the respective horizontal shift parameters α_T (c-d). Dashed lines indicate the separation of two processes.

The second term resembles a Maxwell model in order to describe the terminal relaxation where G_e and τ_2 are the corresponding plateau modulus and terminal relaxation time, respectively. For almost all samples, eq. 7.5 a and b were fitted simultaneously to the G' and G" data with shared parameters.

For PDMS-S-COOH-13, the separation of the segmental relaxation and terminal mode is almost 5 decades (Fig. 7.8), much larger than the non-associated PDMS at this low MW (Fig. 7.9). Meanwhile, the shape of the peak at high frequencies in $G''(\omega)$ get remarkably broad (Fig. 7.9 b). The storage modulus value G_e (estimated by Eq. 7.5) at the onset of the transition from rouse mode to terminal relaxation is even higher than the rubbery plateau value G_e of PDMS-S-COOH-83. To have a deeper insight into this, we compare the rubbery plateau values G_e with the prediction of a network model considering entanglements, and physical crosslinks due to the end-association (Fig. 7.10). G_e here represents the value of the storage modulus $G'(\omega)$ at the frequency where the loss modulus $G''(\omega)$ exhibits a minimum. It is related to the molecular weight between entanglements M_e and between the physical crosslinks M_c by the relation:

$$G_e = \rho RT \left(\frac{1}{M_e} + \frac{1}{M_c}\right) \tag{7.6}$$

where R is the ideal gas constant, M_c is the PDMS molecular weight, and ρ is the mass density of PDMS which equals to 965 kg m^{-3}. The known entanglement molecular weight of PDMS M_e = 12 kg mol^{-1}. Due to different reference temperatures of the constructed master curves, we estimated the model value of G_e at T = 150 and 169 K, accordingly. The extended rubbery plateau values of PDMS-NHCO-COOH (Chapter 5) are also included in Fig. 7.10 for comparison. The difference between experimental results with the model predictions is ~2 times for PDMS-S-COOH-13 and PDMS-NHCO-COOH-74, and it rises to ~10 times for PDMS-NHCO-COOH-22. Obviously, besides possible entanglement and physical crosslinking, it is the hard, glassy phase of the phase-separated end groups that contributes to the additional reinforcement. Comparing with PDMS-NHCO-COOH-22, the enhancement on the mechanical performance is much weaker in PDMS-S-COOH-13, this is possibly because its relatively unstable and less intense formation of aggregates. For PDMS-S-COOH-83, the experimental value agrees well

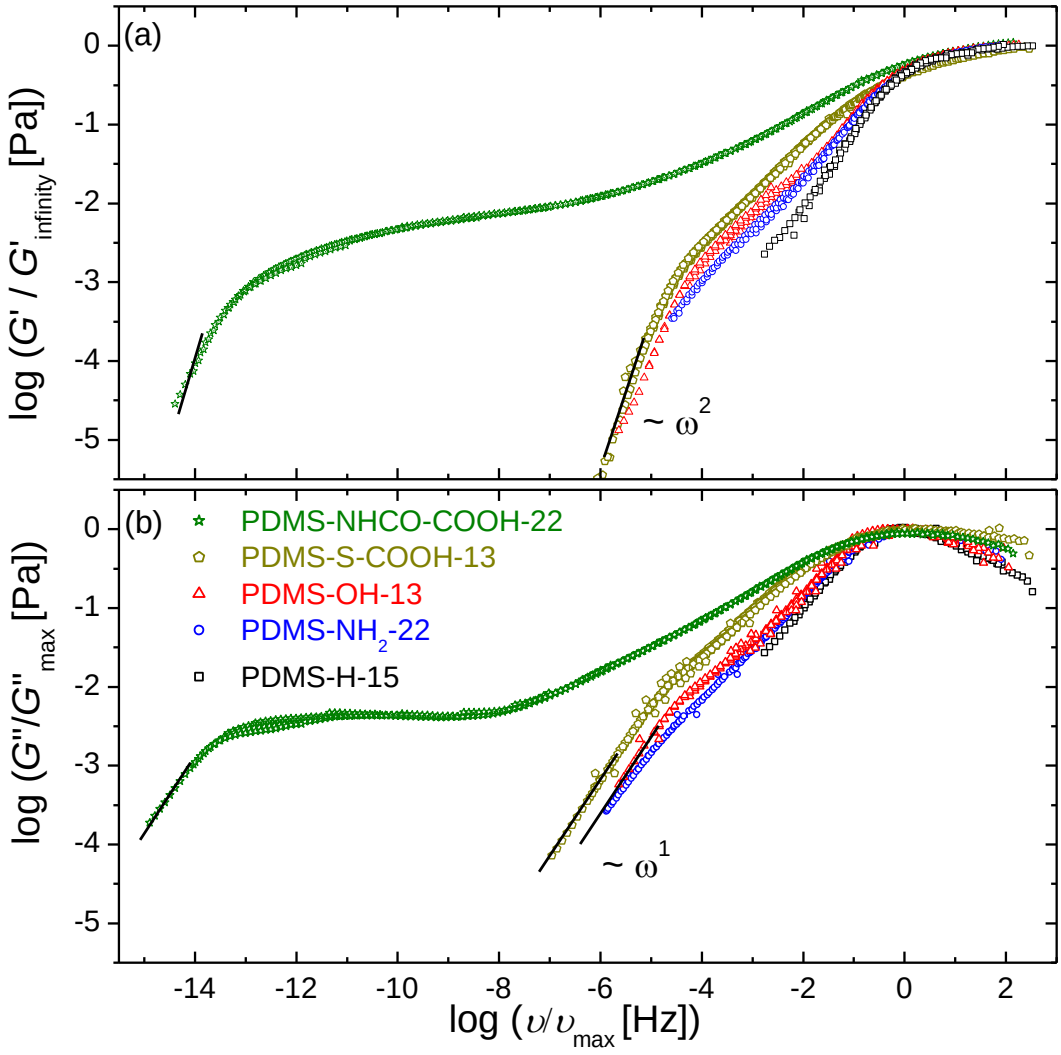

Figure 7. 9. Storage (a) and loss part (b) of the shear modulus master curves normalized according to the respective maxima $G'(\nu/\nu_{max})/G_{\infty}$ and $G''(\nu/\nu_{max})/G''_{max}$ as well as the frequency position ν_{max} of G''_{max} obtained using TTS for PDMS with different end-groups as indicated and similar DP. The solid lines indicate the terminal end of the spectra.

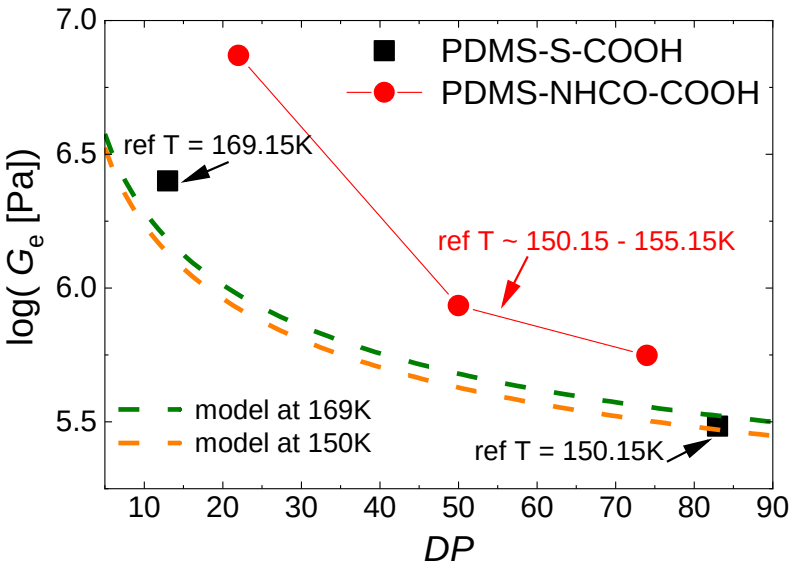

Figure 7. 10. The dependence of the plateau modulus G_e of PDMS-NHCO-COOH (read directly from the master curve, chapter 5) and PDMS-S-COOH on the degree of polymerization (*DP*). Dashed lines are model predictions at T ~ 150 and 169K, estimated by eq. 7.6. The plateau value of PDMS-S-COOH-13 and 83 is calculated according to eq. 7.5.

with the model estimation, which is also consistent with the fact that we didn't find any sign of phase separation in this material.

Comparing telechelic associating PDMS with similar *DP*, the terminal relaxation for all NH_2-, OH-, -S-COOH and -NHCO-COOH terminated PDMS gets much longer in comparison to that of the non-associating one (Fig. 7.9), especially for PDMS-NHCO-COOH-22 and PDMS-S-COOH-13. In non-associating linear polymer systems, the terminal relaxation time reflects the timescale of the motion of a whole chain. The prolonged relaxation time in associating polymers of identical chain length indicates that in these materials the terminal relaxation has a different molecular origin, namely, mechanical stress release enabled by the reorganization of the supramolecular network. In the past, this was considered identical to the dissociation of individual reversible bonds as is reflected in certain theoretical descriptions *e.g.* the Tanaka-Edwards model.[182, 339] However, a direct comparison of the dielectric α*-relaxation time assigned to the dissociation of the reversible bonds and the rheological terminal relaxation time

reveals a clear difference reaching several orders of magnitude (all PDMS-NHCO-COOH in Fig. 7.7 a and PDMS-S-COOH-83 in Fig. 7.7 b). Similar behaviors are also reported in some associating systems.[160, 161] Apparently, the mechanical stress relaxation can take up to several orders of magnitude longer than the dissociation of the bonds. In a systematic study we demonstrate that for short telechelic chains both timescales are almost identical, while longer chains (still below the entanglement length) exhibit large discrepancies.[320, 340]

This difference can be explained by the bond lifetime renormalization model which was developed to describe dynamics and kinetics in self-healing polymers based on end-functionalized polymer strands.[158] The model introduces a rather complex mechanism of mechanical stress release. Breaking the bond between two associated groups does not release mechanical stress if the same groups re-associate again, although this process changes the dipole moment and hence generates a dielectric response (corresponding to the 'actual' bond lifetime). The mechanical relaxation requires a change in the network structure, i.e. an exchange of bond partners. That may happen only after several bond breaks and subsequent re-associations of the same two associating groups. Consequently, the mechanical relaxation in this framework is generally slower than the actual dissociation of end groups. How often two end groups re-associate before they exchange partners depends on the average distance to the next available bond partner. This distance can be expressed in terms of the concentration of end groups, i.e. the chain length in telechelic polymers. Since a longer distance to the next bond partner obviously increases the number of returns to the original partner before connecting to the new one, the model predicts longer stress relaxation times for longer telechelic chains at the same dissociation energy. This agrees well with our experimental results of PDMS-S-COOH (Fig. 7.8, comparing *DP*= 13 and 83) and PDMS-NHCO-COOH systems (Chapter 5, comparing *DP*=22, 50). In addition, in the PDMS-S-COOH systems, while *DP*= 83 with the longer chain has a significant separation between rheological terminal relaxation time and dielectric α*-relaxation time, the terminal relaxation time of *DP* =13 agrees well with its α*-relaxation time.

To evaluate the association mechanism and dynamics in the investigated telechelic associating polymers quantitatively, one may use the separation of the terminal relaxation from the segmental relaxation in the shear modulus master curve as well as the level of the plateau

modulus reached before the terminal regime. In PDMS-S-COOH and PPG-NHCO-COOH (Chapter 6) systems, the separation increases with increasing chain length (Fig. 7.8 and Fig. 6.7 from Chapter 6, *i.e.*, decreasing concentration of end groups in the system). At the same instance the plateau modulus drops with increasing chain length because fewer end groups in the system result in fewer connections in the supramolecular network (Fig. 7.10). Consequently, the mechanical enhancement in this class of systems is characterized by a tradeoff between a high plateau modulus and a long terminal relaxation time. Both cannot be realized at the same time. This clearly limits the performance that can be achieved with these materials.

We want to note that in principle end groups which require a higher activation energy for dissociation would increase the terminal relaxation time; whereby short chains must still be used in order to ensure a high plateau modulus. However, this route merely results in small associating molecules which, for strongly associating moieties, often form crystalline aggregates[142] and, hence, loses the beneficial properties of polymers.

On the other side, we found a tremendous increase of the terminal relaxation time in the shear modulus measurements in telechelic PDMS-NHCO-COOH (Fig. 5.3, Chapter 5), with only slightly different end groups (-NHCO-COOH vs. -S-COOH). This reflects a drastic enhancement of the mechanical properties induced by the amino groups which promote phase separation from the PDMS main chains. Moreover, these samples exhibit an intermediate shear modulus relaxation which is approximately three decades faster than the terminal relaxation. It has been assigned to partial stress release due to the dissociation of dimeric end group association. For either process, the intermediate as well as the terminal relaxation, the extracted plateau moduli and the respective relaxation times both increase as the length of the main chain decreases. Apparently, the phase separation of the end group associations allows to overcome the above described restrictions.

It's paramount to point out that the terminal relaxation of shear modulus came out above ~220 K for all samples of PDMS-S-COOH and PDMS-NHCO-COOH-22, 50 (due to crystallization, we don't have that data for PDMS-NHCO-COOH-74). Meanwhile, we have observed the sign of aggregates of PDMS-S-COOH-13, PDMS-NHCO-COOH-22 and 50 from SAXS

at the room temperature obviously. This clearly suggests that below the room temperature, although the chain motion occurs, the systems are still partially connected, even with aggregates that makes its flow behavior similar to that of star polymers.

7.3.5. Zero shear viscosity

To demonstrate how particular properties of the phase segregated end groups dominate the properties of the system, we evaluate the zero-shear viscosity of telechelic PDMS with different end groups as a function of inverse temperature scaled by their respective T_g (Fig. 7.11). The viscosities of -NH_2, -OH (Chapter 4 and 5) and -S-COOH terminated chains is only slightly enhanced (up to approximately 1 decade) compared to the -H terminated (i.e. non-H-bonding) reference sample (Chapter 5) after the difference of their T_g is compensated by the scaling. This also illustrates the minor impact of the activation energy of the end group association. Only the -NHCO-COOH terminated PDMS exhibits a huge increase in viscosity between 2 and 6 orders of magnitude. Remarkably, after scaling the temperature axis by the second T_g, *i.e.* the glass transition of the end group clusters, the viscosity of PDMS-NHCO-COOH is very close to all the other curves exhibiting a similarly small enhancement (note that in Fig. 7.11 a, the *DP* of the samples varies resulting in higher viscosities for weaker H-bonding end groups if the chains are longer). This clearly indicates that in this material —where the supramolecular network is established via phase segregation— the structural relaxation of this connecting phase is the dominating parameter (and not that one of the main chains as in the other samples). However, the rescaled viscosity seems to have a less steep increase close to the T_g of the clusters. This may indicate that despite the system approaching an effectively permanent network structure, the highly mobile matrix polymer (which is still well above its T_g) provides some structural flexibility.

These results, as well as those of other studies[113, 130, 179, 341-343], indicate that phase separation as driving force for supramolecular association is a promising route to polymers with

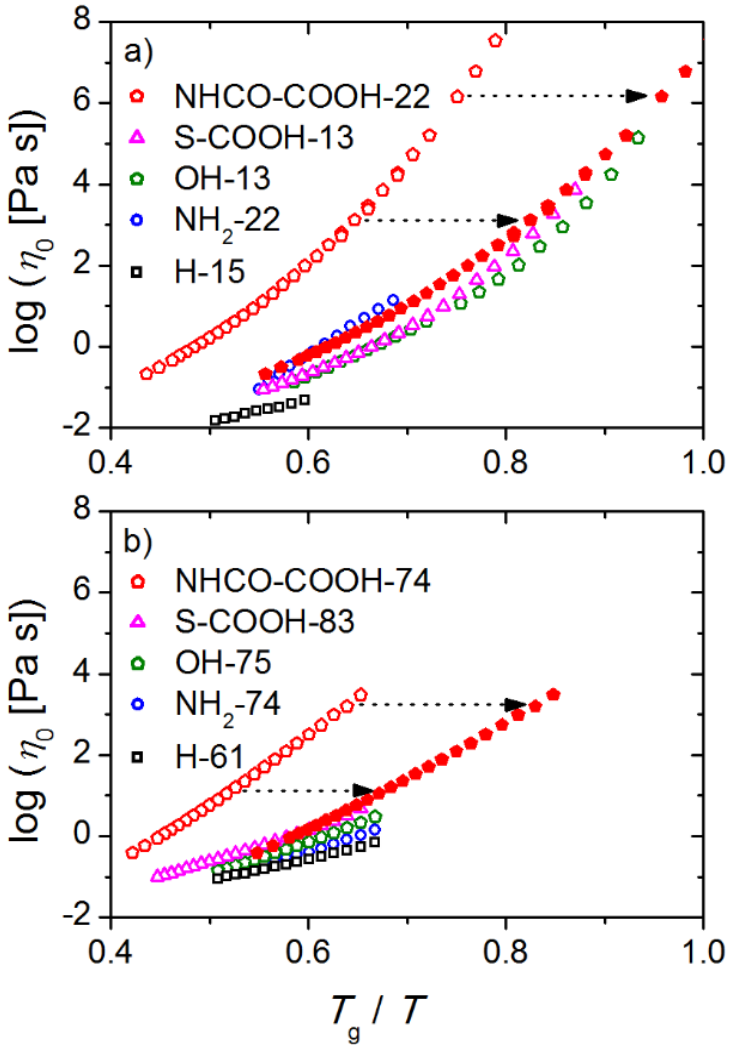

Figure 7. 11. Zero-shear viscosities of telechelic PDMS chains with different types of end groups and *DP* as indicated plotted vs. the inverse temperature normalized by the respective glass transition temperature of the polymer (open symbols) for (a) short and (b) long chains (respective *DP* as indicated in legend). For PDMS-NHCO-COOH, the curve is additionally depicted vs. temperature normalized by the second glass transition temperature, *i.e.* the T_g of the end group clusters (solid red pentagons); the horizontal arrows indicate that shift.

strongly enhanced properties, and that a systematic investigation is highly desirable for a deep understanding to eventually enable rational designs of high-performance materials.

7.4 Conclusions

We studied the dynamics, structure, viscoelastic and mechanical performance of telechelic PDMS with varied H-bonding end-groups and different chain length using DSC, dielectric spectroscopy, linear rheology and SAXS. All systems share the similar trend that their glass transition temperature increases as chain length decreases. For PDMS-S-COOH, we have observed the sign of phase separation in SAXS experiments at both 200 K and room temperature for the short chain, *DP*=13. Although there's only one T_g appeared in DSC results, the terminal relaxation is clearly slowed down comparing to weakly associated PDMS-OH and PDMS-NH_2. For PDMS-NHCO-COOH systems, we have seen phase separation for all investigated chain length at both low and room temperatures from SAXS. This confirms with what we have reported before, that a second T_g in the DSC curves which is about 40-50 K higher than the main chain T_g and an additional relaxation process in the dielectric spectra. The systems exhibit largely enhanced mechanical performance as well as significantly longer terminal relaxation time simultaneously at decreasing chain length.

It's reported by Alegria that monocarboxydecyl-terminated (DMS-DCOOH-14) phase segregated below 230K. In our case, PDMS-S-COOH-13, with similar chain length, but associating groups on both chain ends, exhibits phase separation even at room temperature. But when it comes to longer chain length, only with the extra linker -NHCO-, that the formation of aggregates occurs. By providing possible lateral packing, the PDMS-NHCO-COOH systems possess drastic enhancement in mechanical performance and flow behavior. In conclusion, our analysis clearly demonstrate that phase separation affects viscoelastic properties stronger than the strength of the chain ends interactions.

Concluding Remarks

Associating polymers emerge into a very promising class of functional materials, due to their stimuli-responsive structures, reversible properties, impressive self-healing performance and highly potential recyclability. However, many open questions remain to be solved to obtain associating polymers with specific properties desired for various application.

Currently, many researches are focused on strongly associated supramolecular polymer systems, especially in the polymer solutions. In this study, we presented a systematic investigation on the dynamics and viscoelastic properties of telechelic supramolecular polymers with varied chain end strength (different association lifetimes accordingly), polymer precursor MW, rigidity and polarity in the melt state. The main experimental techniques used were broadband dielectric spectroscopy, rheology and differential scanning calorimetry and small-angle X-ray spectroscopy.

First, we studied the effect of single H-bonding chain ends (hydroxyl group, OH) on the dynamics of associated PDMS. We demonstrate that hydrogen bonding has a strong influence on both segmental and slower dynamics in the systems with low molecular weights. In particular, the decrease in the chain length leads to an increase of the glass transition temperature, viscosity, and fragility index, at variance with the usual behavior of non-associating polymers. The supramolecular association of hydroxyl-terminated chains leads to the emergence in dielectric and mechanical relaxation spectra of the so-called Debye process traditionally observed in monohydroxy alcohols.

Then, we investigated telechelic PDMS of several MW with different hydrogen bonding end groups. Besides the well-established increase of the glass transition temperature T_g with decreasing MW, T_g remains unchanged as the end group varies from NH2 over OH to NHCO-COOH. For the latter system, a 2nd T_g is found which indicates a segregated phase. In contrast, rheological measurements reveal a qualitative difference in the viscoelastic response of NH_2-terminated and NHCO-COOH terminated chains. Both systems show clear signs of end group association, but only the latter exhibits an extended rubbery plateau. All features observed in the rheology experiments have corresponding processes in the dielectric measurements. This

provides insight into the underlying molecular mechanisms, and especially reveals that many end groups of the NHCO-COOH terminated chains phase segregate while a certain fraction forms binary associates and remains non-segregated. In contrast, the NH_2-terminated systems form only binary associates increasing the effective chain length, whereas the NHCO-COOH terminated system consists of two types of associates forming a crosslinked network. Remarkably, a single species of end group forms two qualitatively different types of associates: transient bonds which allow stress release by a bond-partner exchange mechanism, and effectively permanent bonds formed by a phase segregated fraction of end groups which are stable on the timescale of the transient mechanism.

Later we study the impact of H-bonding end-groups on segmental and chain dynamics of telechelic polypropylene glycol (PPG) and poly(dimethylsiloxane) (PDMS). Polymer chains with three types of H-bonding end-groups possessing different interaction strengths and a non-H-bonding end-group as reference were compared. The glass transition temperature (T_g) of H-bonding PPG systems with low molecular weight increases compared to the reference, and the T_g difference varies with chain-end interaction strength. In contrast, their shear viscosities (for T_g -scaled temperature, i.e., when the shift in T_g is accounted for) are similar to that one of the references. This is in strong contrast to the behavior of telechelic PDMS with the same set of endgroups, where the T_g increase of all H-bonding systems is independent of H-bond strengths, while shear viscosity increases significantly only for the strongest H-bonding end-groups. These observations are explained by the difference in lifetime of the end-group associations relative to segmental and chain relaxation times.

In the end, we studied the role of phase separation on the dynamics and mechanical performance of telechelic PDMS by comparing the different behavior of acid-terminated PDMS with different linker groups (-NHCO- vs. -S-). The phase separation in PDMS-NHCO-COOH contribute to the prolonged rubbery plateau in shear modulus with high plateau modulus, especially for the low MW. Meantime, the terminal relaxation time is prominently longer in this system. We demonstrate that comparing to the bond strength, phase separation provides a more remarkable and decisive factor for the dynamics and viscoelastic properties of supramolecular systems.

For all the systems investigated, the mechanical enhancement by the H-bond association is evidenced in the shear rheology measurements which exhibit a terminal relaxation much slower than expected for such short chains. It is shown that the H-bond dissociation time is different from the mechanical stress relaxation time as predicted by the lifetime renormalization model. This model can describe the data quantitatively, and the extracted fit parameters indicate a transition from Rouse to reptation dynamics as chain length increases, although the chain length remains far below entanglement. The latter suggests the formation of super-chains by chain end association. Furthermore, the model can explain why for increasing chain length, the mechanical stress relaxation is prolonged while the plateau modulus is reduced. Our results on telechelic systems with phase segregating ends demonstrate a possible way to increase both, plateau modulus and terminal relaxation times, simultaneously by supramolecular association.

Reference

1. Brunsveld, L.; Folmer, B.; Meijer, E. W.; Sijbesma, R. Supramolecular polymers. *Chem. Rev.* **2001,** 101 (12), 4071-4098.
2. De Greef, T. F.; Smulders, M. M.; Wolffs, M.; Schenning, A. P.; Sijbesma, R. P.; Meijer, E. Supramolecular polymerization. *Chem. Rev.* **2009,** 109 (11), 5687-5754.
3. Huang, F.; Scherman, O. A. Supramolecular polymers. *Chem. Soc. Rev.* **2012,** 41 (18), 5879-5880.
4. Liu, Y.; Wang, Z.; Zhang, X. Characterization of supramolecular polymers. *Chem. Soc. Rev.* **2012,** 41 (18), 5922-32.
5. Seiffert, S.; Sprakel, J. Physical chemistry of supramolecular polymer networks. *Chem. Soc. Rev.* **2012,** 41 (2), 909-930.
6. Sijbesma, R. P.; Beijer, F. H.; Brunsveld, L.; Folmer, B. J.; Hirschberg, J. K.; Lange, R. F.; Lowe, J. K.; Meijer, E. Reversible polymers formed from self-complementary monomers using quadruple hydrogen bonding. *Science* **1997,** 278 (5343), 1601-1604.
7. Sijbesma, R. P.; Meijer, E. Quadruple hydrogen bonded systems. *Chem. Commun.* **2003,** (1), 5-16.
8. Corbin, P. S.; Zimmerman, S. C. Self-association without regard to prototropy. A heterocycle that forms extremely stable quadruply hydrogen-bonded dimers. *J. Am. Chem. Soc.* **1998,** 120 (37), 9710-9711.
9. Wilson, A. J. Non-covalent polymer assembly using arrays of hydrogen-bonds. *Soft Matter* **2007,** 3 (4), 409-425.
10. Wang, X.; McHale, R. Metal‐Containing Polymers: Building Blocks for Functional (Nano) Materials. *Macromol. Rapid Commun.* **2010,** 31 (4), 331-350.
11. Murakami, Y.; Yokoyama, M.; Okano, T.; Nishida, H.; Tomizawa, Y.; Endo, M.; Kurosawa, H. A novel synthetic tissue‐adhesive hydrogel using a crosslinkable polymeric micelle. *Journal of Biomedical Materials Research Part A* **2007,** 80 (2), 421-427.
12. Dobrawa, R.; Lysetska, M.; Ballester, P.; Grüne, M.; Würthner, F. Fluorescent supramolecular polymers: Metal directed self-assembly of perylene bisimide building blocks. *Macromolecules* **2005,** 38 (4), 1315-1325.
13. Burattini, S.; Colquhoun, H. M.; Fox, J. D.; Friedmann, D.; Greenland, B. W.; Harris, P. J.; Hayes, W.; Mackay, M. E.; Rowan, S. J. A Self-repairing, supramolecular polymer system: healability as a consequence of donor–acceptor π–π stacking interactions. *Chem. Commun.* **2009,** (44), 6717-6719.
14. Avestro, A.-J.; Belowich, M. E.; Stoddart, J. F. Cooperative self-assembly: Producing synthetic polymers with precise and concise primary structures. *Chem. Soc. Rev.* **2012,** 41 (18), 5881-5895.
15. Aboudzadeh, M. A.; Munoz, M. E.; Santamaría, A.; Fernandez-Berridi, M. J.; Irusta, L.; Mecerreyes, D. Synthesis and rheological behavior of supramolecular ionic networks based on citric acid and aliphatic diamines. *Macromolecules* **2012,** 45 (18), 7599-7606.
16. Zare, P.; Stojanovic, A.; Herbst, F.; Akbarzadeh, J.; Peterlik, H.; Binder, W. H. Hierarchically nanostructured polyisobutylene-based ionic liquids. *Macromolecules* **2012,** 45 (4), 2074-2084.
17. Li, S.-L.; Xiao, T.; Lin, C.; Wang, L. Advanced supramolecular polymers constructed by orthogonal self-assembly. *Chem. Soc. Rev.* **2012,** 41 (18), 5950-5968.
18. Appel, E. A.; del Barrio, J.; Loh, X. J.; Scherman, O. A. Supramolecular polymeric hydrogels. *Chem. Soc. Rev.* **2012,** 41 (18), 6195-6214.
19. Gröger, G.; Meyer-Zaika, W.; Böttcher, C.; Gröhn, F.; Ruthard, C.; Schmuck, C. Switchable supramolecular polymers from the self-assembly of a small monomer with two orthogonal binding interactions. *J. Am. Chem. Soc.* **2011,** 133 (23), 8961-8971.
20. Tayi, A. S.; Shveyd, A. K.; Sue, A. C.-H.; Szarko, J. M.; Rolczynski, B. S.; Cao, D.; Kennedy, T. J.; Sarjeant, A. A.; Stern, C. L.; Paxton, W. F. Room-temperature ferroelectricity in supramolecular networks of charge-transfer complexes. *Nature* **2012,** 488 (7412), 485.

21. Filot, I. A.; Palmans, A. R.; Hilbers, P. A.; van Santen, R. A.; Pidko, E. A.; de Greef, T. F. Understanding cooperativity in hydrogen-bond-induced supramolecular polymerization: a density functional theory study. *J. Phys. Chem. B* **2010,** 114 (43), 13667-13674.
22. Jeffrey, G. A.; Jeffrey, G. A., *An introduction to hydrogen bonding*. Oxford university press New York: 1997; Vol. 12.
23. Binder, W. H.; Zirbs, R., Supramolecular Polymers and Networks with Hydrogen Bonds in the Main-and Side-Chain. In *Hydrogen bonded polymers*, Springer: 2006; pp 1-78.
24. Pollino, J. M.; Weck, M. Non-covalent side-chain polymers: design principles, functionalization strategies, and perspectives. *Chem. Soc. Rev.* **2005,** 34 (3), 193-207.
25. Murray, T. J.; Zimmerman, S. C. New triply hydrogen bonded complexes with highly variable stabilities. *J. Am. Chem. Soc.* **1992,** 114 (10), 4010-4011.
26. Zimmerman, S. C.; Murray, T. J. Hydrogen bonded complexes with the AA· DD, AA· DDD, and AAA· DD motifs: the role of three centered (bifurcated) hydrogen bonding. *Tetrahedron Lett.* **1994,** 35 (24), 4077-4080.
27. Murray, T. J.; Zimmerman, S. C.; Kolotuchin, S. V. Synthesis of heterocyclic compounds containing three contiguous hydrogen bonding sites in all possible arrangements. *Tetrahedron* **1995,** 51 (2), 635-648.
28. Quinn, J. R.; Zimmerman, S. C.; Del Bene, J. E.; Shavitt, I. Does the A·T or G·C base-pair possess enhanced stability? Quantifying the effects of CH···O interactions and secondary interactions on base-pair stability using a phenomenological analysis and ab initio calculations. *J. Am. Chem. Soc.* **2007,** 129 (4), 934-941.
29. Binder, W. H.; Bernstorff, S.; Kluger, C.; Petraru, L.; Kunz, M. J. Tunable materials from hydrogen-bonded pseudo block copolymers. *Adv. Mater.* **2005,** 17 (23), 2824-2828.
30. Park, T.; Todd, E. M.; Nakashima, S.; Zimmerman, S. C. S. A quadruply hydrogen bonded heterocomplex displaying high-fidelity recognition. *Journal of the American Chemical* **2005,** 127 (51), 18133-18142.
31. Chang, S. K.; Hamilton, A. D. Molecular recognition of biologically interesting substrates: synthesis of an artificial receptor for barbiturates employing six hydrogen bonds. *J. Am. Chem. Soc.* **1988,** 110 (4), 1318-1319.
32. Zeng, H.; Miller, R. S.; Flowers, R. A.; Gong, B. A highly stable, six-hydrogen-bonded molecular duplex. *J. Am. Chem. Soc.* **2000,** 122 (11), 2635-2644.
33. Van Ruymbeke, E.; Orfanou, K.; Kapnistos, M.; Iatrou, H.; Pitsikalis, M.; Hadjichristidis, N.; Lohse, D.; Vlassopoulos, D. Entangled dendritic polymers and beyond: Rheology of symmetric Cayley-tree polymers and macromolecular self-assemblies. *Macromolecules* **2007,** 40 (16), 5941-5952.
34. van Ruymbeke, E.; Vlassopoulos, D.; Mierzwa, M.; Pakula, T.; Charalabidis, D.; Pitsikalis, M.; Hadjichristidis, N. Rheology and structure of entangled telechelic linear and star polyisoprene melts. *Macromolecules* **2010,** 43 (9), 4401-4411.
35. Zhuge, F.; Hawke, L. G.; Fustin, C.-A.; Gohy, J.-F.; Van Ruymbeke, E. Decoding the linear viscoelastic properties of model telechelic metallo-supramolecular polymers. *J. Rheol.* **2017,** 61 (6), 1245-1262.
36. Goldansaz, H.; Voleppe, Q.; Pioge, S.; Fustin, C. A.; Gohy, J. F.; Brassinne, J.; Auhl, D.; van Ruymbeke, E. Controlling the melt rheology of linear entangled metallo-supramolecular polymers. *Soft Matter* **2015,** 11 (4), 762-74 DOI: 10.1039/c4sm02319f.
37. Ciferri, A., *Supramolecular polymers*. 2nd ed.; CRC Press: 2005.
38. Shabbir, A.; Javakhishvili, I.; Cerveny, S.; Hvilsted, S.; Skov, A. L.; Hassager, O.; Alvarez, N. J. Linear viscoelastic and dielectric relaxation response of unentangled UPy-based supramolecular networks. *Macromolecules* **2016,** 49 (10), 3899-3910.

39. Chen, Q.; Tudryn, G. J.; Colby, R. H. Ionomer dynamics and the sticky Rouse model. *J. Rheol.* **2013,** 57 (5), 1441.
40. Cui, G.; Boudara, V. A.; Huang, Q.; Baeza, G. P.; Wilson, A. J.; Hassager, O.; Read, D. J.; Mattsson, J. Linear shear and nonlinear extensional rheology of unentangled supramolecular side-chain polymers. *J. Rheol.* **2018,** 62 (5), 1155-1174.
41. Feldman, K. E.; Kade, M. J.; Meijer, E.; Hawker, C. J.; Kramer, E. J. Model transient networks from strongly hydrogen-bonded polymers. *Macromolecules* **2009,** 42 (22), 9072-9081.
42. Rossow, T.; Habicht, A.; Seiffert, S. Relaxation and dynamics in transient polymer model networks. *Macromolecules* **2014,** 47 (18), 6473-6482.
43. Rossow, T.; Seiffert, S. Supramolecular polymer gels with potential model-network structure. *Polym. Chem.* **2014,** 5 (8), 3018-3029.
44. Yan, X.; Cook, T. R.; Pollock, J. B.; Wei, P.; Zhang, Y.; Yu, Y.; Huang, F.; Stang, P. J. Responsive supramolecular polymer metallogel constructed by orthogonal coordination-driven self-assembly and host/guest interactions. *J. Am. Chem. Soc.* **2014,** 136 (12), 4460-4463.
45. Holten-Andersen, N.; Jaishankar, A.; Harrington, M. J.; Fullenkamp, D. E.; DiMarco, G.; He, L.; McKinley, G. H.; Messersmith, P. B.; Lee, K. Y. C. Metal-coordination: using one of nature's tricks to control soft material mechanics. *Journal of Materials Chemistry B* **2014,** 2 (17), 2467-2472.
46. Eisenberg, A.; Hird, B.; Moore, R. A new multiplet-cluster model for the morphology of random ionomers. *Macromolecules* **1990,** 23 (18), 4098-4107.
47. Ahmadi, M.; Hawke, L. G. D.; Goldansaz, H.; van Ruymbeke, E. Dynamics of Entangled Linear Supramolecular Chains with Sticky Side Groups: Influence of Hindered Fluctuations. *Macromolecules* **2015,** 48 (19), 7300-7310 DOI: 10.1021/acs.macromol.5b00733.
48. Lewis, C. L.; Stewart, K.; Anthamatten, M. The influence of hydrogen bonding side-groups on viscoelastic behavior of linear and network polymers. *Macromolecules* **2014,** 47 (2), 729-740.
49. Shabbir, A.; Goldansaz, H.; Hassager, O.; van Ruymbeke, E.; Alvarez, N. J. Effect of hydrogen bonding on linear and nonlinear rheology of entangled polymer melts. *Macromolecules* **2015,** 48 (16), 5988-5996.
50. Ahmadi, M.; Jangizehi, A.; van Ruymbeke, E.; Seiffert, S. Deconvolution of the effects of binary associations and collective assemblies on the rheological properties of entangled side-chain supramolecular polymer networks. *Macromolecules* **2019**.
51. Yang, L.; Tan, X.; Wang, Z.; Zhang, X. Supramolecular polymers: historical development, preparation, characterization, and functions. *Chem. Rev.* **2015,** 115 (15), 7196-7239.
52. de Greef, T. F.; Meijer, E. Materials science: Supramolecular polymers. *Nature* **2008,** 453 (7192), 171.
53. Aida, T.; Meijer, E.; Stupp, S. I. Functional supramolecular polymers. *Science* **2012,** 335 (6070), 813-817.
54. Du, X.; Zhou, J.; Shi, J.; Xu, B. Supramolecular hydrogelators and hydrogels: from soft matter to molecular biomaterials. *Chem. Rev.* **2015,** 115 (24), 13165-13307.
55. Jin, H.; Huang, W.; Zhu, X.; Zhou, Y.; Yan, D. Biocompatible or biodegradable hyperbranched polymers: from self-assembly to cytomimetic applications. *Chem. Soc. Rev.* **2012,** 41 (18), 5986-5997.
56. Buerkle, L. E.; Rowan, S. J. Supramolecular gels formed from multi-component low molecular weight species. *Chem. Soc. Rev.* **2012,** 41 (18), 6089-6102.
57. de Gennes, P.-G. Reptation of a polymer chain in the presence of fixed obstacles. *J. Chem. Phys.* **1971,** 55 (2), 572-579.
58. Hiemenz, P. C.; Lodge, T. P., *Polymer chemistry*. CRC press: 2007.
59. Cao, P. F.; Li, B.; Hong, T.; Townsend, J.; Qiang, Z.; Xing, K.; Vogiatzis, K. D.; Wang, Y.; Mays, J. W.; Sokolov, A. P. Superstretchable, self‐healing polymeric elastomers with tunable properties. *Adv. Funct. Mater.* **2018**, 1800741.

60. Chen, Y.; Kushner, A. M.; Williams, G. A.; Guan, Z. Multiphase design of autonomic self-healing thermoplastic elastomers. *Nature chemistry* **2012,** 4 (6), 467-472.
61. Phadke, A.; Zhang, C.; Arman, B.; Hsu, C.-C.; Mashelkar, R. A.; Lele, A. K.; Tauber, M. J.; Arya, G.; Varghese, S. Rapid self-healing hydrogels. *Proceedings of the National Academy of Sciences* **2012,** 109 (12), 4383-4388.
62. Cordier, P.; Tournilhac, F.; Soulié-Ziakovic, C.; Leibler, L. Self-healing and thermoreversible rubber from supramolecular assembly. *Nature* **2008,** 451 (7181), 977-980.
63. Burnworth, M.; Tang, L.; Kumpfer, J. R.; Duncan, A. J.; Beyer, F. L.; Fiore, G. L.; Rowan, S. J.; Weder, C. Optically healable supramolecular polymers. *Nature* **2011,** 472 (7343), 334-337.
64. Chen, S.; Mahmood, N.; Beiner, M.; Binder, W. H. Self-healing materials from V-and H-Shaped supramolecular architectures. *Angew. Chem. Int. Ed.* **2015,** 54 (35), 10188-10192.
65. Campanella, A.; Döhler, D.; Binder, W. H. Self-healing in supramolecular polymers. *Macromol. Rapid Commun.* **2018,** 39 (17), 1700739.
66. Yang, Y.; Ding, X.; Urban, M. W. Chemical and physical aspects of self-healing materials. *Prog. Polym. Sci.* **2015,** 49-50, 34-59.
67. Scheiner, M.; Dickens, T. J.; Okoli, O. Progress towards self-healing polymers for composite structural applications. *Polymer* **2016,** 83, 260-282.
68. Harada, A.; Kobayashi, R.; Takashima, Y.; Hashidzume, A.; Yamaguchi, H. Macroscopic self-assembly through molecular recognition. *Nature chemistry* **2011,** 3 (1), 34.
69. Pieters, G. g.; Pezzato, C.; Prins, L. J. Reversible control over the valency of a nanoparticle-based supramolecular system. *J. Am. Chem. Soc.* **2012,** 134 (37), 15289-15292.
70. Ward, M. D.; Raithby, P. R. Functional behaviour from controlled self-assembly: challenges and prospects. *Chem. Soc. Rev.* **2013,** 42 (4), 1619-1636.
71. Langner, A.; Tait, S. L.; Lin, N.; Chandrasekar, R.; Meded, V.; Fink, K.; Ruben, M.; Kern, K. Selective coordination bonding in metallo-supramolecular systems on surfaces. *Angew. Chem. Int. Ed.* **2012,** 51 (18), 4327-4331.
72. Llanes-Pallas, A.; Yoosaf, K.; Traboulsi, H.; Mohanraj, J.; Seldrum, T.; Dumont, J.; Minoia, A.; Lazzaroni, R.; Armaroli, N.; Bonifazi, D. Modular engineering of H-bonded supramolecular polymers for reversible functionalization of carbon nanotubes. *J. Am. Chem. Soc.* **2011,** 133 (39), 15412-15424.
73. Loveless, D. M.; Abu-Lail, N. I.; Kaholek, M.; Zauscher, S.; Craig, S. L. Reversibly cross-linked surface-grafted polymer brushes. *Angew. Chem. Int. Ed.* **2006,** 45 (46), 7812-7814.
74. Weng, W.; Beck, J. B.; Jamieson, A. M.; Rowan, S. J. Understanding the mechanism of gelation and stimuli-responsive nature of a class of metallo-supramolecular gels. *J. Am. Chem. Soc.* **2006,** 128 (35), 11663-11672.
75. Cortese, J.; Soulié-Ziakovic, C.; Cloitre, M.; Tencé-Girault, S.; Leibler, L. Order–disorder transition in supramolecular polymers. *J. Am. Chem. Soc.* **2011,** 133 (49), 19672-19675.
76. Cafferty, B.; Avirah, R.; Schuster, G.; Hud, N. Ultra-sensitive pH control of supramolecular polymers and hydrogels: p K a matching of biomimetic monomers. *Chem. Sci.* **2014,** 5 (12), 4681-4686.
77. Balkenende, D. W.; Coulibaly, S.; Balog, S.; Simon, Y. C.; Fiore, G. L.; Weder, C. Mechanochemistry with metallosupramolecular polymers. *J. Am. Chem. Soc.* **2014,** 136 (29), 10493-10498.
78. Coulibaly, S.; Heinzmann, C.; Beyer, F. L.; Balog, S.; Weder, C.; Fiore, G. L. Supramolecular polymers with orthogonal functionality. *Macromolecules* **2014,** 47 (24), 8487-8496.
79. Cortese, J.; Soulie-Ziakovic, C.; Tence-Girault, S.; Leibler, L. Suppression of mesoscopic order by complementary interactions in supramolecular polymers. *J. Am. Chem. Soc.* **2012,** 134 (8), 3671-4.

80. Brassinne, J.; Stevens, A. M.; Van Ruymbeke, E.; Gohy, J.-F.; Fustin, C.-A. Hydrogels with Dual Relaxation and Two-Step Gel–Sol Transition from Heterotelechelic Polymers. *Macromolecules* **2013,** 46 (22), 9134-9143 DOI: 10.1021/ma401657f.
81. Hu, J.; Zhang, G.; Liu, S. Enzyme-responsive polymeric assemblies, nanoparticles and hydrogels. *Chem. Soc. Rev.* **2012,** 41 (18), 5933-5949.
82. Yan, X.; Wang, F.; Zheng, B.; Huang, F. Stimuli-responsive supramolecular polymeric materials. *Chem. Soc. Rev.* **2012,** 41 (18), 6042-6065.
83. Zhang, H.; Liu, Y.; Yao, D.; Yang, B. Hybridization of inorganic nanoparticles and polymers to create regular and reversible self-assembly architectures. *Chem. Soc. Rev.* **2012,** 41 (18), 6066-6088.
84. Safont-Sempere, M. M.; Fernández, G.; Würthner, F. Self-sorting phenomena in complex supramolecular systems. *Chem. Rev.* **2011,** 111 (9), 5784-5814.
85. Chakrabarty, R.; Mukherjee, P. S.; Stang, P. J. Supramolecular coordination: self-assembly of finite two-and three-dimensional ensembles. *Chem. Rev.* **2011,** 111 (11), 6810-6918.
86. Park, C.; Lee, J.; Kim, C. Functional supramolecular assemblies derived from dendritic building blocks. *Chem. Commun.* **2011,** 47 (44), 12042-12056.
87. Adisoejoso, J.; Li, Y.; Liu, J.; Liu, P. N.; Lin, N. Two-dimensional metallo-supramolecular polymerization: toward size-controlled multi-strand polymers. *J. Am. Chem. Soc.* **2012,** 134 (45), 18526-18529.
88. Li, J.; Viveros, J. A.; Wrue, M. H.; Anthamatten, M. Shape‐memory effects in polymer networks containing reversibly associating side‐groups. *Adv. Mater.* **2007,** 19 (19), 2851-2855.
89. Li, J.; Lewis, C. L.; Chen, D. L.; Anthamatten, M. Dynamic mechanical behavior of photo-cross-linked shape-memory elastomers. *Macromolecules* **2011,** 44 (13), 5336-5343.
90. Ware, T.; Hearon, K.; Lonnecker, A.; Wooley, K. L.; Maitland, D. J.; Voit, W. Triple-shape memory polymers based on self-complementary hydrogen bonding. *Macromolecules* **2012,** 45 (2), 1062-1069.
91. You, L.; Zha, D.; Anslyn, E. V. Recent advances in supramolecular analytical chemistry using optical sensing. *Chem. Rev.* **2015,** 115 (15), 7840-7892.
92. Bae, Y.; Fukushima, S.; Harada, A.; Kataoka, K. Design of environment‐sensitive supramolecular assemblies for intracellular drug delivery: Polymeric micelles that are responsive to intracellular pH change. *Angew. Chem. Int. Ed.* **2003,** 42 (38), 4640-4643.
93. Hirschberg, J. K.; Brunsveld, L.; Ramzi, A.; Vekemans, J. A.; Sijbesma, R. P.; Meijer, E. Helical self-assembled polymers from cooperative stacking of hydrogen-bonded pairs. *Nature* **2000,** 407 (6801), 167.
94. Brochu, A. B.; Craig, S. L.; Reichert, W. M. Self‐healing biomaterials. *Journal of Biomedical Materials Research Part A* **2011,** 96 (2), 492-506.
95. Chen, S.-G.; Yu, Y.; Zhao, X.; Ma, Y.; Jiang, X.-K.; Li, Z.-T. Highly stable chiral (A) 6–B supramolecular copolymers: a multivalency-based self-assembly process. *J. Am. Chem. Soc.* **2011,** 133 (29), 11124-11127.
96. Dudowicz, J.; Freed, K. F. Generalized entropy theory of polymer glass formation. *Adv. Chem. Phys.* **2008,** 137, 125-222.
97. Sokolov, A.; Novikov, V.; Ding, Y. Why many polymers are so fragile. *J. Phys. Condens. Matter* **2007,** 19 (20), 205116.
98. Kunal, K.; Robertson, C. G.; Pawlus, S.; Hahn, S. F.; Sokolov, A. P. Role of chemical structure in fragility of polymers: a qualitative picture. *Macromolecules* **2008,** 41 (19), 7232-7238.
99. Stukalin, E. B.; Douglas, J. F.; Freed, K. F. Application of the entropy theory of glass formation to poly(alpha-olefins). *J. Chem. Phys.* **2009,** 131 (11), 114905.
100. Dudowicz, J.; Freed, K. F.; Douglas, J. F. The glass transition temperature of polymer melts. *J. Phys. Chem. B* **2005,** 109 (45), 21285-21292.

101. Adam, G.; Gibbs, J. H. On the temperature dependence of cooperative relaxation properties in glass-forming liquids. *J. Chem. Phys.* **1965,** 43 (1), 139-146.
102. Roland, C.; Hensel-Bielowka, S.; Paluch, M.; Casalini, R. Supercooled dynamics of glass-forming liquids and polymers under hydrostatic pressure. *Rep. Prog. Phys.* **2005,** 68 (6), 1405.
103. Amann-Winkel, K.; Gainaru, C.; Handle, P. H.; Seidl, M.; Nelson, H.; Bohmer, R.; Loerting, T. Water's second glass transition. *PNAS* **2013,** 110 (44), 17720-5.
104. Loerting, T.; Fuentes-Landete, V.; Handle, P. H.; Seidl, M.; Amann-Winkel, K.; Gainaru, C.; Bohmer, R. The glass transition in high-density amorphous ice. *J Non Cryst Solids* **2015,** 407, 423-430.
105. Hansen, J. S.; Kisliuk, A.; Sokolov, A. P.; Gainaru, C. J. P. r. l. Identification of structural relaxation in the dielectric response of water. **2016,** 116 (23), 237601.
106. Gainaru, C.; Bauer, S.; Vynokur, E.; Wittkamp, H.; Hiller, W.; Richert, R.; Bohmer, R. Dynamics in supercooled secondary amide mixtures: dielectric and hydrogen bond specific spectroscopies. *J. Phys. Chem. B* **2015,** 119 (51), 15769-79.
107. Böhmer, R.; Gainaru, C.; Richert, R. Structure and dynamics of monohydroxy alcohols—Milestones towards their microscopic understanding, 100 years after Debye. *Phys. Rep.* **2014,** 545 (4), 125-195.
108. Gainaru, C.; Kastner, S.; Mayr, F.; Lunkenheimer, P.; Schildmann, S.; Weber, H. J.; Hiller, W.; Loidl, A.; Böhmer, R. Hydrogen-bond equilibria and lifetimes in a monohydroxy alcohol. *Phys. Rev. Lett.* **2011,** 107 (11).
109. Gainaru, C.; Meier, R.; Schildmann, S.; Lederle, C.; Hiller, W.; Rössler, E.; Böhmer, R. Nuclear-magnetic-resonance measurements reveal the origin of the debye process in monohydroxy alcohols. *Phys. Rev. Lett.* **2010,** 105 (25), 258303.
110. Kremer, F. S., A., *Broadband dielectric spectroscopy*. Springer-Verlag, Berlin: 2002.
111. Adachi, K.; Kotaka, T. Dielectric normal mode relaxation. *Prog. Polym. Sci.* **1993,** 18 (3), 585-622.
112. Lou, N.; Wang, Y.; Li, X.; Li, H.; Wang, P.; Wesdemiotis, C.; Sokolov, A. P.; Xiong, H. Dielectric relaxation and rheological behavior of supramolecular polymeric liquid. *Macromolecules* **2013,** 46 (8), 3160-3166.
113. Herbst, F.; Schröter, K.; Gunkel, I.; Gröger, S.; Thurn-Albrecht, T.; Balbach, J.; Binder, W. H. Aggregation and chain dynamics in supramolecular polymers by dynamic rheology: cluster formation and self-aggregation. *Macromolecules* **2010,** 43 (23), 10006-10016.
114. Pensec, S.; Nouvel, N.; Guilleman, A.; Creton, C.; Boué, F. o.; Bouteiller, L. Self-assembly in solution of a reversible comb-shaped supramolecular polymer. *Macromolecules* **2010,** 43 (5), 2529-2534.
115. Staropoli, M.; Raba, A.; Hövelmann, C. H.; Appavou, M.-S.; Allgaier, J.; Krutyeva, M.; Pyckhout-Hintzen, W.; Wischnewski, A.; Richter, D. Melt dynamics of supramolecular comb polymers: Viscoelastic and dielectric response. *J. Rheol.* **2017,** 61 (6), 1185-1196.
116. Staropoli, M.; Raba, A.; Hövelmann, C. H.; Krutyeva, M.; Allgaier, J.; Appavou, M.-S.; Keiderling, U.; Stadler, F. J.; Pyckhout-Hintzen, W.; Wischnewski, A.; Richter, D. Hydrogen bonding in a reversible comb polymer architecture: A microscopic and macroscopic investigation. *Macromolecules* **2016,** 49 (15), 5692-5703.
117. Nyrkova, I. A.; Khokhlov, A. R.; Doi, M. Microdomains in block copolymers and multiplets in ionomers: parallels in behavior. *Macromolecules* **1993,** 26 (14), 3601-3610.
118. Semenov, A.; Joanny, J.-F.; Khokhlov, A. Associating polymers: equilibrium and linear viscoelasticity. *Macromolecules* **1995,** 28 (4), 1066-1075.
119. Semenov, A. Contribution to the theory of microphase layering in block-copolymer melts. *Zh. Eksp. Teor. Fiz* **1985,** 88 (4), 1242-1256.
120. Lange, R. F.; Van Gurp, M.; Meijer, E. Hydrogen-bonded supramolecular polymer networks. *J. Polym. Sci., Part A: Polym. Chem.* **1999,** 37 (19), 3657-3670.

121. Schubert, U. S.; Hofmeier, H.; Newkome, G. R., *Modern terpyridine chemistry*. John Wiley & Sons: 2006.
122. Serero, Y.; Aznar, R.; Porte, G.; Berret, J.-F.; Calvet, D.; Collet, A.; Viguier, M. Associating polymers: from "flowers" to transient networks. *Phys. Rev. Lett.* **1998,** 81 (25), 5584.
123. Brassinne, J. r. m.; Stevens, A. M.; Van Ruymbeke, E.; Gohy, J.-F. o.; Fustin, C.-A. Hydrogels with dual relaxation and two-step gel–sol transition from heterotelechelic polymers. *Macromolecules* **2013,** 46 (22), 9134-9143.
124. Zhang, Z.; Liu, C.; Cao, X.; Gao, L.; Chen, Q. Linear viscoelastic and dielectric properties of strongly hydrogen-bonded polymers near the sol–gel transition. *Macromolecules* **2016,** 49 (23), 9192-9202.
125. Cates, M. E. Reptation of living polymers: dynamics of entangled polymers in the presence of reversible chain-scission reactions. *Macromolecules* **1987,** 20, 2289-2296.
126. Cates, M. E. Theory of the viscosity of polymeric liquid sulfur. *Europhys. Lett.* **1987,** 4, 497-502.
127. Marques, C. M.; Turner, M. S.; Cates, M. E. Relaxation mechanisms in worm-like micelles. *J. Non-Cryst. Solids* **1994,** 172-174, 1168-1172.
128. Tang, S.; Wang, M.; Olsen, B. D. Anomalous self-diffusion and sticky Rouse dynamics in associative protein hydrogels. *J. Am. Chem. Soc.* **2015,** 137 (11), 3946-3957.
129. Rubinstein, M.; Semenov, A. N. Dynamics of entangled solutions of associating polymers. *Macromolecules* **2001,** 34, 1058-1068.
130. Semenov, A. N.; Rubinstein, M. Dynamics of entangled associating polymers with large aggregates. *Macromolecules* **2002,** 35, 4821-4837.
131. Leibler, L.; Rubinstein, M.; Colby, R. H. Dynamics of reversible networks. *Macromolecules* **1991,** 24 (16), 4701-4707.
132. Rubinstein, M.; Semenov, A. N. Dynamics of entangled solutions of associating polymers. *Macromolecules* **2001,** 34 (4), 1058-1068.
133. Green, M. S.; Tobolsky, A. V. A new approach to the theory of relaxing polymeric media. *J. Chem. Phys.* **1946,** 14 (2), 80.
134. Lodge, A. A network theory of flow birefringence and stress in concentrated polymer solutions. *Trans. Faraday Soc.* **1956,** 52, 120-130.
135. Tanaka, F.; Edwards, S. F. Viscoelastic properties of physically cross-linked networks. Transient network theory. *Macromolecules* **1992,** 25, 1516-1523.
136. Yamamoto, M. J. J. o. t. p. s. o. J. The visco-elastic properties of network structure I. General formalism. *J. Phys. Soc. Jpn.* **1956,** 11 (4), 413-421.
137. Yamamoto, M. The visco-elastic properties of network structure II. Structural viscosity. *J. Phys. Soc. Jpn.* **1957,** 12 (10), 1148-1158.
138. Yamamoto, M. The visco-elastic properties of network structure III. Normal stress effect (Weissenberg effect). *J. Phys. Soc. Jpn.* **1958,** 13 (10), 1200-1211.
139. Jongschaap, R. J. J.; Wientjes, R. H. W.; Duits, M. H. G.; Mellema, J. A generalized transient network model for associative polymer networks. *Macromolecules* **2001,** 34 (4), 1031-1038.
140. Vermonden, T.; van Steenbergen, M. J.; Besseling, N. A. M.; Marcelis, A. T. M.; Hennink, W. E.; Sudhölter, E. J. R.; Cohen Stuart, M. A. Linear rheology of water-soluble reversible neodymium(III) coordination polymers. *J. Am. Chem. Soc.* **2004,** 126 (48), 15802-15808.
141. Knoben, W.; Besseling, N.; Bouteiller, L.; Stuart, M. C. Dynamics of reversible supramolecular polymers: Independent determination of the dependence of linear viscoelasticity on concentration and chain length by using chain stoppers. *Phys. Chem. Chem. Phys.* **2005,** 7 (11), 2390-2398.
142. Hirschberg, J. H. K. K.; Beijer, F. H.; van Aert, H. A.; Magusin, P. C. M. M.; Sijbesma, R. P.; Meijer, E. W. Supramolecular polymers from linear telechelic siloxanes with quadruple-hydrogen-bonded units. *Macromolecules* **1999,** 32 (8), 2696-2705.

143. Castellano, R. K.; Clark, R.; Craig, S. L.; Nuckolls, C.; Rebek, J. Emergent mechanical properties of self-assembled polymeric capsules. *Proceedings of the National Academy of Sciences* **2000,** 97 (23), 12418-12421.
144. Xu, J.; Fogleman, E. A.; Craig, S. L. Structure and properties of DNA-based reversible polymers. *Macromolecules* **2004,** 37 (5), 1863-1870.
145. Fogleman, E. A.; Yount, W. C.; Xu, J.; Craig, S. L. Modular, well-behaved reversible polymers from DNA-based monomers. *Angew. Chem. Int. Ed.* **2002,** 41 (21), 4026-4028.
146. Graessley, W. W., The entanglement concept in polymer rheology. In *The entanglement concept in polymer rheology*, Springer: 1974; pp 1-179.
147. Granek, R.; Cates, M. Stress relaxation in living polymers: results from a poisson renewal model. *J. Chem. Phys.* **1992,** 96 (6), 4758-4767.
148. Cates, M. E.; Candau, S. J. Statics and dynamics of worm-like surfactant micelles. *J. Phys. Condens. Matter* **1990,** 2, 6869-6892.
149. Cates, M. Nonlinear viscoelasticity of wormlike micelles (and other reversibly breakable polymers). *Journal of Physical Chemistry* **1990,** 94 (1), 371-375.
150. Baxandall, L. G. Dynamics of reversibly cross-linked chains. *Macromolecules* **1989,** 22, 1982-1988.
151. Rouse, P. E. A theory of the linear viscoelastic properties of dilute solutions of coiling polymers. *J. Chem. Phys.* **1953,** 21 (7), 1272.
152. Marrucci, G.; Bhargava, S.; Cooper, S. Models of shear-thickening behavior in physically crosslinked networks. *Macromolecules* **1993,** 26 (24), 6483-6488.
153. Colby, R. H.; Zheng, X.; Rafailovich, M. H.; Sokolov, J.; Peiffer, D. G.; Schwarz, S. A.; Strzhemechny, Y.; Nguyen, D. Dynamics of Lightly Sulfonated Polystyrene Ionomers. *Phys. Rev. Lett.* **1998,** 81 (18), 3876-3879.
154. Tierney, N. K.; Register, R. A. Ion hopping in ethylene− methacrylic acid ionomer melts as probed by rheometry and cation diffusion measurements. *Macromolecules* **2002,** 35 (6), 2358-2364.
155. Semenov, A. N.; Rubinstein, M. Thermoreversible gelation in solutions of associative polymers. 1. Statics. *Macromolecules* **1998,** 31 (4), 1373-1385.
156. Rubinstein, M.; Semenov, A. N. Thermoreversible gelation in solutions of associating polymers. 2. Linear dynamics. *Macromolecules* **1998,** 31 (4), 1386-1397.
157. Semenov, A.; Charlot, A.; Auzély-Velty, R.; Rinaudo, M. Rheological properties of binary associating polymers. *Rheol. Acta* **2007,** 46 (5), 541-568.
158. Stukalin, E. B.; Cai, L.-H.; Kumar, N. A.; Leibler, L.; Rubinstein, M. Self-healing of unentangled polymer networks with reversible bonds. *Macromolecules* **2013,** 46 (18), 7525-7541.
159. Wang, S.-Q., *Nonlinear polymer rheology*. Wiley Online Library: 2018.
160. Gold, B.; Hövelmann, C.; Lühmann, N.; Székely, N.; Pyckhout-Hintzen, W.; Wischnewski, A.; Richter, D. Importance of Compact Random Walks for the Rheology of Transient Networks. *ACS Macro Letters* **2017,** 6 (2), 73-77.
161. Gold, B.; Hövelmann, C.; Lühmann, N.; Pyckhout-Hintzen, W.; Wischnewski, A.; Richter, D. The microscopic origin of the rheology in supramolecular entangled polymer networks. *J. Rheol.* **2017,** 61 (6), 1211-1226.
162. Roovers, J.; Hadjichristidis, N.; Fetters, L. J. Analysis and dilute solution properties of 12-and 18-arm-star polystyrenes. *Macromolecules* **1983,** 16 (2), 214-220.
163. Xuexin, C.; Zhongde, X.; Von Meerwall, E.; Seung, N.; Hadjichristidis, N.; Fetters, L. J. Self-diffusion of linear and 4-and 18-armed star polyisoprenes in tetrachloromethane solution. *Macromolecules* **1984,** 17 (7), 1343-1348.

164. Suzuki, S.; Uneyama, T.; Watanabe, H. Concentration dependence of nonlinear rheological properties of hydrophobically modified ethoxylated urethane aqueous solutions. *Macromolecules* **2013,** 46 (9), 3497-3504.
165. Annable, T.; Buscall, R.; Ettelaie, R.; Whittlestone, D. The rheology of solutions of associating polymers: Comparison of experimental behavior with transient network theory. *J. Rheol.* **1993,** 37 (4), 695-726.
166. Milner, S. T.; Witten, T. A. Bridging attraction by telechelic polymers. *Macromolecules* **1992,** 25 (20), 5495-5503.
167. Charlier, P.; Jerome, R.; Teyssie, P.; Utracki, L. Viscoelastic properties of telechelic ionomers. 2. Complexed α, ι-diaminopolydienes. *Macromolecules* **1990,** 23 (13), 3313-3321.
168. Suzuki, S.; Uneyama, T.; Inoue, T.; Watanabe, H. Nonlinear rheology of telechelic associative polymer networks: Shear thickening and thinning behavior of hydrophobically modified ethoxylated urethane (HEUR) in aqueous solution. *Macromolecules* **2012,** 45 (2), 888-898.
169. Stadler, F. J.; Pyckhout-Hintzen, W.; Schumers, J.-M.; Fustin, C.-A.; Gohy, J.-F. o.; Bailly, C. Linear viscoelastic rheology of moderately entangled telechelic polybutadiene temporary networks. *Macromolecules* **2009,** 42 (16), 6181-6192.
170. Stadler, F. J.; Still, T.; Fytas, G.; Bailly, C. Elongational rheology and brillouin light scattering of entangled telechelic polybutadiene based temporary networks. *Macromolecules* **2010,** 43 (18), 7771-7778.
171. Zhang, L.; Brostowitz, N. R.; Cavicchi, K. A.; Weiss, R. Perspective: Ionomer research and applications. *Macromol. React. Eng.* **2014,** 8 (2), 81-99.
172. Kwon, Y.; Matsumiya, Y.; Watanabe, H. Viscoelastic and orientational relaxation of linear and ring rouse chains undergoing reversible end-association and dissociation. *Macromolecules* **2016,** 49 (9), 3593-3607.
173. Zhuge, F.; Brassinne, J. r. m.; Fustin, C.-A.; Van Ruymbeke, E.; Gohy, J.-F. o. Synthesis and rheology of bulk metallo-supramolecular polymers from telechelic entangled precursors. *Macromolecules* **2017,** 50 (13), 5165-5175.
174. Park, G. W.; Ianniruberto, G. A new stochastic simulation for the rheology of telechelic associating polymers. *J. Rheol.* **2017,** 61 (6), 1293-1305.
175. Fetters, L. J.; Graessley, W. W.; Hadjichristidis, N.; Kiss, A. D.; Pearson, D. S.; Younghouse, L. B. Association behavior of end-functionalized polymers. 2. Melt rheology of polyisoprenes with carboxylate, amine, and zwitterion end groups. *Macromolecules* **1988,** 21 (6), 1644-1653.
176. Davidson, N. S.; Fetters, L. J.; Funk, W. G.; Graessley, W. W.; Hadjichristidis, N. Association behavior in end-functionalized polymers. 1. Dilute solution properties of polyisoprenes with amine and zwitterion end groups. *Macromolecules* **1988,** 21 (1), 112-121.
177. Amin, D.; Likhtman, A. E.; Wang, Z. Dynamics in supramolecular polymer networks formed by associating telechelic chains. *Macromolecules* **2016,** 49 (19), 7510-7524.
178. Binder, W. H.; Kunz, M. J.; Kluger, C.; Hayn, G.; Saf, R. Synthesis and analysis of telechelic polyisobutylenes for hydrogen-bonded supramolecular pseudo-block copolymers. *Macromolecules* **2004,** 37 (5), 1749-1759.
179. Yan, T.; Schröter, K.; Herbst, F.; Binder, W. H.; Thurn-Albrecht, T. What controls the structure and the linear and nonlinear rheological properties of dense, dynamic supramolecular polymer networks? *Macromolecules* **2017**.
180. Brás, A. R.; Hövelmann, C. H.; Antonius, W.; Teixeira, J.; Radulescu, A.; Allgaier, J. r.; Pyckhout-Hintzen, W.; Wischnewski, A.; Richter, D. Molecular approach to supramolecular polymer assembly by small angle neutron scattering. *Macromolecules* **2013,** 46 (23), 9446-9454.

181. Yan, T.; Schröter, K.; Herbst, F.; Binder, W. H.; Thurn-Albrecht, T. Nanostructure and rheology of hydrogen-bonding telechelic polymers in the melt: from micellar liquids and solids to supramolecular gels. *Macromolecules* **2014,** 47 (6), 2122-2130.
182. Tanaka, F.; Edwards, S. Viscoelastic properties of physically crosslinked networks. 1. Transient network theory. *Macromolecules* **1992,** 25 (5), 1516-1523.
183. Hadjichristidis, N.; Pispas, S.; Pitsikalis, M. End-functionalized polymers with zwitterionic end-groups. *Prog. Polym. Sci.* **1999,** 24 (6), 875-915.
184. Antonietti, M.; Ehlich, D.; Foelsch, K. J.; Sillescu, H.; Schmidt, M.; Lindner, P. Micronetworks by end-linking of polystyrene. 1. Synthesis and characterization by light and neutron scattering. *Macromolecules* **1989,** 22 (6), 2802-2812.
185. Antonietti, M.; Foelsch, K. J.; Sillescu, H.; Pakula, T. Micronetworks by end-linking of polystyrene. 2. Dynamic mechanical behavior and diffusion experiments in the bulk. *Macromolecules* **1989,** 22 (6), 2812-2817.
186. Vlassopoulos, D.; Pitsikalis, M.; Hadjichristidis, N. Linear dynamics of end-functionalized polymer melts: Linear chains, stars, and blends. *Macromolecules* **2000,** 33 (26), 9740-9746.
187. Pispas, S.; Hadjichristidis, N. End-functionalized block copolymers of styrene and isoprene: synthesis and association behavior in dilute solution. *Macromolecules* **1994,** 27 (7), 1891-1896.
188. Müller, M.; Dardin, A.; Seidel, U.; Balsamo, V.; Iván, B.; Spiess, H. W.; Stadler, R. Junction dynamics in telechelic hydrogen bonded polyisobutylene networks. *Macromolecules* **1996,** 29 (7), 2577-2583.
189. Wu, S.; Liu, S.; Zhang, Z.; Chen, Q. Dynamics of telechelic ionomers with distribution of number of ionic stickers at chain ends. *Macromolecules* **2019,** 52 (6), 2265-2276.
190. Li, Z.; Djohari, H.; Dormidontova, E. E. Molecular dynamics simulations of supramolecular polymer rheology. *J. Chem. Phys.* **2010,** 133 (18), 184904.
191. Huang, C.-C.; Xu, H.; Ryckaert, J.-P. Kinetics and dynamic properties of equilibrium polymers. *J. Chem. Phys.* **2006,** 125 (9), 094901.
192. Watanabe, H.; Matsumiya, Y.; Masubuchi, Y.; Urakawa, O.; Inoue, T. Viscoelastic relaxation of rouse chains undergoing head-to-head association and dissociation: Motional coupling through chemical equilibrium. *Macromolecules* **2015,** 48 (9), 3014-3030.
193. Watanabe, H.; Matsumiya, Y.; Kwon, Y. Viscoelastic and dielectric relaxation of reptating type-A chains affected by reversible head-to-head association and dissociation. *Macromolecules* **2018,** 51 (16), 6476-6496.
194. Watanabe, H.; Matsumiya, Y.; Kwon, Y. Dynamics of rouse chains undergoing head-to-head association and dissociation: Difference between dielectric and viscoelastic relaxation. *J. Rheol.* **2017,** 61 (6), 1151-1170.
195. Rubinstein, M.; Colby, R. H., *Polymer physics*. Oxford university press New York: 2003; Vol. 23.
196. Yan, T.; Schroter, K.; Herbst, F.; Binder, W. H.; Thurn-Albrecht, T. Unveiling the molecular mechanism of self-healing in a telechelic, supramolecular polymer network. *Sci Rep* **2016,** 6, 32356.
197. Herbst, F.; Döhler, D.; Michael, P.; Binder, W. H. Self‐healing polymers via supramolecular forces. *Macromol. Rapid Commun.* **2013,** 34 (3), 203-220.
198. Herbst, F.; Seiffert, S.; Binder, W. H. Dynamic supramolecular poly (isobutylene) s for self-healing materials. *Polym. Chem.* **2012,** 3 (11), 3084-3092.
199. Binder, W. H. The past 40 years of macromolecular sciences: reflections on challenges in synthetic polymer and material science. *Macromol. Rapid Commun.* **2019,** 40 (1), 1800610.
200. Zhang, Z.; Chen, Q.; Colby, R. H. Dynamics of associative polymers. *Soft Matter* **2018,** 14 (16), 2961-2977.
201. Israelachvili, J., Intermolecular and surface forces. Burlington, MA: Academic Press: 2011.

202. Khokhlov, A.; de Gennes, P.-G., *Giant molecules: here, there, and everywhere*. World Scientific: 2011.
203. Biedermann, F.; Schneider, H. J. Experimental binding energies in supramolecular complexes. *Chem. Rev.* **2016,** 116 (9), 5216-300.
204. Chen, Q.; Huang, C.; Weiss, R.; Colby, R. H. Viscoelasticity of reversible gelation for ionomers. *Macromolecules* **2015,** 48 (4), 1221-1230.
205. Huang, C.; Wang, C.; Chen, Q.; Colby, R. H.; Weiss, R. Reversible gelation model predictions of the linear viscoelasticity of oligomeric sulfonated polystyrene ionomer blends. *Macromolecules* **2016,** 49 (10), 3936-3947.
206. Zhang, Z.; Huang, C.; Weiss, R.; Chen, Q. Association energy in strongly associative polymers. *J. Rheol.* **2017,** 61 (6), 1199-1207.
207. Huang, C.; Chen, Q.; Weiss, R. Nonlinear Rheology of Random Sulfonated Polystyrene Ionomers: The Role of the Sol–Gel Transition. *Macromolecules* **2016,** 49 (23), 9203-9214.
208. Matsumiya, Y.; Watanabe, H.; Urakawa, O.; Inoue, T. Experimental Test for Viscoelastic Relaxation of Polyisoprene Undergoing Monofunctional Head-to-Head Association and Dissociation. *Macromolecules* **2016,** 49 (18), 7088-7095.
209. Van Ruymbeke, E. Preface: Special issue on associating polymers. *J. Rheol.* **2017,** 61 (6), 1099-1102.
210. Watanabe, H. Dielectric Relaxation of Type‐A Polymers in Melts and Solutions. *Macromol. Rapid Commun.* **2001,** 22 (3), 127-175.
211. Wübbenhorst, M.; Van Turnhout, J. Analysis of complex dielectric spectra. I. One-dimensional derivative techniques and three-dimensional modelling. *J. Non-Cryst. Solids* **2002,** 305 (1-3), 40-49.
212. Spink, C. H. Differential scanning calorimetry. *Methods in cell biology* **2008,** 84, 115-141.
213. Charsley, E.; Price, D.; Hunter, N.; Gabbott, P.; Kett, V.; Gaisford, S.; Priestley, I.; Duncan, J.; Royall, P.; Scowen, I., *Principles of thermal analysis and calorimetry*. Royal society of chemistry: 2019.
214. Zheng, Q.; Zhang, Y.; Montazerian, M.; Gulbiten, O.; Mauro, J. C.; Zanotto, E. D.; Yue, Y. Understanding glass through differential scanning calorimetry. *Chem. Rev.* **2019,** 119 (13), 7848-7939.
215. Moynihan, C.; Macedo, P.; Montrose, C.; Montrose, C.; Gupta, P.; DeBolt, M.; Dill, J.; Dom, B.; Drake, P.; Easteal, A. Structural relaxation in vitreous materials. *Ann. N.Y. Acad. Sci.* **1976,** 279 (1), 15-35.
216. Gulbiten, O.; Mauro, J. C.; Lucas, P. Relaxation of enthalpy fluctuations during sub-Tg annealing of glassy selenium. *J. Chem. Phys.* **2013,** 138 (24), 244504.
217. Kelly, P. Solid mechanics part I: An introduction to solid mechanics. **2013,** 94042.
218. Deegan, R. D.; Leheny, R. L.; Menon, N.; Nagel, S. R.; Venerus, D. C. Dynamic shear modulus of tricresyl phosphate and squalane. *J. Phys. Chem. B* **1999,** 103 (20), 4066-4070.
219. Kopf, A.; Dünweg, B.; Paul, W. Dynamics of polymer "isotope" mixtures: Molecular dynamics simulation and Rouse model analysis. *J. Chem. Phys.* **1997,** 107 (17), 6945-6955.
220. Aharoni, S. M. On entanglements of flexible and rodlike polymers. *Macromolecules* **1983,** 16 (11), 1722-1728.
221. Mark, J. E., *Physical properties of polymers handbook*. Springer: 2007; Vol. 1076.
222. Fetters, L.; Lohse, D.; Richter, D.; Witten, T.; Zirkel, A. Connection between polymer molecular weight, density, chain dimensions, and melt viscoelastic properties. *Macromolecules* **1994,** 27 (17), 4639-4647.
223. Kavassalis, T. A.; Noolandi, J. Entanglement scaling in polymer melts and solutions. *Macromolecules* **1989,** 22 (6), 2709-2720.
224. Wang, S.-Q. On chain statistics and entanglement of flexible linear polymer melts. *Macromolecules* **2007,** 40 (24), 8684-8694.
225. Wool, R. P. Polymer entanglements. *Macromolecules* **1993,** 26 (7), 1564-1569.

226. Guo, J.; Grassia, L.; Simon, S. L. Bulk and shear rheology of a symmetric three‐arm star polystyrene. *J. Polym. Sci., Part B: Polym. Phys.* **2012,** 50 (17), 1233-1244.
227. Zhao, Z. Understanding melt-deformation effect on mechanical behavior of polymer glasses. University of Akron, 2019.
228. Plazek, D. J.; O'Rourke, V. M. Viscoelastic behavior of low molecular weight polystyrene. *Journal of Polymer Science Part A‐2: Polymer Physics* **1971,** 9 (2), 209-243.
229. Xing, K.; Tress, M.; Cao, P.; Cheng, S.; Saito, T.; Novikov, V. N.; Sokolov, A. P. Hydrogen-bond strength changes network dynamics in associating telechelic PDMS. *Soft Matter* **2018**.
230. Xing, K.; Tress, M.; Cao, P.-F.; Fan, F.; Cheng, S.; Saito, T.; Sokolov, A. P. The role of chain-end association lifetime in segmental and chain dynamics of telechelic polymers. *Macromolecules* **2018,** 51 (21), 8561-8573.
231. Osterwinter, C.; Schubert, C.; Tonhauser, C.; Wilms, D.; Frey, H.; Friedrich, C. Rheological Consequences of Hydrogen Bonding: Linear Viscoelastic Response of Linear Polyglycerol and Its Permethylated Analogues as a General Model for Hydroxyl-Functional Polymers. *Macromolecules* **2015,** 48 (1), 119-130 DOI: 10.1021/ma501674x.
232. Yan, T.; Schröter, K.; Herbst, F.; Binder, W. H.; Thurn-Albrecht, T. Nanostructure and Rheology of Hydrogen-Bonding Telechelic Polymers in the Melt: From Micellar Liquids and Solids to Supramolecular Gels. *Macromolecules* **2014,** 47 (6), 2122-2130 DOI: 10.1021/ma402007f.
233. Xing, K.; Chatterjee, S.; Saito, T.; Gainaru, C.; Sokolov, A. P. Impact of hydrogen bonding on dynamics of hydroxyl-terminated polydimethylsiloxane. *Macromolecules* **2016,** 49 (8), 3138-3147.
234. Ferry, A. Ionic interactions and transport properties in methyl terminated poly (propylene glycol)(4000) complexed with LiCF3SO3. *J. Phys. Chem. B* **1997,** 101 (2), 150-157.
235. Ferry, A.; Tian, M. Influence of hydroxyl terminal groups on the ionic speciation and ionic conductivity in complexes of poly (propylene glycol)(4000) and LiCF3SO3 salt. *Macromolecules* **1997,** 30 (4), 1214-1215.
236. Sijbesma, R. P.; Beijer, F. H.; Brunsveld, L.; Folmer, B. J. B.; Ky Hirschberg, J. H. K.; Lange, R. F. M.; Lowe, J. K. L.; Meijer, E. W. Reversible polymers formed from self-complementary monomers using quadruple hydrogen bonding. *Science* **1997,** 278, 1601-1604.
237. Sijbesma, R. P.; Meijer, E. W. Quadruple hydrogen bonded systems. *Chem. Commun.* **2003,** (1), 5-16.
238. Wagner, H.; Richert, R. Equilibrium and non-equilibrium type β-relaxations: D-sorbitol versus o-terphenyl. *J. Phys. Chem. B* **1999,** 103 (20), 4071-4077.
239. Fan, F.; Wang, Y.; Sokolov, A. P. Ionic transport, microphase separation, and polymer relaxation in poly(propylene glycol) and lithium perchlorate mixtures. *Macromolecules* **2013,** 46 (23), 9380-9389 DOI: 10.1021/ma401238k.
240. Kudlik, A.; Benkhof, S.; Blochowicz, T.; Tschirwitz, C.; Rössler, E. The dielectric response of simple organic glass formers. *J. Mol. Struct.* **1999,** 479 (2), 201-218.
241. Hintermeyer, J.; Herrmann, A.; Kahlau, R.; Goiceanu, C.; Rossler, E. Molecular weight dependence of glassy dynamics in linear polymers revisited. *Macromolecules* **2008,** 41 (23), 9335-9344.
242. Böttcher;, C. J. F.; Bordewijk, P., *Theory of electric polarization II: Dielectrics in time-dependent fields*. Elsevier, New York: 1978.
243. Davidson, D.; Cole, R. Dielectric relaxation in glycerine. *J. Chem. Phys.* **1950,** 18 (10), 1417-1417.
244. Maggi, C.; Jakobsen, B.; Christensen, T.; Olsen, N. B.; Dyre, J. C. Supercooled liquid dynamics studied via shear-mechanical spectroscopy. *J. Phys. Chem. B* **2008,** 112 (51), 16320-16325.
245. Ferry, J. D., *Viscoelastic properties of polymers*. John Wiley & Sons: 1980.
246. Roland, C. M., *Viscoelastic behavior of rubbery materials*. Oxford University Press: 2011.
247. Cowie, J.; McEwen, I. Molecular motions in poly (dimethyl siloxane) oligomers and polymers. *Polymer* **1973,** 14 (9), 423-426.

248. Kirst, K.; Kremer, F.; Pakula, T.; Hollingshurst, J. Molecular dynamics of cyclic and linear poly (dimethylsiloxanes). *Colloid. Polym. Sci.* **1994,** 272 (11), 1420-1429.
249. Böhmer, R.; Ngai, K. L.; Angell, C. A.; Plazek, D. J. Nonexponential relaxations in strong and fragile glass formers. *J. Chem. Phys.* **1993,** 99 (5), 4201 DOI: 10.1063/1.466117.
250. Dudowicz, J.; Freed, K. F.; Douglas, J. F. Fragility of glass-forming polymer liquids. *J. Phys. Chem. B* **2005,** 109 (45), 21350-21356.
251. Bass, S.; Nathan, W.; Meighan, R.; Cole, R. Dielectric properties of alkyl amides. II. Liquid dielectric constant and loss. *J. Phys. Chem.* **1964,** 68 (3), 509-515.
252. Adrjanowicz, K.; Kaminski, K.; Dulski, M.; Wlodarczyk, P.; Bartkowiak, G.; Popenda, L.; Jurga, S.; Kujawski, J.; Kruk, J.; Bernard, M. K.; Paluch, M. Communication: Synperiplanar to antiperiplanar conformation changes as underlying the mechanism of Debye process in supercooled ibuprofen. *J. Chem. Phys.* **2013,** 139 (11), 111103 DOI: 10.1063/1.4820492.
253. Kwon, H.-J.; Kim, T. H.; Ko, J.-H.; Hwang, Y.-H. Relaxation phenomena in supercooled liquid and glassy acetaminophen studied by dielectric, photon correlation and Brillouin light scattering spectroscopies. *Chem. Phys. Lett.* **2013,** 556, 117-121 DOI: 10.1016/j.cplett.2012.11.072.
254. Rams-Baron, M.; Wojnarowska, Z.; Dulski, M.; Ratuszna, A.; Paluch, M. Evidence of slow Debye-like relaxation in the anti-inflammatory agent etoricoxib. *Phys Rev E Stat Nonlin Soft Matter Phys* **2015,** 92 (2), 022309 DOI: 10.1103/PhysRevE.92.022309.
255. Wang, Y.; Griffin, P. J.; Holt, A.; Fan, F.; Sokolov, A. P. Observation of the slow, Debye-like relaxation in hydrogen-bonded liquids by dynamic light scattering. *J. Chem. Phys.* **2014,** 140 (10), 104510 DOI: 10.1063/1.4867913.
256. Cosby, T.; Holt, A.; Griffin, P. J.; Wang, Y.; Sangoro, J. Proton transport in imidazoles: unraveling the role of supramolecular structure. *J. Phys. Chem. Lett.* **2015,** 6 (19), 3961-5.
257. MacCallum, J. L.; Tieleman, D. P. Structures of neat and hydrated 1-octanol from computer simulations. *J. Am. Chem. Soc.* **2002,** 124 (50), 15085-15093.
258. Gómez-Álvarez, P.; Romaní, L.; González-Salgado, D. Association effects in pure methanol via Monte Carlo simulations. I. Structure. *J. Chem. Phys.* **2013,** 138 (4), 044509.
259. Zoranic, L.; Sokolic, F.; Perera, A. Microstructure of neat alcohols: a molecular dynamics study. *J. Chem. Phys.* **2007,** 127 (2), 024502 DOI: 10.1063/1.2753482.
260. Tomšič, M.; Jamnik, A.; Fritz-Popovski, G.; Glatter, O.; Vlček, L. Structural properties of pure simple alcohols from ethanol, propanol, butanol, pentanol, to hexanol: comparing monte carlo simulations with experimental SAXS data. *J. Phys. Chem. B* **2007,** 111 (7), 1738-1751.
261. Sillren, P.; Bielecki, J.; Mattsson, J.; Borjesson, L.; Matic, A. A statistical model of hydrogen bond networks in liquid alcohols. *J. Chem. Phys.* **2012,** 136 (9), 094514 DOI: 10.1063/1.3690137.
262. Franks, N.; Abraham, M.; Lieb, W. Molecular organization of liquid n-octanol: An X-ray diffraction analysis. *J. Pharm. Sci.* **1993,** 82 (5), 466-470.
263. Stewart, G.; Morrow, R. M. X-ray diffraction in liquids: primary normal alcohols. *Physical Review* **1927,** 30 (3), 232.
264. Vahvaselkä, K.; Serimaa, R.; Torkkeli, M. Determination of liquid structures of the primary alcohols methanol, ethanol, 1-propanol, 1-butanol and 1-octanol by X-ray scattering. *J. Appl. Crystallogr.* **1995,** 28 (2), 189-195.
265. Narten, A. H.; Habenschuss, A. Hydrogen bonding in liquid methanol and ethanol determined by x-ray diffraction. *J. Chem. Phys.* **1984,** 80 (7), 3387 DOI: 10.1063/1.447093.
266. Fukasawa, T.; Sato, T. Versatile application of indirect Fourier transformation to structure factor analysis: from X-ray diffraction of molecular liquids to small angle scattering of protein solutions. *Phys. Chem. Chem. Phys.* **2011,** 13 (8), 3187-96 DOI: 10.1039/c0cp01679a.

267. Whitfield, T.; Martyna, G.; Allison, S.; Bates, S.; Vass, H.; Crain, J. Structure and hydrogen bonding in neat N-methylacetamide: Classical molecular dynamics and Raman spectroscopy studies of a liquid of peptidic fragments. *J. Phys. Chem. B* **2006,** 110 (8), 3624-3637.
268. Herrebout, W.; Clou, K.; Desseyn, H. Vibrational spectroscopy of N-methylacetamide revisited. *J. Phys. Chem. A* **2001,** 105 (20), 4865-4881.
269. Turton, D. A.; Wynne, K. Structural relaxation in the hydrogen-bonding liquids N-methylacetamide and water studied by optical Kerr effect spectroscopy. *J. Chem. Phys.* **2008,** 128 (15), 154516.
270. Bauer, S.; Burlafinger, K.; Gainaru, C.; Lunkenheimer, P.; Hiller, W.; Loidl, A.; Bohmer, R. Debye relaxation and 250 K anomaly in glass forming monohydroxy alcohols. *J. Chem. Phys.* **2013,** 138 (9), 094505 DOI: 10.1063/1.4793469.
271. Bierwirth, S. P.; Buning, T.; Gainaru, C.; Sternemann, C.; Tolan, M.; Bohmer, R. Supramolecular x-ray signature of susceptibility amplification in hydrogen-bonded liquids. *Phys. Rev E* **2014,** 90 (5-1), 052807 DOI: 10.1103/PhysRevE.90.052807.
272. Rössler, E. Private communications.
273. Börner, H. G.; Beers, K.; Matyjaszewski, K.; Sheiko, S. S.; Möller, M. Synthesis of molecular brushes with block copolymer side chains using atom transfer radical polymerization. *Macromolecules* **2001,** 34 (13), 4375-4383.
274. Ludwig, R. The structure of liquid methanol. *ChemPhysChem* **2005,** 6 (7), 1369-75 DOI: 10.1002/cphc.200400663.
275. Ludwig, R.; Weinhold, F.; Farrar, T. Quantum cluster equilibrium theory of liquids: temperature dependent chemical shifts, quadrupole coupling constants and vibrational frequencies in liquid ethanol. *Mol. Phys.* **1999,** 97 (4), 479-486.
276. Zarzycki, P.; Rustad, J. R. Theoretical determination of the NMR spectrum of liquid ethanol. *J. Phys. Chem. A* **2009,** 113 (1), 291-297.
277. Bauer, S.; Stern, J.; Böhm, F.; Gainaru, C.; Havenith, M.; Loerting, T.; Böhmer, R. Vibrational study of anharmonicity, supramolecular structure, and hydrogen bonding in two octanol isomers. *Vib. Spectrosc.* **2015,** 79, 59-66 DOI: 10.1016/j.vibspec.2015.05.001.
278. Gainaru, C.; Figuli, R.; Hecksher, T.; Jakobsen, B.; Dyre, J.; Wilhelm, M.; Böhmer, R. Shear-modulus investigations of monohydroxy alcohols: evidence for a short-chain-polymer rheological response. *Phys. Rev. Lett.* **2014,** 112 (9), 098301.
279. Fox Jr, T. G.; Flory, P. J. Second‐order transition temperatures and related properties of polystyrene. I. Influence of molecular weight. *J. Appl. Phys.* **1950,** 21 (6), 581-591.
280. Gold, B. J.; Hövelmann, C. H.; Weiss, C.; Radulescu, A.; Allgaier, J.; Pyckhout-Hintzen, W.; Wischnewski, A.; Richter, D. Sacrificial bonds enhance toughness of dual polybutadiene networks. *Polymer* **2016,** 87, 123-128.
281. Vogel, H. Flűssigkeiten das temperaturabhängigkeitsgesetz der viskosität von. *Phys Zeitschr* **1921,** 22, 645-646.
282. Tammann, G.; Hesse, W., *Die abhangigkeit der viscositat von der temperatur bei unterkuhlten flussigkeiten*. Zeitschrift fur anorganische und allgemeine Chemie: 1926; Vol. 156, p 245-257.
283. Fulcher, G. S. Analysis of recent measurements of the viscosity of glasses. *J. Am. Ceram. Soc.* **1925,** 8 (6), 339-355.
284. Müller, M.; Fischer, E.; Kremer, F.; Seidel, U.; Stadler, R. The molecular dynamics of thermoreversible networks as studied by broadband dielectric spectroscopy. *Colloid & Polymer Science* **1995,** 273 (1), 38-46.
285. Goldansaz, H.; Fustin, C.-A.; Wübbenhorst, M.; van Ruymbeke, E. How supramolecular assemblies control dynamics of associative polymers: toward a general picture. *Macromolecules* **2016,** 49 (5), 1890-1902.

286. Marten, B.; Kim, K.; Cortis, C.; Friesner, R. A.; Murphy, R. B.; Ringnalda, M. N.; Sitkoff, D.; Honig, B. New model for calculation of solvation free energies: correction of self-consistent reaction field continuum dielectric theory for short-range hydrogen-bonding effects. *J. Phys. Chem.* **1996,** 100 (28), 11775-11788.
287. Matsumiya, Y.; Watanabe, H.; Urakawa, O.; Inoue, T. Experimental Test for Viscoelastic Relaxation of Polyisoprene Undergoing Monofunctional Head-to-Head Association and Dissociation. *Macromolecules* **2016**, DOI: 10.1021/acs.macromol.6b01313.
288. Stephen A. Perusich, P. A., Mimi Y. Keating. Dielectric relaxation studies of perfluorocarboxylate polymers. *Macromolecules* **1993,** 26, 4756-4764.
289. Peter Pulay, G. F., Frank Pang, James E. Boggs. Systematic ab initio gradient calculation of molecular geometries, force constants, and dipole moment derivatives. *J. Am. Chem. Soc.* **1979,** 101, 2550-2560.
290. Ding, Y.; Novikov, V.; Sokolov, A.; Cailliaux, A.; Dalle-Ferrier, C.; Alba-Simionesco, C.; Frick, B. Influence of molecular weight on fast dynamics and fragility of polymers. *Macromolecules* **2004,** 37 (24), 9264-9272.
291. Ngai, K.; Roland, C. Chemical structure and intermolecular cooperativity: dielectric relaxation results. *Macromolecules* **1993,** 26 (25), 6824-6830.
292. Leibler, L.; Rubinstein, M.; Colby, R. Dynamics of telechelic ionomers. Can polymers diffuse large distances without relaxing stress? *J. Phys. II* **1993,** 3 (10), 1581-1590.
293. Gainaru, C.; Hiller, W.; Böhmer, R. A Dielectric Study of Oligo- and Poly(propylene glycol). *Macromolecules* **2010,** 43 (4), 1907-1914 DOI: 10.1021/ma9026383.
294. Gainaru, C.; Böhmer, R. Oligomer-to-Polymer Transition of Poly(propylene glycol) Revealed by Dielectric Normal Modes. *Macromolecules* **2009,** 42 (20), 7616-7618 DOI: 10.1021/ma901805c.
295. Dyre, J. C.; Olsen, N. B. Minimal model for Beta relaxation in viscous liquids. *Phys. Rev. Lett.* **2003,** 91 (15), 155703 DOI: 10.1103/PhysRevLett.91.155703.
296. Mattsson, J.; Bergman, R.; Jacobsson, P.; Borjesson, L. Chain-length-dependent relaxation scenarios in an oligomeric glass-forming system: from merged to well-separated alpha and beta loss peaks. *Phys. Rev. Lett.* **2003,** 90 (7), 075702 DOI: 10.1103/PhysRevLett.90.075702.
297. Grzybowska, K.; Grzybowski, A.; Ziolo, J.; Paluch, M.; Capaccioli, S. Dielectric secondary relaxations in polypropylene glycols. *J. Chem. Phys.* **2006,** 125 (4), 44904 DOI: 10.1063/1.2219112.
298. Grzybowska, K.; Grzybowski, A.; Ziolo, J.; Rzoska, S. J.; Paluch, M. Anomalous behavior of secondary dielectric relaxation in polypropylene glycols. *J. Phys. Condens. Matter* **2007,** 19 (37), 376105 DOI: 10.1088/0953-8984/19/37/376105.
299. Pawlus, S.; Hensel-Bielowka, S.; Grzybowska, K.; Zioło, J.; Paluch, M. Temperature behavior of secondary relaxation dynamics in tripropylene glycol. *Phys. Rev. B* **2005,** 71 (17), DOI: 10.1103/PhysRevB.71.174107.
300. Ngai, K. L.; Pawlus, S.; Grzybowska, K.; Kaminski, K.; Capaccioli, S.; Paluch, M. Does the Johari–Goldstein β-Relaxation Exist in Polypropylene Glycols? *Macromolecules* **2015,** 48 (12), 4151-4157 DOI: 10.1021/acs.macromol.5b00832.
301. Moon, I.; Jeong, Y.; Furukawa, T. Enthalpy and dielectric relaxation in the glass transition region of polypropylene glycol. *Thermochim. Acta* **2001,** 377 (1-2), 97-104.
302. Hofmann, M.; Gainaru, C.; Cetinkaya, B.; Valiullin, R.; Fatkullin, N.; Rössler, E. Field-cycling relaxometry as a molecular rheology technique: common analysis of NMR, shear modulus and dielectric loss data of polymers vs dendrimers. *Macromolecules* **2015,** 48 (20), 7521-7534.
303. Gainaru, C.; Hecksher, T.; Fan, F.; Xing, K.; Cetinkaya, B.; Olsen, N. B.; Dyre, J. C.; Sokolov, A. P.; Böhmer, R. Simple-liquid dynamics emerging in the mechanical shear spectra of poly (propylene glycol). *Colloid. Polym. Sci.* **2017,** 295 (12), 2433-2437.

304. Cochrane, J.; Harrison, G.; Lamb, J.; Phillips, D. W. Creep, creep recovery and dynamic mechanical measurements of a poly(propylene glycol) oligomer. *Polymer* **1980,** 21, 837-844.
305. Nicolai, T.; Floudas, G. Dynamics of linear and star poly (oxypropylene) studied by dielectric spectroscopy and rheology. *Macromolecules* **1998,** 31 (8), 2578-2585.
306. Swenson, J.; Köper, I.; Telling, M. Dynamics of propylene glycol and its 7-mer by neutron scattering. *J. Chem. Phys.* **2002,** 116 (12), 5073-5079.
307. Wang, C.-H.; Fytas, G.; Lilge, D.; Dorfmüller, T. Laser light beating spectroscopic studies of dynamics in bulk polymers: poly (propylene glycol). *Macromolecules* **1981,** 14 (5), 1363-1370.
308. Engberg, D.; Schüller, J.; Strube, B.; Sokolov, A.; Torell, L. Brillouin scattering and dielectric relaxation in PPG of different chain lengths and end groups. *Polymer* **1999,** 40 (17), 4755-4761.
309. Eckert, S.; Meier, G.; Alig, I. Phase behaviour of mixtures of polyethylene glycol and polypropylene glycol: Influence of hydrogen bond clusters on the phase diagram. *Phys. Chem. Chem. Phys.* **2002,** 4 (15), 3743-3749 DOI: 10.1039/b203060h.
310. Kaminski, K.; Kipnusu, W.; Adrjanowicz, K.; Mapesa, E.; Iacob, C.; Jasiurkowska, M.; Wlodarczyk, P.; Grzybowska, K.; Paluch, M.; Kremer, F. Comparative study on the molecular dynamics of a series of polypropylene glycols. *Macromolecules* **2013,** 46 (5), 1973-1980.
311. Kaminski, K.; Kipnusu, W. K.; Adrjanowicz, K.; Mapesa, E. U.; Iacob, C.; Jasiurkowska, M.; Wlodarczyk, P.; Grzybowska, K.; Paluch, M.; Kremer, F. Comparative Study on the Molecular Dynamics of a Series of Polypropylene Glycols. *Macromolecules* **2013,** 46 (5), 1973-1980 DOI: 10.1021/ma302611x.
312. Callies, X.; Véchambre, C.; Fonteneau, C.; Pensec, S.; Chenal, J. M.; Chazeau, L.; Bouteiller, L.; Ducouret, G.; Creton, C. Linear Rheology of Supramolecular Polymers Center-Functionalized with Strong Stickers. *Macromolecules* **2015,** 48 (19), 7320-7326 DOI: 10.1021/acs.macromol.5b01583.
313. Stockmayer, W. H. Dielectric dispersion in solutions of flexible polymers. *Pure Appl. Chem.* **1967,** 15 (3-4), 539-554.
314. Roland, C.; Psurek, T.; Pawlus, S.; Paluch, M. Segmental-and normal-mode dielectric relaxation of poly (propylene glycol) under pressure. *J. Polym. Sci., Part B: Polym. Phys.* **2003,** 41 (23), 3047-3052.
315. Schlosser, E.; Schönhals, A. Relation between main-and normal-mode relaxation. A dielectric study on poly (propyleneoxide). *Application of Scattering Methods to the Dynamics of Polymer Systems* **1993**, 158-161.
316. Schüller, J.; Mel'Nichenko, Y. B.; Richert, R.; Fischer, E. W. Dielectric studies of the glass transition in porous media. *Phys. Rev. Lett.* **1994,** 73 (16), 2224.
317. Schönhals, A.; Stauga, R. Broadband dielectric study of anomalous diffusion in a poly(propylene glycol) melt confined to nanopores. *J. Chem. Phys.* **1998,** 108 (12), 5130-5136 DOI: 10.1063/1.475918.
318. Hayakawa, T.; Adachi, K. Dielectric normal mode relaxation of undiluted poly (propylene glycol) s. *Polymer* **2001,** 42 (4), 1725-1732.
319. Gainaru, C.; Bohmer, R. Oligomer-to-Polymer Transition of Poly (propylene glycol) Revealed by Dielectric Normal Modes. *Macromolecules* **2009,** 42 (20), 7616-7618.
320. Ge, S.; Tress, M.; Xing, K.; Cao, P.-F.; Saito, T.; Sokolov, A. P. Viscoelasticity in associating oligomers and polymers: experimental test of the bond lifetime renormalization model. [submitted].
321. Kautz, H.; Van Beek, D.; Sijbesma, R. P.; Meijer, E. Cooperative end-to-end and lateral hydrogen-bonding motifs in supramolecular thermoplastic elastomers. *Macromolecules* **2006,** 39 (13), 4265-4267.
322. Appel, W. P. J.; Portale, G.; Wisse, E.; Dankers, P. Y. W.; Meijer, E. W. Aggregation of ureido-pyrimidinone supramolecular thermoplastic elastomers into nanofibers: A kinetic analysis. *Macromolecules* **2011,** 44 (17), 6776-6784 DOI: 10.1021/ma201303s.
323. Chen, S.; Binder, W. H. Dynamic ordering and phase segregation in hydrogen-bonded polymers. *Acc Chem Res* **2016,** 49 (7), 1409-20 DOI: 10.1021/acs.accounts.6b00174.

324. Chen, S.; Yan, T.; Fischer, M.; Mordvinkin, A.; Saalwächter, K.; Thurn‐Albrecht, T.; Binder, W. H. Opposing phase‐segregation and hydrogen‐bonding forces in supramolecular polymers. *Angew. Chem. Int. Ed.* **2017,** 56 (42), 13016-13020.
325. Merino, D. H.; Feula, A.; Melia, K.; Slark, A. T.; Giannakopoulos, I.; Siviour, C. R.; Buckley, C. P.; Greenland, B. W.; Liu, D.; Gan, Y. A systematic study of the effect of the hard end-group composition on the microphase separation, thermal and mechanical properties of supramolecular polyurethanes. *Polymer* **2016,** 107, 368-378.
326. Sivakova, S.; Bohnsack, D. A.; Mackay, M. E.; Suwanmala, P.; Rowan, S. J. Utilization of a combination of weak hydrogen-bonding interactions and phase segregation to yield highly thermosensitive supramolecular polymers. *J. Am. Chem. Soc.* **2005,** 127 (51), 18202-18211.
327. Ferahian, A.-C. c.; Balog, S.; Oveisi, E.; Weder, C.; Montero de Espinosa, L. Hard phase crystallization directs the phase segregation of hydrogen-bonded supramolecular polymers. *Macromolecules* **2019,** 52 (5), 2164-2172.
328. Botterhuis, N. E.; van Beek, D. J. M.; van Gemert, G. M. L.; Bosman, A. W.; Sijbesma, R. P. Self-assembly and morphology of polydimethylsiloxane supramolecular thermoplastic elastomers. *J. Polym. Sci., Part A: Polym. Chem.* **2008,** 46 (12), 3877-3885.
329. Herbst, F.; Binder, W. H. Comparing solution and melt-state association of hydrogen bonds in supramolecular polymers. *Polym. Chem.* **2013,** 4 (12), 3602.
330. Binder, W. H., *Self-healing polymers: from principles to applications*. John Wiley & Sons: 2013.
331. Woodward, P. J.; Hermida Merino, D.; Greenland, B. W.; Hamley, I. W.; Light, Z.; Slark, A. T.; Hayes, W. Hydrogen bonded supramolecular elastomers: Correlating hydrogen bonding strength with morphology and rheology. *Macromolecules* **2010,** 43 (5), 2512-2517.
332. Callies, X.; Fonteneau, C.; Véchambre, C.; Pensec, S.; Chenal, J. M.; Chazeau, L.; Bouteiller, L.; Ducouret, G.; Creton, C. Linear rheology of bis-urea functionalized supramolecular poly(butylacrylate)s: Part I – weak stickers. *Polymer* **2015,** 69, 233-240 DOI: 10.1016/j.polymer.2014.12.053.
333. Mitchell, G. R.; Odajima, A. The local conformation of poly (dimethylsiloxane). *Polym. J.* **1984,** 16 (4), 351.
334. Schwab, M.; Stühn, B. Thermotropic transition from a state of liquid order to a macrolattice in asymmetric diblock copolymers. *Phys. Rev. Lett.* **1996,** 76 (6), 924.
335. Kinning, D. J.; Thomas, E. L. Hard-sphere interactions between spherical domains in diblock copolymers. *Macromolecules* **1984,** 17 (9), 1712-1718.
336. Ding, Y.; Sokolov, A. P. Comment on the dynamic bead size and Kuhn segment length in polymers: Example of polystyrene. *J. Polym. Sci., Part B: Polym. Phys.* **2004,** 42 (18), 3505-3511.
337. Mark, J.; Curro, J. A non‐Gaussian theory of rubberlike elasticity based on rotational isomeric state simulations of network chain configurations. I. Polyethylene and polydimethylsiloxane short‐chain unimodal networks. *J. Chem. Phys.* **1983,** 79 (11), 5705-5709.
338. Müller, M.; Stadler, R.; Kremer, F.; Williams, G. On the motional coupling between chain and junction dynamics in thermoreversible networks. *Macromolecules* **1995,** 28 (20), 6942-6949.
339. Tanaka, F.; Edwards, S. Viscoelastic properties of physically crosslinked networks: Part 1. Non-linear stationary viscoelasticity. *J. Non-Newtonian Fluid Mech.* **1992,** 43 (2-3), 247-271.
340. Tress, M.; Xing, K.; Ge, S.; Cao, P.; Saito, T.; Sokolov, A. What dielectric spectroscopy can tell us about supramolecular networks⋆. *Eur Phys J E* **2019,** 42 (10), 133.
341. Chen, S.; Döhler, D.; Binder, W. H. Rheology of hydrogen-bonded dendritic supramolecular polymer networks in the melt state. *Polymer* **2016,** 107, 466-473 DOI: 10.1016/j.polymer.2016.08.046.
342. Jangizehi, A.; Ghaffarian, S. R.; Nikravan, G.; Jamalpour, S. Thermal and viscoelastic properties of entangled supramolecular polymer networks as a powerful tool for prediction of their microstructure. *Thermochim. Acta* **2018,** 661, 34-40.

343. de Espinosa, L. M.; Balog, S.; Weder, C. Isophthalic Acid-Pyridine H-Bonding: Simplicity in the Design of Mechanically Robust Phase-Segregated Suprannolecular Polymers. *ACS Macro Letters* **2014,** 3 (6), 540-543.

Vita

Kunyue Xing was born in Shijiazhuang, Hebei, China in 1991 (Year of the Horse). She graduated from Shijiazhuang No. 1 High School in 2009 and entered Sun Yat-Sen University at the same year. She received her B.S. degree in Chemistry in June 2013 and came to the University of Tennessee, Knoxville to pursue Ph.D. degree in Polymer chemistry. She joined Professor Alexei P. Sokolov's group in September 2014 with a research focus on dynamics and viscoelastic properties of associating polymers. She won 3rd Prize of Poster Presentation Awards in the 12th National Graduate Research Polymer Conference, Akron in June 2016 and Best Poster Awards (Division of Polymer Materials: Science and Engineering) in American Chemistry Society National Meeting, Boston in August 2018. She worked as a research co-op at Toyota Research Institute, North America in Ann Arbor from January to May 2019 on future all-solid-state batteries. By December 2019, she has authored or coauthored nine peer-reviewed publications.